Keck Adaptive Optics Note 768

NEXT GENERATION ADAPTIVE OPTICS: PRELIMINARY DESIGN MANUAL

May 24, 2010

Author List

Name	Function
Peter Wizinowich	NGAO Project Manager
Sean Adkins	NGAO Senior Manager (WMKO)
Richard Dekany	NGAO Senior Manager (COO)
Don Gavel	NGAO Senior Manager (UCO)
Claire Max	NGAO Project Scientist (UCO)
From Caltech Optical Observatories (COO): Viswa Velur Alex Delacroix Antonin Bouchez Kent Wallace Randy Bartos Gautam Vasisht Mitchell Troy Lewis Roberts	 Optical system engineer Mechanical engineer AO scientist JPL optics engineer JPL mechanical engineer JPL scientist JPL AO scientist JPL engineer
From University California Observatories (UCO): Elizabeth McGrath Renate Kupke Marco Reinig Chris Lockwood Sandrine Thomas	 Astronomer Optical system engineer AO software engineer Mechanical engineer AO scientist
From W. M. Keck Observatory (WMKO): Jason Chin Al Conrad Jimmy Johnson Jim Lyke Drew Medeiros Doug Morrison Chris Neyman Sergey Panteleev Mike Pollard Thomas Stalcup Kevin Tsubota Ed Wetherell	 LGSF lead & electronics engineer Support astronomer Software engineer Support astronomer Mechanical engineer Software engineer AO scientist Optics engineer Mechanical engineer AO scientist Controls lead & software engineer Electronics engineer

Approval Control

Control	Name	Function
Revised by:		
Approved by:		
Authorized by:		

Document Change Record

Version	Date	Change Description
1.0	May 24, 2010	Release for PDR

Table of Contents

Table of Contents

Figures and Tables

Figures and Tables

Figures and Tables

Figures and Tables

Figures and Tables

1 INTRODUCTION

This document describes the preliminary design for the Next Generation Adaptive Optics (NGAO) system to be built for the W. M. Keck Observatory (WMKO). This document is one of the key preliminary design phase deliverables as discussed in the Preliminary Design Report (KAON 770). It is intended to provide an overview of the preliminary design, while referencing the appropriate documents containing additional technical detail. This document replaces the System Design Manual (KAON 511) and the Build-to-Cost design update (KAON 642).

Some areas that could have been included in this document such as the NGAO integration and test strategy and the approach to component failures and spares are instead addressed in the Systems Engineering Management Plan (KAON 769). Similarly, a discussion of NGAO risks is instead presented in KAON 720.

We begin with an overview of the preliminary design that includes major sections on the AO system, laser facility, controls hardware and software, science operations, science instruments and facilities. The performance budgets are addressed in Section 4. Section 5 provides an overview of the requirements and documents under configuration control. The final section provides a summary of trade studies performed in the process of arriving at the preliminary design. A glossary can be found at the end of this document.

2 REFERENCES

A list of all Keck Adaptive Optics Notes for NGAO can be found in an Appendix to the Preliminary Design Report (KAON 770). These documents are available at http://www.oir.caltech.edu/twiki_oir/bin/view/Keck/NGAO/NewKAONs.

3 DESIGN OVERVIEW

3.1 AO System Overview

All of the NGAO science cases require essentially diffraction-limited performance (Strehl > 0.6) in the near-IR. A number of Solar System and Galactic science cases have requirements for at least modest Strehl at visible wavelengths. All of the science cases also require high sensitivity with most of the targets of interest being too faint to use as references for wavefront sensing in the AO system. This high Strehl, faint object performance is required with reasonable (≥ 30%) sky coverage averaged over the sky.

NGAO science cases require observation of only a modest to narrow field of view, ranging from 2" to 30" diameter. This is generally within the natural isoplanatic angle of the atmosphere at corresponding wavelengths, allowing NGAO to meet performance requirements by applying wavefront correction at only a single conjugate altitude. Excellent spatial control of the wavefront requires the use of a high-order deformable mirror (DM) in the science path.

The requirements for sky coverage and high sensitivity are both met by using a laser of 589 nm wavelength to illuminate the mesospheric sodium layer, producing an artificial laser guide star (LGS)

for AO wavefront sensing. To achieve the desired level of Strehl performance we must overcome the effect of focus anisoplanatism (the "cone effect"), which we do by projecting multiple laser beacons to form an on-sky asterism of LGS as shown in Figure 1. Four central LGS are viewed with four Shack-Hartmann wavefront sensors (WFS's), providing information to tomographically estimate the three-dimensional atmospheric turbulence over the telescope aperture. We have concluded that a fixed diameter LGS asterism with one in the center and three equally spaced around a circle provides the optimal sampling of the atmosphere above the telescope with respect to tomography error for the science field (KAON 644). The radius of the circle is set at 10".

To provide excellent sky coverage and overcome limitations imposed by the central tomographic sensing system, NGAO employs a low-order wavefront sensor (LOWFS) subsystem, consisting of three additional LGS WFS and DM's operating as three independently controlled AO loops, to provide high-fidelity, near-infrared wavelength image sharpening of three natural guide stars (NGS). Each NGS sensor arm contains an articulating object selection mechanism (OSM) and its own high-order DM to allow optimal sharpening of NGS spread over a 120" diameter field of view. To provide sensitive and accurate measurement of un-sensed atmospheric modes, two of the NGS sensors are assigned to measure atmospheric tip and tip (TT) and a third sensor to measure tip, tilt, focus, and astigmatism (TTFA).

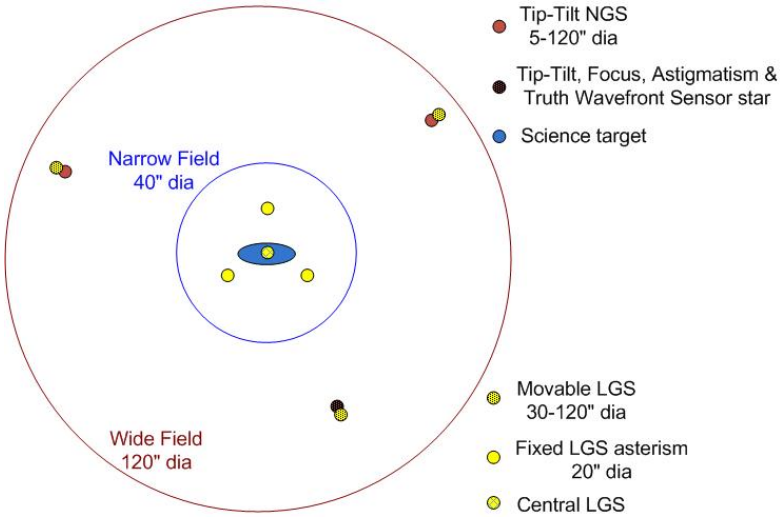

Figure 1: LGS "3+1" asterism for tomography of the central science field, plus three patrolling LGS for image sharpening two TT and one TTFA NGS

A block diagram of the AO system architecture that we have selected to deliver high Strehl correction with excellent sky coverage is shown in Figure 2. We refer to this design as a "cascaded relay" because it uses two AO optical relays in series: an initial wide-field relay for large NGS field of regard followed by a narrow-field relay for exquisite science path spatial correction. Starting at the lower left hand side of the figure, an enclosure on the elevation ring of the telescope houses three ~25W CW format sodium D_2 wavelength lasers. Laser output is sent via a free space beam transfer system to a multiple beam asterism generator and controller located at the top end of the Keck II telescope. The output of this asterism generator is projected onto the mesospheric sodium layer by a

laser launch telescope located behind the telescope secondary mirror as shown just to the left of center in Figure 2.

Light collected by the Keck telescope is directed to the AO system shown in the lower right in Figure 2. The AO system and instruments are located on the telescope's left Nasmyth platform at the f/15 focus. The AO system science path is enclosed and cooled to -15°C below ambient (~260 K) to reduce the thermal emissivity of the optical surfaces. An entrance window is provided to isolate the enclosure from the dome environment. Output windows are provided to feed the appropriate light to the LGS WFS assembly and the interferometer dual star module (DSM). The science instrument cryostat forms a seal with the cooled enclosure at one of the AO system's two science ports.

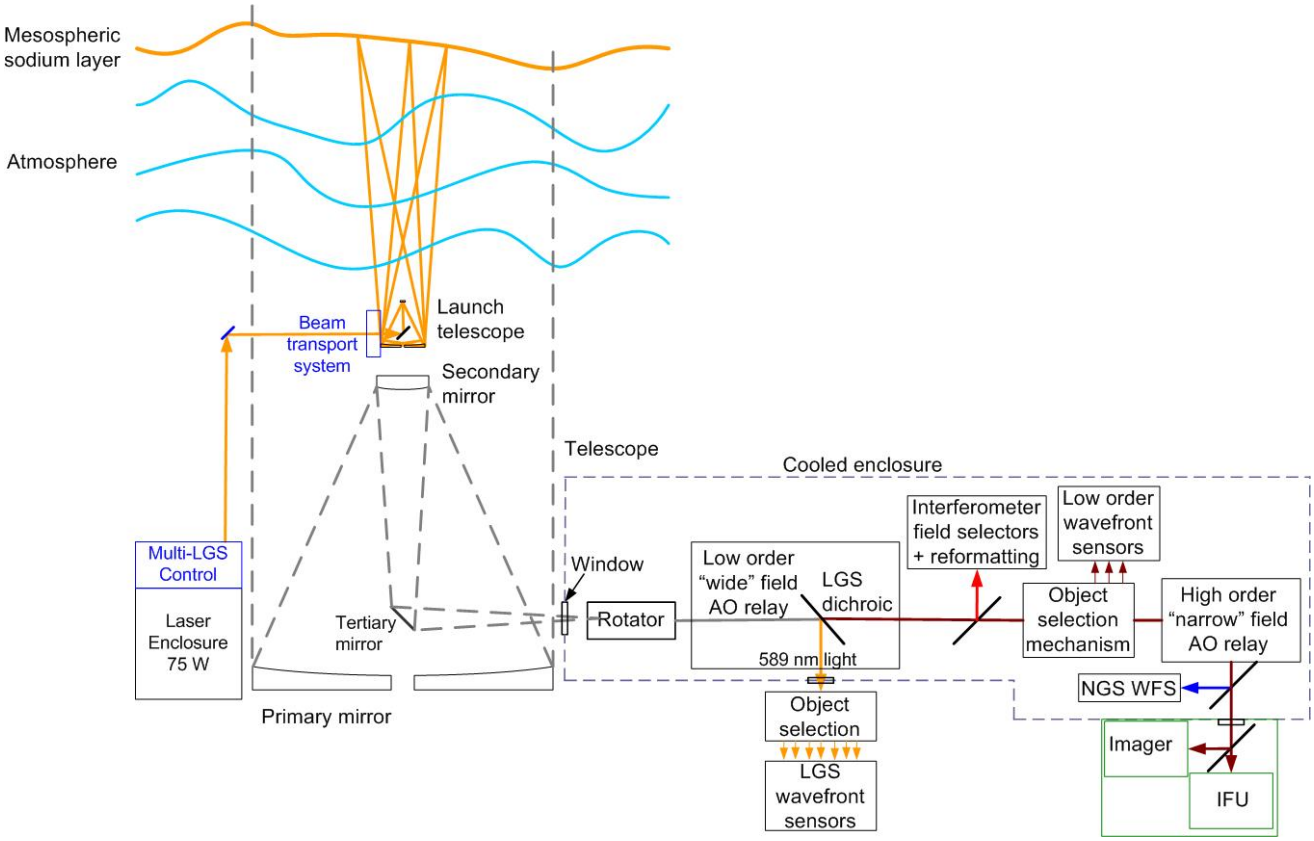

Figure 2: NGAO Block Diagram

Within the cooled enclosure, the light from the telescope passes through an image de-rotator. A "wide" field, low-order AO relay incorporating a single DM provides moderate spatial order AO correction (comparable to the correction provided by the existing Keck AO systems). This DM operates in a closed loop in conjunction with the LGS wavefront sensors. Just after the DM, a dichroic beamsplitter is used to send the 589 nm light from the LGS asterism to the LGS WFS assembly. The light from the wide field relay is transmitted directly to the object selection mechanism for the LOWFS, which also contains a visible-light truth wavefront sensor (TWFS) that monitors slow calibration changes in the system. A dichroic can be inserted to feed light to the Keck interferometer. A pickoff mirror (not shown) can be inserted to feed light to the acquisition camera.

Light not otherwise directed then passes through a "narrow" field, high-order AO relay. High-order corresponds to nine times the DM actuator areal density of the low-order DM. This relay provides light to a visible light NGS wavefront sensor and the science instrument corrected with a low-latency "go-to" AO control law and highly stable DM (utilizing micro-electromechanical systems (MEMS) technology). The NGAO science instrument is a combined imager and integral field spectrograph, called DAVINCI (for Diffraction limited Adaptive optics Visible and Infrared iNtegral field spectrograph and Coronagraphic Imager), working from I-band to K-band. Another instrument port is provided for a future instrument capability.

For NGS AO observations only the NGS WFS is required. For LGS AO observations, the LGS and LOWFS are required.

The following is a brief summary of the key architectural features of NGAO and why they were selected (i.e., flowed down from the science requirements):

- Laser tomography to measure wavefronts and overcome the cone effect over the science field. This is supported by the fixed "3+1" LGS asterism and LGS WFS.
- LGS projection from behind the telescope's secondary mirror to minimize perspective elongation.
- Location of the AO system on the Keck II telescope left Nasmyth platform to have sufficient space for the AO system and science instruments in a gravity constant environment.
- A cooled AO system to meet the near-infrared background requirements.
- A K-mirror rotator at the input to the AO system to keep either the field or pupil fixed. The AO system would need to be cooled even without a rotator and this approach allows the most stability for the AO system and instruments.
- A wide-field (120" diameter) relay to feed light to the LGS wavefront sensors and the three LOWFS.
- A conventional (5 mm pitch) DM was chosen to transmit a wide field in the wide-field relay.
- A low-order (20 actuators across the pupil) DM (LODM) was chosen for the wide-field relay to limit the size of the relay, to permit closed loop AO correction on the LGS wavefront sensors and to keep the LGS wavefront sensors in their linear range, reducing the requirement on downstream open loop correction.
- Open loop AO-corrected near-IR tip-tilt sensors to maximize sky coverage. This is supported by three patrolling laser beacons and LGS WFS.
- Open loop AO-correction to the narrow field science instrument(s) in LGS mode.
- MEMS DM's for the AO-correction. These are very compact devices and have been lab demonstrated to accurately go where they are commanded. Small, modest-cost 32x32 element MEMS DM's provide the required correction for the tip-tilt sensors. A 64x64 element MEMS, similar to that developed for the Gemini Planet Imager (GPI), is needed to provide the required AO correction to the narrow field science instrument(s).
- A high order, narrow-field (40"x60" diameter) AO relay to feed light to the narrow field science instrument(s) and NGS wavefront sensor. The science instruments fed by this relay only require a narrow-field (32"x32") and the narrow field facilitates the use of a single MEMS DM for all narrow-field instruments.

3.2 Telescope

The NGAO design and plan currently assumes implementation on the Keck II telescope. This replaces the older AO system and laser and takes advantage of existing AO and laser infrastructure. It would be straightforward to modify the design for implementation on Keck I. The design and plan assumes that the existing Keck II AO and laser systems will be removed from the summit facility to make room for the NGAO system. In addition to providing physical space for the system this will also free up power and cooling capacity, as well as cable wrap space.

A Solidworks model of the Keck II telescope has been generated in order to clearly define the available space and interfaces for the NGAO system. A view of this model is shown in Figure 3 with a possible AO enclosure on the left Nasmyth platform. This tool can be used to provide the details of areas like the Nasmyth platform or secondary mirror socket which the NGAO system will need for interface purposes. The details of this model are suitable for preliminary design. Critical dimensions will need to be field verified before detailed design.

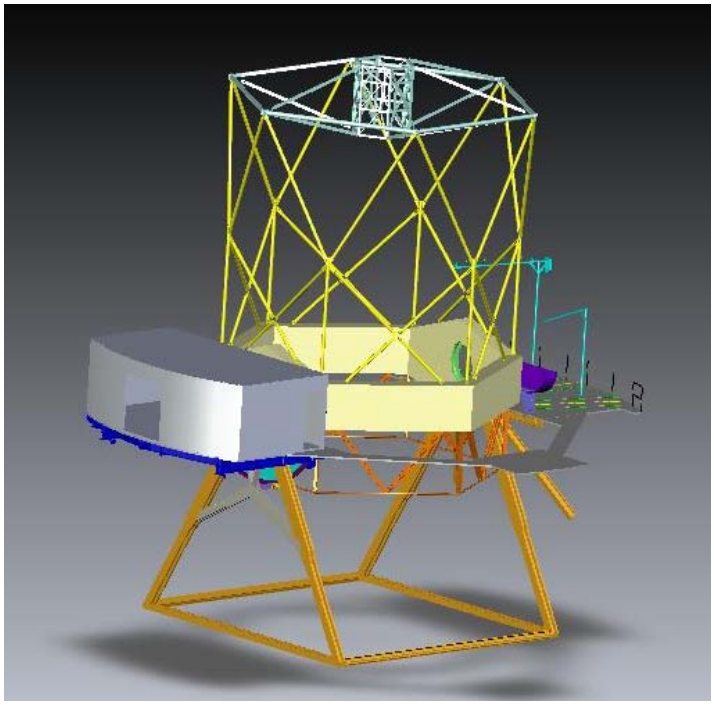

Figure 3: Telescope Solidworks model

3.3 AO System Description

The AO system description begins with the AO opto-mechanical design (section 3.3.1). This includes the AO bench and everything on it except for the systems used by the real-time control system (wavefront sensor cameras and correction elements). The correction elements are discussed in section 3.3.3 and the wavefront sensors in section 3.3.3. The AO enclosures including the cold enclosure for the AO bench, the room housing the AO bench and instruments and the electronics vault are discussed in section 3.3.5. Ancillary systems and procedures (alignment, calibration, metrology, atmospheric monitoring, etc.) are discussed in section 3.3.7.

3.3.1 AO Opto-Mechanical Design

The opto-mechanical design for the AO bench, documented in KAON 685, is summarized in this section. Figure 4 and Figure 5 provide top and perspective views, respectively, of the AO bench and NGAO science instruments on the Nasmyth platform. Annotated optical and mechanical layouts are provided in Figure 6 and Figure 7. We first discuss the rotator and wide field relay design followed by discussions of the optical feeds to the LGS WFS, interferometer and acquisition camera. We then discuss the narrow field relay, including the high order deformable mirror, followed by the optical feeds to the NGS WFS and the science instruments.

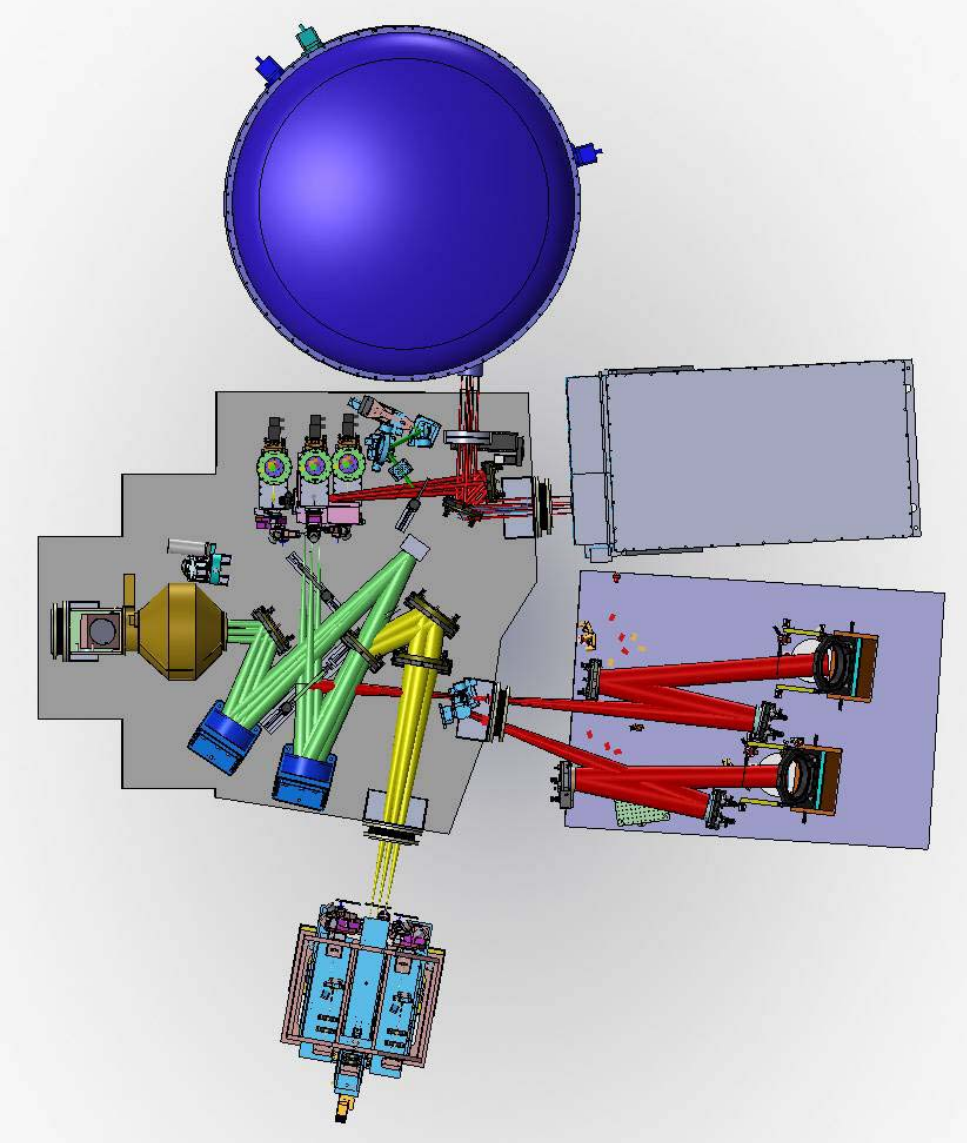

Figure 4: Top view of the AO bench and science instruments

The AO bench (center left) is surrounded by the LGS WFS assembly (bottom), the interferometer dual star module (bottom right), a nominal volume for a future science instrument (top right) and the NGAO science instrument, DAVINCI (top). Light from the telescope enters from the left of this figure along the axis of the rotator (shown in gold on the AO bench).

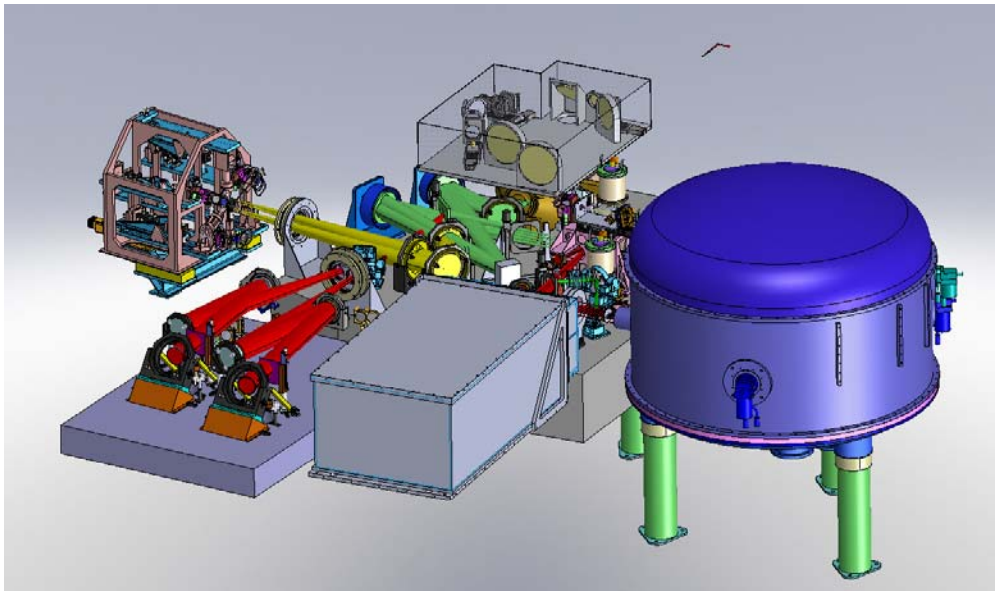

Figure 5: A perspective view of the AO bench and science instruments

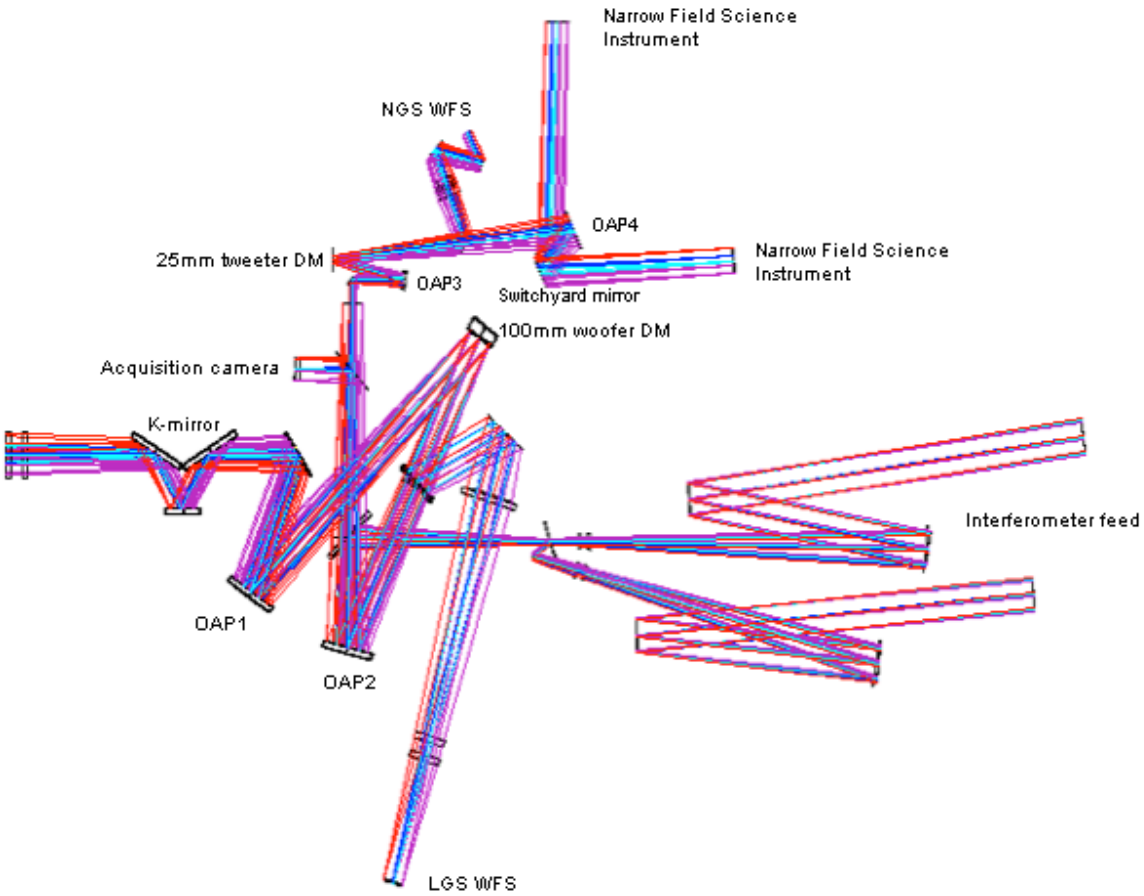

Figure 6: Annotated optical layout of the AO relays and feeds

Light from the telescope enters from the left. Multiple field points are shown in different colors.

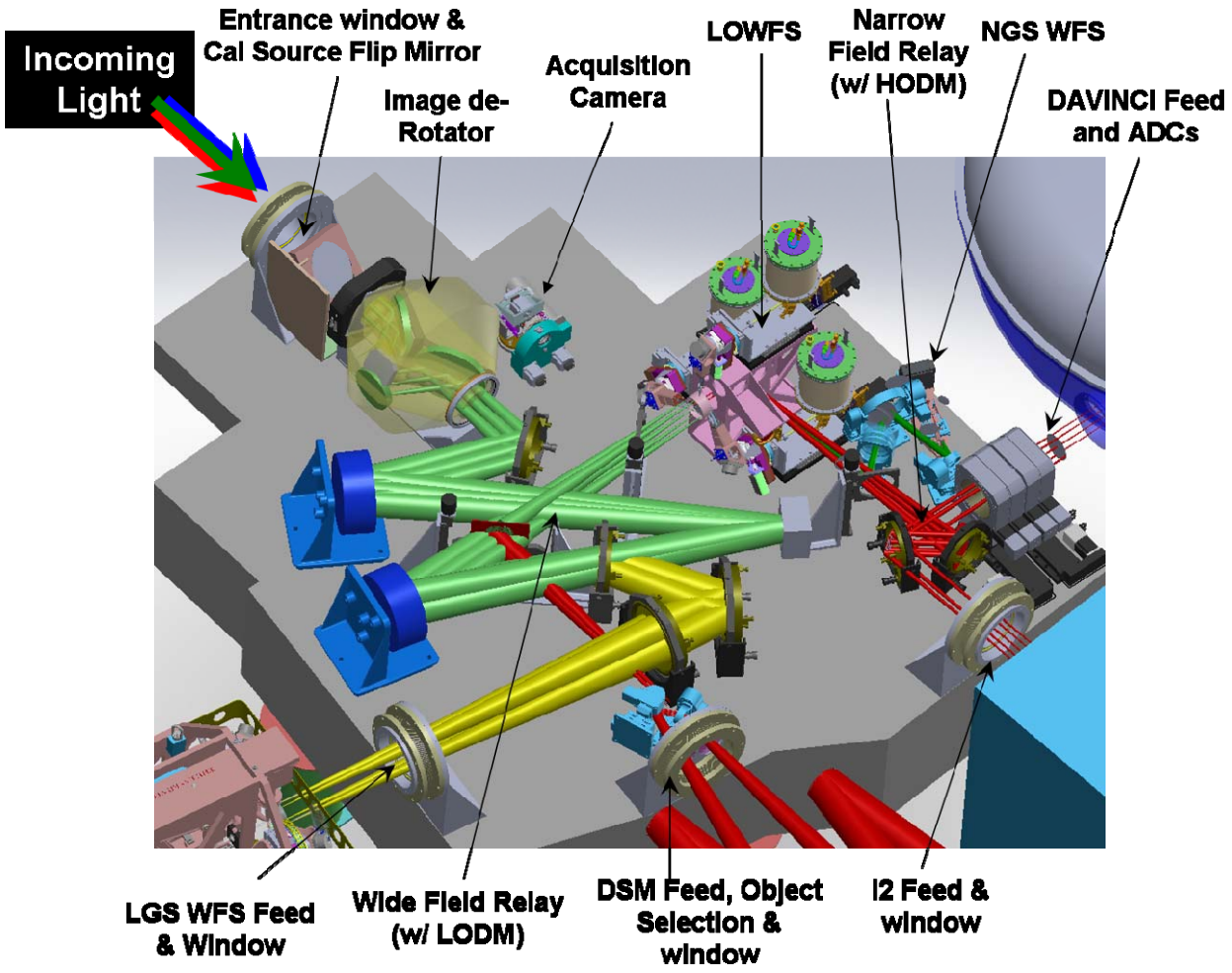

Figure 7: AO bench components

3.3.1.1 Entrance and Exit Windows and Ports

The AO bench is enclosed in a cold enclosure operated at -15° C. The enclosure is sealed from the ambient environment either by windows or sealed ports. The windows include the entrance window in front of the rotator, a window to the LGS WFS and a window to the interferometer dual star module. In the case of the interferometer separate windows are provided for the on- and off-axis targets. All of the windows are double-pane, with dry nitrogen between the two panes, to prevent condensation and AR-coated to optimize throughput. These windows have been included in the Zemax optical design.

The preliminary design has the windows mounted to the optical bench, in order to maintain their tilt requirements, as shown in Figure 8. They then need to be sealed to the inside wall of the cold enclosure, that surrounds the bench, with flex-bellows.

The front face of the first entrance window lies 795 mm before the telescope focus. Each of the 180 mm diameter windows, to accommodate the 120" diameter field, is 25 mm thick. The entrance

window and interferometer exit windows are currently planned to be CaF_2 substrates to provide wavelength coverage to L-band.

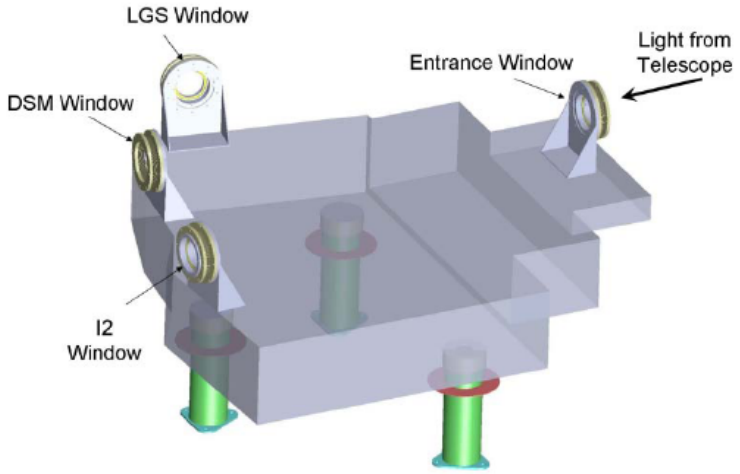

Figure 8: Entrance and exit windows

The science instrument DAVINCI will mate with the cold enclosure so as to provide a thermal and vapor seal. A similar arrangement could be used for a future science instrument to remove the light loss from an exit window.

3.3.1.2 Rotator

The rotator, shown in Figure 9, is a K-mirror that can be used to either keep the field or pupil fixed. The Keck telescope's f/15 Nasmyth focal plane is located ~270 mm past the telescope's elevation bearing, and 121 mm after the first mirror of the rotator. We have not yet evaluated the impact of the focal plane proximity to mirror surfaces upon thermal background uniformity or its impact on our high-contrast science goals (for reference the focal plane is located 110 mm before the first mirror of the existing Keck AO rotator).

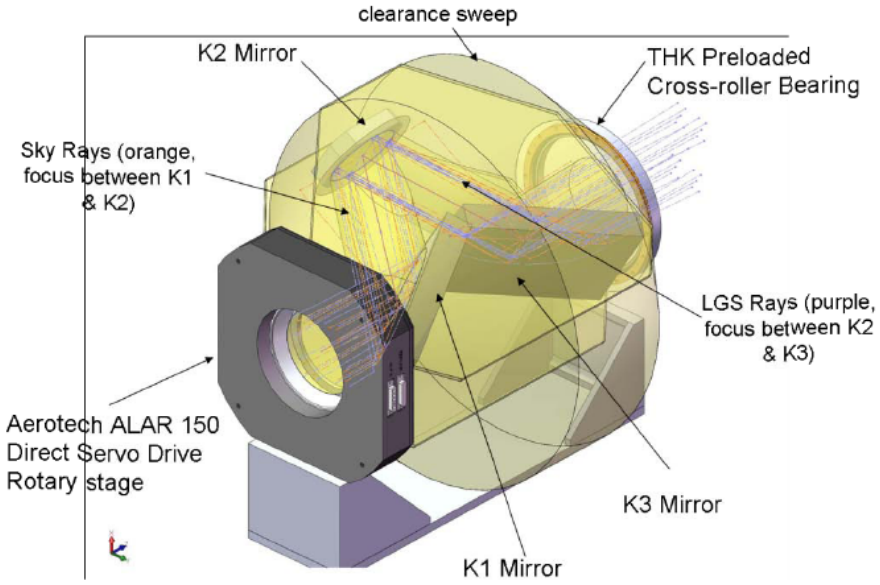

Figure 9: Rotator

The NGAO rotator is very close to the size of the existing Keck AO rotator and it is intentionally kept similar in order to maintain the polarization characteristics in support of interferometer operations. The mirror tilts and separations are identical between the two rotators. The first mirror is slightly larger in the NGAO rotator (250 mm in the long dimension) due to the need to accommodate a 120" diameter NGS field of view (FOV) and a 120" diameter LGS FOV (for the case of an LGS at 80 km). The 2nd mirror is the same size and the 3rd mirror is slightly smaller than their Keck AO counterparts. It will also be desirable to match the coatings between the NGAO and Keck I rotators (currently the 1st and 3rd mirrors are Al, and the 2nd mirror is protected silver in Keck I).

3.3.1.3 Wide Field Relay

The wide field relay is located after the rotator, as shown in Figure 10. For packaging reasons a fold mirror (conjugate to 22 km above the telescope) is located after the rotator. We will determine during the detailed design whether this mirror should be mounted on a slow tip-tilt stage to provide pupil motion compensation. Pupil nutation in the current Keck AO systems is ~70 mm on the telescope primary mirror and we plan to improve this to ~30 mm through improved alignments. The fold is followed by the wide field relay.

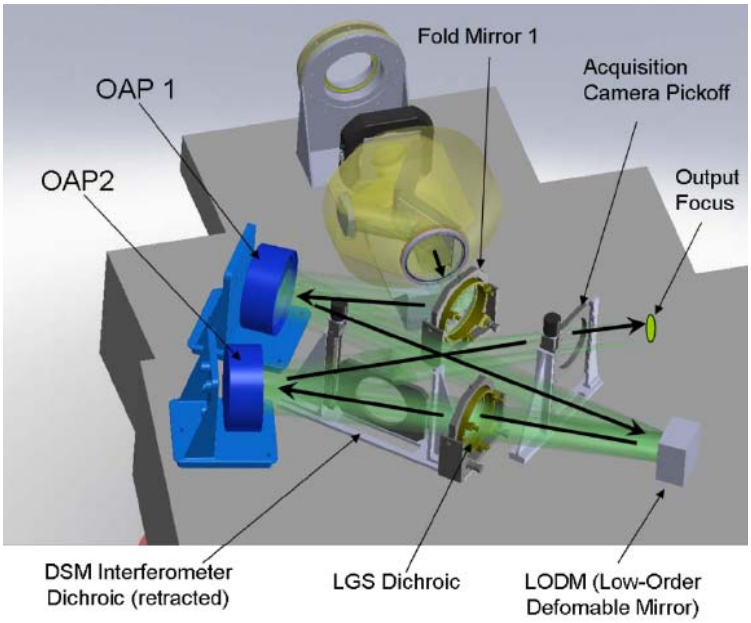

Figure 10: Wide field relay
The entrance window and rotator are also shown for reference.

The wide field relay is a one-to-one magnification relay consisting of an off-axis parabola (OAP1) to collimate the light and reimage the primary mirror onto the DM, and a second identical OAP (OAP2) to converge the light with the same focal ratio as the telescope and a telecentric pupil. The third-order optical aberrations can be minimized by two approaches using a collimated beam between two identical OAPs; of these the off-centered pupil approach was chosen since it maintains a non-tilted focal plane (Korsch, Reflective Optics, p. 171, 1991). The focal length of the OAP was selected to map the primary mirror to a 5 mm (d_{DM}) pitch DM with 22x22 actuators as shown in Figure 11. The OAPs are mounted in commercial SORL OAP mounts.

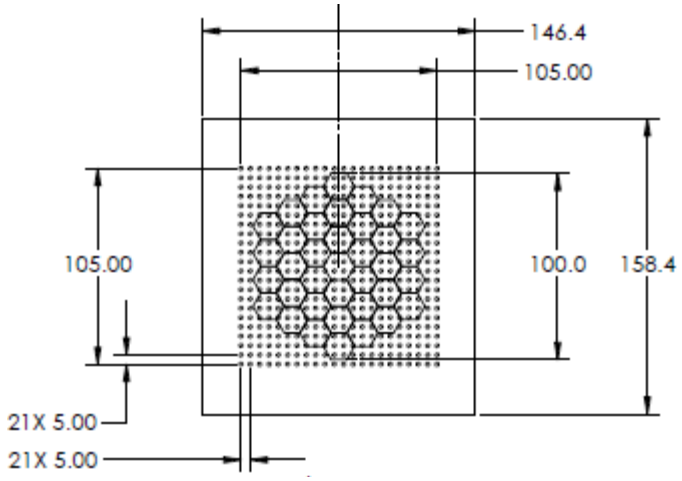

Figure 11: Mapping of Keck primary mirror onto a 22x22 actuator low order DM
The (vertical, horizontal) mapping = (547.45, 555.90) mm/subaperture. Keck drawing 1410-CM0010.

The DM is placed at an optical conjugate to the primary mirror and is mounted on a fast tip-tilt controllable mount (see section 3.3.3.1). The second OAP is located its focal length from the DM in order to project the pupil to infinity and hence generate a telecentric output beam.

The output of the first relay goes directly to the object selection mechanism (OSM) that feeds the low order wavefront sensors (LOWFS). A dichroic or mirror can be inserted into this beam to feed the interferometer or the acquisition camera, respectively.

Some key design numbers:

- Telescope parameters (from KOTN 163 or KAON 107).
  - Telescope focal length, f_{Tel} = 149.583 m.
  - Telescope entrance pupil diameter D_{Tel} = 10.949 m.
  - Telescope exit pupil diameter, D_{EP} = 1460 mm.
  - Distance from telescope exit pupil to focus, t_{EP} = 19948 mm.
  - Telescope $f/\#_{Tel} = f_{Tel}/D_{Tel}$ = 13.66.
  - Telescope plate scale, PS = 0.727 mm/".
- Chosen design parameters for the AO optics up through the wide field relay.
  - LOWFS NGS field of view diameter, Φ_{NGS} = 120".
  - Rotator mirror angles of incidence are 60º for mirrors 1 and 3, and 30º for mirror 2.
  - Rotator mirror diameters (assuming a 90% clear aperture) are 250 mm, 160 mm and 270 mm. The separation of mirrors is 243.5 mm.
  - 190 mm diameter fold mirror located 397.5 mm after the last mirror of the rotator at an incidence angle of 34.5°.
  - OAP1 and OAP2 off-axis angle = 25º
  - DM conjugate to the telescope primary mirror.
  - DM incidence angle, α_{DM} = 10°.
  - DM subaperture size, d_{DM} = 5 mm.
  - Primary mirror subaperture size = 547.45 mm.
  - Output pupil from 1st relay at infinity.
- 1st order calculated parameters.
  - OAP focal length, $f_{OAP} = (d_{DM}/d_{PM})\, f_{Tel}$ = 1366.2 mm.
  - Required OAP diameter to accept the pupil and field, $d_{OAP} = (f_{OAP}/t_{EP})D_{EP} + (f_{OAP}+t_{EP})\Phi_{NGS}*PS/t_{EP}$ = 193.2 mm.
  - Distance of DM from OAP1 in order to be conjugate to the primary, $t_{DM} = [1/f_{OAP} - 1/(t_{EP}+f_{OAP})]^{-1}$ = 1459.7 mm.
  - Pupil elongation on the DM due to the angle of incidence, % elongation = $[1-\cos(\alpha_{DM})]*100\%$ = 1.5%.
  - Distance of OAP2 from the DM in order to project the pupil to infinity, $t_{OAP2} = f_{OAP}$ = 1366.2 mm.

3.3.1.4 LGS Wavefront Sensor Feed

The LGS WFS feed is shown in Figure 12. A fixed dichroic (190 mm diameter, 25 mm thick and at a 19° angle of incidence), located in the collimated beam between the DM and OAP2, reflects the sodium wavelength light over the full 120" diameter field. This location was chosen to minimize the

aberrations in the transmitted beam to the science instruments and LOWFS; and in the LGS beam since the LGS light does not receive a performance benefit from the matched OAPs. The dichroic is mounted in a fixed Aerotech gimbal mount.

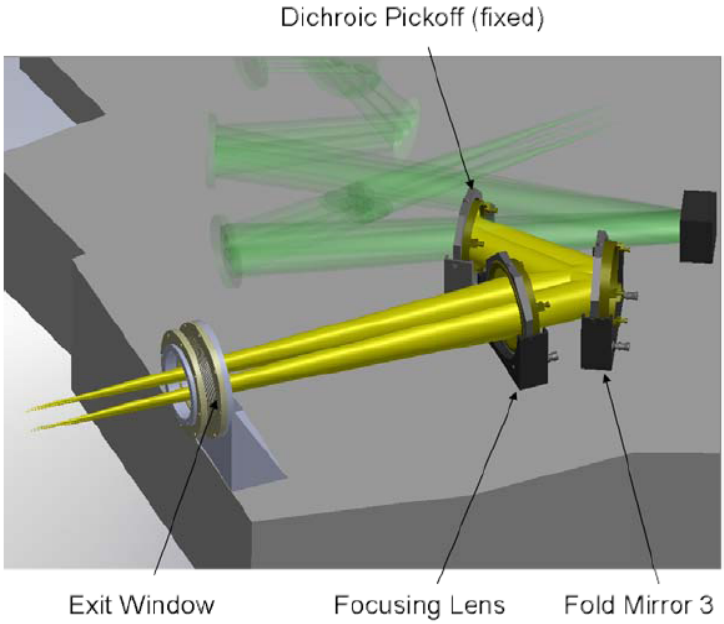

Figure 12: LGS WFS feed

The dichroic is followed by a 250 mm diameter fold mirror used to locate the LGS WFS on the side of the AO bench away from the science instruments. A plano-convex lens, located its focal length from the LODM, is used to produce a f/13.4 beam with a pupil at infinity. A 140 mm diameter double-paned (nominally BK7) exit window is located 950 mm after the lens. The dichroic, fold mirror and focusing lens are all mounted in 10 inch Aerotech gimbal mounts.

3.3.1.5 Interferometer Feed

A removable 190 mm diameter interferometer feed dichroic located 500 mm after OAP2, at an angle of incidence of 42.75° (and with a 0.17° wedge to remove lateral color), sends a 60" diameter field to a pair of field selector mirrors (see Figure 13). The first of these mirrors is located near the focus and has a hole in it to transmit a small on-axis field. The first field selector steers the desired off-axis point to the center of the second field selector mirror, which in turn steers the off-axis field along the desired axis. Similar field steering mirrors are used in the existing Keck AO system and this approach has been implemented for the ASTRA upgrade to the interferometer. The on-axis and off-axis beams go to the dual star module where OAPs are used to collimate the light and fold mirrors are used to steer the beam to the existing coude train.

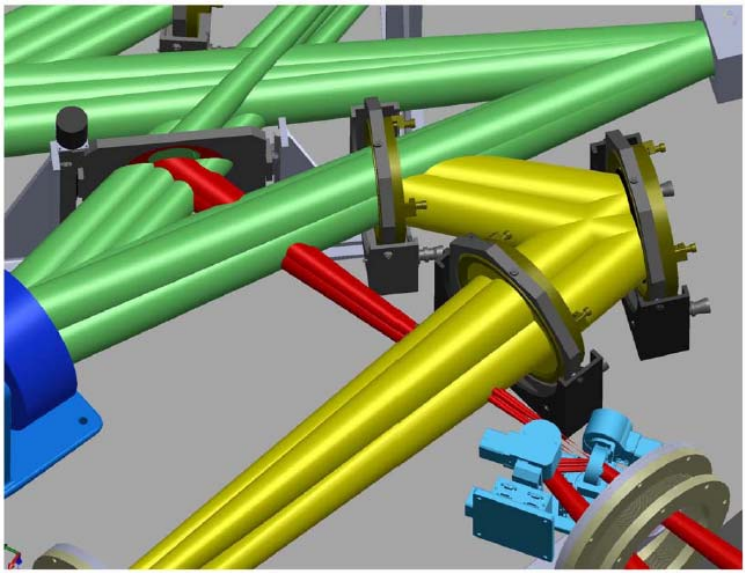

Figure 13: Interferometer feed
The beam from the interferometer dichroic through the field selector mirrors is shown in red.

The interferometer dichroic is mounted in a THK LM stage with ball screw driven shaft encoding.

Note that the LOWFS are not used for interferometer science since the near-IR light is needed by the interferometer. Instead the NGS WFS is used as a low order WFS to provide tip-tilt and truth (TWFS) sensing.

3.3.1.6 Acquisition Camera and Pickoff

A removable 45º incidence angle mirror (or dichroic) folds the entire 120" diameter wide field relay output to the acquisition camera. We have determined (KAON 567 and section 3.6.2.4) that a visible camera is adequate (versus a NIR camera) and that this camera can therefore be used for both NGS and LGS acquisition. The camera is mounted on a focus translation stage to go between the NGS and LGS foci as is done with the acquisition camera for the current Keck AO system. A simple focal reducer is used to obtain the required plate scale on the Keck standard MAGIQ acquisition camera.

The acquisition camera fold stage was planned to be identical to the interferometer, however we recently recognized the need to also provide a blue reflective dichroic to support the ASTRA upgrade to the Interferometer (KAON 748) which will require space for a 3 position stage.

3.3.1.7 Narrow-Field Relay

The narrow-field relay provides a high order of correction for the narrow-field science instrument(s). It also provides a magnification of ~3 in order to provide separation between the instruments and an optimal plate scale for the science instruments. The narrow field relay is shown in Figure 14.

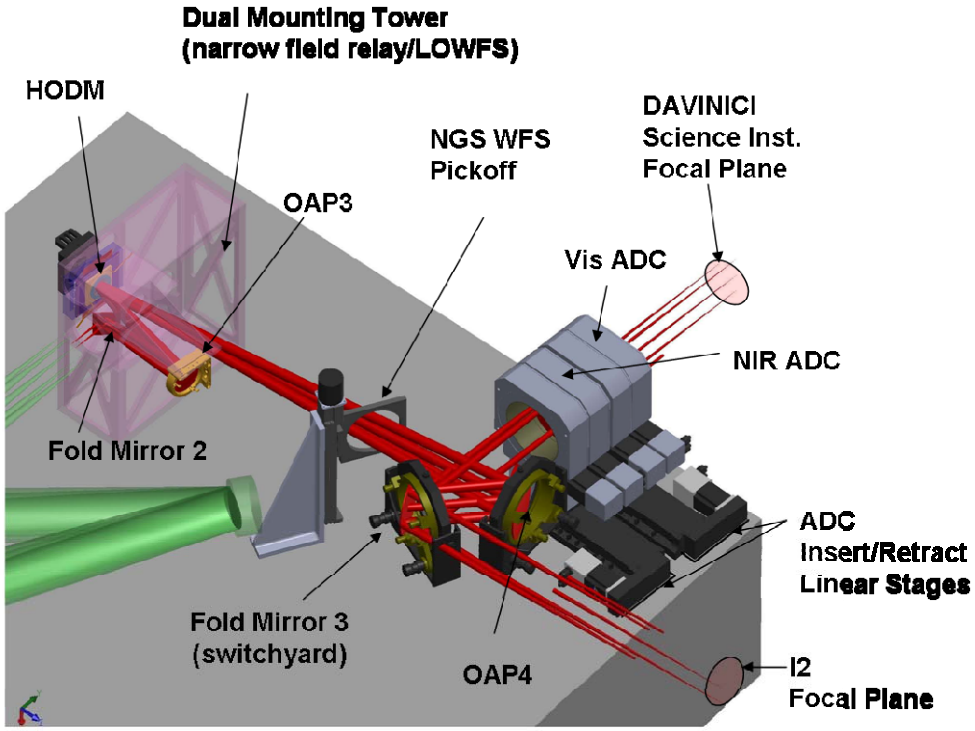

Figure 14: Narrow field relay

The dual mounting tower which supports the HODM and a LOWFS is shown as transparent pink. The wide field relay light is shown as green and the narrow field relay light as red.

The central 60" diameter beam from the wide field relay is reflected by fold mirror 2 before passing through focus to OAP3 which collimates the light and reimages the telescope primary mirror onto a 64x64 MEMS DM as shown in Figure 15. The DM is mounted on a slow tip-tilt stage in order to facilitate science instrument dithering and differential tip-tilt corrections (KAON 669 and section 3.5.2). OAP4 is chosen to provide a factor of ~3 magnification and is located its focal length from the MEMS in order to project the pupil to infinity. Fold mirror 3, located 350 mm after OAP4, allows the beam to be directed to either of two instrument ports. This mirror would be motorized prior to the arrival of a 2nd science instrument.

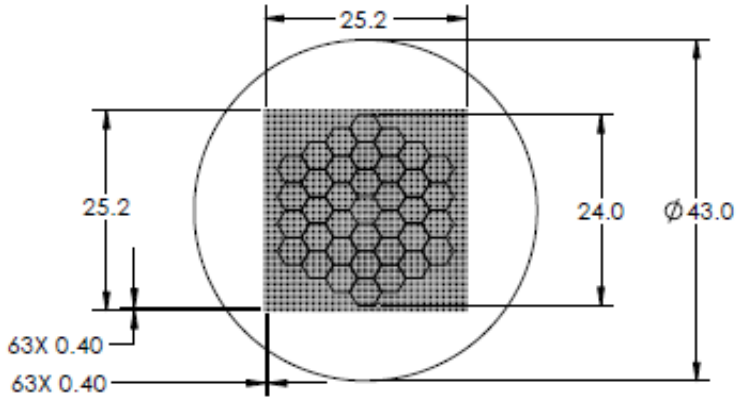

Figure 15: Mapping of Keck primary mirror to a 64x64 actuator high order DM

The (vertical, horizontal) mapping = (182.48, 185.30) mm/subaperture. Keck drawing 1410-CM0010.

The first three narrow field relay elements are closely located with the LOWFS assembly as shown in Figure 16.

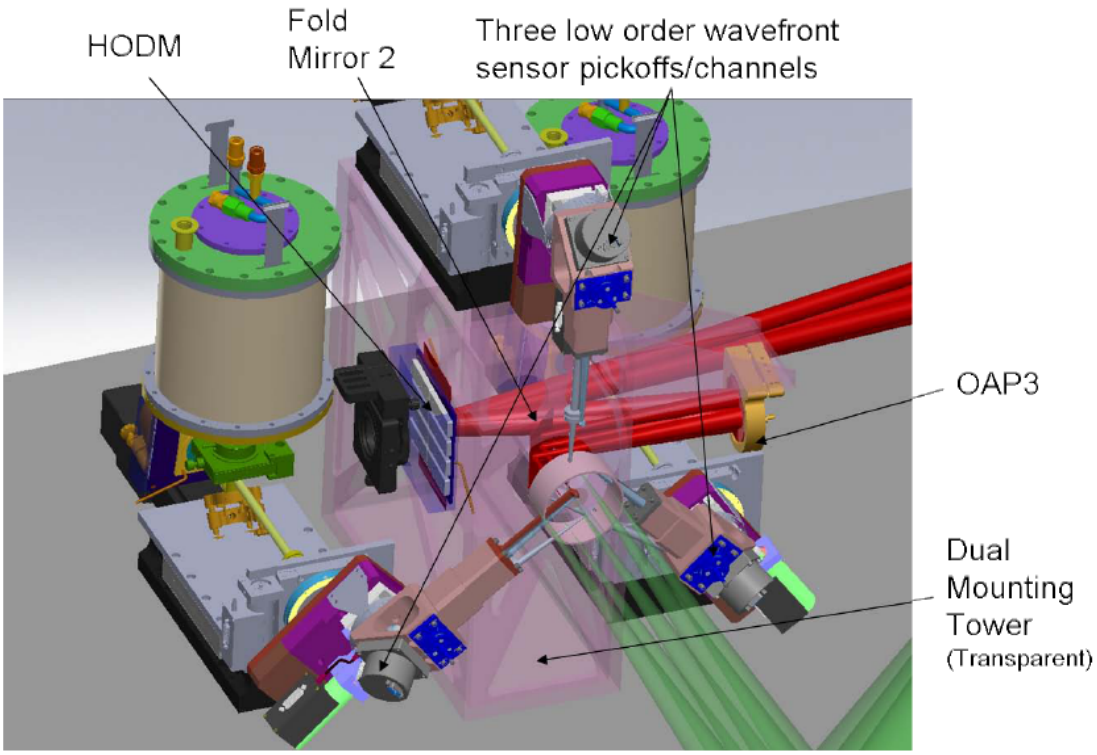

Figure 16: Narrow field relay within the surrounding LOWFS assembly

The following is a summary of the design and calculated parameters for the narrow field relay:

- Chosen design parameters.
  - NGS field of view diameter, $\Phi_{NGS,narrow}$ = 40"x60" for NGS WFS and science instruments.
  - OAP3 off-axis angle = 13º.
  - Telescope primary mirror subaperture size, d_{PM2} = 182.48 mm.
  - MEMS angle of incidence, α_{MEMS} = 10º.
  - MEMS conjugate to the telescope primary mirror.
  - MEMS subaperture size, d_{MEMS} = 0.40 mm.
  - f/46.3 output beam
  - OAP4 off-axis angle = 41.9º.
  - Output pupil from narrow field relay at infinity.
- 1st order calculated parameters.
  - OAP focal length, $f_{OAP3} = (d_{MEMS}/d_{PM2})\ f_{Tel}$ = 327.9 mm
  - Required OAP3 diameter to accept the pupil and field, $d_{OAP3} = f_{OAP3}/f/\#_{Tel} + \Phi_{NGS,narrow}$*PS = 67.6 mm.
  - Distance of MEMS from OAP3 in order to be conjugate to the primary, $t_{DM} = f_{OAP3}$.

- Pupil elongation on the DM due to the angle of incidence, % elongation = [1–cos(α_{MEMS})]*100% = 1.5%.
- OAP4 focal length for a (46.3/13.66)x magnification, $f_{OAP4} = 3.39 f_{OAP3} = 1111$ mm.
- Distance of OAP4 from the DM in order to project the pupil to infinity, $t_{OAP4} = f_{OAP4}$.
- Required OAP4 diameter to accept the pupil and field, $d_{OAP4} = f_{OAP4}/f/\# + \Phi_{NGS,narrow}*3.39PS = 172$ mm.

3.3.1.8 Natural Guide Star Wavefront Sensor Feed

The NGS WFS assembly is fed by an insertable dichroic, in collimated space, located 727 mm after the HODM. The dichroic is at an angle of incidence of 30º. A triplet in the collimated beam is used to produce an f/20 beam that is steered by two field steering mirrors into the NGS WFS (see section 3.3.4.2).

3.3.1.9 Narrow Field Science Instrument Feed

Two science instruments can be fed by the narrow field relay as shown in Figure 14. The light reflected by a fold mirror just after OAP4 goes directly to the combined imager and IFU (DAVINCI). This fold can be motorized and tilted to feed a future science instrument.

3.3.1.10 Atmospheric Dispersion Correctors

Two atmospheric dispersion correctors (ADCs), one for the NIR and one for the visible, have been designed for the DAVINCI science instrument. The ADC is removable for science near the zenith or IFS science where higher throughput or lower emissivity is preferred. The design is based on the design of the NIRC2 NIR ADC (KAON 134). Two Amici prism pairs are used as shown in Figure 17. These are counter-rotated to introduce dispersion and co-rotated to keep the dispersion in the zenith direction.

The current design has the visible and NIR ADCs on separate insertion stages. During detailed design we will work on a design simplification that would allow a single, three position stage to be used. Insertion of the NIR ADC into the beam will shift the focus by 10.4 mm. The telescope will therefore need to be refocused to maintain the focus on the science instrument (the LOWFS are also repositioned to compensate for the resultant focal plane shift).

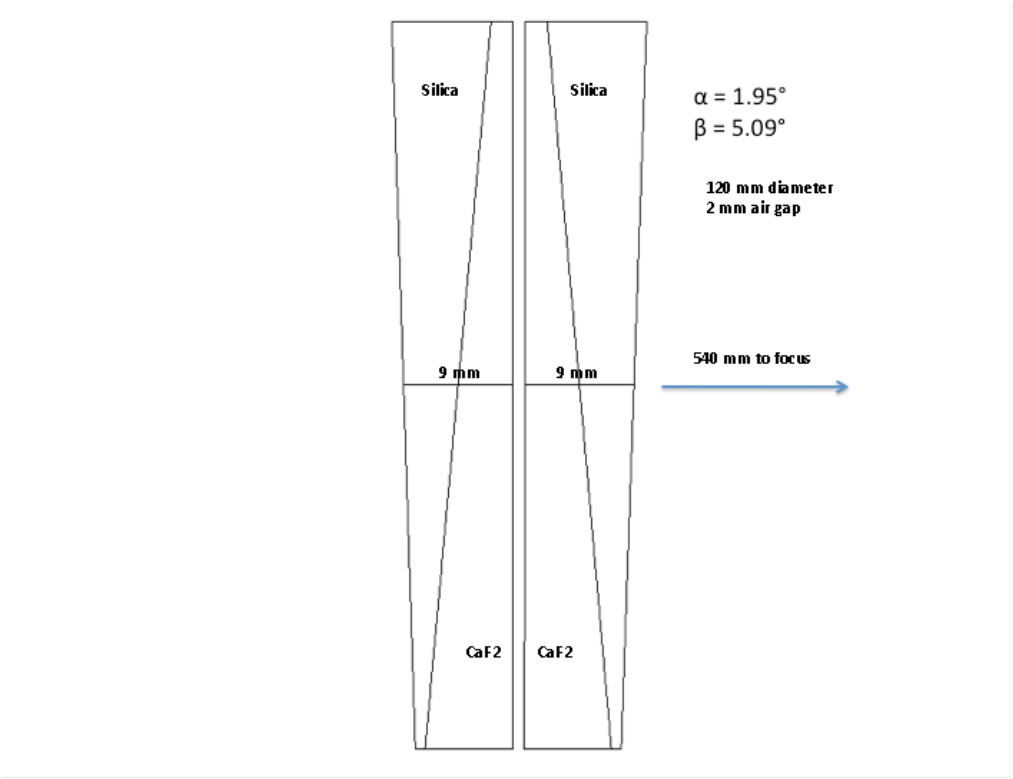

Figure 17: NIR atmospheric dispersion corrector design

3.3.1.11 Summary of Required Dichroics and Mirrors

The above sections only described the location of the required pickoffs. Table 1 provides a summary of the required dichroics and mirrors and their properties.

Table 1: Summary of Required Dichroics and Mirrors

Dichroic or Fold	#	Options	Transmit	Reflect	Notes
Na Dichroic	1	Always in	0.4-L	589 nm	Notch filter ideal. ≥ 600nm an option
Interfer-ometer Fold	1	Out	All	None	
	2	Science reflect	< 1.0 μm	JHKL	
Acquisition Fold	1	Out	All	None	IF dichroic reflects ~470 nm light to the IBM-T camera mounted on the acquisition camera
	2	Mirror	None	All	
	3	IF Dichroic	> 0.5 mm	< 0.5 μm	
NGS WFS Fold	1	Science transmit	~0.92μm-K	0.5-0.9 μm	NGS WFS unlikely for short λ science
	2	Out	All	None	

3.3.1.12 Optics Bench Structure

The AO components described above will be mounted on a typical honeycomb core optical table. The plan-form of the table will be a custom shape to both minimize the volume of the cold enclosure and to provide edges normal to the entry and exit beams. The impacts of thermal contraction and the selection of the table thickness will be performed during detailed design.

Attachment of the optics bench to the Nasmyth platform will be via support legs with a kinematic interface to the bench (as is done for the current Keck AO benches). The optimal location of the cone, V-groove and flat should be determined to minimize the lateral motion of the bench with respect to the science instruments and telescope as the telescope and Nasmyth platform change temperature. Differential focus motion is more acceptable since it has less impact and can be more easily corrected. Assuming the Nasmyth platform behaves isothermally then all points will move radially toward or away from any reference points.

Figure 18 is a top-down view of the AO bench on the Nasmyth platform showing the kinematic cone position below the telescope's optical (i.e., elevation) axis. In theory this means that the bench cone can only move in focus (toward or away from the tertiary mirror). The bench cone is also located below the projected optical axis of DAVINCI.

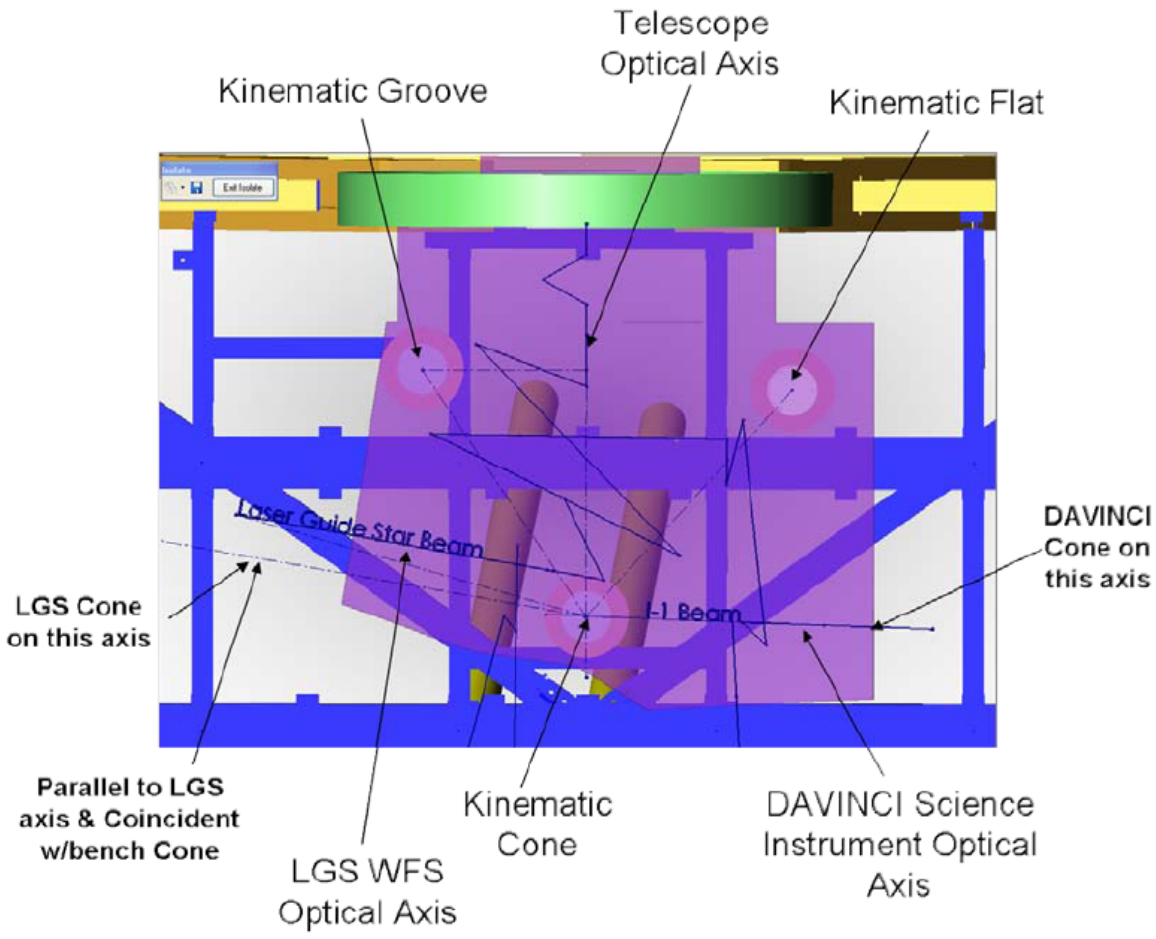

Figure 18: Plan view of AO bench on Nasmyth platform

The elevation ring is shown in green. The Nasmyth platform structure is shown in blue and, where it extends under the AO bench it is shown in purple.

The LGS WFS optical axis intersects the telescope axis before the bench cone. However, its support cone could be placed on the axis parallel to its optical axis and coincident with the bench cone. During the detailed design we will optimize the location of the kinematic points for the various

components that sit on the Nasmyth platform. For perspective, to maintain a 5 μm decenter stability for DAVINCI given a 1500 mm separation between the bench and DAVINCI cones and a 2° C temperature change requires that the misalignment of the DAVINCI optical axis from the direction of the bench cone must be less than 18°.

3.3.2 AO Relay Optical Performance

To determine the performance of the optical system, several sources of optical degradation were analyzed using Zemax in the wavelength passbands used by the individual science instruments and wavefront sensors. The passbands are defined in KAON 530.

The optical relay was modeled in conjunction with the Keck primary and secondary mirrors, to ascertain the combined effects of the two optical systems. Field points used were the maximum off-axis fields defined for each instrument.

According to Zemax, the working f/# of the wide-field relay is f/13.66 and of the narrow-field relay is f/46.3. Airy disk sizes are defined by

$$r_{airy} = 1.22\lambda F/\# \qquad (1)$$

and the depth of focus (DOF) is defined by $DOF = 4\lambda(F/\#)^2$.

Chromatic focal shift and lateral color, where applicable, were evaluated for different wavelength ranges using the Zemax analysis tools. Lateral color and chromatic focal shift arise from the transmissive optics (i.e., windows and beamsplitters).

3.3.2.1 Optical Performance of the LGS WFS Optical Feed

The Keck telescope and first OAP in the wide field relay are both implemented for an object at infinity. To this is added, in the LGS WFS optical feed, a focusing lens designed for a compromise of sodium layer distances. The performance of the LGS WFS feed is summarized in Table 2. The spot diagrams for zenith pointing and a sodium layer at 90 km is shown in Figure 19 over the 120" diameter field. The 727 μm reference bar in the top left of this Figure corresponds to 1.0". The focal plane is both tilted and curved.

Table 2: Performance of the LGS WFS feed

Conjugate height	FOV (arcsec)	Focal plane tilt (°)	Field Curvature (mm)	Grid distortion	RMS WFE, on axis (nm)	RMS WFE, at 60" radius (μ)	RMS Spot Radius, on axis (mas)	RMS Spot Radius , 60" radius, (mas)
90 km	120	4	4000	0.7%	140	1.8	33	253
115 km	120	3	9500	0.7%	140	1.9	33	285
180 km	120	2	>10,000	0.8%	140	2.2	33	323

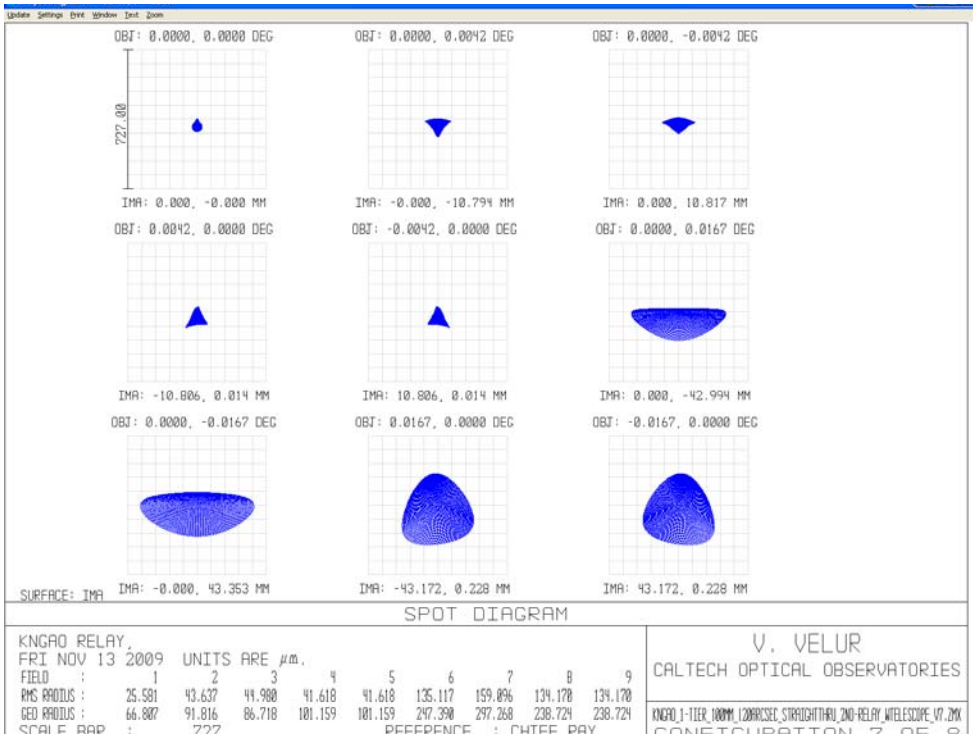

Figure 19: LGS WFS spot diagram for zenith pointing and a 90 km sodium altitude

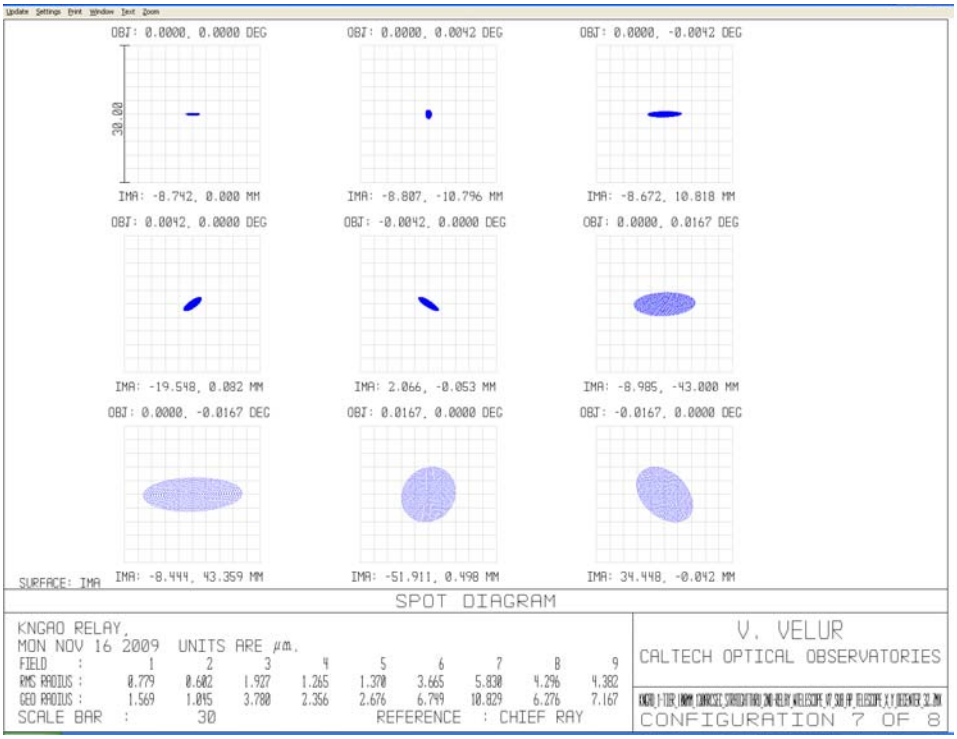

Figure 20: Patrolling LGS WFS spot diagram for a subaperture at the edge of the pupil

Although the entire beam has large aberrations, the degradation in a subaperture is considerably less. For example, for the patrolling LGS WFS which are the only WFS used beyond a field radius of 10",

the performance of a single subaperture (1/31st of the primary mirror) at the edge of the pupil is shown in Figure 20. The spot size radius is < 6 μm rms corresponding to a FWHM of < 20 mas. The worst case centroid shift is 15.5 mas.

3.3.2.2 Optical Performance to the Low Order Wavefront Sensors

Thanks to the matched OAPs, the wide field relay gives diffraction-limited performance over the entire 120" diameter field as seen in Figure 11. Chromatic aberrations are due to the entrance window at the front of the AO relay and the sodium transmissive dichroic. The focal plane has a 1200 mm radius of curvature.

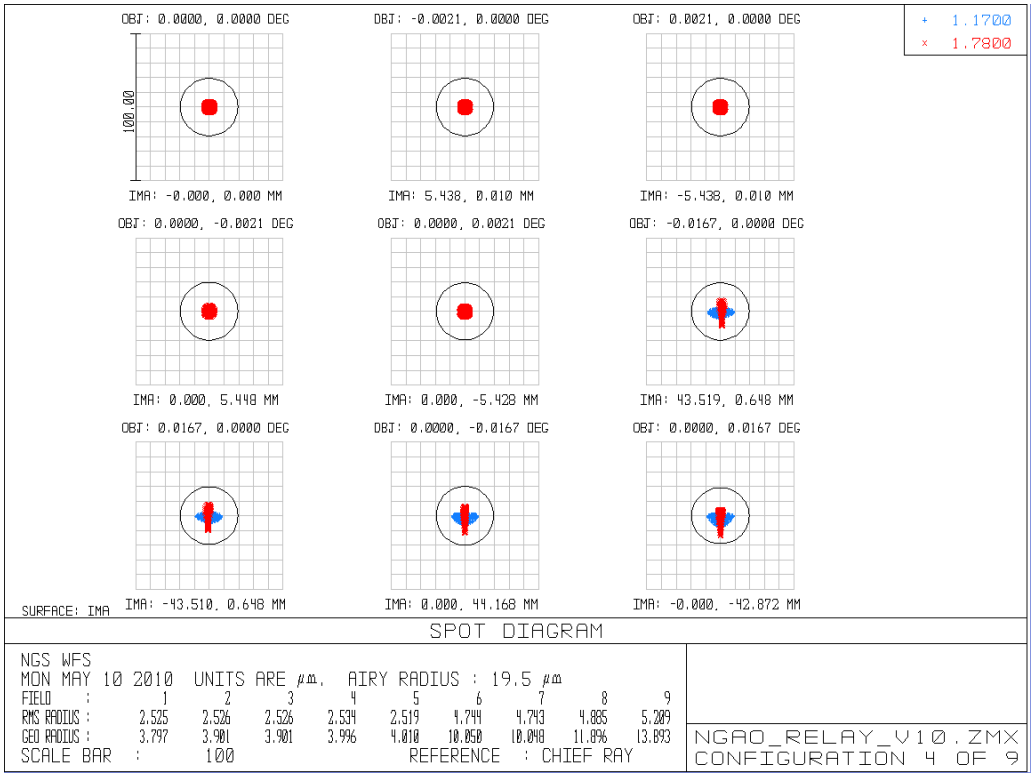

Figure 21: Spot diagrams delivered to the LOWFS focal plane.

3.3.2.3 Narrow Field Relay Optical Performance

The narrow field relay consists of two unmatched OAPs with an output focal ratio of f/46.3, a plate scale of 2.46 mm/arcsec and a focal plane radius of curvature of 220 mm. The narrow field relay performance is summarized in Table 3. The aberrations resulting from the unmatched OAPs are strongly field dependent as shown in Figure 22. The performance is just diffraction-limited at the 20" radius shown.

Table 3: Performance to the narrow field science instruments

Observing band	λ (μ)	Field cur-vature. (mm)	RMS WFE (nm), on axis	RMS WFE (nm), 10" off axis	RMS WFE (nm), 20" off axis	RMS Spot Radius, on axis (mas)	RMS Spot Radius, 10" off axis (mas)	Airy radius (mas)	Chrom. Focal shift (mm)	Depth of focus (mm)
i-band	0.7-0.85	220	29	18	70	10	10	14	1.5	6
z-band	0.85-1.05	220	29	18	70	10	10	17.5	1.5	7
Y-band	0.97-1.07	220	29	18	70	10	10	20	0.7	8
J-band	1.17-1.33	220	29	18	70	10	10	24	1	10
H-band	1.49-1.78	220	29	18	70	10	10	31	2	12
K-band	2.03-2.37	220	29	18	70	10	10	42	3	17

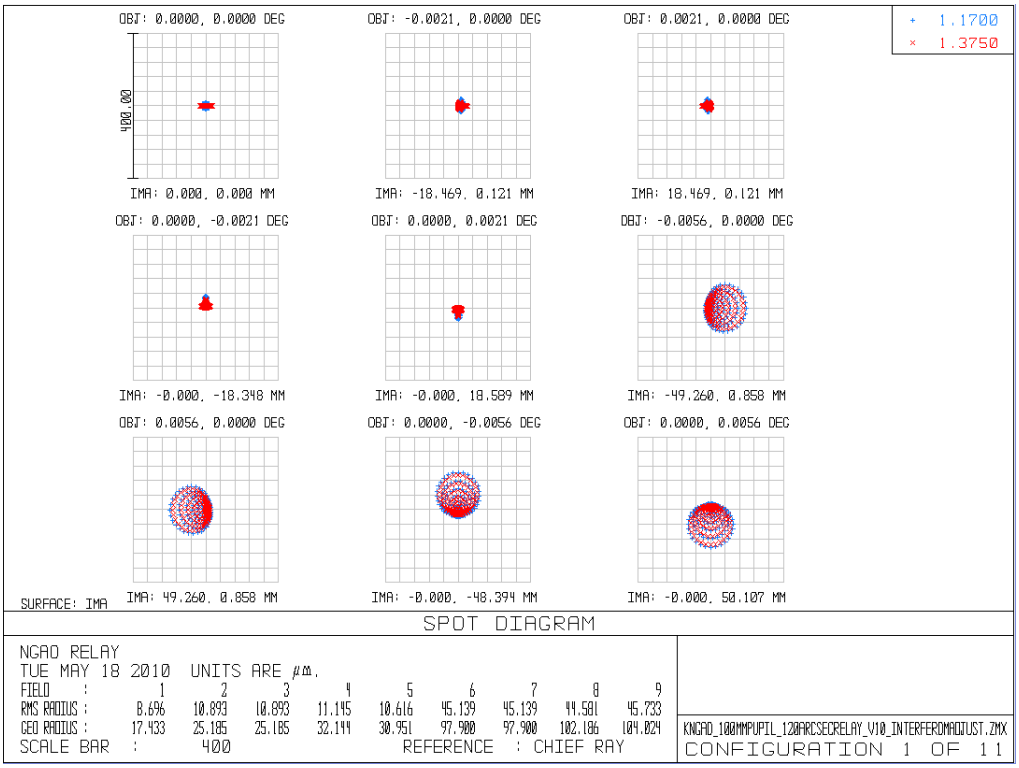

Figure 22: J-band spots at the narrow field relay output focal plane

3.3.2.4 Pupil Distortion

Pupil distortion in the NGAO cascaded relay manifests itself in several ways. The first two of these are evaluated in this section: the degree to which a grid of points on the primary mirror maps to a square grid on the DM on axis and the field dependent pupil aberrations.

Two other factors are: pupil tilt on the DM's (this manifests itself not only as an uncertainty in the conjugate height of the correction, but also in plate scale errors that can degrade the astrometric accuracy) and DM-to-lenslet misregistration and scale errors (these are dependent on the pupil reimaging optics chosen for the wavefront sensors).

In the analysis, the telescope primary became the "object", and field points were defined on the edges of the primary mirror. Observed field angle was set by adjusting the "stop" size placed at the Nasmyth focus to accommodate a 120" diameter field for the LODM, and a 40" diameter field for the HODM in the narrow-field relay. Results are shown in Table 4. Figure 23 provides a geometric spot analysis of the telescope primary mirror mapped onto the LODM (pupil tilt and curvature are included). Figure 24 shows the same things for the HODM.

Table 4: Characteristics of the pupil image on the deformable mirrors

	Diameter (mm)	Field (″)	# actuators	Tilt (meters on sky, peak)	Curvature (mm)	Max Grid Distortion	Pupil PSF, (μ)
DM1, woofer	100	120	20x20	134	3000	0.4%	400
DM2, tweeter	24	40	60x60	366	275	0.5%	81

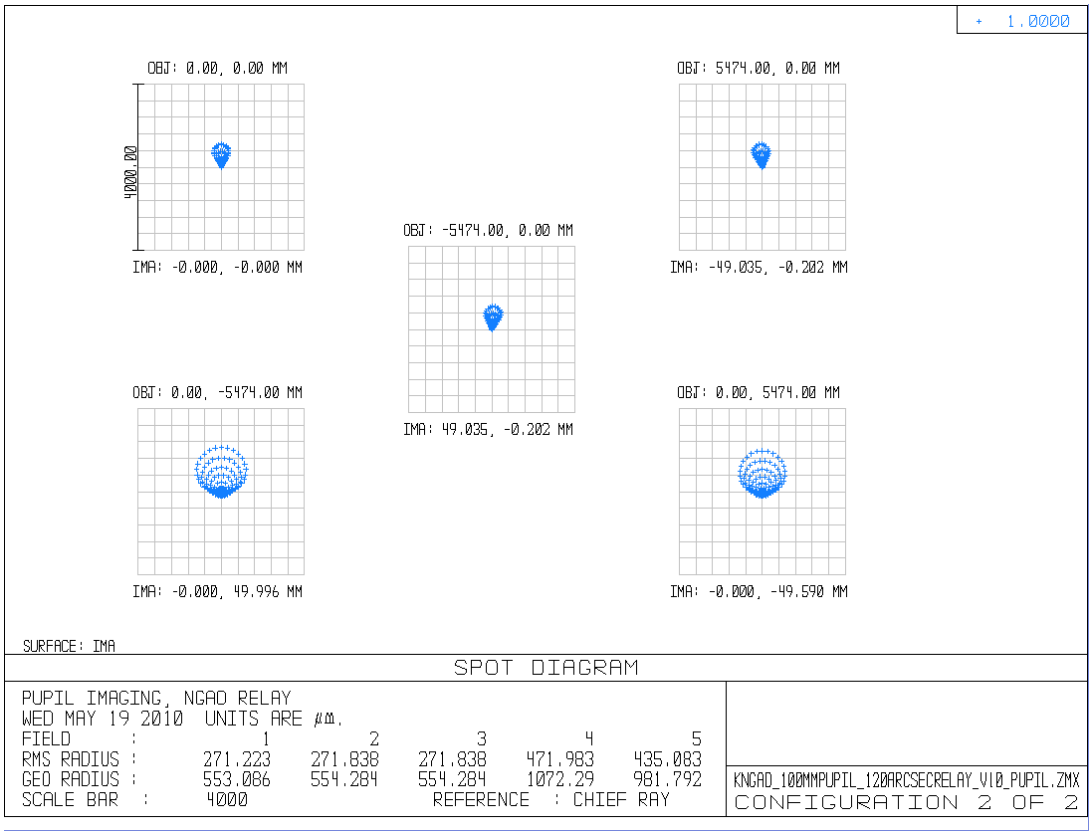

Figure 23: Spot diagrams for 5 locations on the primary mirror imaged onto the LODM
Field considered is 120" diameter. Chief rays from the on-axis field angles make up the point of the comatic pattern, while chief rays for off-axis field angles make up the outer "radius" of comatic points.

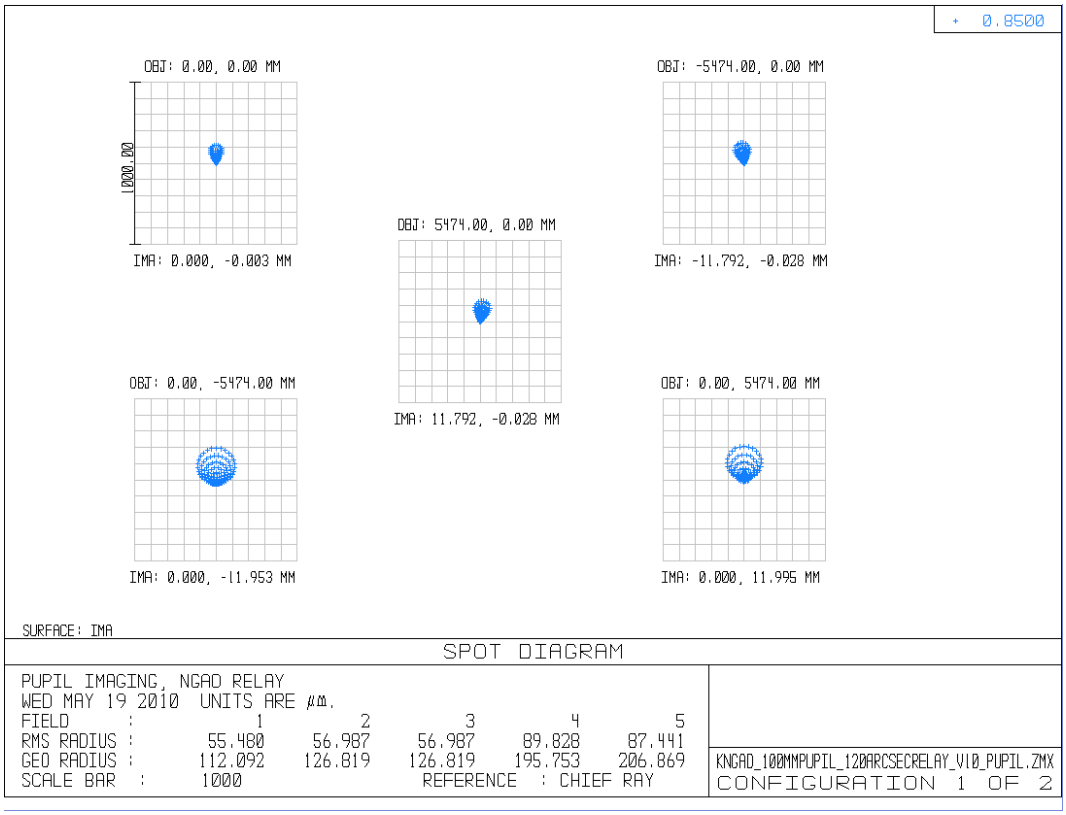

Figure 24: Spot diagrams for 5 locations on the primary mirror imaged onto the HODM

3.3.2.5 Tolerance Analysis

Tolerancing was performed in KAON 685 both analytically and with Zemax. The wide and narrow field relay OAPs in particular were subjected to an analytical tolerance analysis similar to that performed for the existing Keck AO system in KAON 107 for both focal length and off-axis angle errors.

As an example, Table 5 shows the impact on the alignments from a 1% error in the focal length in one or both of the wide field relay OAPs. If OAP1's focal length is 1% larger then the first step is to minimize the impact by shifting OAP1 by 13.7 mm away from the telescope. This collimated beam diameter will therefore be 1% larger. The LODM must then be moved by 13.7 mm to stay conjugate to the telescope primary (which will appear 1% larger on the LODM). The second OAP needs to maintain its nominal distance from the LODM in order to produce a telecentric output. The final output focal ratio will be reduced by 1%.

Table 5: Impact of a 1% OAP focal length error for the wide field relay

OAP with error	OAP1 and 2	OAP1 only	OAP2 only
Shift in OAP1 (mm)	13.7	13.7	0
Ratio of new to old pupil size at DM	1.01	1.01	1
Shift in DM distance from OAP1 (mm)	13.7	13.7	0
Shift in OAP2 from DM (mm)	13.7	0	13.7

Ratio of output focal ratio to telescope's	1	0.99	1.01

A preliminary tolerance analysis was also performed with the Zemax EE tolerancing tool, for both mounting and manufacturing errors, using the rms wavefront error merit criteria. Once reasonable tolerances are determined using the sensitivity analysis a Monte Carlo analysis simulates the simultaneous impact of all the tolerance perturbations.

Assembly tolerances resulting in acceptable performance for the NGAO relays are listed in Table 6. These tolerances are typical of standard assembly methods. Thickness tolerances were applied to distances between optical elements, decentration was applied to OAPs, and tilt tolerances were applied to every optical element, including the OAPs, the DMs, the fold mirrors, and the dichroic beamsplitters. The tilt and decenter of the K-mirror's individual mirrors, and the K-mirror unit as a whole, were included for completeness.

Table 6: Mechanical tolerance values used in Zemax

Parameter	Value	Units
Thickness (TTHI)	±0.200	mm
Decentration (TEDX/Y)	±0.100	mm
Element Tilt (TETX/Y)	±0.004	degrees

Table 7 summarizes the worst offenders that had an appreciable effect on the RMS wavefront error. The sensitivity analysis indicates that the worst offenders are tilt errors in the LODM and OAP mounts. However, a tilt of 14.2" at OAP1 results in less than 1 nm of additional rms wavefront error.

Table 7: Worst offenders from the mechanical tolerance analysis
See Table 6 for parameter definitions.

Tolerance	Value (degrees tilt)	Criterion (RMS WFE, nm, nominal 18.8)
TETY 19, woofer	0.004	22.1
TETY 19, woofer	-0.004	22.1
TETY 16, OAP1	-0.004	19.7
TETY 16, OAP1	0.004	19.7
TETY 27, OAP2	-0.004	19.7
TETY 27, OAP2	0.004	19.7

A Monte Carlo analysis of mounting errors leads to a similar conclusion. The nominal RMS wavefront error due to static aberrations for a perfectly aligned system is 18.8 nm. For the tolerances listed in Table 6, a 2401 iteration Monte Carlo analysis predicts that 90% of the configurations will have less than 23.7 nm RMS wavefront error. This includes contributions from tilt error in the LODM mount (which in practice will be mitigated by its attachment to the tip/tilt stage).

A boresight analysis was also performed to ensure that mechanical tilts and decenters resulted in movement on the camera of much less than a tenth of a pixel.

Manufacturing tolerances, to be specified to the vendors, were considered separately. Table 8 details the manufacturing tolerances used in the Zemax analysis. The OAP radius of curvature was assigned a tolerance of 0.5% of the radius, as given by Space Optics Research Labs (SORL) as a standard tolerance. The flatness of dichroics and folds was assumed to be within 0.200 fringes, as measured in a double pass Newton's rings type test. The off-axis angles (OAA) of the OAPs were given tolerances of 0.125", again as specified by SORL. The figure errors for the OAPs were considered with an analytic approximation outside of Zemax.

Table 8: Manufacturing Tolerances

Parameter	Value	Units
Radius (TRAD)	0.5%	Unitless
Flatness (TFRN)	±0.200	Fringes
Off-axis angle (TPAR)	$\pm 3.5 \times 10^{-5}$	Degrees

Table 9 summarizes the worst offenders that made an appreciable effect on the rms wavefront error. If distance from Nasmyth focus to OAP1 had been allowed as a compensator (in effect, adjusting the position of the OAP to ensure that the optic produces a collimated beam as discussed earlier) the criterion change is negligible.

Table 9: Worst offenders from the manufacturing tolerances analysis
See Table 8 for parameter definitions.

Tolerance	Value	Criterion (RMS WFE, waves, nominal 18.8)
TRAD 16, OAP1	6.8 mm	0.0221
TRAD 16, OAP1	-6.8 mm	0.0204
TRAD 34, OAP3	-1.75 mm	0.0189

A Monte Carlo simulation of manufacturing tolerances shows that these tolerances, like those adopted for mechanical mounting, are acceptable in terms of degradation to image quality. The 256 iteration Monte Carlo predicts that 90% of configurations will produce less that 20.5nm RMS wavefront error.

3.3.3 Deformable Mirrors and Tip-Tilt Correctors

The NGAO system has a total of five deformable mirrors, one high speed tip-tilt platform and 10 high-speed tip/tilt mirrors. A traditional piezo-electric tranducer low order ("woofer") deformable mirror is mounted on a high-speed tip/tilt stage and located at a pupil in the wide field relay, optically ahead of all the other DMs in the system. The other DMs ("tweeters") are also located at pupil conjugates and provide correction in a) the on-axis science path and in b) the three tip-tilt NGS directions. All the tweeters are micro-electromechanical systems (MEMS) devices. These are small electro-statically actuated devices built using a silicon wafer fabrication process.

3.3.3.1 Low Order DM and Tip/Tilt Stage

The most promising selection for a woofer mirror is a Cilas SAM ("Stacked Actuator Module") series piezo-electrically actuated device with glass continuous face sheet mirror. Cilas has successfully

developed 10-micron stroke DMs with 5 mm inter-actuator spacing, allowing for 300+ degrees of freedom of wavefront control in the NGAO first relay. The small spacing has a key advantage in keeping the size and weight of the overall device low so that it is feasible to mount it on a high-speed tip/tilt stage, which is also supplied by Cilas.

Cilas has delivered a "SAM 416" mirror to the Gemini Observatory to use as the 4.5 km conjugate DM in the GEMS AO system. This device is the closest to NGAO specifications and is bracketed by other delivered DMs in both actuator count and actuator spacing. The SAM 416 has not been engineered for a tip/tilt stage mount. However Cilas has mounted a SAM 100 actuator DM on a tip/tilt stage for the Gemini Planet Imager (GPI) and plans to mount a 3000 actuator DM on a tip/tilt stage for the TMT NFIRAOS system. Discussions with company technical representatives have provided assurance that a tip/tilt stage having a >100 Hz bandwidth can be engineered for the SAM 416.

3.3.3.2 MEMS DMs

MEMS deformable mirrors are relatively new technology to the astronomical community but have been proven capable in a number of on-sky experimental systems. The Boston Micromachines Corporation (BMC) has developed large-actuator count devices and sells them off-the-shelf in 140-actuator ("Multi-DM") and 1020-actuator ("Kilo-DM") packages. The Kilo-DMs meet the NGAO needs for the adaptively corrected LOWFS tip/tilt stars. The 4092-actuator device called for in the NGAO design (providing 2827 actuators inscribed in the 60x60 NGAO aperture) is now currently under development by BMC under contract to the GPI project. The high-contrast needs of GPI have put extraordinary demands on the yield performance of the silicon foundry fabricating the devices. While they are yet to produce a 4K device with 100% working actuators, they have fabricated several 4K devices with over 99% working actuators. Our calculations show that, while this might be unacceptable for planet detection at $>10^{-6}$ contrast, it is perfectly suitable for general purpose high Strehl application; the loss of 1% of the actuators is equivalent to 1% Strehl loss, well within the error budget tolerance of NGAO. In other words, the NGAO MEMS DM's are all already available.

The BMC devices are driven by 200-Volt multi-channel D/A electronics through megarray flex cables. 16 of these 256-channel driver cards are needed for the 4K device, and 4 cards are needed for each of the 3 LOWFS DMs. The cards are manufactured by Cambridge Innovations, being built around the 14-bit Supertex HV256 chip.

3.3.3.3 Tip-Tilt Mirrors

The precision and usability of piezo-actuated tip-tilt mirrors have improved greatly during the years of AO development. The tip-tilt mirrors produced by Physik Instrumente (PI) are precise go-to devices with strain gauge position feedback. The three tip-tilt mirrors in the LOWFS will be running in a local closed loop with the LOWFS sensors, so each LOWFS measurement of tip-tilt is actually derived from the position of the mirror. The 4.7" (on-sky) dynamic range of the PI S330.8, with 0.2 milli-radian precision, is more than adequate for meeting NGAO functional requirements and error budgets.

Seven additional tip-tilt mirrors are needed for each of the LGS WFS. These provide high-speed closed-loop re-centering of the LGS on the Hartmann sensor in order to improve the linear dynamic

range of these sensors. The LGS tip-tilt information is not further useful for AO reconstruction and is therefore discarded for use other than in these local tip-tilt loops.

The tip-tilt piezos require high-voltage drives which are available in 2-channel and multi-channel modules. Strain-gauge feedback control is provided with these units. PI has provided NGAO with a quotation for a complete turn-key 10 tip/tilt mirror system.

3.3.4 Wavefront Sensor Opto-Mechanical Design

Two wavefront sensor (WFS) assemblies are fed by the wide field optical relay: the LGS WFS assembly and the low-order WFS (LOWFS) assembly. The NGS WFS assembly is fed by the narrow-field relay. Each of these assemblies includes an object selection mechanism (OSM) that selects the appropriate NGS or LGS and feeds the light to the appropriate wavefront sensor(s). Two versions of the same multi-target mechanism have been chosen for the LGS WFS and LOWFS object selection mechanisms, while a different single-object selection approach has been taken for the NGS WFS assembly as described in section 3.3.4.2. The LGS WFS assembly includes a total of seven LGS wavefront sensors. The NGS WFS is a single WFS with three modes: high order WFS, low order (TT + truth wavefront sensing) and pupil imaging. The LOWFS assembly includes two NIR tip-tilt (TT) sensors, a NIR tip-tilt-focus-astigmatism (TTFA) sensor and a visible truth wavefront sensor (TWFS). The design reports for the multi-target OSM and the LGS WFS can be found in KAON 692. The LOWFS design report can be found in KAON 730 and the NGS WFS design in KAON 729.

We begin this section by discussing the LGS and NGS WFS assemblies followed by a description of the WFS CCD camera. The two varieties of LOWFS (TT and TTFA) are then discussed followed by a description of the NIR sensor used for these LOWFS. We close this section with a description of the truth wavefront sensor that is co-mounted with the TTFA.

3.3.4.1 LGS Wavefront Sensor Assembly

3.3.4.1.1 LGS WFS Optical Design

The LGS WFS opto-mechanical design is documented in KAON 692. The LGS WFS assembly consists of four fixed LGS WFS and three patrolling LGS WFS to acquire the laser asterism shown in Figure 1. Two of the fixed LGS WFS and one patrolling LGS WFS are shown schematically in Figure 25. The optical feed to the LGS WFS, schematically represented at the top of Figure 25 and described in sections 3.3.1.4 and 3.3.2.1, consists of a sodium reflective dichroic in collimated light after the LODM, a fold mirror, a focusing lens and a window sealing the AO bench cold enclosure.

All of the LGS WFS have a collimating lens located at its focal length from the (tilted) input focal plane. The central LGS WFS has a fold mirror after the collimator while the off-axis LGS WFS have a fold mirror before the collimator. In all three cases the next optic is a fast tip-tilt mirror that is controlled to drive the average tip-tilt error to zero for each WFS. In the fixed LGS WFS cases the tip-tilt mirror is followed by a focusing lens. The patrolling LGS WFS has two additional fold mirrors, that are part of two (θ,ϕ) rotation stages used to position this sensor in the field, prior to the focusing lens. The patrolling LGS WFS also has two additional fold mirrors after the focusing lens,

one of which is a slow tip-tilt mirror to maintain the LODM-to-lenslet registration as a function of field position.

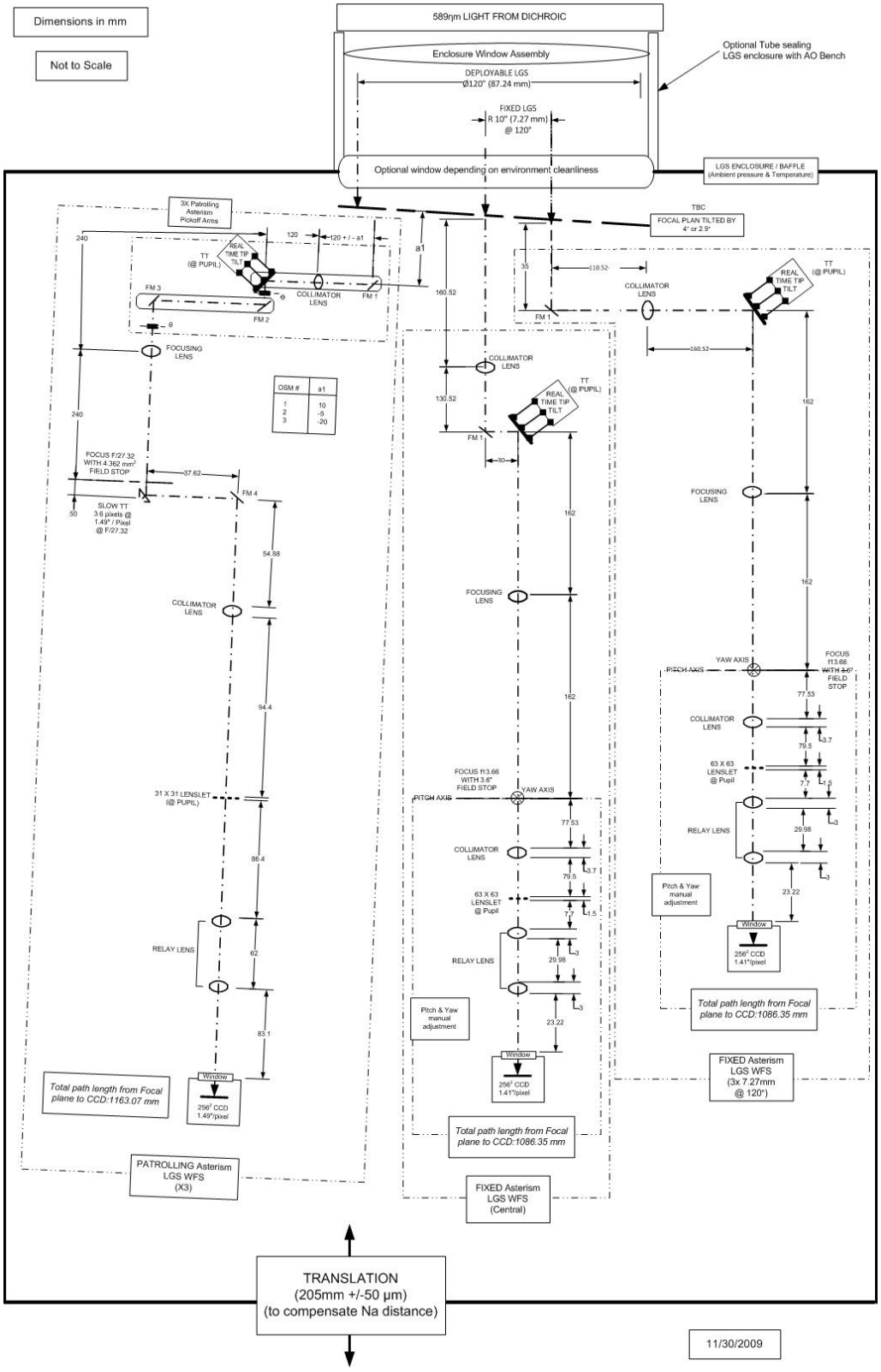

Figure 25: LGS WFS assembly schematic showing two fixed and one patrolling WFS channel

The remaining parts of each LGS WFS are conceptually the same. There is a field stop at the focal plane of the focusing lens followed by a collimator lens that reimages the LODM onto a lenslet array. The focal plane of the lenslet array is then relayed with the desired magnification onto the CCD.

The entire assembly, as illustrated at the bottom of Figure 25, moves in focus to stay conjugate to the sodium layer. The relative focus positions of each LGS WFS will be set as a compromise taking into account the change in focus with off-axis distance for the patrolling LGS WFS and the change in radius of curvature of the focal plane with sodium layer distance. The radius of curvature changes from 883 mm for 90 km to 2064 mm for 180 km corresponding to a change in focus for the patrolling LGS WFS at the edge of the field of 617 μm or 0.52 waves (4 μm for the fixed LGS WFS). This error is deterministic and can be addressed by automatically updating the centroid offsets used by the real-time control system as a function of sodium distance and patrolling LGS WFS off-axis distance.

Figure 26 shows the optical elements of one of the fixed LGS WFS after the field stop. The total length from field stop to CCD is 232 mm. All of these optics are singlets anti-reflection coated for 589 nm. The resultant plate scale is 0.705"/pixel with 4x4 pixels used per subaperture. The custom lenslet, with 63x63 subapertures, is on a 101 μm pitch and the relay optics provide a 0.83 magnification to match the 4x 21 μm pixels. The resultant spot diagrams are shown in Figure 27 with a 1 pixel (21 μm) reference scale. The worst case spot size is 0.90 μm (30 mas) rms radius. The grid distortion of the relay is 0.03%.

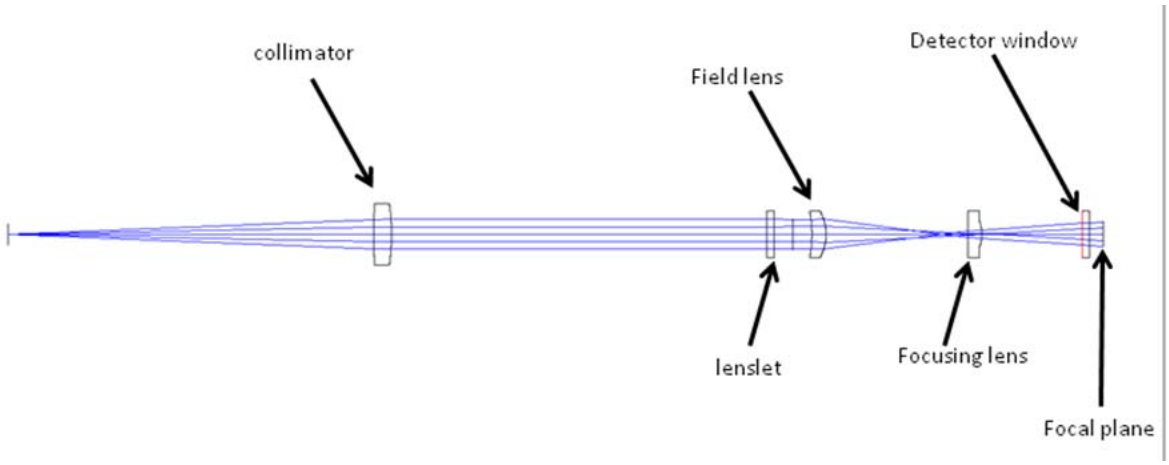

Figure 26: Fixed LGS WFS optics post-field stop

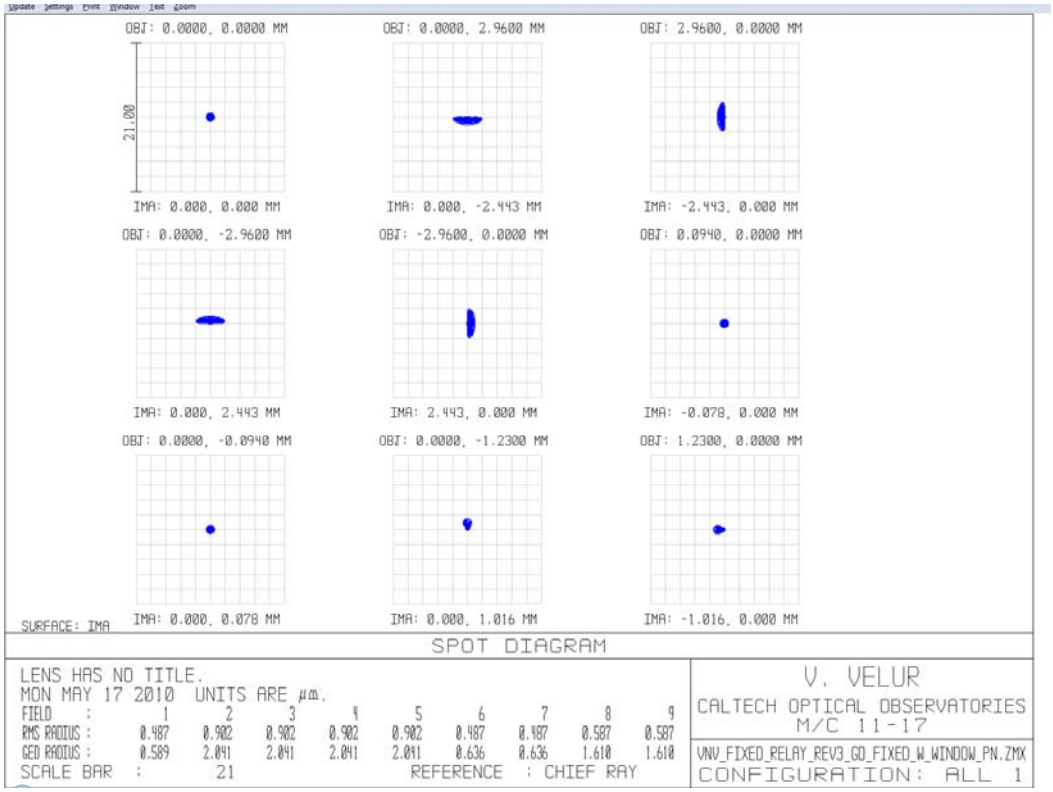

Figure 27: Spot diagram for the central fixed LGS WFS post-lenslet relay

The plate scale for the patrolling LGS WFS is 1.49"/pixel. The custom lenslet, with 31x31 subapertures, is on a 122 μm pitch and the relay optics provide a 0.69 magnification to match the 4x 21 μm pixels. We will look at whether we can make this design more consistent with the fixed LGS WFS design during the detailed design. We will also look at a much more compact and light efficient WFS design involving direct bonding of the lenslet array to the CCD package, as demonstrated at the University of Arizona and briefly explored in KAON 692, during the detailed design.

The LGS WFS error budget is summarized in Table 10. The various contributors to blurring and to shifting the spot in the subaperture at the edge of the pupil are listed along with the overall available allocation. The design to the extent it has been currently evaluated (the tolerance analysis will be performed during the detailed design) easily meets the allocation.

Table 10: LGS WFS error budget

Blurring of Shack-Hartmann spot		
Error source	**Fixed LGS WFS spot size**	**Patrolling LGS WFS spot size**
AO relay	20 mas	20 mas
Focal plane curvature	0	
Object Selection Mechanism	50 mas	50 mas
WFS relay	60 mas	60 mas
Allocation	250 mas	250 mas
Diffraction spot size (for ref.)	666 mas	350 mas

Shift of the worst case sub-aperture		
Error source	**Fixed LGS WFS spot size**	**Patrolling LGS WFS spot size**
AO relay	20 mas	120 mas
Focal plane curvature	22 mas	
Object Selection Mechanism	TBD	TBD
WFS relay	TBD	TBD
Allocation (10% of sub-aperture)	300 mas	600 mas

3.3.4.1.2 LGS WFS Assembly Mechanical Design

The LGS WFS assembly mechanical design is documented as KAON 692. The LGS WFS assembly and its supports which mount directly to the Nasmyth platform are shown in Figure 28. The assembly translates in focus to stay conjugate to the sodium layer as shown in Figure 29; the kinematic mount interfaces to the support legs are also shown in this Figure.

There are a total of seven LGS wavefront sensors as shown in Figure 30. There is a fixed component shown in Figure 31 consisting of three WFS on the vertices of a 10" (14.5 mm) equilateral triangle and one at the triangle's center. And there is a patrolling component consisting of three WFS that can be pointed anywhere in the field of regard in order to sharpen the three TT(FA) stars. One of the fixed off-axis LGS WFS units is shown in Figure 32.

The three patrolling LGS WFS probe arms do not collide during normal operation since they are in different planes, although they are capable of vignetting either a patrolling LGS WFS further downstream or a fixed LGS WFS. A collision hardware prevention mechanism has been designed to ensure that the pick-off arms never collide, even when the software forces the motors to position the probe arms outside of the 120" field. The probe arm and the camera assembly of one of the patrolling LGS WFS units are shown in Figure 33 and Figure 34, respectively. Each patrolling LGS WFS has a 5" (3.64 mm) diameter field of view; the probe tip diameter is 8 mm. The maximum probe tip deflection is 1 μm. The lowest resonant frequency of the probe tip is 236 Hz.

The probe arm is a compact 2-motor device as shown in Figure 33. The 2 degrees of freedom probe arm consists of 2 individual arms: a crank arm and a lever arm, driven by 2 corresponding rotation motors: the crank and lever motors. The crank motor is secured to the main structural plate. It rotates the crank arm, and all hardware attached to it that includes the lever arm and lever arm motor, precisely about the rotation axis of the crank motor (θ rotation). The lever arm motor provides the necessary second degree of freedom by rotating the lever arm and all associated optics (φ rotation). The lengths of the crank and lever arms were chosen to provide full coverage of the field of view. Any position in the LOWFS OSM field of view can be acquired by calculating appropriate values for θ and φ, noting that there are always two possible solutions. A major reason for our selection of the θ, φ approach over an r, θ approach is that the pathlength does not change versus field position.

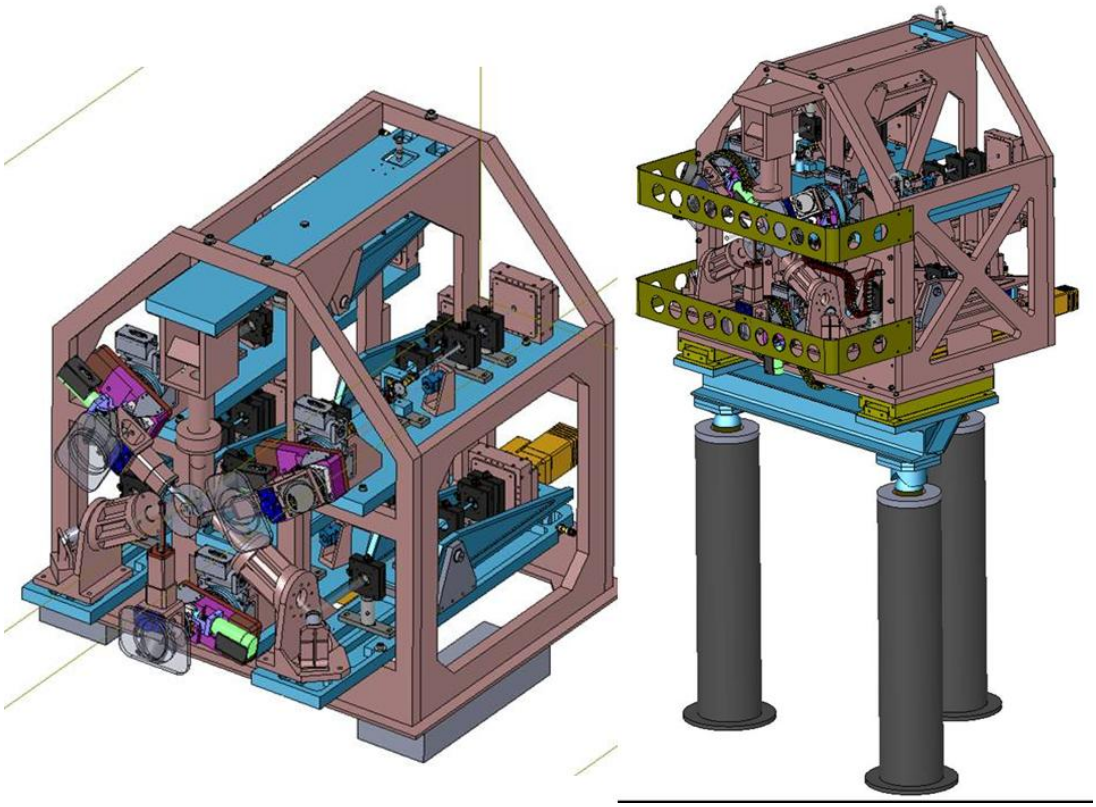

Figure 28: LGS WFS assembly (left) and with support legs to the Nasmyth platform (right)

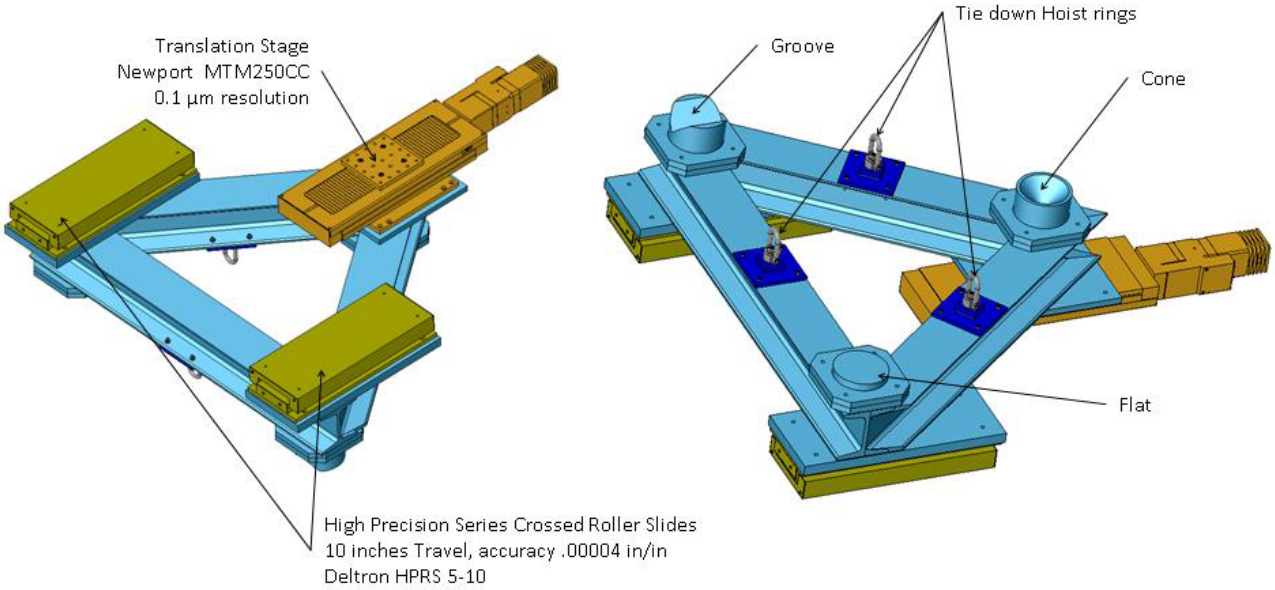

Figure 29: LGS WFS assembly translation mechanism (top view at left) and kinematic mounting mechanism to the support legs (bottom view at right)

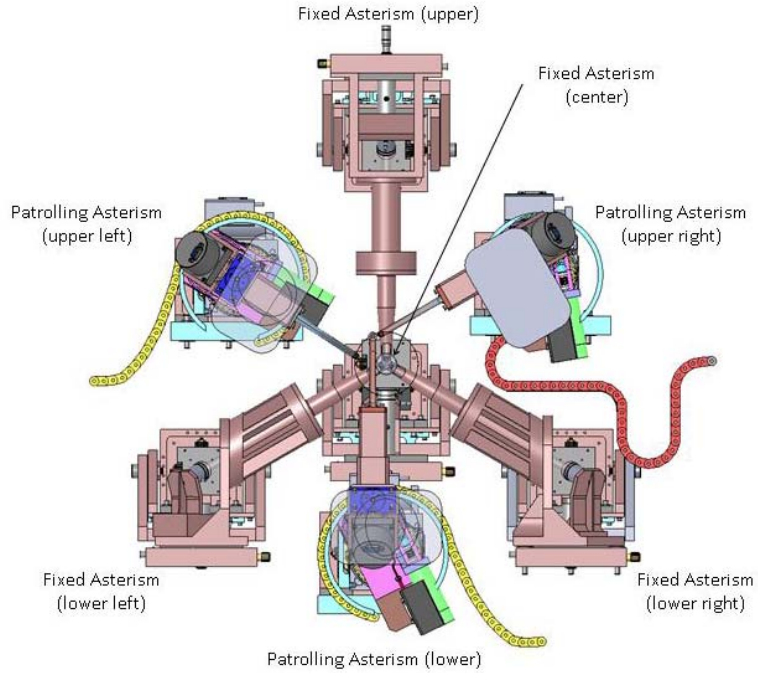

Figure 30: LGS WFS asterism

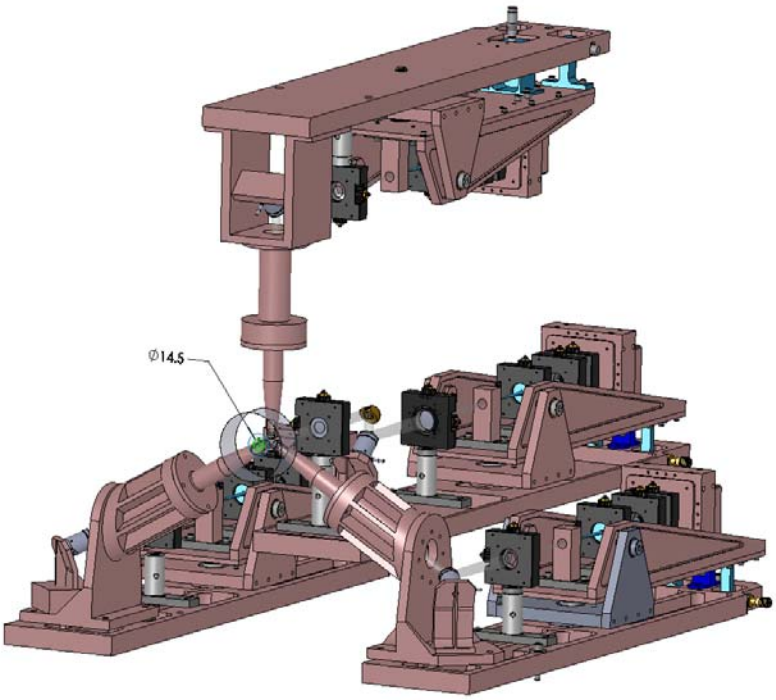

Figure 31: Fixed asterism LGS WFS

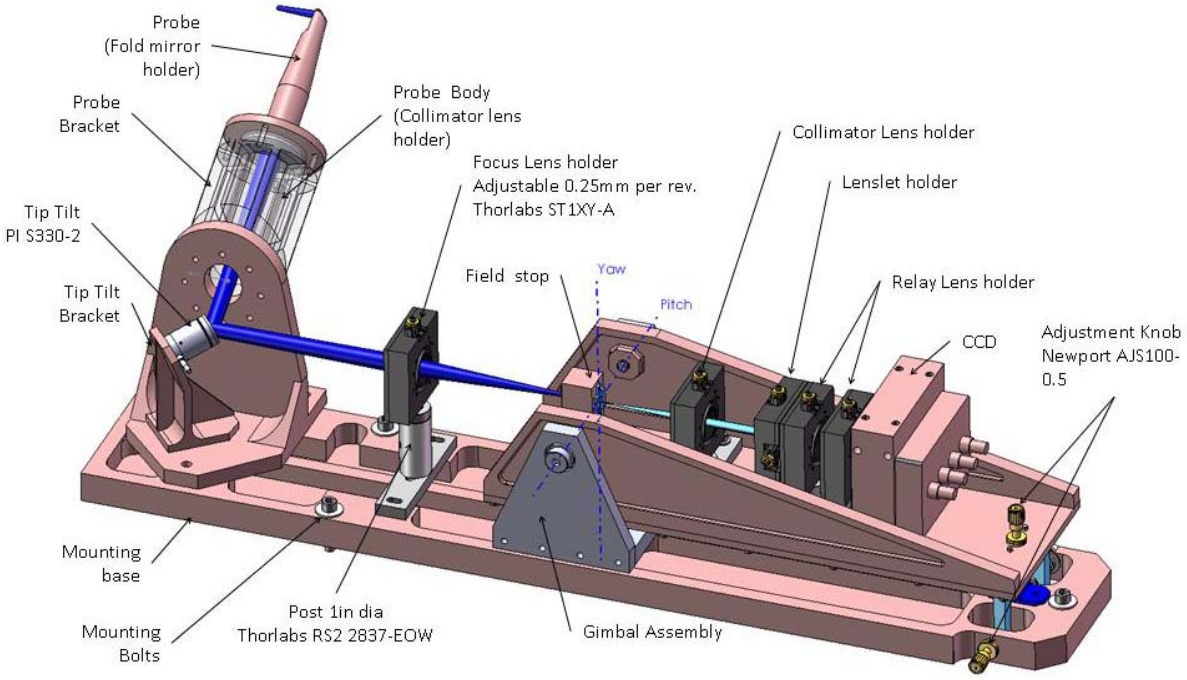

Figure 32: A single off-axis fixed LGS WFS

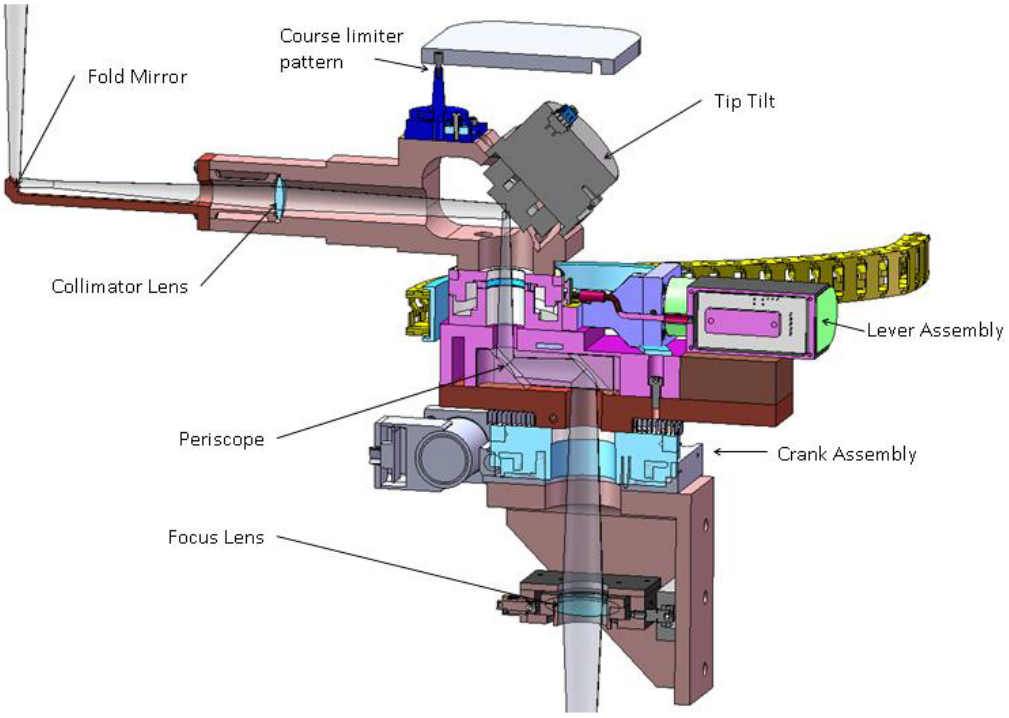

Figure 33: Cross section of patrolling LGS WFS probe (pick-off) arm

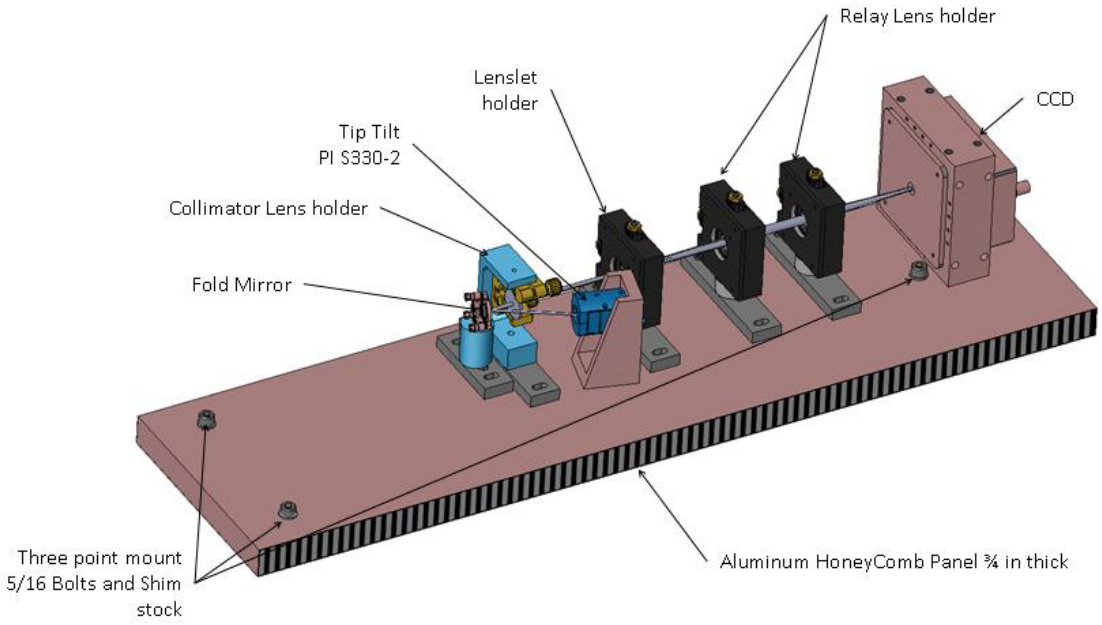

Figure 34: Patrolling LGS WFS camera assembly

3.3.4.2 NGS Wavefront Sensor Assembly

The NGS WFS design is documented in KAON 729. The NGS WFS has multiple roles:

- High spatial order (63x63 subaperture) wavefront sensing for NGS AO science. This mode works with objects as large as 4" diameter (i.e., Uranus).
- High bandwidth tip-tilt sensing and low bandwidth, low order truth wavefront sensing for some LGS AO science (e.g., fixed pupil mode science (KAON 669), interferometer science (KAON 748) and occasional fixed field science where the science target needs to be used for tip-tilt). In this mode the NGS WFS is used with 5x5 subapertures.
- High spatial resolution truth WFS for LGS AO engineering.
- Pupil imaging for alignment purposes (see section 3.3.7.1).

Four pixels are used per sub-aperture which can be binned on chip and read as 2x2 pixels per sub-aperture with almost zero read noise penalty. This provides the flexibility of 2 modes, one with high linearity and another with lower read noise. A build-to-cost design choice was made not to provide an atmospheric dispersion corrector for the NGS WFS.

Although not yet a part of the design we plan to add a lower spatial order NGS AO WFS mode to support interferometer science during the detailed design.

The opto-mechanical layout of the NGS WFS is shown in Figure 35. The light to the NGS WFS is picked off in collimated light with a dichroic as discussed in section 3.3.1.8. A refractive triplet is used to produce a converging ~f/20 beam. The selection of the NGS from within the field is performed with a pair of field steering mirrors.

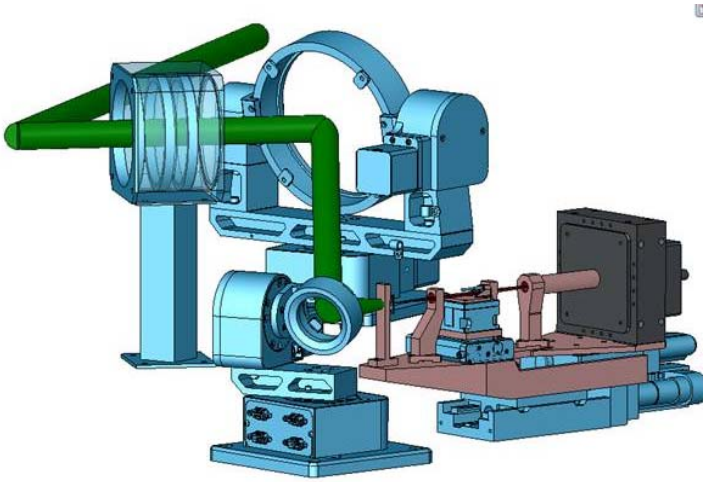

Figure 35: NGS WFS assembly

The NGS WFS camera, shown in more detail in Figure 36, is mounted on a focus translation stage to stay conjugate to the science instrument focal plane. The optical elements are shown in Figure 37. The light passes through a field stop (at left), a collimating doublet to reimage the primary mirror (DM) onto the lenslet array, the lenslet array, relay optics (a field singlet and focusing doublet) that reimage the lenslet focal plane onto the CCD (a magnification of 0.59 which produces a 4 pixel separation for the 63x63 subaperture lenslet), and the window just in front of the CCD (at right). The overall relay length shown in Figure 37 is 269 mm for the 5x5 subaperture lenslet. The lenslet to singlet separation is reduced by 7 mm when going to the 63x63 subaperture lenslet and by another 2 mm when the lenslet is removed for pupil imaging mode. The relay optics and CCD are mounted on a translation stage to allow refocusing for each lenslet.

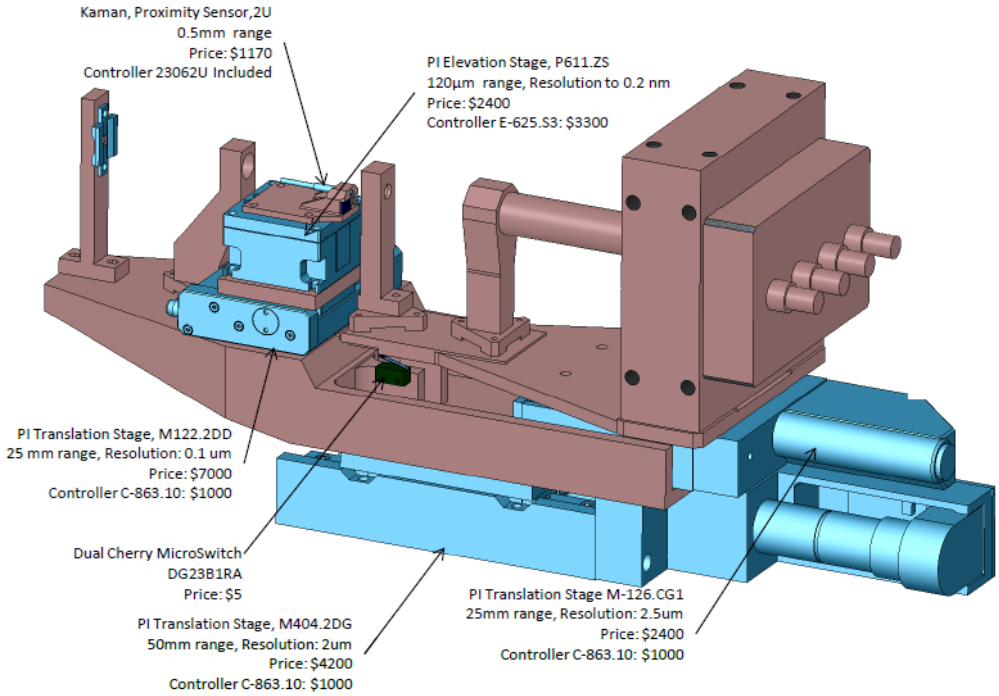

Figure 36: NGS WFS camera

Figure 37: NGS WFS optical elements (field stop at left to CCD at right)

The NGS WFS is designed to use light from 500 to 900 nm. The images produced by the triplet at the input to NGS WFS camera (i.e., the field stop location), where the plate scale is 1.06 mm/arcsec are shown in Figure 38. The worst case spot is 97 μm (0.092") rms radius.

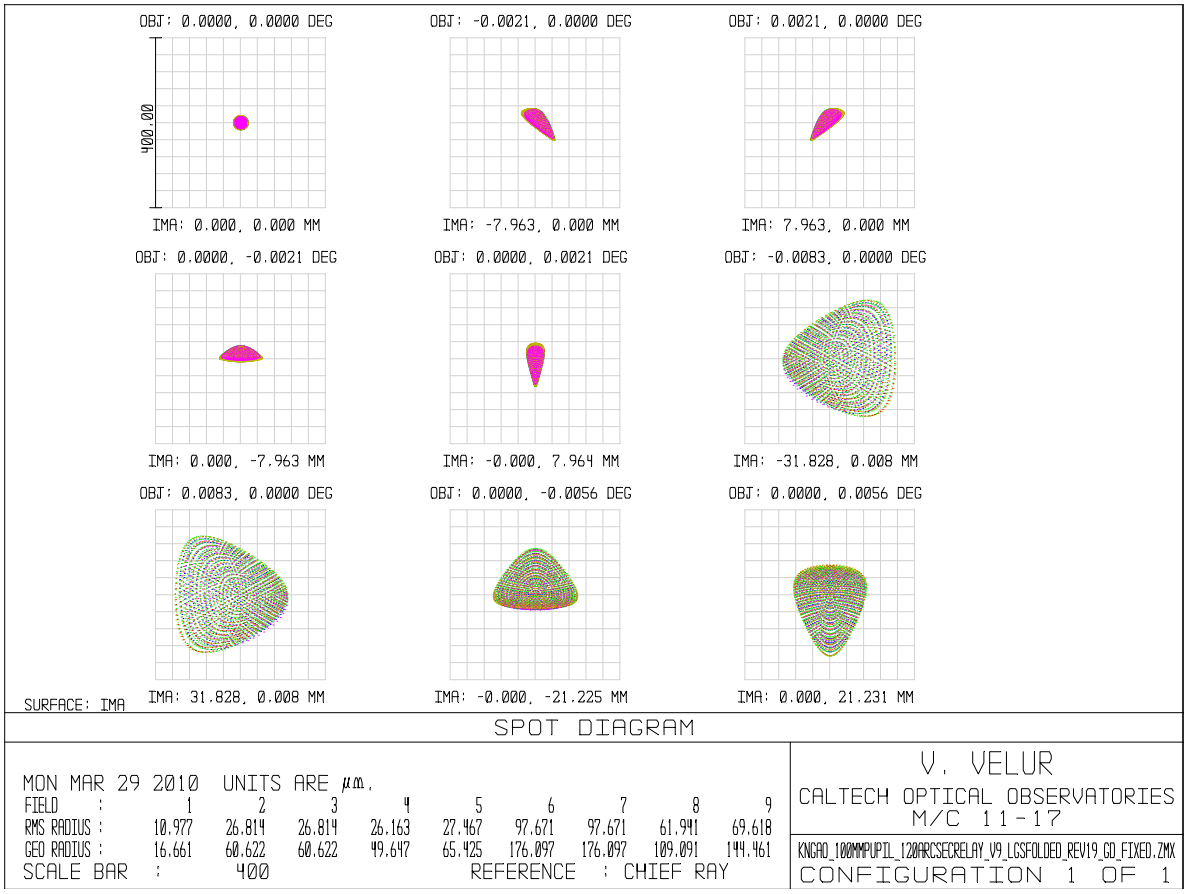

Figure 38: Spot diagrams at the NGS WFS field stop location as delivered by the AO relay

The distortion of mapping HODM actuators to NGS WFS lenslets is <2% at the extreme subapertures. The chromatic effect of imaging the HODM onto the lenslet array is shown in the Figure 39.

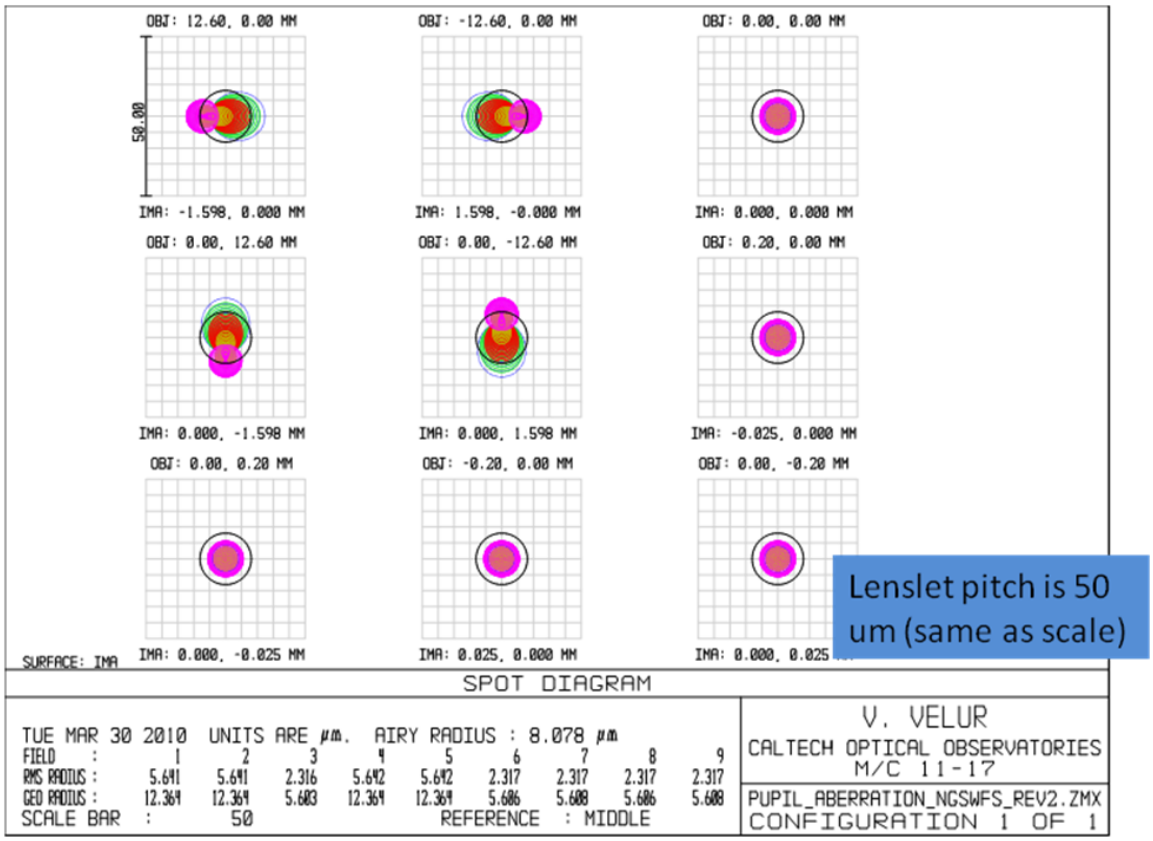

Figure 39: Pupil image spot diagrams at the NGS WFS lenslet for 0.5 to 0.9 µm operation
The 63x63 subaperture lenslet pitch is shown for reference.

The optical relay performance is good. Figure 40 shows the 3 µm (0.33") rms spots generated by the post-lenslet relay. The grid distortion produced by the relay is 0.08% which leads to a worst case grid distortion of 0.1 pixels.

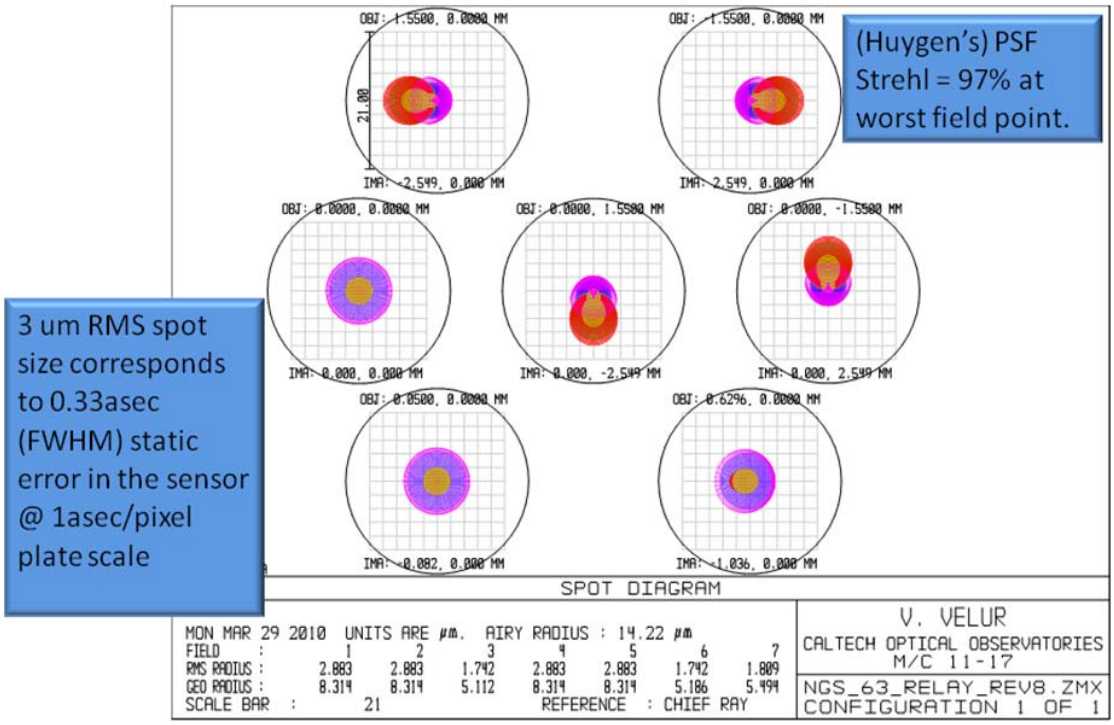

Figure 40: Spot diagrams at the NGS WFS CCD from the post-lenslet relay

3.3.4.3 Wavefront Sensor CCD Detectors and Cameras

A separate WMKO project has been developing low noise, high performance AO imagers in collaboration with the Lincoln Laboratory (see KAON 718). The NGAO baseline is to use the combination of the 256x256 pixel CCID-74 and a proposed 64 channel readout system with focal plane electronics for all of the LGS and NGS WFS cameras. A CCID-74 wafer run is currently in progress at MIT/LL with completion of back illuminated packaged devices expected in October 2010. The readout system is based on the design proposed for the polar coordinate detector wavefront sensor cameras that are the baseline LGS wavefront sensors for the TMT. The TMT is also planning to use the CCID-74 as their NGS wavefront sensor.

The 256 x 256 pixel format is required for the four fixed LGS WFS and the NGS WFS (all of these use 63 x 63 subapertures with 4 x 4 pixels per subaperture). An existing 240 x 240 pixel EM CCD and 60 x 60 subapertures is a potential fallback option although it will have higher noise due to the EM chain as well as potential linearity issues with bright LGS and NGS. The patrolling LGS WFS could also use a smaller format CCDs (such as the CCID-66 in a 31 x 31 subaperture format with 4 x 4 pixel subapertures) with lower performance. Four SciMeasure cameras based on the 160x160 pixel CCID-66 are currently being installed as part of the upgrade to the AO system on the 3.5 m telescope at the Starfire Optical Range 3.5 m telescope AO system. Although it is unlikely that we would need to fall back this far, we could potentially also consider using the same E2V CCD-39 based SciMeasure cameras for the patrolling LGS WFS as we are using with our current Keck AO systems.

The performance predictions for the CCID-74 are based on measurements of the CCID-66 devices. The assumed read noise is 1.7 e- and 2.6 e- rms at a 1 kHz and 2 kHz frame rates, respectively.

The CCID-74 is packaged in a 131 pin hermetic windowed package with a two stage thermoelectric cooler (TEC). The CCID-74 camera and the camera for the polar coordinate detector share a common overall envelope. The polar coordinate detector package will also be a hermetic package with a window and a two stage TEC, but will be larger than the CCID-74 with 286 pins. The detectors are connected to the electronics using zero insertion force sockets that are mounted on a printed circuit board that serves as a motherboard for the focal plane electronics. The hot side of the TEC is cooled by a cold plate in the camera head.

The focal plane electronics are based on two board sets that provide analog and digital processing for 32 channels of video from the CCD. For the CCID-74 a pair of these two board sets would be used to readout the 64 channels of the CCID-74. The higher power dissipation digital board will be cooled by a cold plate with the thermal connection made using thermally conductive foam pads (Bergquist Gap Pad).

Each of the digital boards has a low voltage digital signaling (LVDS) interface connector (~44 pins), and the camera also has a power connector for DC power input, and power to the TEC. Closed loop operation of the TEC is supported by a temperature sensor mounted in the CCID-74 package.

The LVDS connectors and the power connector interface the camera to a 1U high EIA 19 inch rack mounted interface controller module (see KAON 718). The LVDS cables are limited to a maximum length of ~3 m. The interface controller is designed for mounting in a sealed enclosure cooled by a liquid to air heat exchanger.

3.3.4.4 Tip-Tilt (Focus and Astigmatism) Sensors

There are three low order wavefront sensors (LOWFS), two providing fast tip-tilt (TT) measurements and one providing tip-tilt-focus-astigmatism (TTFA). To provide the needed sky coverage each LOWFS contains a MEMS DM that, in combination with a patrolling LGS WFS, provides AO correction to the NGS used by the LOWFS. This improves the availability of suitable stars of sufficient brightness at the near-IR wavelengths used by the LOWFS. Optimal performance is obtained using combined J and H band light. A direct image of the NGS is used for the TT sensors. The TTFA sensor has 2 x 2 subapertures to additionally provide sensing of focus and astigmatism.

Operationally, each sensor drives its own LOWFS tip-tilt mirror in a very low-latency closed loop. The tip-tilt measurement is then read back from the tip-tilt mirror strain gauge (which may be temperature-stabilized, depending on the results of mirror testing planned during DD phase). This approach increases the rejection of tip-tilt anisoplanatism induced differential motion on the LOWFS detectors, allowing smaller region of interest readout and thus lower read noise for a given frame rate. In return, we must have high stability and reliability of the LOWFS tip-tilt mirrors, as their linearity is directly traceable to science path tip-tilt performance. In addition, there is somewhat more complexity for the control system, which must track ‘strain offsets’ in the LOWFS, alongside the more traditional ‘centroid offsets’ used for calibration in the LGS WFS and NGS WFS.

The opto-mechanical design of the TT and TTFA WFS is documented in KAON 730. Two views of the three LOWFS with their object selection mechanisms crossing in the 120" diameter field are shown in Figure 41 and Figure 42.

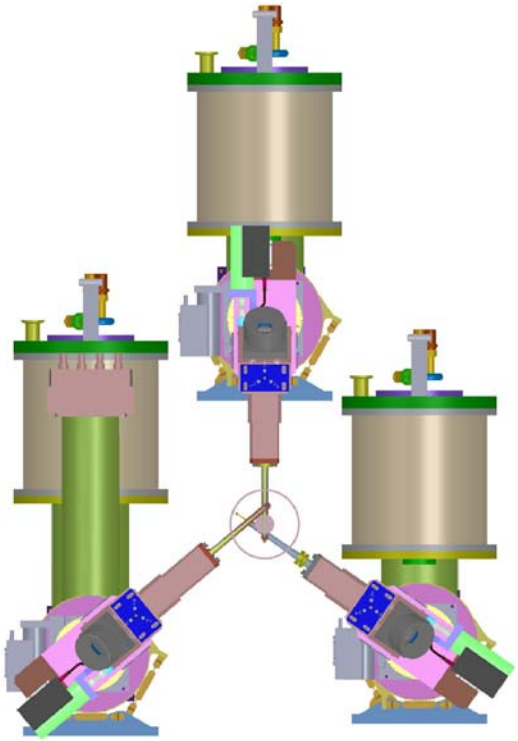

Figure 41: Face on view of the LOWFS assembly
All three probes are shown within the 120" diameter circle drawn in this figure.

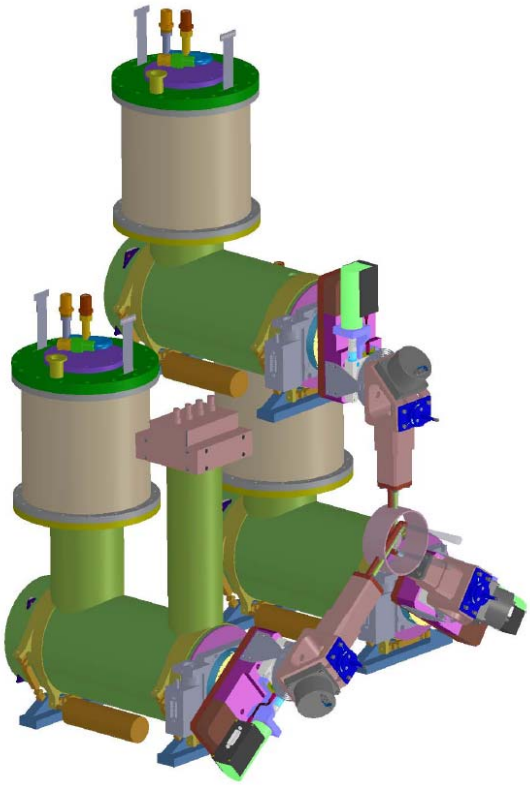

Figure 42: Perspective view of the LOWFS assembly

A cartoon of the LOWF optical system is shown in Figure 43. The elements above the dashed line are part of the object selection mechanism (OSM). The OSM is the same design as used for the patrolling LGS WFS. The elements below the dashed line are specific to the LOWFS. The image plane is produced by the wide field relay. Each LOWFS is mounted on its own focus stage to compensate for field curvature as a function of off-axis distance and to stay conjugate to the science instrument focal plane (which changes as different elements are inserted in the narrow field relay, such as the atmospheric dispersion corrector). Lens 1 in Figure 43 is an air spaced achromat that collimates the light. A tip-tilt mirror at a pupil plane is used to keep the image centered on the LOWFS detector. The light then reflects off the fold mirrors at the center of the OSM lever and crank assemblies before being refocused by lens 4 (there is no lens 3). The telescope pupil is reimaged onto the LOWFS DM with the mapping shown in Figure 44. The beam is folded once more before being imaged onto the IR sensor array.

The optical performance at the TT sensor is shown in Figure 45. The 40 μm scale shown corresponds to 118 mas. The system is diffraction-limited over the field of view.

The optics for the TT and TTFA are identical up through lens 4. Two additional elements, shown in Figure 46, a collimating achromat and a lenslet array are added to provide 2x2 subapertures for the TTFA.

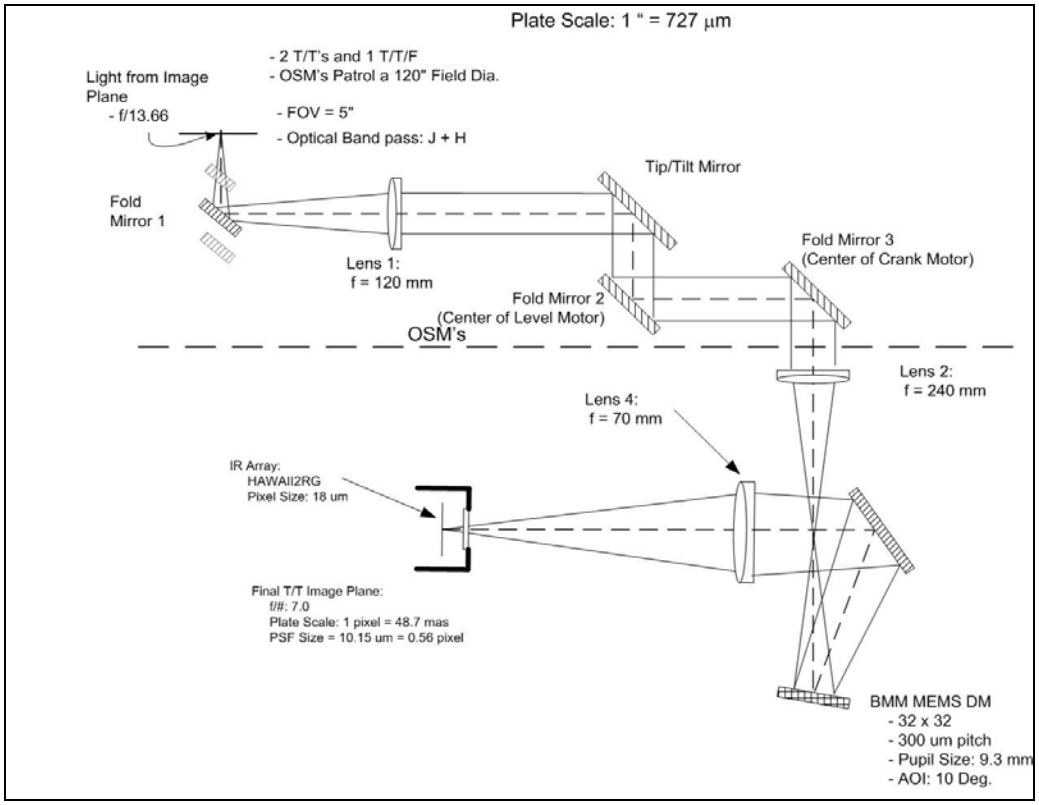

Figure 43: Cartoon of the LOWFS optical system

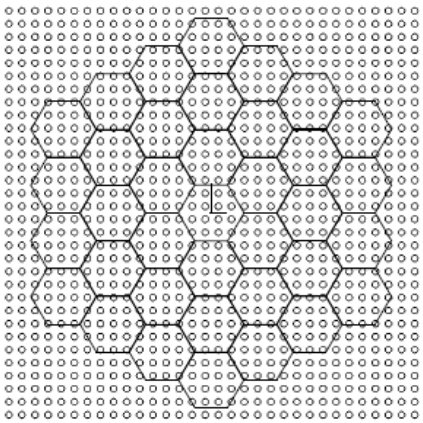

Figure 44: Mapping of Keck primary mirror to a 32x32 actuator LOWFS DM
The (vertical, horizontal) mapping = (346.97, 370.60) mm/subaperture. Keck drawing 1410-CM0010.

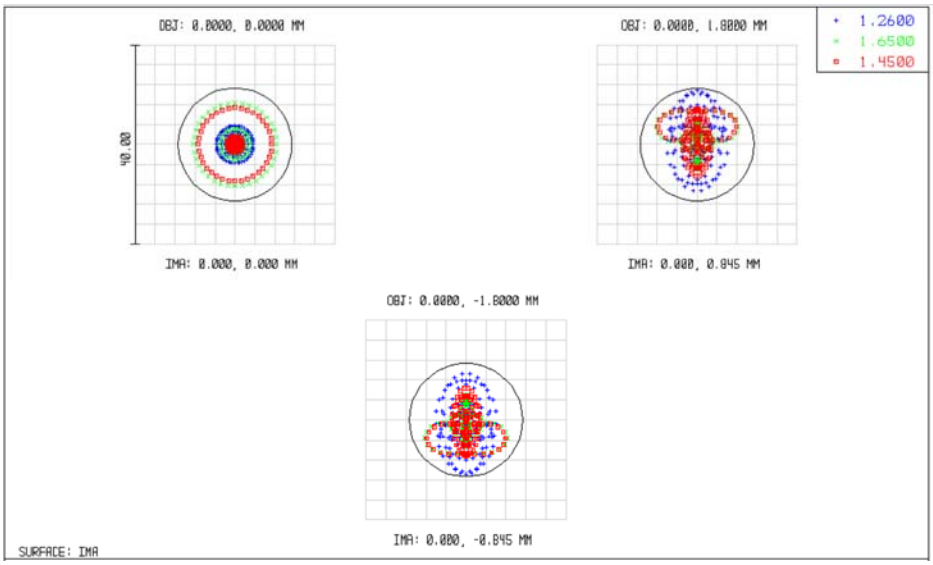

Figure 45: Optical performance of the TT sensor over the 2.5" radius field

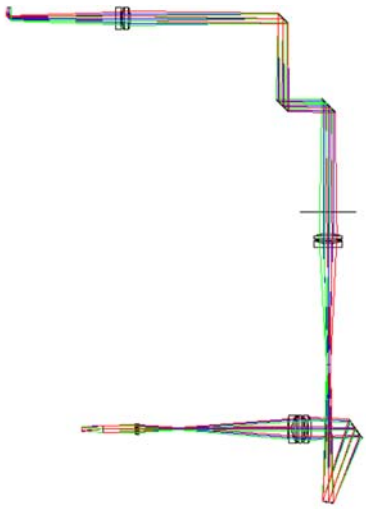

Figure 46: TTFA optical path from wide field relay focal plane (top left) to detector

The mechanical design of a single LOWFS arm is shown in Figure 47. The unit is supported on a focus stage. Commercial mounts are used for the optical components. The MEMS DM mounting will require careful thought during the detailed design.

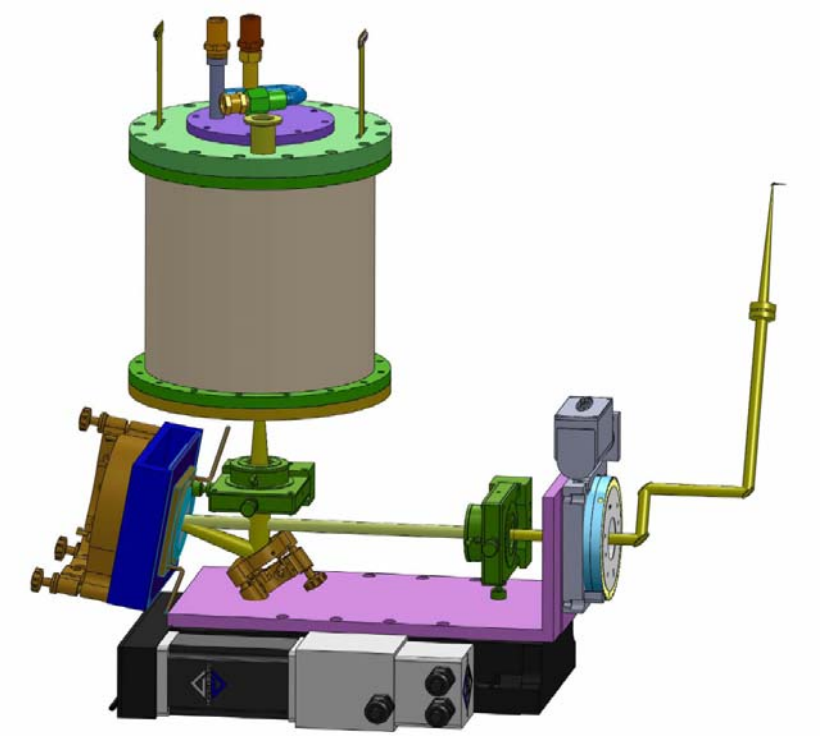

Figure 47: Mechanical design of a single LOWFS
This image shows an earlier concept of the focus stage.

3.3.4.5 LOWFS Cryostat

The opto-mechanics for the LOWFS cryostat is shown in Figure 48. The outer flanges are 8 inches in diameter and the chamber itself is 7 inches in diameter. The cryocooler is a CryoTiger mixed gas Joule-Thompson cooler. All the electronics, not shown, will be mounted externally.

An ion pump will be used to remove residual gas molecules inside the cryostat after initial pump down and gas molecules that permeate the O-ring seals of the cryostat. The vacuum ports of the three cryostats can be connected to a single ion pump using a vacuum manifold. Ion pumps can provide a service life up to 80,000 hours (9 years). An ion pump has no moving parts and will hold vacuum in the event of a power failure.

Mounting locations and containers for traditional charcoal and zeolite getter materials are also planned to be included in the cryostat design. The inclusion of removable getter containers will permit the cryostat to operate in the absence of an ion pump if desired when the getter materials are installed. The charcoal getter shall be mounted such that it can be maintained at the cold temperature.

A rear view of the cryostat is shown in Figure 49. The vacuum port valve is shown as the yellow plug in the outer green ring.

The Teledyne Hawaii 2RG array comes with three and four mounting leg options. We have chosen the three leg option since it is more properly constrained. This array mount is mated to the detector cold plate via three linear blade flexures (shown as the green circular disk) as shown in Figure 50.

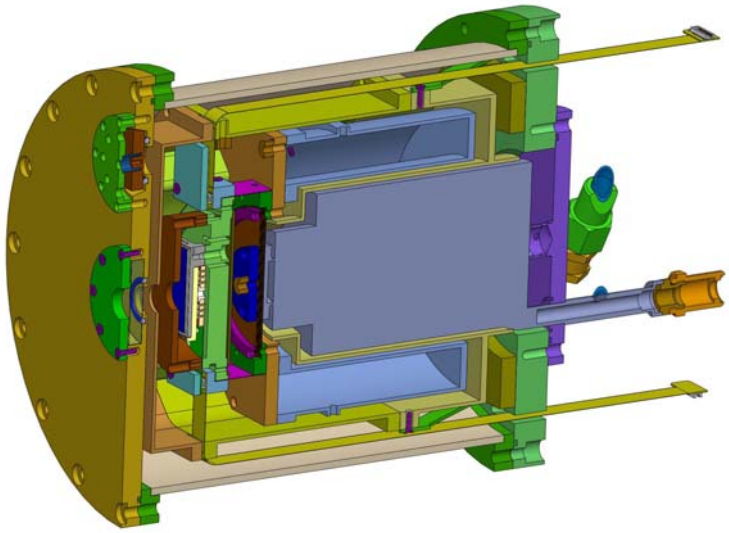

Figure 48: LOWFS cryostat

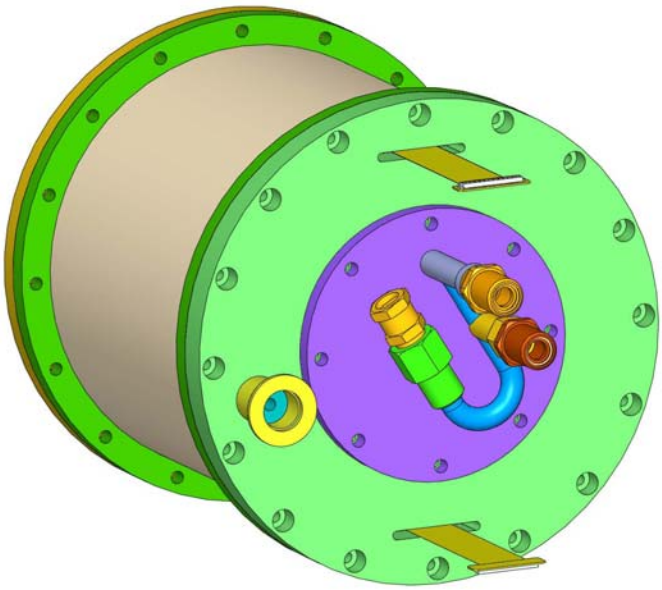

Figure 49: Rear view of LOWFS cryostat

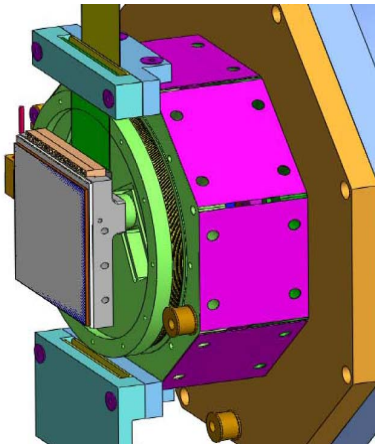

Figure 50: Mechanics for the H2RG array mounting

Thermal loading calculations were performed to determine the required cooling capacity of the cryocooler and its steady state operational temperature. A lumped parameter thermal model was used and the thermal model differential equations were solved using MATLAB. The simulation model that was developed for the dewar took ~10 hours to reach a steady state temperature below 80K assuming 7 W of cooling power. The dewar radiation shields reached their steady state temperature after ~ 40 hours. Once the 80K detector temperature was achieved it took ~2 W of cooling power to maintain temperature in a 258K environment and assuming a maximum detector heat load of 0.25 W.

3.3.4.6 Near-IR Detector

The TT and TTFA each require a small format, low noise and fast readout detector with high quantum efficiency at J and H-bands. We have chosen the Teledyne Hawaii-xRG detectors for their demonstrated performance and in particular the H2RG for its availability.

A H2RG detector was demonstrated to meet our requirements by a team at COO (Smith et al, NIR Detector Design Study for the OIWFS for IRIS on TMT, February 28, 2010). In collaboration with Smith we (PI: Wizinowich) submitted a NSF ATI proposal in November 2009 to implement one of these detectors as a near-IR tip-tilt sensor with the Keck I AO system as a risk reduction for NGAO as well as a significant performance improvement for the existing AO system.

The detector is read out non-destructively in window mode, through a single channel. The window coordinates are updated prior to each window scan by issuing command over a high speed serial line to the H2RG multiplexer taking ~5 µs and allowing the readout of multiple windows at any location during any given exposure. This flexibility can be utilized to accommodate some combination of multiple guide stars (when available with sufficient brightness).

Conventional readout algorithms employing multiple sampling to beat down the read noise suffer a >50% duty cycle penalty at high frame rates. This limitation can be overcome by using the readout mode tested at COO in which the detector is only reset when the integrated signal level approaches saturation as shown in Figure 51, typically every 100 to 1000 exposures for guide stars faint enough to be impacted by read noise. The “exposures” are then synthesized by using the group of samples

representing the end of one exposure as the "zero level" for the next exposure to obtain duty cycles of >99%. When reset becomes necessary there will be a gap in the data stream that will be small compared to the update rate.

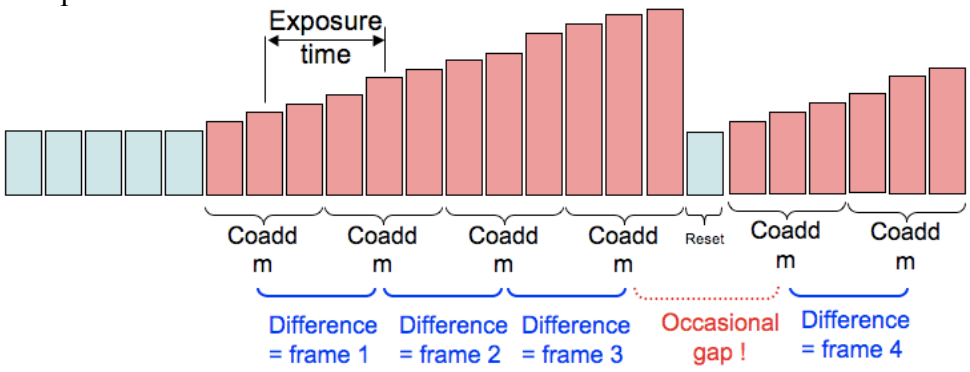

Figure 51: s"Differential Multi-Accumulate" readout mode
The detector is reset only when necessary to avoid saturation to obtain ~100% duty cycle. Non destructive reads are averaged and exposures are synthesized by differencing averaged frames.

For an N pixel square window, the frame scan time, $t_s = 5.16N^2 + 10.32N + 5.28$ µs = 143 µs for a 4x4 pixel window, or 47 µs for a 2x2 window. A representative low noise 2.5 µm cut-off H2RG tested at COO, exhibited the following noise components added in quadrature: 11 e- of white noise, which scales as the square root number of samples per exposure, 0.06 e- of dark noise which scales inversely with the square root number of samples per exposure and a 2.4 e- floor due to 1/f noise. The total noise as a function of exposure rate and number of pixels per frame is shown in Figure 52. The choice of read mode can be adjusted according to the brightness of the guide stars.

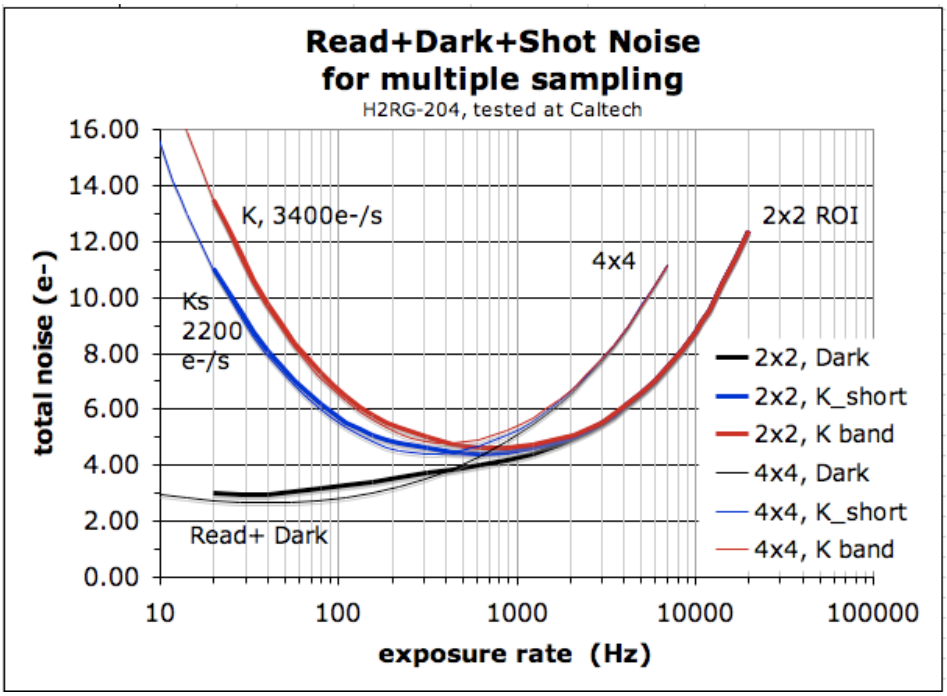

Figure 52: H2RG laboratory noise measurements

After coadding non-destructive reads for a low noise 2.5 µm cutoff H2RG in the dark and with projected background (sky, telescope and AO) noise added.

Full field readout can be used for confirmation of guide star positions, reading out through multiple channels to keep read time down to ~1 second. A larger (~1") region centered on the TT star can be read out at 1 kHz, but elevated read noise (12 e-), to provide initial guiding until the TT loop is closed. As the spot position is stabilized by the TT feedback, the window size will be reduced to 2x2 or 4x4 pixels.

3.3.4.7 Near-IR Detector Electronics

The current electronics design, shown in Figure 53, assumes the array will be read out with a set of Leach electronics (i.e., Astronomical Research Cameras SDSU-III readout electronics) that includes boards for clocks, biases and video. The flex cable from the array is extended through the back of the cryostat to an external interface board. The readout electronics interface to the computer via a communications card.

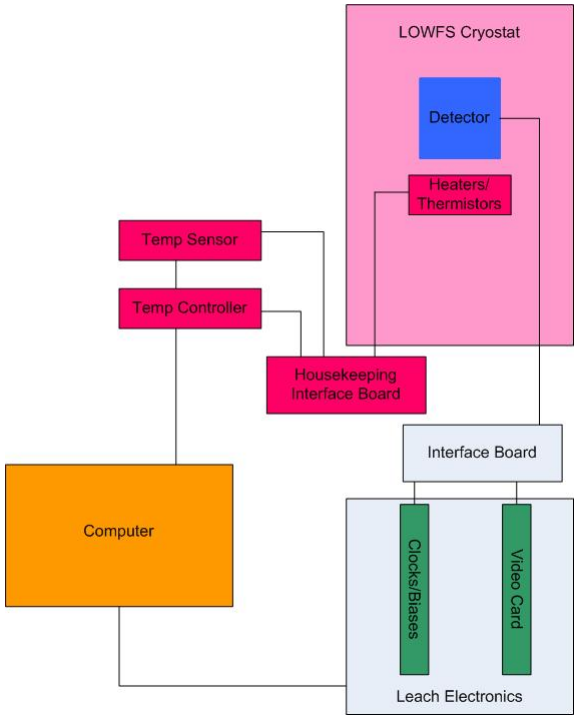

Figure 53: Near-IR detector electronics with the ARC SDSU-III readout electronics

We are also considering the use of the Sidecar ASIC from Teledyne as another possible means of reading out the array. The Sidecar has the distinct advantage of providing digital values very early in the detector signal path making it much less susceptible to noise pick-up. A functional block diagram of the HAWAII implemented with an ASIC is shown in Figure 54. The USB driver is strictly MS windows based.

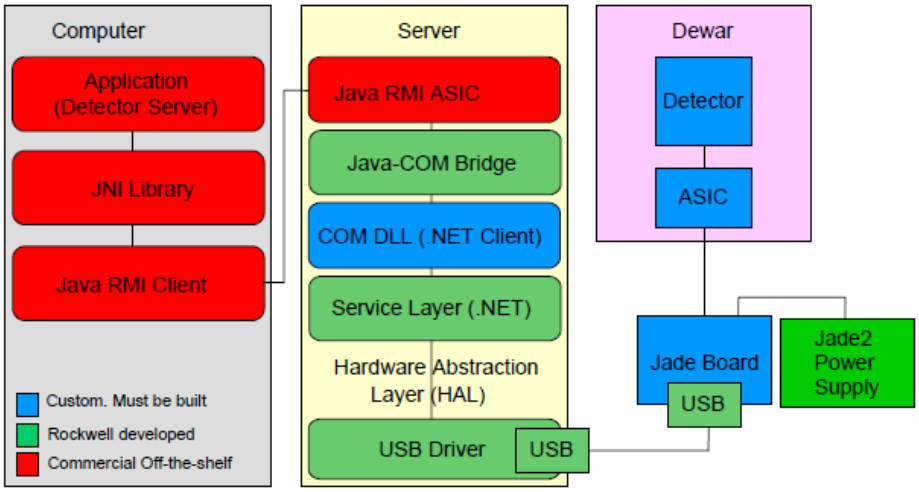

Figure 54: Block diagram of detector readout with the Teledyne Sidecar ASIC.

3.3.4.8 Truth Wavefront Sensors

The TWFS is used to calibrate biases that arise when using LGS in an AO system; in the existing Keck AO system we refer to this as the Low Bandwidth Wavefront Sensor. The biases are principally caused by the elongated nature of the LGS when viewed by sub-apertures of the LGS wavefront sensor and the changing sodium layer density profile. The truth wavefront sensor measures these biases by sensing the time-average wavefront from a NGS. These biases are slowly varying and are of a low spatial order. So, a NGS WFS using long exposures and only measuring the lowest spatial wavefront error is sufficient. The TWFS also measures focus which is used to correct the position of the LGS WFS focus stage.

A dichroic just after the TTFA object selection mechanism sends the visible NGS light (0.5 to 1.0 μm) to the TWFS while transmitting the J and H band light to the TTFA. The TWFS optics after this dichroic, to reimage the pupil onto the lenslet array and to relay the lenslet focal plane to the detector, are shown in Figure 55. The TWFS has 5x5, 0.732 mm square, subapertures across the pupil and a plate scale of 177 μm/arcsec on the detector. The images are diffraction-limited.

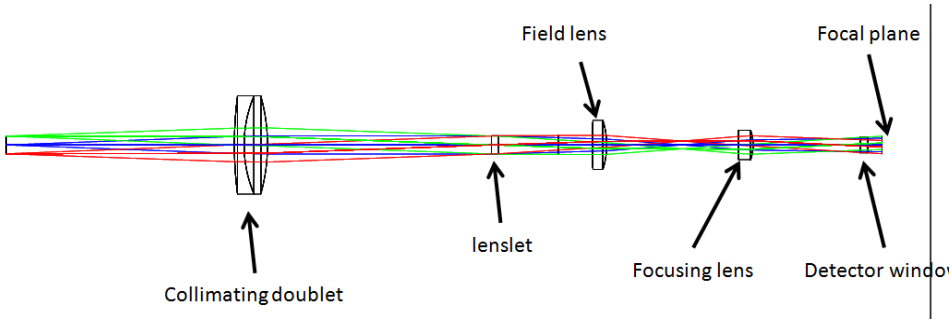

Figure 55: TWFS optical relay

Figure 56 shows the TWFS CCD as part of the TTFA LOWFS.

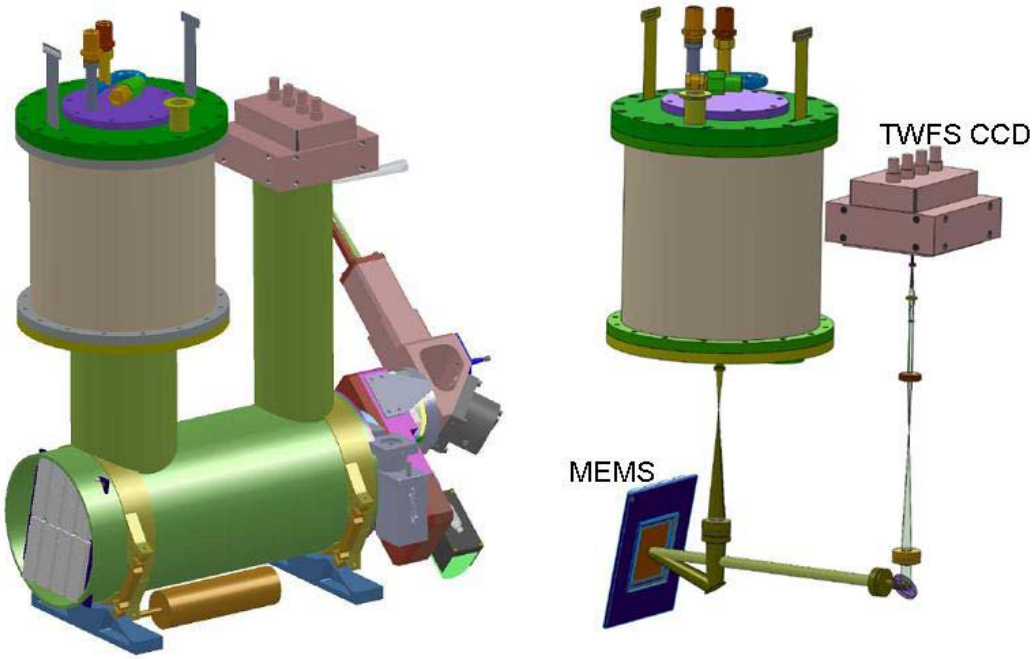

Figure 56: TTFA assembly with the TWFS arm (left) and with the post-OSM optics shown (right)
The TWFS CCD is just to the right of the near-IR cryostat

3.3.5 AO Cold Enclosure

The AO cold enclosure design is documented in KAON 766. Much of this work was performed by Quartus Engineering. The cold enclosure requirements include a normal operating temperature of -15 º C, class 1,000 clean room and humidity ≤ 50%.

The key features of the cold enclosure design include:

- High thermal resistance insulation panels built into the supporting frame for the enclosure
- Actively cooled walls to mitigate parasitic loads from ambient environment
- Individually cooled thermal loads on the AO optical bench
- Maintain positive nitrogen or dry air purge pressure during "observe" state
- Replaceable desiccant for humidity removal
- Controlled high volume "chilled air" flow to facilitate the "cool down" state
- Health monitoring points employed to feedback to system control for safety interlocks

Figure 57 is a representation of the overall cooling system, showing the chiller loop for the chilled air purge and individual component heat load cooling. This system utilizes the existing glycol infrastructure with a heat exchanger to remove heat from the cold enclosure chiller system. During cool down mode, the internal volume cooling is maximized through both wall cooling and heat exchange with the interior air volume. In observing and standby mode, the heat exchange with the internal air volume is stopped to eliminate turbulence. In this operating mode the system relies on the wall cooling to address the parasitic load from the ambient environment, and glycol connection to the individual, high heat load components.

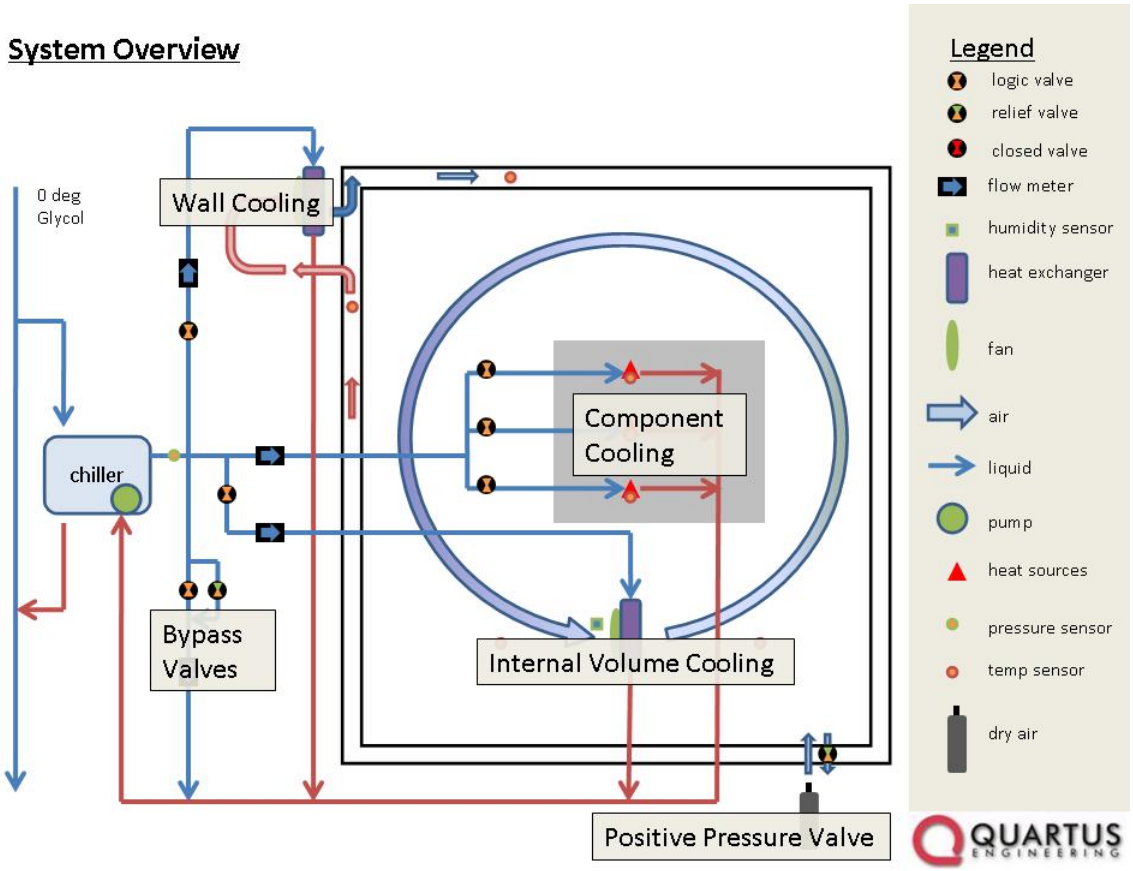

Figure 57: Cooling system overview

The enclosure wall design concept is shown in Figure 58. The foam is encapsulated with an aluminum cap on the inside of the enclosure, with a composite (fiberglass/carbon-fiber) shell on the outer three sides. Chilled air is fed through the wall and into a cooling cavity formed by the aluminum cap for convective cooling of the walls. This part of the design architecture ensures that the parasitic load from the ambient environment is eliminated.

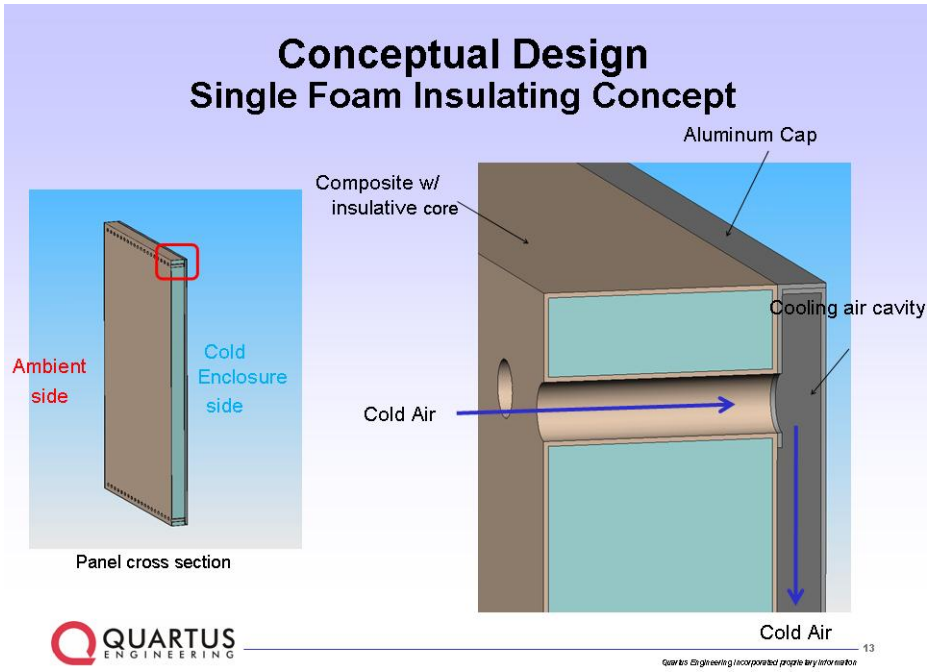

Figure 58: Single foam insulating core design concept

Figure 59 shows the conceptual design of the enclosure, with the air-cooled panels supported by an aluminum frame. The enclosure decoupling from the AO bench is maximized through floor support. Isolation of the windows will be accomplished with a TBD damping material where the bellows connections are made. Also considered in the design is the parasitic load of the metallic legs, which can be managed using insulating materials such as ceramics for the balls in the kinematic mounts and insulation of the leg intrusion into the enclosure. More detailed analysis of these parts will take place in the detailed design phase.

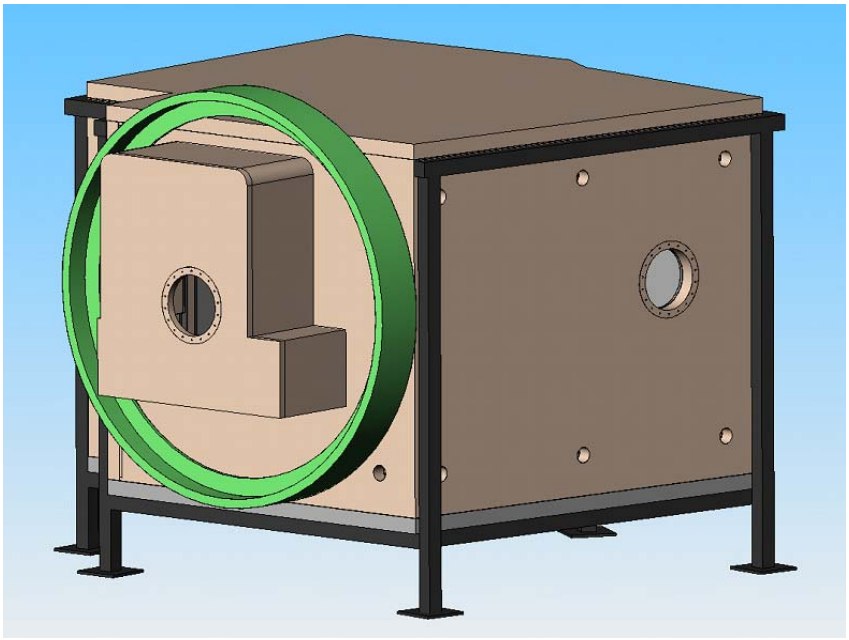

Figure 59: Cold enclosure conceptual design
The front end of the cold enclosure sits inside the telescope's elevation ring (shown in green).

The cold enclosure system must provide a means to achieve a set point temperature below ambient. The proposed design will utilize -20°C to -15°C glycol fluid as the heat transfer media. Two options are being investigated for the glycol chiller in discussions with vendors: a vapor compression cycle (VCC) chiller or a thermally electrically cooler (TEC) driven chiller.

Two glycol-to-air heat exchangers with fans will be employed: one to cool the cold enclosure walls and one to cool the air and component cold plates inside the cold enclosure. The former will be outside the AO enclosure and the latter would be under the AO bench.

Additional work is currently being performed (that will be documented in KAON 766) to complete the preliminary design in the areas of cold plate thermal analysis, air quality management system, elevation ring and enclosure clearances, airflow to panel interface design, design features to allow removable panels, window interfaces, and shipping interfaces.

3.3.6 AO Enclosure

The AO enclosure preliminary design is documented in KAON 767. The 3D model shown in Figure 60 was developed to support this design. The current design makes full use of the entire left Nasmyth platform, an area of ~6.1 x 9.1 m, and much of the existing thermally insulated AO enclosure. The enclosure includes the room housing the AO bench, LGS WFS and science instruments, a separate electronics vault and an ante-room for changing into clean room garb.

The existing AO enclosure will require modifications for fitting the AO bench cold enclosure into the elevation ring and for changing the location of the ante-room. The Nasmyth platform structure under the enclosure will be modified to add some additional structure under the support legs for the AO

bench, LGS WFS and DAVINCI. The six electronics racks are also laid out differently than the electronics racks in the existing vault area. Some additional cable trays will be added. The interferometer module will normally be housed in this enclosure but can be removed as it is now, through the large double door, via the existing motorized cart and rails that extend off the telescope to the Nasmyth deck.

The roof of the existing enclosure can be removed to install major components with the dome crane.

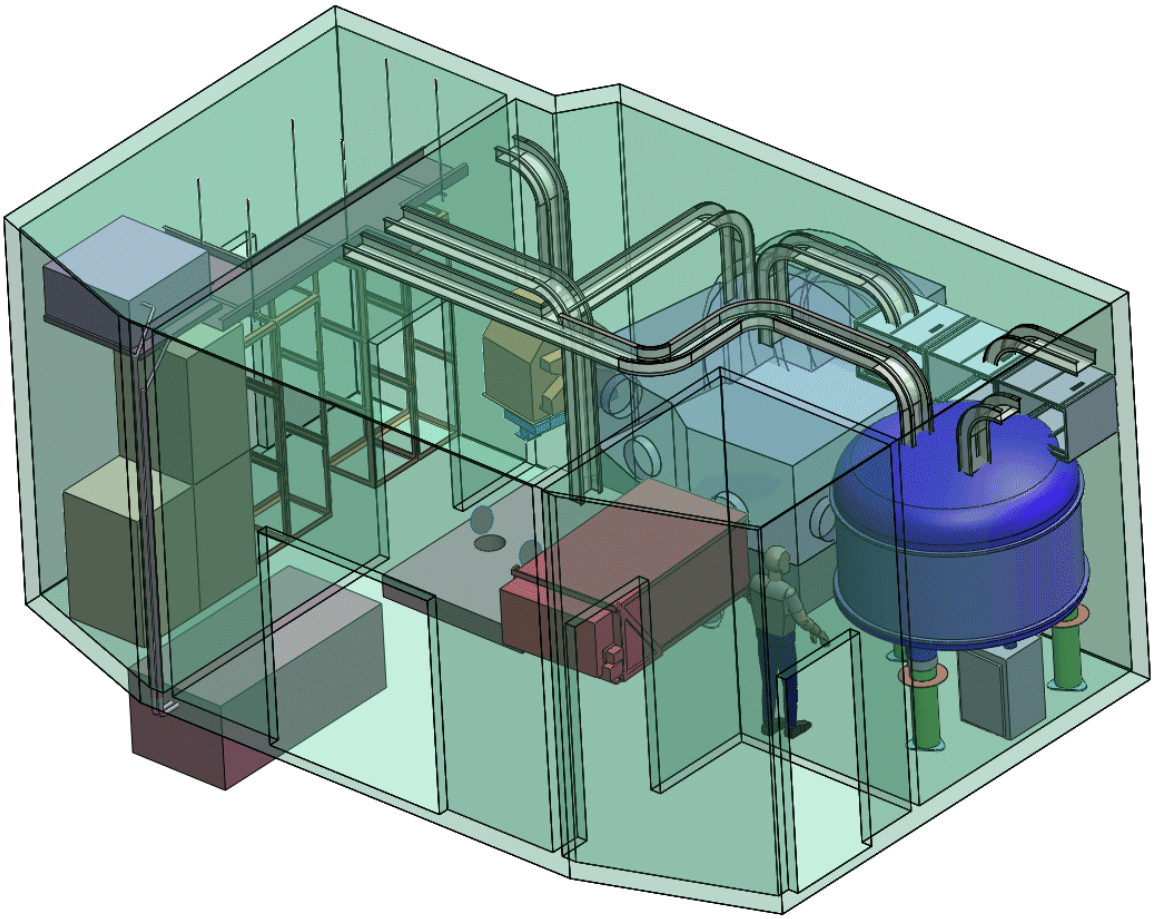

Figure 60: Nasmyth platform AO enclosure

3.3.7 Alignment, Calibration, Metrology, Vibration Mitigation and Atmospheric Profiling

3.3.7.1 Alignment

KAON 719 defines and describes the alignments that will need to be performed to assemble the AO subsystems into the overall AO system and to align this system to the telescope. Subsystem alignments will be documented as detailed design phase deliverables for each subsystem.

The key axes to be co-aligned are the telescope elevation axis (assuming the telescope optical axis overlaps this), the AO rotator mechanical axis, the science instrument optical axis and the optical axes for each subsystem. The key points along the telescope elevation axis are the telescope focal

plane and the telescope pupil plane. These points need to be co-located with the appropriate foci and pupil planes for the AO subsystems and science instrument.

The models used for alignment will include the Zemax optical prescription and tolerance analysis and the SolidWorks model of the AO bench and AO system on the Nasmyth platform. If appropriate the SolidWorks model will be exported to coordinate measuring machine (CMM) software to allow the use of a probe arm or laser tracker to locate components. The models will be produced at the lab and operating temperatures.

The alignment requirements to the telescope (SR-55) include making the NGAO bench's optical axis coincident with the telescope elevation axis to within 1 mm at the telescope focal plane (2 mm in focus) and 30 mm at the telescope pupil at all telescope elevations from zenith to 70°, all rotator angles and all operating temperatures. These requirements are flowed down to requirements on the alignment of AO subsystems and the science instrument to the AO rotator in KAON 719.

The alignment of the NGAO system in the lab is broken into the following sequence in KAON 719. Preliminary procedures are provided for each of the install and align steps:

- Install and level the AO bench.
- Mark out location of all components on the bench based on the SolidWorks model and the optical tolerances.
- Install and align the rotator.
- Install and align the low order relay.
- Install and align the high order relay.
- Install and align the LGS WFS feed optics.
- Install and align the acquisition camera.
- Install and align the calibration unit and its fold mirror.
- Install and align the NGS WFS assembly.
- Install and align the LOWFS assembly.
- Install and align the ADC.
- Install and align the LGS WFS cold enclosure exit window.
- Install and align the LGS WFS to the AO bench.
- Install and align DAVINCI to the AO bench.
- Install and align the interferometer exit windows.
- Install and align the AO bench entrance window.
- Install and align the AO bench alignment fiducial in front of the AO bench entrance window. The fiducial is a partially reflective mirror to be aligned perpendicular to the rotator axis with a cross-hair centered on the rotator axis.
- Align the interferometer dual star module to the AO bench (summit only).

Lab alignment testing is performed with the bench at room temperature and at the cold enclosure temperature.

A key question is how much we will need to or want to disassemble the fully assembled lab I&T system for shipment to the summit. The lowest risk shipment approach is to fully disassemble and pack the lab system. The quickest and less error prone re-assembly approach is to leave the aligned

AO bench and aligned LGS WFS fully assembled. For the purpose of this alignment procedure we assumed that the AO bench and LGS WFS will be shipped fully assembled to the summit. We are therefore assuming that the internal alignments will only need to be verified at the summit.

The installation process will require removal of the AO room and electronics vault roofs. In order to ensure optics cleanliness during the summit shipment and installation the AO bench and LGS WFS will have been sealed in some manner (preferably with the cold enclosure) to prevent air/dust inflow. These seals will not be removed until after all the required components (AO bench, LGS WFS assembly, science instrument, electronics in the AO room, etc.) have been installed, the AO room roof has been replaced, cables have been routed and connected to the extent possible and the AO room has been thoroughly cleaned. At this point the AO room will become a clean room.

The AO bench will be aligned to the telescope using an autocollimating theodolite, cross-hairs on the elevation journals and the AO bench alignment fiducial.

3.3.7.2 Calibration Methods and Procedures

Before AO observations can begin, the various WFS, DMs, and science instruments should be calibrated. This is a necessary process so that the non-ideal features of these components do not compromise the systems scientific utility. Calibrations are considered here as operations or procedures performed with the NGAO system that can be completed during the daytime and do not require access to celestial sources. Measurements that could be similar to calibrations but are made with celestial sources are considered part of the operations and optimization tasks of the NGAO system. These operations can occur before, during, or after science observations. Such on sky operations include:

- Observation of NGS sources with the Truth Wavefront Sensor (TWFS)
- Dithering of LGS and NGS to calibrate the systems for wavefront sensor image size changes
- Optimization of the control loop bandwidth from AO WFS and DM data

As discussed at some length in the NGAO System Design Review presentation (KAON 584), AO correction without feedback, known as ‘open-loop’ or ‘go-to’ adaptive optics, requires the following:

- Predictable deformable mirror response
- Absolute measurement of the wavefront with high dynamic range

It has been suggested (Gavel et al., SPIE 7015, 2008) that errors in these two calibrations limited the low frequency error rejection of the VILLAGES experiment, see Figure 61.

NGAO will mitigate the issue of calibration errors by the use of a Truth Wavefront Sensor (TWFS) which will monitor the steady state performance of the AO system while observing and the use of daytime calibrations discussed in the remainder of this section. The methods suggested for calibrating the NGAO systems are based on experience testing ‘go-to’ AO systems at the UC Santa Cruz Laboratory for Adaptive Optics test bench and the VILLAGES experiment at Lick Observatory.

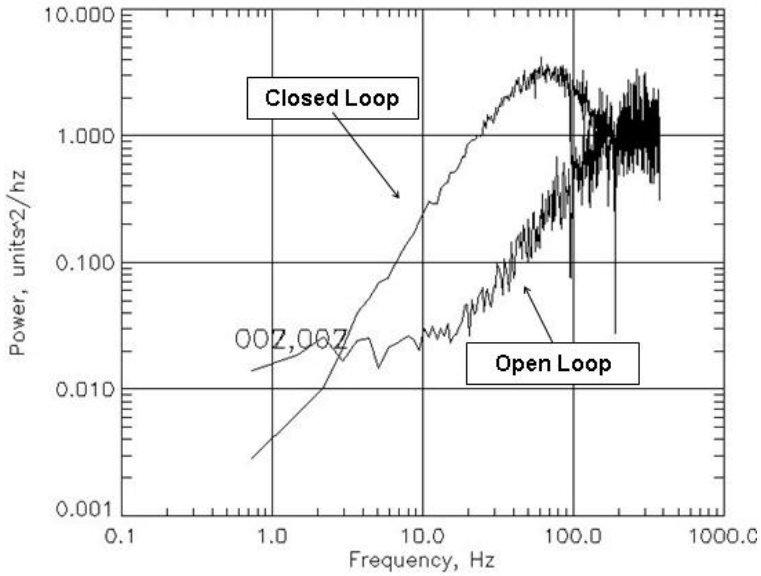

Figure 61: AO error rejection curves from the VILLAGES experiment
The 'go-to' AO system shows higher unit response or 'cross over' frequency compared to conventional 'closed loop' AO. However, the 'go-to' system exhibits worse performance at frequencies below 3 Hz.

The following were identified as NGAO daytime calibration tasks. An abbreviated discussion is given below of possible methods and techniques to address each item. More details are given in KAON 739.

1. Detector Calibration of Science Instrument and AO Wavefront Sensors:
This item includes the sources and optics needed to produce both 'white light' and spectrally filtered 'flat fields' and narrow wavelength line sources for spectrograph dispersion calibration. This function is needed to calibrate the science instrument and the same sources might also be useful for calibration of the various wavefront sensors in the system. This calls for a "flat field" source and spectral line sources to be part of the AO calibration unit.

2. Astrometric Calibration of AO System and Science Instrument Distortion:
The AO systems will need a means to measure the optical distortion across the science instruments field of view and across the LOWFS and LGS WFS input fields of regard. The current Keck AO system science instrument NIRC2 has a grid of holes that can be inserted at a focus internal to the instrument. It has been used successfully to calibrate the optical distortion of the NIRC2 instrument. We propose a similar source for the calibration unit for NGAO.

3. Determine Static Wavefronts for Best Science Image:
The AO system needs a means to measure non-common path (NCP) errors and determine the bias or offset figure for all science path deformable mirrors. Recently high sensitivity phase diversity techniques have been demonstrated. The phase diversity algorithm used to calibrate the AO system by Sauvage et al. (JOSA A 24, 2007) reports rms wavefront errors of 12 nm with only 4.5 nm attributed to modes the DM could remove. The remaining error belongs to spatial frequencies higher than the DM's spatial cutoff frequency. Bikkannavara et al. (SPIE 7015, 2008) report an

error of 35 nm rms when used with the Palomar AO system. Improvements to the calibration scheme have lowered this value to 25 nm rms. Under laboratory conditions, the same algorithm achieved a wavefront measurement error of 3 rms in direct comparison to a WYKO interferometer.

4. Determine Static Wavefronts for Best LOWFS Image:
The AO system needs a means to calibrate NCP errors and determine the bias or offset figure for all the LOWFS DM's. Phase diversity algorithms can also be used for this task. An additional factor with the LOWFS is the need to sub-sample the image. The LOWFS currently will have pixels that will under sample the image relative to the Nyquist criterion. In the case of under sampled images, a higher resolution image can be synthesized from sub pixel stepping of the image across the detector. This idea is the basis of the DRIZZLE algorithm (Fruchter and Hook, PASP 114, 2002) used on the Hubble Space Telescope. Other image interlacing methods may also be useful for this task.

5. Calibrate LGS WFS Response for 'Go-To' Operation:
The LGS WFS will need to operate over an extended dynamic range for 'go-to' as compared to conventional 'closed loop' AO. The LGS WFS response must be calibrated or made linear in some fashion. The baseline design of these sensors is a Shack-Hartmann type sensor with a grid of 4 by 4 pixels per subaperture as opposed to the conventional 2 by 2 pixel quad cell arrangement. The response of the 4 by 4 pixel sensor will be somewhat nonlinear to input wavefronts. A means to calibrate such a sensor has been demonstrated at the Laboratory for Adaptive Optics at UCSC by Ammons, et al. (http://arxiv.org/abs/0901.1716). Their method uses an artificial calibration source that resembles the LGS in size and wavelength. The method consists of scanning the LGS source across the pixels of each subaperture to map their response. The known input tilt and the wavefront response are used to develop lookup tables that correct for the non-linear response of the sensor. The final "calibration" for the LGS aberration that results from the LGS passing through the AO relay at the incorrect focus will be done on-sky with the TWFS.

6. Calibrate LOWFS Response:
Each LOWFS unit will be located behind both a dedicated MEMS DM and the shared main LODM. The AO system needs to calibrate the response of these sensors for operation with an AO-corrected near IR image.

7. Calibrate NGS Wavefront Sensor Response:
This sensor has three functions:

- The main wavefront sensor for the NGS science modes, where LGS are not used.
- Low order wavefront sensing when the NGS WFS is used to determine tip-tilt and other low-order modes from the science object itself.
- Calibration wavefront sensor used for characterizing AO performance with high pupil sampling and checking or performing various other calibrations in this document.

This last item may require a means to distinguish internal aberrations within the NGS wavefront sensor itself from upstream aberrations of the other AO components. This can be achieved by adding a reference point source to the NGS WFS optics.

8. Calibrate the DM Response:
Successful operation of NGAO will require measurement or knowledge of the optical figure of a DM as a function of commanded position. The NGAO system will have four MEMS deformable mirrors. Based on current experience it has been suggested that small commercial high resolution Shack-Hartmann sensors (see for example Thorlabs and Imagine Optic) could be placed into the AO bench periodically on kinematic fixtures as needed, perhaps once a year. While this would provide a high quality calibration of the MEMS response, this proposal has the disadvantage of requiring access to the AO cold enclosure. That would require warming up the AO bench, but only at times when the system would be down for other maintenance tasks and upgrades. The calibration of currently used MEMS suggests this calibration will be stable on periods up to 6 months and possibly longer.

9. Registration of Each Wavefront Sensor to Corresponding Correction Elements:
This operation is termed 'lenslet-to-DM registration' in conventional AO systems. NGAO has multiple correctors that are located in optical paths separate from many of its sensors. This is in contrast to conventional closed loop AO where the sensors are always located downstream of the correcting elements. All the wavefront sensors in the AO system "see" the LODM. Using the technique of moving a few LODM actuators and measuring the response on the respective wavefront sensors, we can set the registration of each LGS WFS channel and the NGS WFS to the LODM. This calibration would proceed similarly to current waffle pattern DM-to-Lenslet registration algorithms (Oliker, SPIE 3126, 1997) used at Keck today. The current AO wavefront sensor designs have a subaperture centered Fried geometry so this algorithm is directly applicable. LOWFS MEMS need to be registered to each patrolling LGS WFS (3 sets total). Also the HODM needs to be registered to the on axis LGS wavefront sensors (1 MEMS to 4 on axis LGS WFS). Since these elements are in different optical paths, modifications to the Oliker's method used in the previous section are not applicable. Instead, one can use the nature of 'go-to' correction to determine the registration. Unlike a closed loop AO system, misregistration between the WFS and the correction element (DM) does not cause control loop instability but instead results in static errors in the corrected wavefront. In the case of linear translation between LGS WFS and LOWFS DM, the error resembles NGS anisoplanatism (see KAON 704 for more details on this effect). If the static offset wavefront error can be measured on the LOWFS detector, then the registration errors could be determined for use by the RTC or corrected by adjusting the LOWFS optical alignment.

This section has outlined the methods for calibrating the AO system and the science instrument before an observing run. In some cases, these methods are unique to NGAO and should be tested during the detailed design phase on an actual 'go-to' adaptive optics system. Possible locations include the UCSC Laboratory for Adaptive Optics and the VILLAGES system at Lick Observatory.

3.3.7.3 Calibration Unit

The calibration unit will provide an input to the AO bench that simulates the telescope optical characteristics. This will be used during the initial system assembly, alignment, and optimization in the lab as well as for the continuing calibration requirements at the summit. The calibration unit will

also have flat field, spectral line, and pinhole array sources for science instrument calibration tasks. KAON 745 has a detailed description of the design of the calibration unit, and KAON 568 outlines some early thoughts on requirements for the calibration unit. KAON 739 discusses in detail the calibration procedures and requirements and its appendix discusses why wavefront error in the calibration unit does not directly transfer to calibration errors in the AO system since it is measured as a common term in the wavefront sensor and the science path.

The current Keck AO system places a single mode fiber at the NGS telescope focus to provide a calibration point source. Unfortunately, this will not work for the NGAO system because the NGS focus is inside the AO rotator, so an optical relay must be used to produce a point source image at the correct location. The multiple wavefront sensors require multiple sources to be available simultaneously to properly test the system, so the calibration source relay field of regard needs to match that of the NGAO system. It also needs to function at both NGS and LGS conjugates simultaneously.

Although the wavefront error of the calibration unit does not directly translate into calibration error in the AO system, it is still desirable to keep the wavefront error as low as practical. Keeping the common mode error small reduces the amount of residual error due to higher order effects. The goal was to keep the total rms wavefront error from the calibration unit less than 35 nm or even lower if reasonable. This means that the number of surfaces in the system must be minimized, since random figure errors would quickly add up and dominate the system error.

The desire to minimize the number of surfaces dictated several features of the design. If the calibration unit was placed outside the cold enclosure it would require a few extra mirrors and also a window, so the decision was made early on to keep the calibration unit inside the cold enclosure. A few different optical designs involving off-axis parabolas or other aspheric elements were investigated, but they required either lots of space or highly aspheric elements. Producing these aspheric elements with a figure error of 10 nm rms or less would be difficult and expensive, so a design based on an Offner relay was examined. Its single biggest advantage is that it uses all spherical elements which will allow low figure errors resulting in reasonable fabrication costs. Unfortunately, although it does have a real pupil image it is located on one of the mirrors. This will result in a small amount of blurring of the edges of the pupil mask which can be minimized by placing the mask as close as possible to the mirror. An arrangement of two beam splitters allows the selection of NGS, LGS, or spectral line sources without the need for selection stages. The system layout is shown in Figure 62, and the rms wavefront error for the NGS and two LGS conjugates is shown in Figure 63.

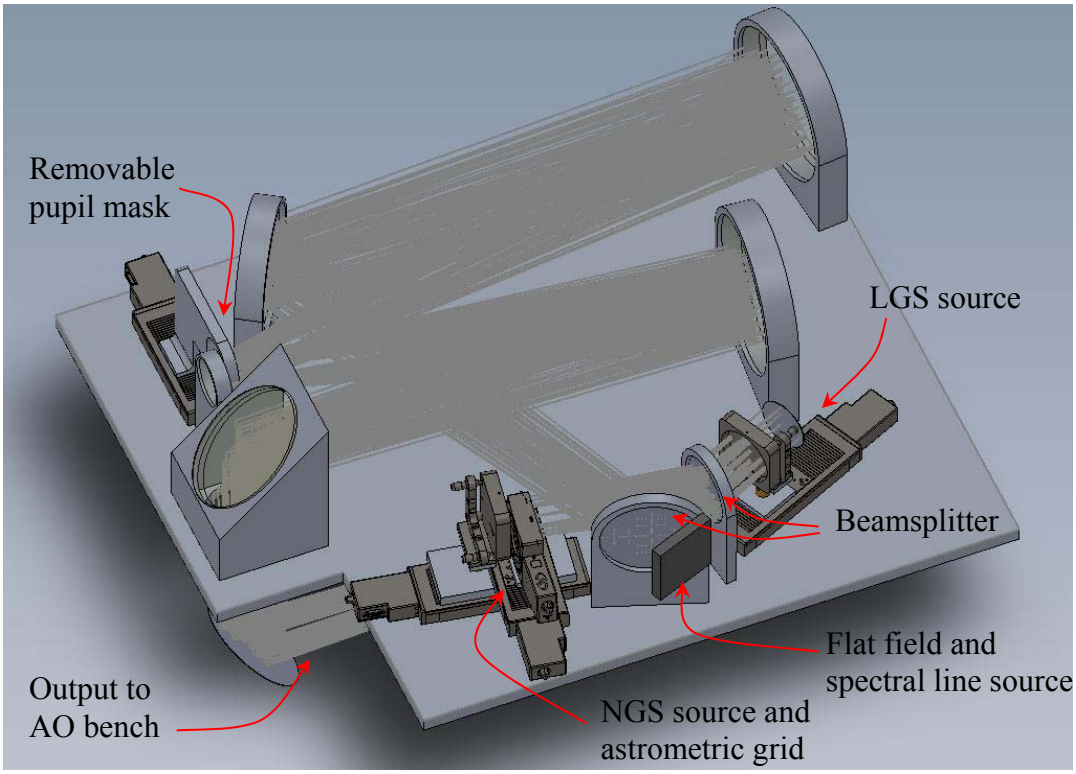

Figure 62: Calibration unit layout

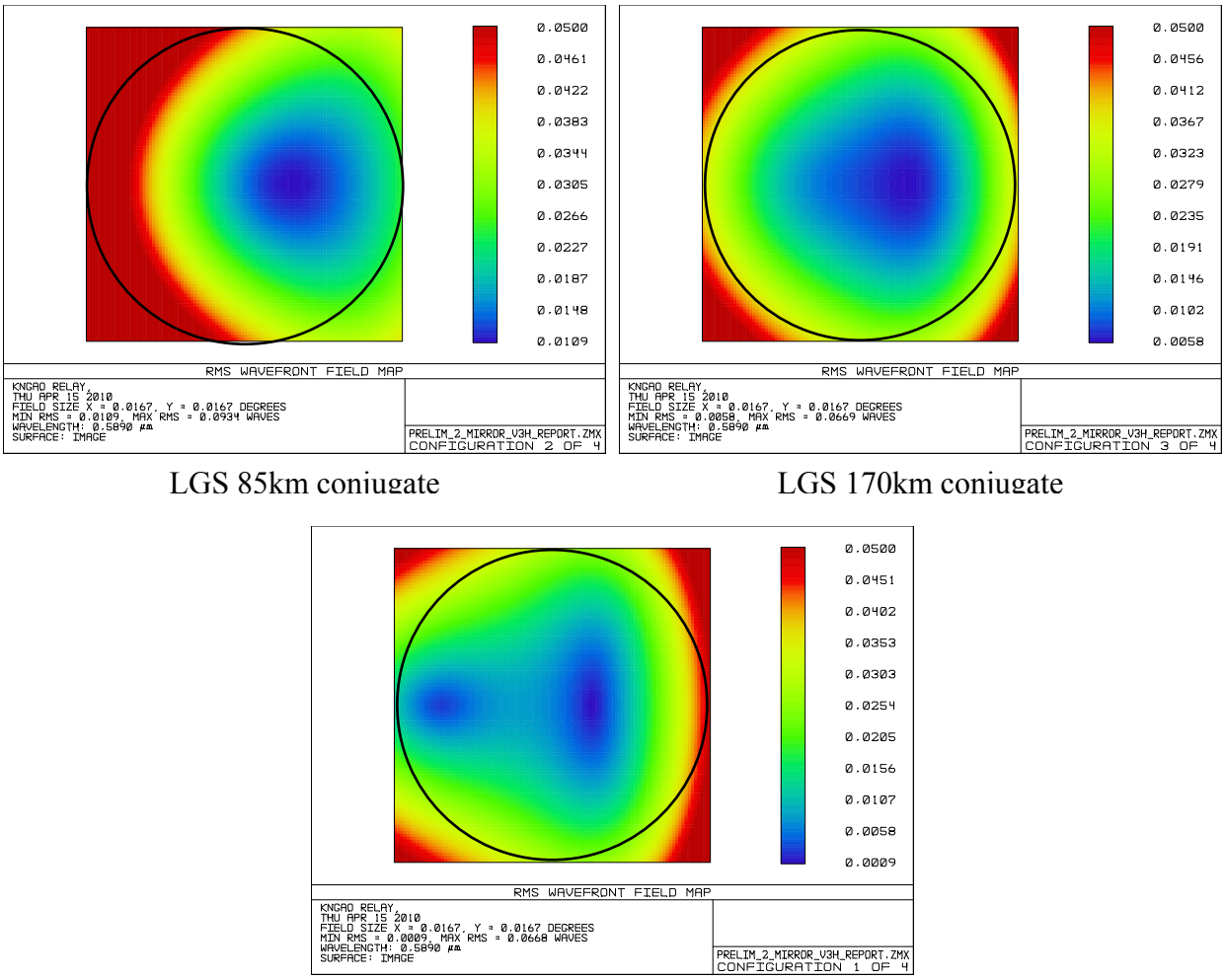

LGS 85km conjugate

LGS 170km conjugate

NGS conjugate

Figure 63: Calibration unit field dependent wavefront error
Error is given in rms waves at 589 nm, so the full scale of 0.05 waves corresponds to 30 nm rms. The black circle is the two arcminute diameter NGAO field of view.

To minimize heat loading inside the cold enclosure and to prevent the need to warm up the AO bench to replace a failed lamp, all sources will be fiber fed with the lamps placed outside the cold enclosure. Multiple NGS and LGS source points will be placed across the field to allow calibration and testing for different source geometries without the need for complicated x-y positioning systems. These will include both unresolved and resolved sources, with the resolved source size simulating median seeing conditions.

The flat field and spectral line sources will share a common element in the calibration unit. Typically this is an integration sphere, but an alternative is being considered to reduce the size and cost. Woven fiber optic panels produce a uniform surface illumination due to the controlled bending loss produced when the fiber optic strands are weaved into a panel. The uniformity of this panel will be

confirmed during the detailed design phase. A design using an integrating sphere is a contingency plan if the woven fiber optic panel is not suitable.

The asterism grid is an accurate array of unresolved sources used to calibrate field distortion as seen by the science camera. It is capable of translation and rotation to allow separation of errors in the source grid from the true field distortions. It will be backlit by a similar fiber optic panel to that used for the flat field and spectral line sources.

The calibration source will be placed above the rotator on the AO bench, with the front end inside the telescope elevation bearing. Maintenance in this location would be difficult, so it will be mounted such that it can be slid clear of the elevation bearing on rails and then hoisted off of the bench. This will also allow easier access to the components on the AO bench that are underneath the calibration unit. Figure 64 shows a view of the calibration unit from the telescope side looking through the elevation bearing. The outer blue circle is the inner diameter of the elevation bearing and the inner blue circle is the maximum dimension of the calibration unit enclosure. The clearance is currently 50 mm, although this could easily be increased to 100 mm with changes to the shape of the calibration unit enclosure. Figure 65 shows a view of the calibration unit on the AO bench from above.

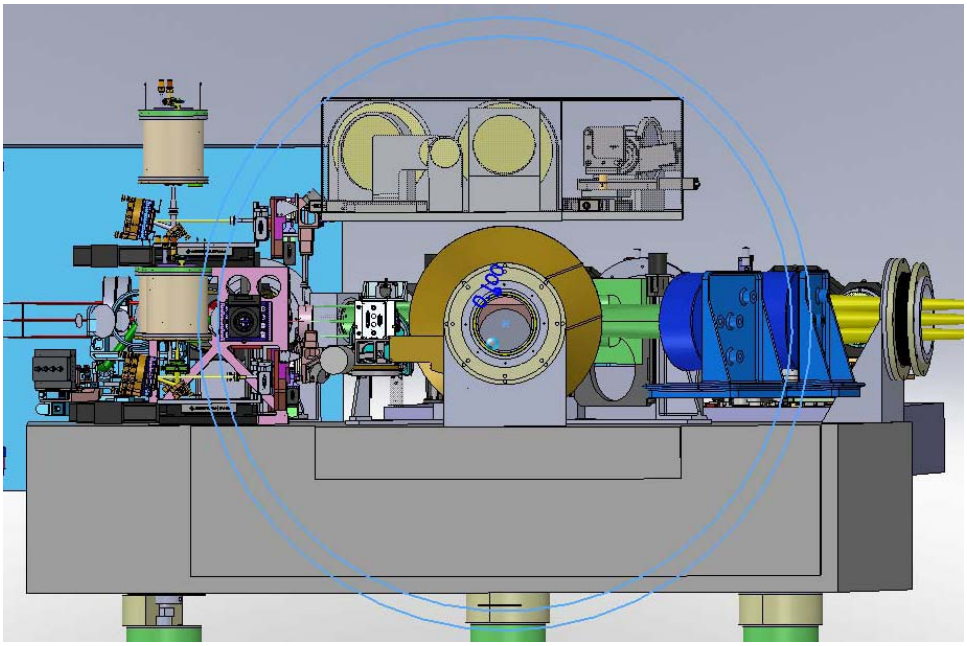

Figure 64: View of AO bench with calibration unit from telescope side

Outer circle is the telescope elevation bearing and the inner circle is the maximum dimension of the calibration unit.

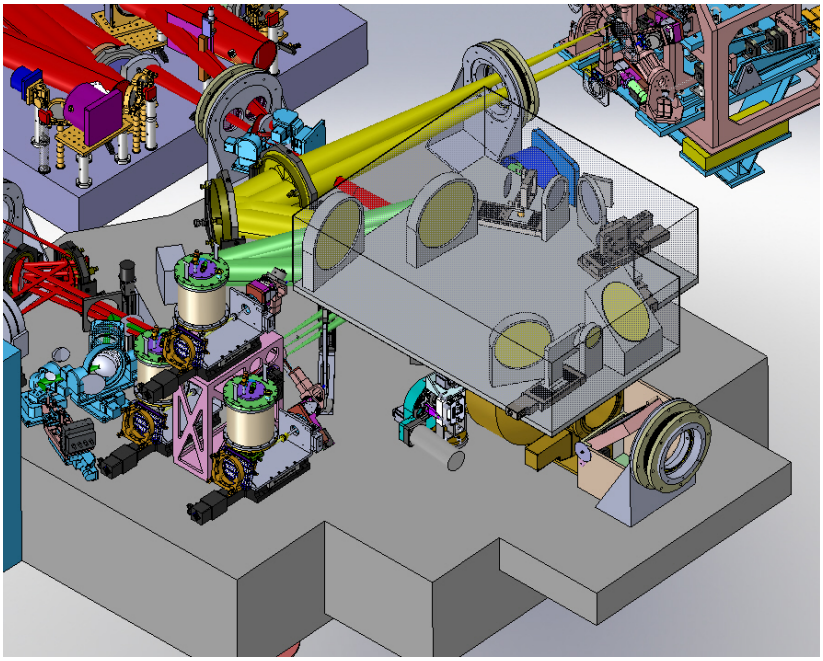

Figure 65: Calibration unit on the AO bench

3.3.7.4 Atmospheric Simulator

KAON 739 section 4.9 states that an atmospheric turbulence simulator is required for the initial integration and testing, but that it does not necessarily need to be part of the calibration unit and that it should not drive the optical design complexity or cost.

There are a few technologies for simulating atmospheric turbulence, but given the requirement for repeatable turbulence and the relatively large beam size devices based on plates with fixed optical phase distributions are the most appropriate. These are produced by creating a thickness profile in the plate that results in the desired optical phase distribution. This can be done with direct etching into fused silica, lithographic techniques and photoresist, or by milling directly into a polymer plate. After generation of the profile, some type of secondary material that has a close index match may be applied to reduce the required tolerances during the machining process. One drawback to these fixed phase plates is their chromaticity. By careful selection of materials, the near-index-matched solution can be made relatively achromatic, but temperature dependence of the index will complicate this process for NGAO. Additionally, as will be seen shortly one of the phase plates required for the calibration unit will be large enough that it may be impractical to manufacture in this way.

One alternative that should be considered is applying a random disturbance function directly to the deformable mirrors. This has the advantage that it is achromatic and does not require any additional hardware. The high spatial frequency range is limited by the actuator spacing, and the results need to be carefully interpreted since by definition it is impossible to introduce any aberration that is not in the control space of the DM that applies it.

Another alternative is a generator based on heated air. It will not create reproducible turbulence, but it may be more appropriate for the larger size beams. Obviously, operating this in the cold enclosure

would require very careful design. An alternative to heated air could be a gas with a different index than air, such as helium. This could be supplied and evacuated from the enclosed calibration unit with less of an effect on the rest of the cold enclosure than a heated air source. The strength of the turbulence could be adjusted by changing index of the gas by mixing with air.

The current design for the calibration unit does have two positions that are appropriate for turbulence generator mechanisms, and are conjugate to the ground layer and also to 11.5 km altitude. These may not be suitable for permanent mounting of phase plates, however, due to interference with the AO cold enclosure. The layout is shown in Figure 66.

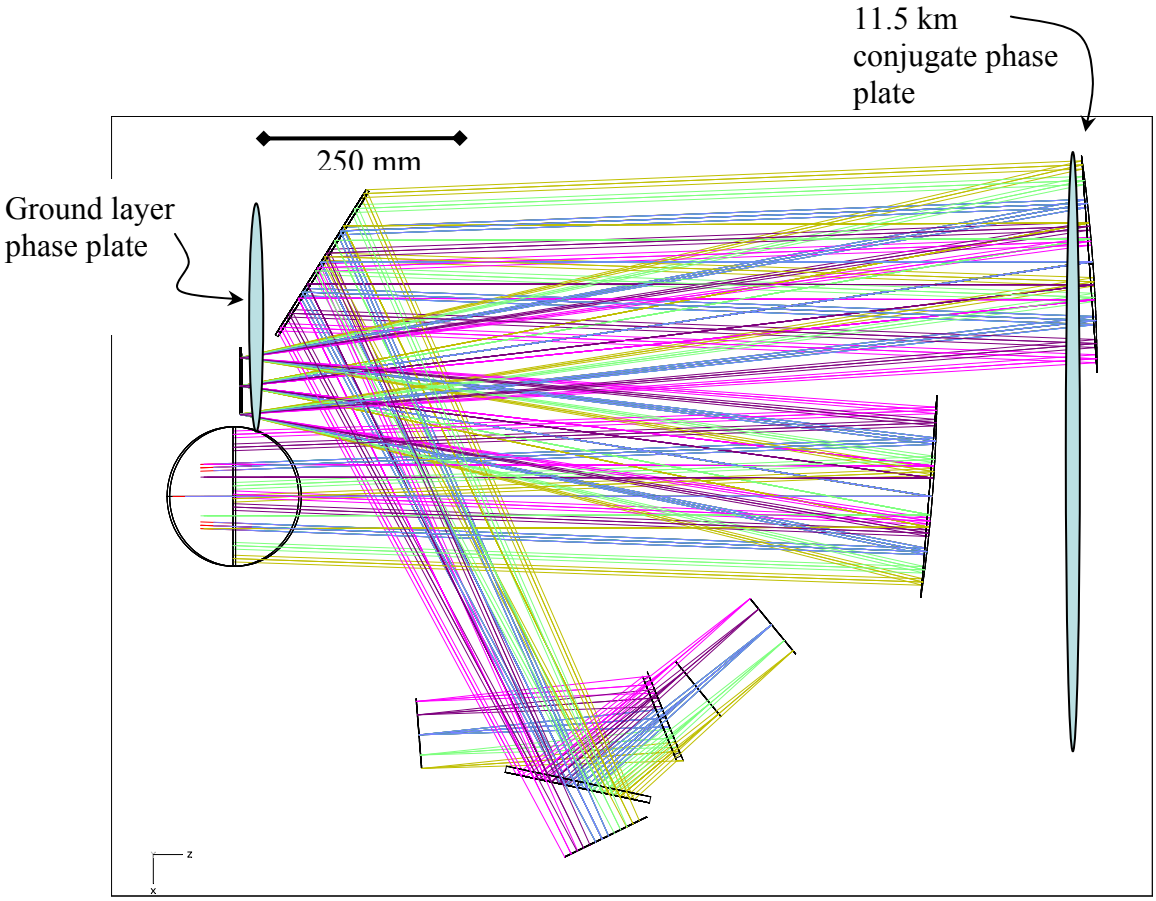

Figure 66: Turbulence simulator phase plate locations

The ground layer plate will be about 250 mm in diameter and there is a possibility that it could fit completely inside the enclosure. However, it does not appear that there is room for a removal mechanism. This would likely be ok during the initial integration and testing but would need to be removed prior to installation at the summit. The 11.5 km conjugate plate needs to be at least 600 mm diameter which may present fabrication problems. The sheer size of the area to be patterned may drive up the cost, but this could be balanced by the larger phase element size possible due to the large size beam. This design space will be explored during the detailed design phase.

An alternative to placing the turbulence generation mechanisms inside the calibration unit would be to create an auxiliary unit solely for the integration and testing at HQ. Since it would only be used at HQ it could be physically larger and so may be easier to design. Allowing larger static wavefront errors and reducing the spectral bandwidth could also make it much easier to design, and might not impact the ability to characterize the system performance if the new limits are chosen carefully.

3.3.7.5 Metrology

A metrology system could potentially be needed to monitor and correct for the alignments between the NGAO system and the science instruments, especially given the tight tip-tilt requirements and the significant non-common path between the LOWFS and the narrow field science instruments. A "metrology like" alignment system (KAON 35) was proposed originally for the Keck AO system. Some parts were installed in the NIRC2 camera but it was later decided not to be needed. A laser metrology system for the Palomar AO system was also considered but was not installed. We plan to perform a test with NIRC2 to better understand the stability of the existing system to determine if such a system might be required for NGAO.

3.3.7.6 Vibration Mitigation

The NGAO requirement to produce high Strehl observations over a significant fraction of the sky implies the ability to track on several natural guide stars that are as faint as J~16 with exposure times as short as 5 msec. In addition to the tip-tilt errors caused by atmospheric turbulence, the tracking system must be able to correct for errors in telescope guiding, wind shake, and mechanical vibrations.

High frequency mechanical vibrations have long been a limiting factor for high-resolution astronomy at WMKO. The presence of vibration in the Keck telescope segments was noted as early as 1994. The effect was extensively studied by Dekens in his PhD thesis using optical measurement with a high-speed CCD camera. Dekens reported both tip-tilt motion of individual segments and full aperture tip tilt motion with the dominate frequency being located around 29 Hz. This frequency is typical of electrical motors that run at 1700-1800 revolutions per minute (28-30 Hz) used throughout the observatory. More recently, an independent survey of vibrations at Keck was made by Tomas Erm of the Thirty Meter Telescope project. The measurements by Erm confirmed that the dominate vibration is centered around 29 Hz. An attempt to determine if this is a resonant frequency of the telescope azimuth and elevation drive was inconclusive.

The current Keck AO systems also observe 29 Hz vibrations in both full aperture tip-tilt and higher order phase aberrations. The AO error budget for tracking bright stars is much higher than would be expected from the simple AO scaling laws. All the above sources have reported that the 29 Hz vibration amplitude is highly variable with time although the frequency is very stable.

During the installation of the Keck interferometer, a large amount of effort was put forth by both the WMKO and JPL team to understand the vibration problem and reduce its effects. These efforts were successful and the interferometer was able to meet its fringe tracking requirements although it did not meet its goal specification of working at the atmospheric limit of the site. The interferometer success was due to a reduction in vibrations by isolation of vibration sources such as pumps and air

conditioners, and the use of a modified control system (parametric oscillator) for the interferometer tracking system.

The use of accelerometers by the interferometer to sense and correct tip-tilt vibrations did not prove successful although it has indicated that the worst offender is likely the secondary mirrors, with the tertiary also providing significant jitter. The interferometer has been able to suppress the residual beam wander that is not corrected by the AO systems with its own tracking systems. The jitter is removed by the Keck Angle Tracker (KAT), which is composed of a tracking mirror and position sensitive detector for each telescope. These components are in the interferometer beam combiner located in the Keck basement. Although the sampling frequency of this servo is as low as 100 Hz, the controller is able to reject a significant amount of 29 Hz by the use of a specialized control technique. This method makes use of the fact that the vibration is located at a precise frequency of 29 Hz. Colavita named this technique the "parametric oscillator" and it is similar to the standard control method of "higher harmonic control" used in other dynamic systems such as helicopter rotors. This method appears to be promising for our application. A more detailed discussion of the vibration modeling discussed below can be found in KAON 680.

Atmospheric turbulence produces random motion of astronomical targets as well as higher order distortions. KAON 680 used the standard gradient or G-tilt formalism devolved by Tyler (JOSA A, 1994). Tyler's expressions were evaluated for the standard median profile of the Mauna Kea Ridge (MKR) atmospheric model (KAON 503) that is used in the NGAO error budget and other performance estimates. The formalism of Tyler assumes an infinite outer scale. The result of this assumption is excess tip-tilt power at very low frequencies, approximately 0.1 Hz and lower. Since any tracking system will be very efficient at removing these frequencies, little performance penalty is associated with the unphysical assumption of an infinite outer scale.

With these assumptions, the atmosphere used in KAON 680 has a fundamental tip-tilt tracking frequency, f_T, of 2.8 Hz and uncorrected RMS tilt error of 1.31". The G-tilt power spectral density (PSD) is proportional to $f^{-2/3}$ at low frequencies and behaves as $f^{-11/3}$ at high frequencies. A bend in the PSD is expected at the intersection of these two asymptotes. For the MKR model, this is at a frequency of approximately 2.8 Hz. Our tip-tilt compensation techniques were tested with random time series of one axis tilt. These random samples were generated to have an ensemble average consistent with the PSD in Tyler's paper. The samples were generated from the inverse Fourier transform of filtering white noise. This technique is the one dimensional analog of the standard atmospheric phase screen generation technique commonly used in AO simulations.

The Keck telescope mechanical vibration is known to be located close to 29 Hz. The amplitude of the resulting disturbance is variable in amplitude but its frequency is typically stable over many seconds. The resulting rms jitter has been measured by several groups and found to be between 0.010" and 0.020". We assume a value of 0.020" as a worse case value. Vibrations were modeled as a pure sine function with a frequency at precisely 29.0 Hz. The phase of the sine wave was a uniform random variable in the range 0-2π. The variability is an attempt to simulate the slowly variable nature of the 29 Hz disturbance. In the simulation, a sine function with random phase is produced for each atmospheric time series generated with the technique described in section above.

A continuous time model of the tracking system of NGAO was developed using the standard Laplace transform techniques for AO, given by Madec ("Control techniques" in Adaptive Optics in Astronomy, F. Roddier, ed., 1999). The Laplace transform techniques were also used to model the parametric oscillator for compensation of the 29 Hz vibrations. A real AO system is actually a combination of discrete and continuous time (CT) components. However, the continuous approximation is often acceptable. Starting from these basic control functions, a model of a single channel of the tip tilt tracker was developed using the MATLAB add-on package Simulink. Simulink is a time domain differential equation solver that has a graphical interface that resembles a control system block diagram. This technique was chosen for the flexibility and the expansion capabilities it provides for future design of AO control models.

The overall Simulink block diagram for an AO tip tilt loop with a parametric oscillator is shown in Figure 67. A few features of the overall model should be noted. At the left of Figure 67, several different types of input signals can be used in the simulation by selecting the desired input with the multiple port switch. The chirp signal and sine wave inputs proved useful in setting up the control loop and verifying the operation of the model. The white noise input was used to measure the error transfer function of the overall system. The "TipTilt" input block reads an input variable from the MATLAB workspace. This function links the Simulink model to the MATLAB code that generates random tip-tilt time series of atmospheric tip-tilt disturbances with or without vibrations.

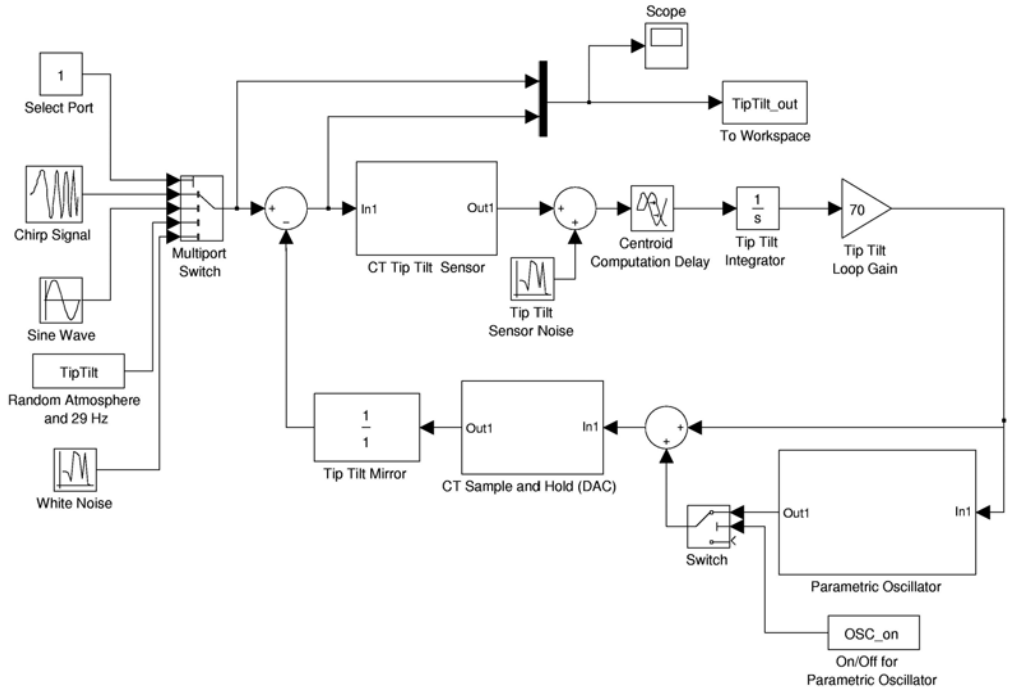

Figure 67: Simulink single channel AO control loop model with a parametric oscillator

The input signal and the error in the control correction are both output to the MATLAB workspace for further analysis via the block labeled "*TipTilt_out*". The Scope block allows monitoring of these signals as the simulation runs. Complicated control functions are combined into subsystem blocks that make the top-level control diagram of Figure 67 appear simpler. Examples of such blocks are

the "*CT Tip Tilt Sensor*", the "*Parametric Oscillator*", and the "*CT Sample and Hold*". The parametric oscillator can be switched on or off from the MATLAB workspace using the variable "*OSC_on*". The *"Tip Tilt Sensor Noise"* block allows the simulation to have white noise added to the output of the tip-tilt sensor measurement.

Tracker performance was estimated directly from the Simulink model, see Figure 68. The input signal was a random atmospheric time series with 29 Hz vibration. The atmospheric signal was generated from the inverse FFT of filtered white noise. The 29 Hz vibration had a 20 mas rms disturbance. The rms tip tilt error was estimated directly from the output time series. The results were averaged over 100 random 26 second time series for a total sample time of 2600 seconds. The time step of the simulation was set to 50 μs (20 kHz update rate). The AO tracker was setup to run at 100 Hz update rate, although the time steps in the simulation are much faster to limit any effect from under sampling in the simulation. The tip-tilt sensor noise equivalent angle was set to 2 mas, a value consistent with the error budget.

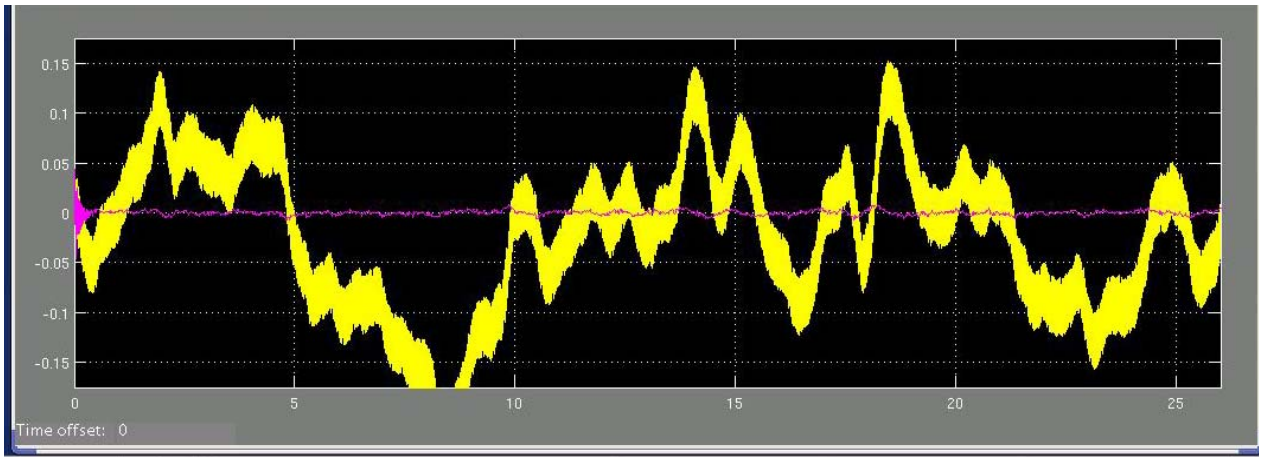

Figure 68: Sample Simulink "Scope Block" display
Arcseconds of tilt versus time for the input signal (yellow), a random atmospheric disturbance with 29 Hz vibrations, and the corrected signal (pink) provided by the tracker and parametric oscillator.

The one-axis uncorrected tracking error was 132 mas rms. This was reduced to 27 mas rms with the tracker and further reduced (by a factor of 7) to 3.7 mas rms with the parametric oscillator. These results are a combination of the NGAO error budget terms: tracker bandwidth, tracker measurement noise and telescope tracking residual (vibration).

The NGAO Error budget total for these terms is an error of ~0.002" rms. However, the simulation results are for more stressing conditions than what is assumed in the error budget. The differences are shown in Table 11. Detailed design phase tasks will include adding a finite outer scale and a detailed study of the tracker performance at other frame rates with a parametric oscillator.

Table 11: Comparison of the Simulink modeling result with the NGAO error budget assumptions

Parameter	Simulink	Error Budget	Comments
Frame rate (Hz)	100	200	Simulation tracker is running at a slower update rate.

Outer scale (m)	Infinite	75	Finite outer scale removes mostly low frequency power < 1Hz.
F_Tyler (Hz)	2.7	1.3	Outer scale reduction assumed in error budget should not change the fundamental tilt frequency. Error budget should probably be revised.

3.3.7.7 Atmospheric Profiler

The initial requirements and design for an atmospheric profiler are found in KAON 552. A profiler was deemed to be useful for NGAO for the following reasons:

- Acceptance testing and performance verification (in order to know the performance versus the current conditions).
- Diagnostic tool during observing.
- Aid to planning observations.
- Improve accuracy or speed up the convergence of the laser tomography algorithm.
- Useful as an aid in estimating the AO PSF across the instrument field of view.

The highest level requirements were determined to be (detailed requirements can be found in the functional requirements):

- Measure atmospheric profile at low resolution in six or more altitude bins between 1 km and 20 km altitude.
- Measure the profile once every 2 minutes.
- Measurement accuracy of 10% or better for r_0.
- Operate automatically when conditions are suitable for operating the Keck telescopes.
- Small physical size.

A MASS/DIMM system was recommended as the best system to meet the NGAO requirements (KAON 552). The NGAO team has significant experience utilizing and interpreting the data from the TMT MASS/DIMM that was located on Mauna Kea (KAONs 415, 420 and 496). A TMT MASS/DIMM was donated to WMKO and installed by CFHT and UH at the CFHT weather tower site between CFHT and Gemini as shown in Figure 69. This facility is operational and the data are published throughout each night at http://mkwc.ifa.hawaii.edu/current/seeing/.

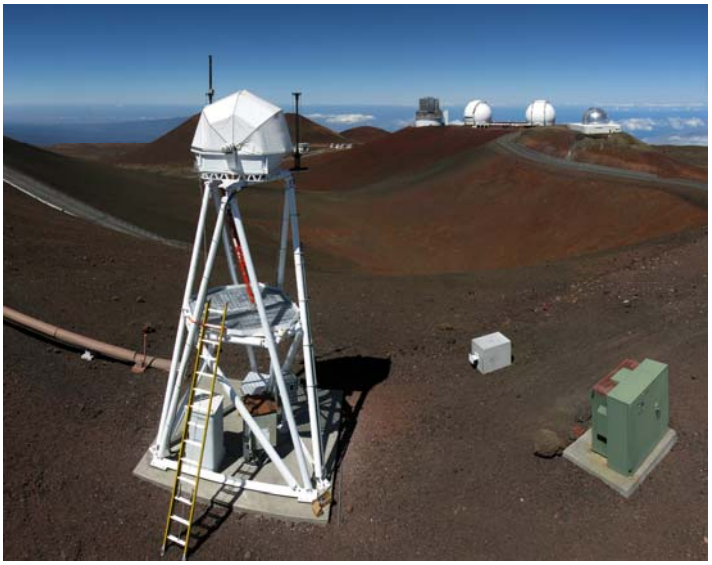

Figure 69: Mauna Kea seeing monitor

3.4 Laser Guide Star Facility Description

The Laser Guide Star Facility (LGSF) layout is shown in Figure 70. The three lasers are located in a laser enclosure on the elevation ring similar to the existing Keck II laser table. The laser beams travel into the Laser Launch Facility (LLF) from the elevation ring to the secondary socket location. The LLF is comprised of the SwitchYarD (SYD), the Beam Transport Optics (BTO), the Beam Generation System (BGS) and the Launch Telescope (LT). The SYD receives and formats the three beams and sends them to the BTO where the beams travel to the secondary socket along the telescope support structure. At the secondary socket, the BGS will receive the three beams and creates the four beam central asterism and three patrolling beam asterism as shown in Figure 1. The BGS will also provide the needed tracking, steering and off-loading to maintain the LGS on the LGS wavefront sensors. The final element is a LT similar to one produced for the Keck I LGS AO project. Diagnostics will be placed throughout the LGSF to monitor the laser beams prior to the LT. The following sections will present the LGSF in the order from laser beam production to on-sky propagation.

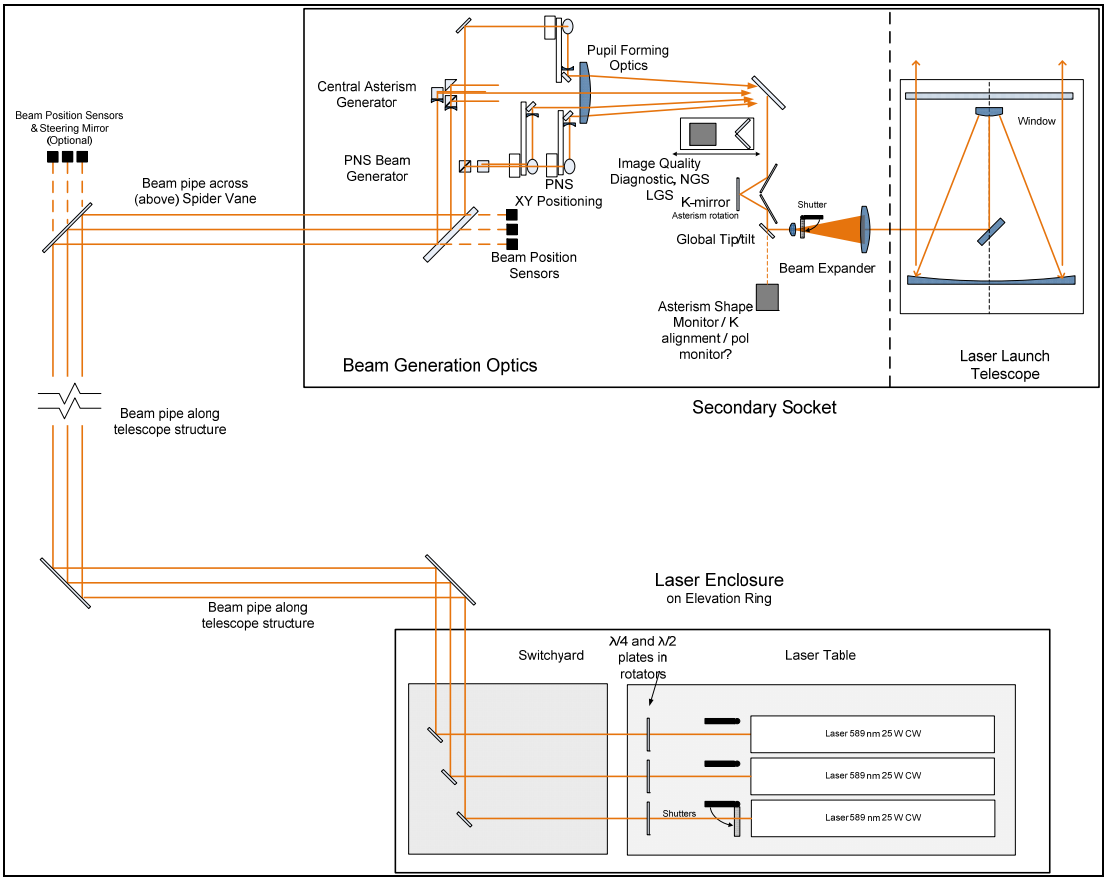

Figure 70: Laser Guide Star Facility

3.4.1 Lasers

The laser planned for NGAO is the result of two down-select processes (WMKO has been involved in both) based on technical, management and budget criteria. The first down-select involved the review of 5 proposals (one of the proposers was LMCT, which recently provided lasers for Keck I and Gemini-South, but which was not found to be cost competitive). Two laser vendors were selected and funded by ESO to produce preliminary designs, completed in December 2009, and firm fixed price quotations for 20 W lasers. WMKO, on behalf of a consortium of U.S. observatories (AURA, GMT and TMT), also placed contracts with these two vendors to perform risk reduction activities in support of these preliminary designs; primarily using $300k of AURA-NSF funding intended to support the development of the next generation of commercial lasers suitable for the future needs of our communities. As a result, all of our organizations participated in the vendor progress review meetings and preliminary design reviews.

In the second down-select, based on the preliminary designs and quotations, ESO has selected the "Laser Guide Star Alliance" of MPB Communications Inc. and TOPTICA Photonics to produce a final design, a pre-production laser and four lasers. This laser strongly leverages the expertise and existing products of these two world-leading laser companies. The TOPTICA/MPBC laser design also meets the WMKO/TMT requirements.

The proposed laser will have a minimum output power of 18 W within the sodium D2a line and 2 W within the D2b line. This re-pumping concept is predicted to improve the sodium return by a factor of 2 or more. A 40% improvement was demonstrated in a preliminary on-sky experiment at Starfire Optical Range. During the preliminary design phase TOPTICA/MPBC produced a demonstrator laser that achieved output powers of up to 30 W at 589 nm wavelength. This demonstrator was shown to operate under variable gravity (see Figure 71) which allows it to be mounted to the elevation ring, thereby lowering beam transport complexity and throughput loss. An electro-optic modulator was also demonstrated to produce the required D2b line with good beam quality.

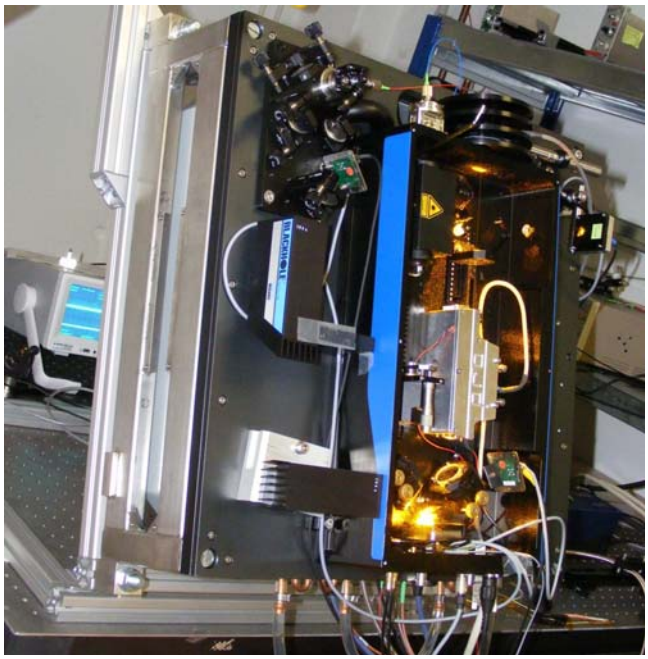

Figure 71: TOPTICA/MPBC demonstrator laser head
Tilt test carried out at a power level of 23W at 589 nm.

The demonstrator laser is based on the Raman Fiber Amplifier (RFA) approach first demonstrated by ESO at 1178 nm and high powers. The TOPTICA/MPBC demonstrator included two RFAs, whose output signals are coherently combined in fiber. Due to successful higher power RFA demonstrations the proposed laser will be simplified significantly by the use of a single RFA, as represented schematically in Figure 72. A master oscillator provides a low power narrow-band signal at a wavelength of 1178 nm to the RFA. The RFA is pumped by an ytterbium fiber pump laser. The 1178 nm RFA output is frequency doubled to the sodium D2a wavelength in a resonant cavity using a lithium triborate crystal. The sodium D2b line is then generated as a sideband when the beam passes through an electro-optic modulator.

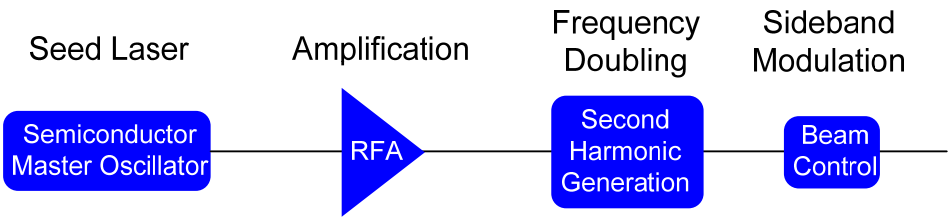

Figure 72: Schematic diagram of the laser

The technologies used for the lasers allow them to be significantly smaller and lighter than lasers of previous generations. The three lasers will each consist of a laser head mounted on the telescope's elevation ring. The laser head will contain the second harmonic generation module, RFA, and electronics for control and diagnostics. The bulk of the laser system will be electronics consisting of the seed laser, pump lasers, power supplies and controller; all mounted in the existing Nasmyth platform AO electronics enclosure (thereby greatly easing the heat removal task). A single heat exchanger cabinet for all three lasers will also be mounted at the Nasmyth platform to support the laser electronics and laser heads and will be cooled by instrument glycol on the telescope.

The infrastructure requirements for the lasers are significantly less than that of the current Keck II dye laser system. For comparison, the three lasers will require a total of 5kW of electrical power as compared to 90kW when all supporting equipments are considered for the current Keck II laser. Removal of the Keck II laser will provide the much needed power to support the entire NGAO system. The lasers along with the entire NGAO system will be provided UPS power to smooth out power bumps that often occur at Mauna Kea. The UPS are not intended to operate the system during longer power outages.

From a cooling standpoint, the combination of the lasers and other NGAO systems will require an upgrade to the instrument glycol system on the summit. The capacity increase resulting from the removal of the Keck II laser will mainly impact the facility glycol system and not the instrument glycol system on the telescope where increased cooling capacity will be needed for NGAO. To remedy this deficiency, the plan is to tie the Keck I and II instrument glycol system together. The Keck I system was upgraded during the Keck I LGSAO project. By tying the two systems together, some level of redundancy is also provided. The cost of merging the systems is significantly less than installation of a new facility in Keck II.

Laser control is done via a standard Ethernet network using the TCP/IP protocol. A laser controller server will be implemented to communicate with the lasers. Through this interface, the controller can initiate startup, shutdown, and monitor and collect internal diagnostics such as laser power, pump powers and currents, temperatures, diode performances, and overall system status. The lasers are equipped with internal self checks to warn users of impending problems prior to failure.

In addition to the network port, each laser will have a hardware port to the safety system. The safety system can override any software commands by shutting down the laser or closing of the laser output shutter. Laser system safety is improved by the use of fiber technology. Laser radiation is contained within the laser components except for the exit window port.

3.4.1 Laser Enclosure

For reference, the Keck II telescope including the existing AO and laser enclosures and laser launch tube are shown in Figure 73.

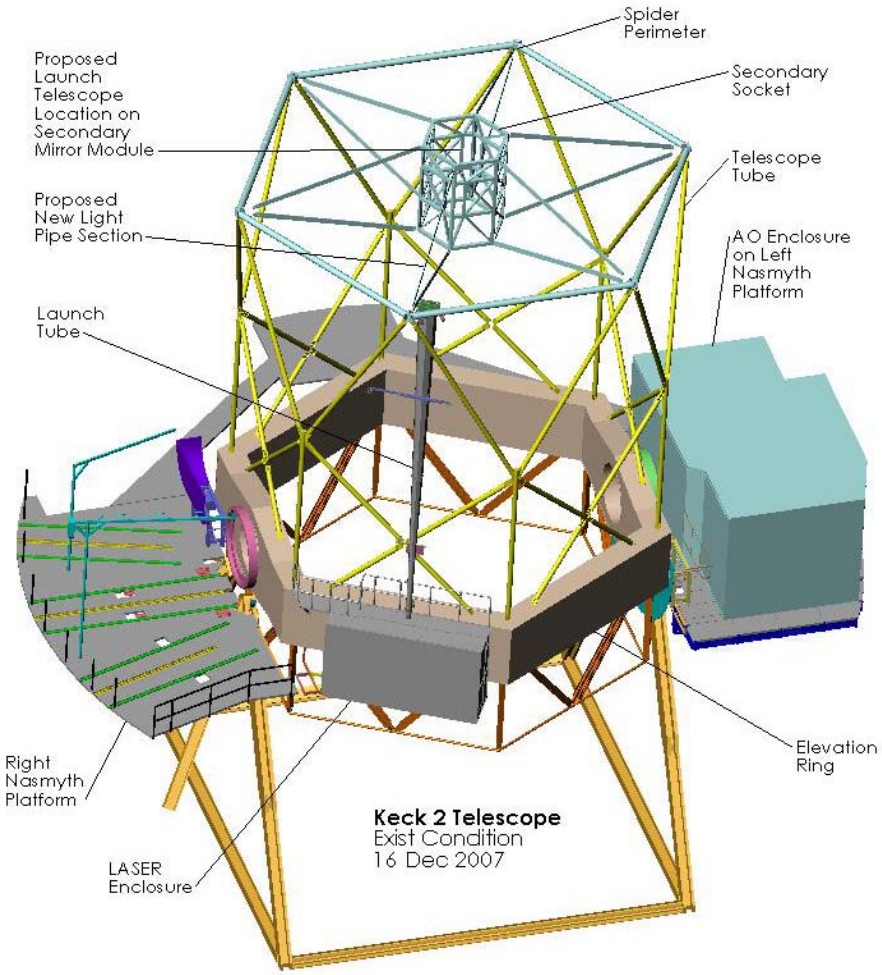

Figure 73: Existing Keck II Telescope and Laser Enclosure.

The use of fiber laser technology in the TOPTICA/MPBC design allows the laser to operate in a moving gravity vector environment as shown in Figure 71. This makes it possible to install the laser heads on the elevation ring structure similar to the Keck II dye laser table in the existing Laser Enclosure. The re-use of the existing laser enclosure will greatly minimize the cost associated with delivering a new enclosure. Infrastructure support such as electricity, pneumatics, and glycol are all readily available in the enclosure. The enclosure also has existing safety system infrastructure to support a class IV laser. Interfaces such as Ethernet, phone and video monitoring already exist and will not have to be designed. The TOPTICA/MPBC laser heads are also sealed and insulated; it has its own internal environmental controls via its heat exchanger. This minimizes the need for an environmental control system within the laser enclosure. The current Keck II laser enclosure does not have an environmental control system.

Mounting of the laser heads on the elevation ring also greatly simplifies the Beam Transport System design. Figure 74 shows a front and right side view of the existing laser enclosure with the three laser heads (yellow) mounted. Personnel enter the laser enclosure via a door on the left from the Left Nasmyth Platform when the telescope is rotated to the zenith position. There is ample room in front

of the laser units and switchyard for servicing. Only the laser heads will need to be located in this enclosure, as the pump lasers, seed lasers, and the controllers are located in the AO electronics room on the Nasmyth Platform. No additional volume is needed in this enclosure for the lasers as all electronics are enclosed within the laser heads. The distances between the enclosure and the pump lasers have been factored into the existing laser design.

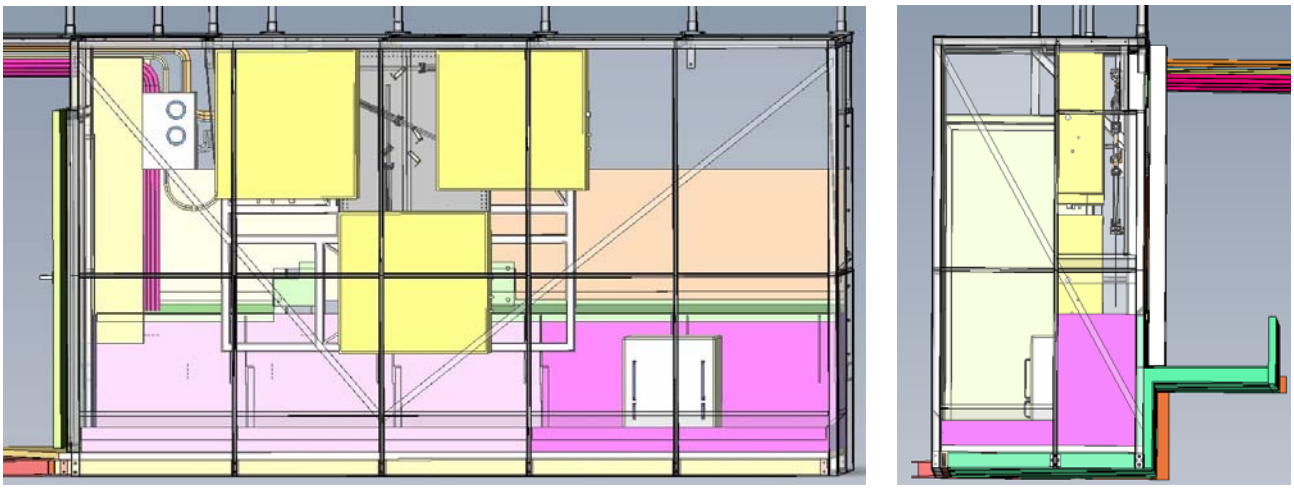

Figure 74: Laser enclosure with laser heads mounted

The right side of the enclosure will be reserved for electronics to support motion control, environmental sensing and safety system infrastructure. The three laser heads are oriented around the optical bench of the SYD where the beams will be formatted and sent to the BTO. To support the SYD and the laser heads, a rigid frame (Figure 75) will be fabricated similar to an existing unit used to support the Keck II laser table. The frame will be mounted via the six existing contact pads which are tied to structural elements within the elevation ring. The elevation ring itself was stiffened to support the Keck II laser. For comparison, the weight of the new systems will be half of the original Keck II laser table system.

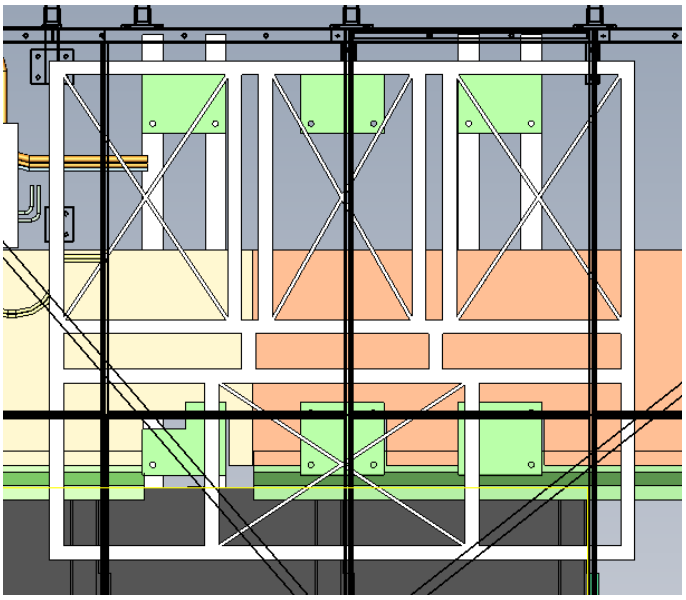

Figure 75: Laser head mounting frame

The delivery of the lasers will likely be in phases with the delivery of the initial laser and subsequent two lasers to follow many months later. The design of the existing enclosure allows the outer shell to be removed as a single unit while leaving the floor intact. The laser enclosure shell and the laser table can be removed using the dome's 5-ton crane. The goal is not to require a telescope shutdown (loss of observing) to remove the existing laser table. Once the enclosure shell is removed, the new mounting frame can be mounted onto the existing pads. The roof of the enclosure shell will be modified to allow installation and removal of subsequent laser heads without the need to remove the entire enclosure.

3.4.2 Laser Launch Facility Optical Design

From the lasers, the beams will travel to the SYD (Figure 76) in the LLF. The SYD formats the three laser beams and sends them to the BTO in a compact volume. In case of a single laser failure, the SYD includes opto-mechanics to split one of the two remaining lasers into two beams to replace the output from the failed laser. This results in one full power beam and two half-power beams. In order to account for flexure, vibration and beam wander due to turbulence in the beam path, each laser beam will include a fast piezo tip-tilt stage. Position of the beams at the BGS is maintained by position sensors which form a feedback control loop with these tip-tilt stages. Polarization control is also available at the SYD to modify the laser's native linear polarization to project a circular polarization from the LT for maximum sodium return. In practice, the motorized waveplate will be set based on optimizing the real time sodium return on the wavefront sensors; but is not expected to change once it is set.

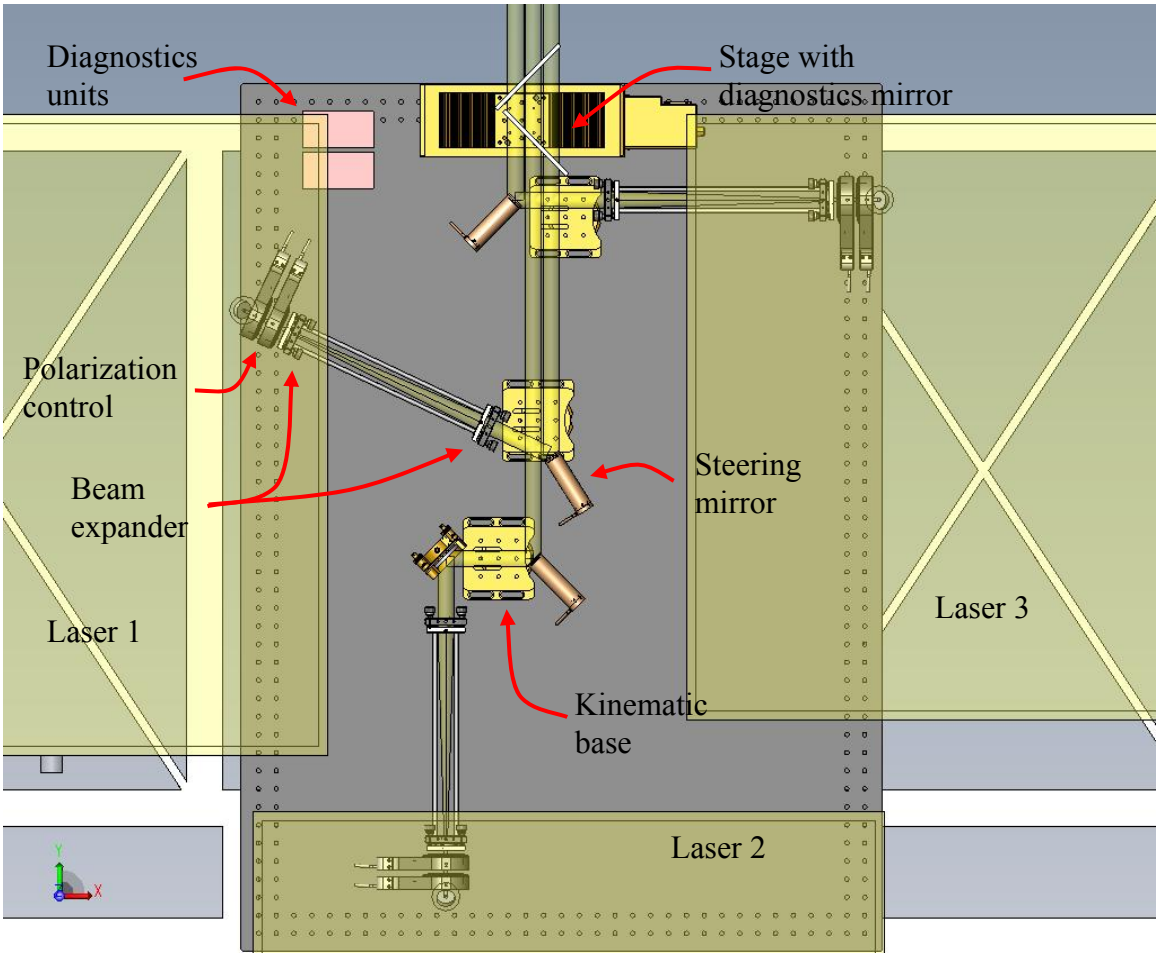

Figure 76: Switchyard opto-mechanical layout

Diagnostics will also be available at the SYD. A motorized linear stage can insert a beam splitter to attenuate the beams for a low power alignment mode in the LLF. The reflected power will be sent to one of three measurement stations selected by the stage position. The three measurements are wavefront error (M^2), polarization state and power.

A window will be installed between the SYD and the BTO interface to prevent chimney effects in the beam tube as the laser beams travel up toward the secondary module. During the PD phase, two designs (short and long relay) were examined for the beams to travel from the laser enclosure to the secondary socket. The short relay design, SRD, (Figure 77) was chosen as the preferred solution since it is a more direct path to the secondary socket as well as providing greater ease of installation and servicing.

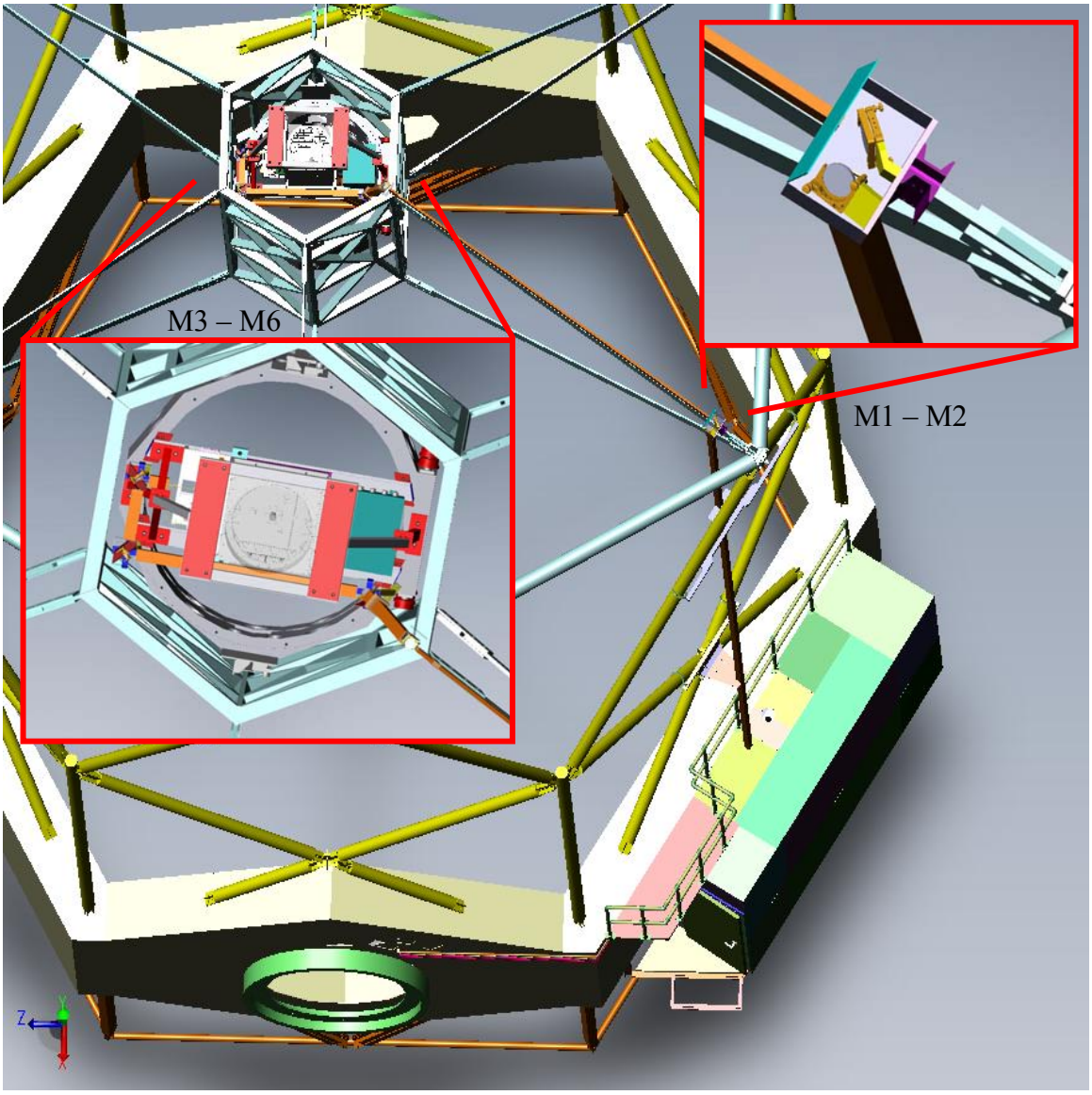

Figure 77: Short relay design

The beams will travel in a similar path as the current Keck II side launched laser up toward the existing output L4 lens location (Figure 78) from the LE. At this corner, two mirrors will jog the beam on top of the spider after which it will enter the telescope fixed hub. There will be a combination of four mirrors, M3 through M6, in the secondary socket to propagate the beam into the BGS. All motion control for the LLF will be in the BGS and SYD, the BTO will not require actively controlled optics according to flexure data taken on the telescope. However, as a contingency plan in case the flexure is larger than expected, the enclosures for the BTO mirrors will be sized to support motion control. The entire BTO path between the LE and the BGS will be enclosed in a rigid tube for safety as well as cleanliness. The tubes will run over the existing telescope spiders so as not to increase existing vignetting. The tube mounting points will be semi-compliant to not induce any mechanical stress on the telescope.

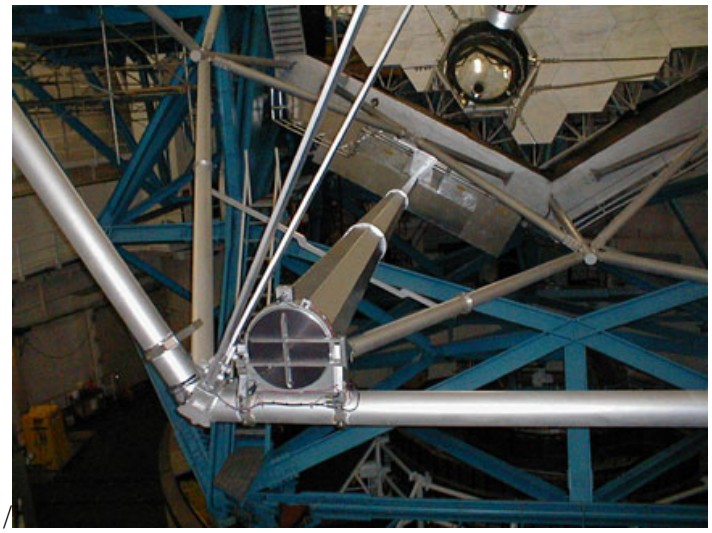

Figure 78: Current L4 beam tube

Prior to entry into the BGS, a section of the BTO will be removable to support servicing of the f/15 secondary module. A kinematic interface shall be provided on M3 (Figure 79) to ensure proper alignment after f/15 module servicing. The path in the secondary module was chosen to fit close to the LT support structure to maximize service accessibility within the f/15 module.

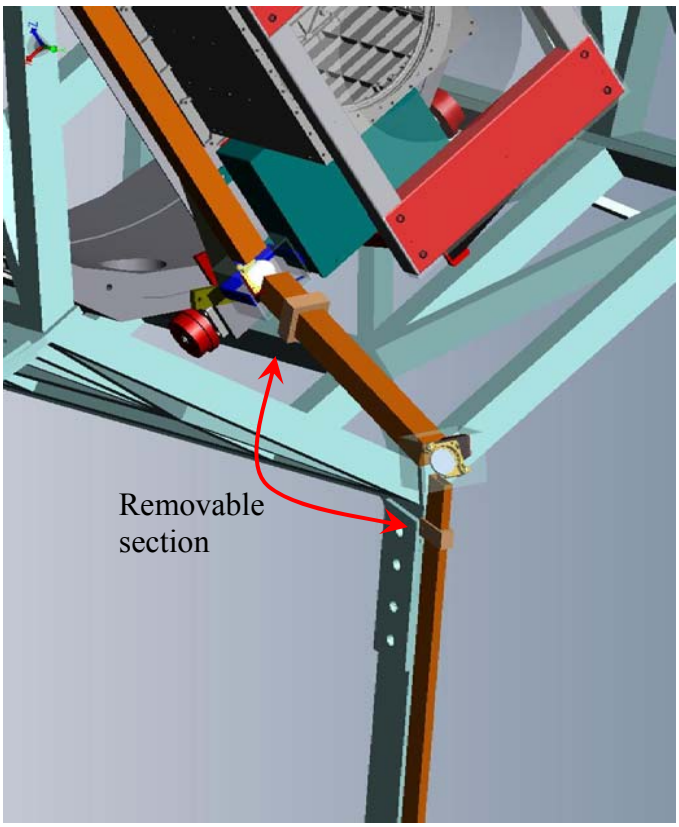

Figure 79: Removable beam tube section at secondary module

In addition to the advantage of a shorter path that minimizes telescope flexure impacts, the SRD offers easier access to its components for installation, alignment, and servicing. The telescope can be lowered in elevation making the components closer to ground level for access. Access can be provided using the JLG (extended boom lift) instead of the man-basket and shutter crane which would be required for the LRD. The current mechanical supports for the existing L4 launch tube can also be reused for part of the BTO structure saving additional cost.

From the BTO, the beams travel to the BGS mounted on the LT (Figure 80); mounting the BGS on top of the LT when horizon pointing allows for easier servicing of the BGS. An iso-view of the BGS is provided in Figure 81 with its protective cover removed. The BGS design has three main components that drive the design choices: the patrolling asterism generator, the central asterism generator, and the beam expander. The patrolling asterism generator requires positioning three beams in arbitrary locations over a 120" field; its design influences much of the rest of the system. For this design the LT input/output beam specifications were taken from the recently awarded contract for the Keck II center launch telescope which are substantially similar to those for the recently delivered Keck I LT.

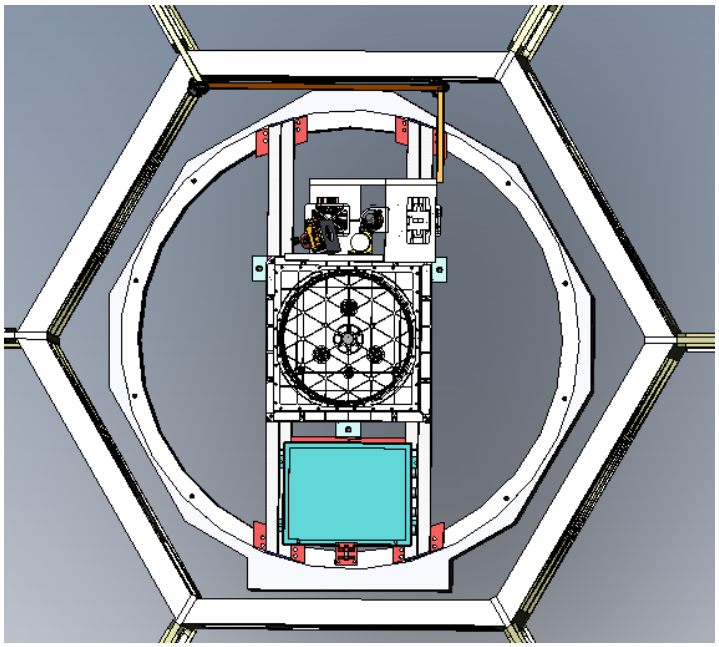

Figure 80: BGS location

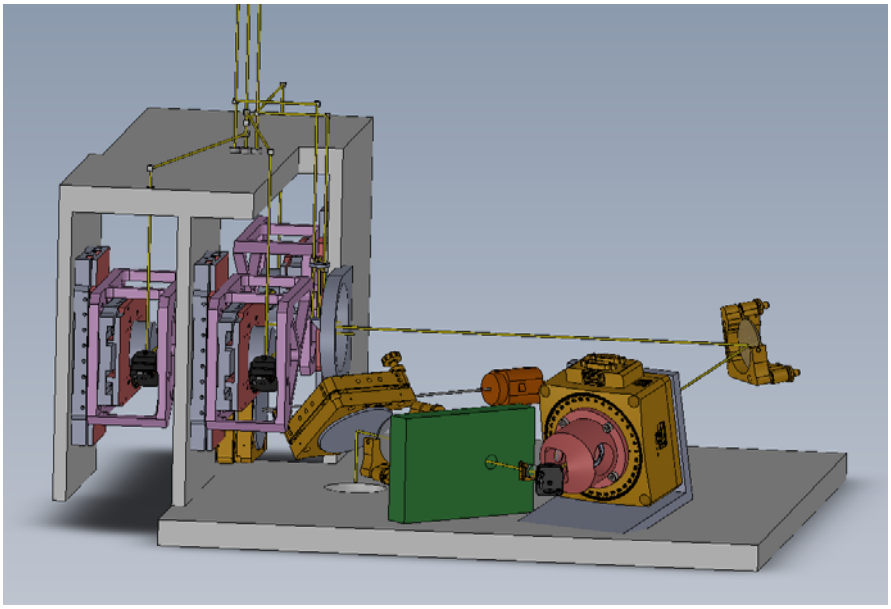

Figure 81: Beam generation system

Two methods were considered to design the patrolling asterism generator (PAG). The PAG must not only position the beam at the desired location in the field, but it must also adjust the angle of the beam such that it is centered on the entrance pupil of the LT. This is shown in Figure 82.

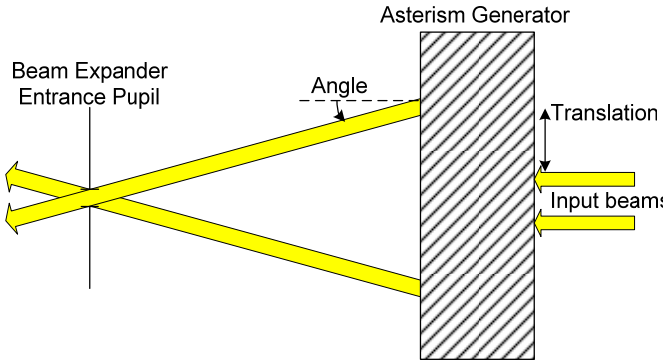

Figure 82: PAG must set both the field position and angle to properly illuminate the pupil

An early concept was to use an actuated tip/tilt mirror at the input to the PAG to steer each input beam to the desired point in the output plane. A mirror split into three segments with independent tip/tilt control would then steer that beam onto the LT input pupil. This concept is shown in Figure 83 .

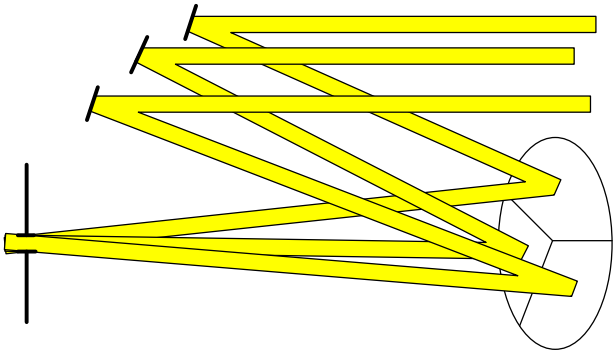

Figure 83: Split mirror concept

This concept has the advantage that all of the control is done by six tip/tilt mirrors, resulting in a reasonably simple, compact system with a minimum number of surfaces that is also light weight. It does not allow arbitrary patrolling beacon placement which is a key requirement for NGAO. To meet this requirement, an alternative two-mirror control using x,y stages was considered. These stages position the beams at the desired field points, while a positive lens then takes these parallel beams and forms a pupil image. A negative lens is included to counteract the power of the positive lens to maintain collimated beams (see Figure 84). From a controls point of view, this method provides a more straightforward implementation. The first method requires synchronization of the two mirrors for each beam to center the pupil on the LT secondary. In the second concept, three separate x-y stages and lenses will be needed to generate the full field PAG (Figure 85). The weight of the patrolling arms is relatively light and may not require the large Newport x-y stage as shown in the figure. Discussions have started with a manufacturer to use a lighter piezo stepping stage with a linear encoder; significantly reducing the BGS mass. Reducing the BGS mass is critical to minimize flexure due to the changing gravity vector. Instead of x,y stages, two rotation stages could be used in a θ,φ arrangement such as used for the LOWFS pickoffs, but this was not practical due to the space constraints in the BGS.

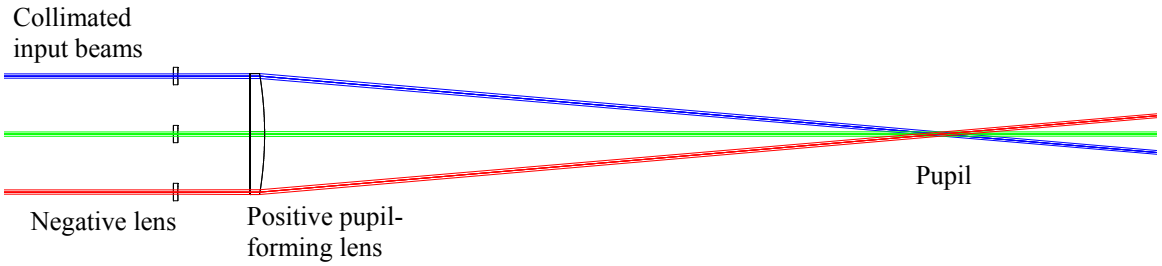

Figure 84: Pupil forming optics

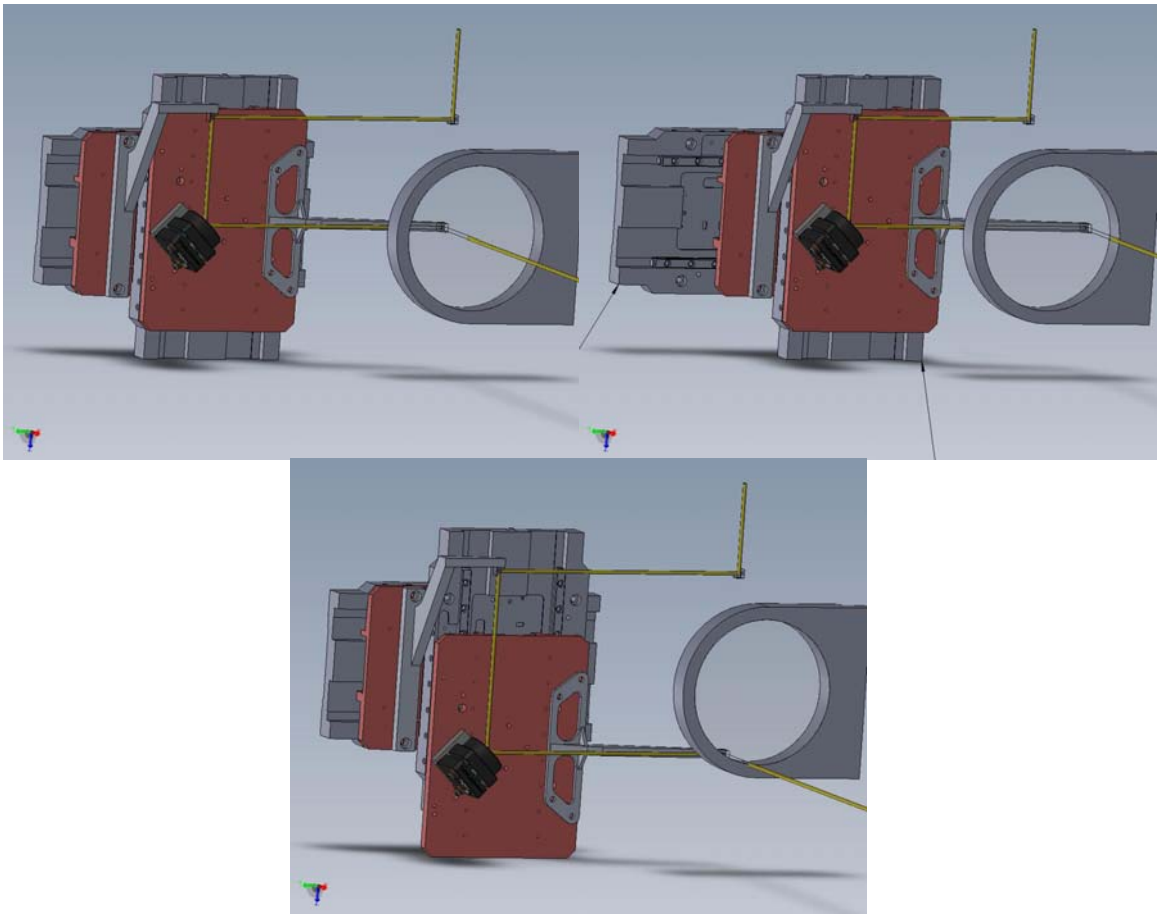

Figure 85: Layout for patrolling asterism generator x,y stages

To split the three laser beams into the required seven beams, a series of beam splitters and mirrors are implemented. For the PAG, a single input beam is split into three parts to generate the three patrolling beacons by using two beam splitters. The first beam splitter has a 33/66 ratio, while the following unit has a 50/50 split. This results in three equal intensity beams. If there are fewer than three patrolling targets, mounting the beam splitters on stages allows sending the unused laser power to the remaining targets as required. To generate the fixed pattern of four beams for the central asterism, a 50/50 beam splitter and mirror is used for each input beam. A set of position sensing devices (PSD) is located at the BGS entrance to ensure proper beam location at the input to the BGS. This position is controlled using the tip-tilt mirrors in the SYD. The overall configuration of the input is shown in Figure 86.

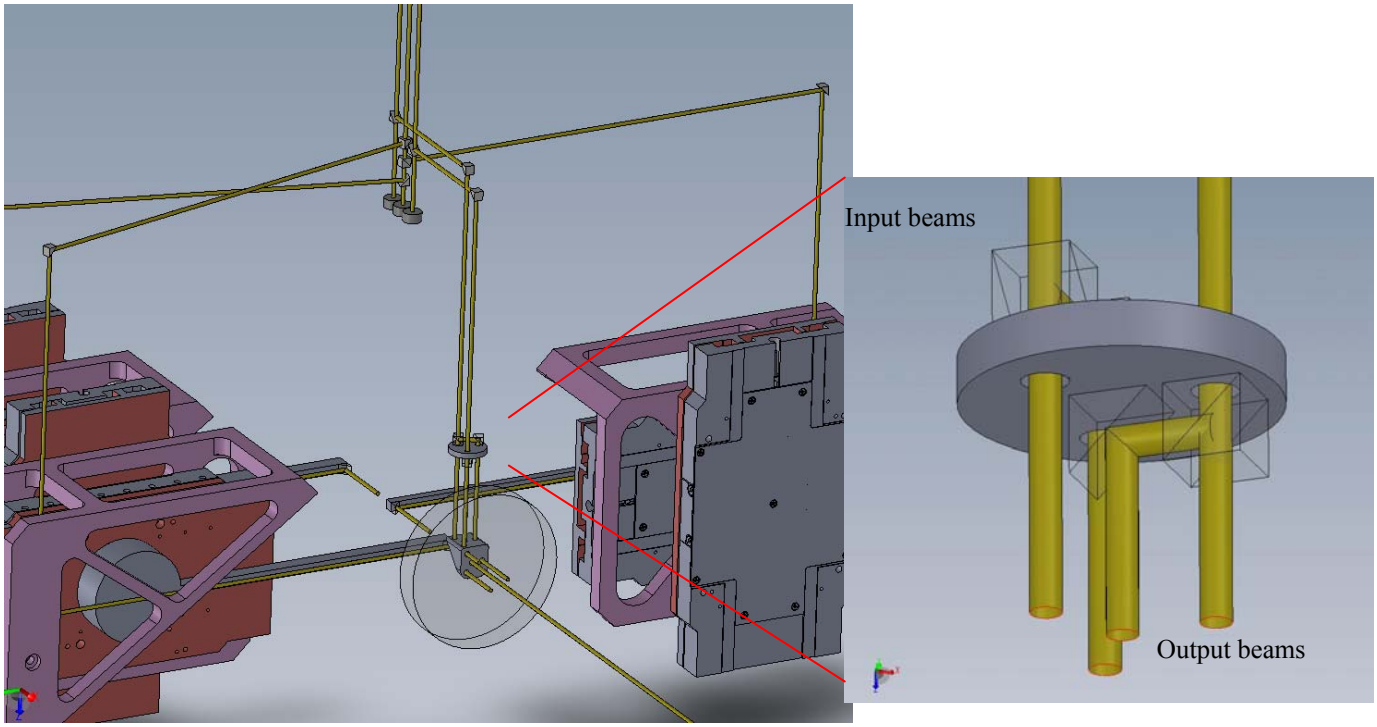

Figure 86: Asterism generation

Subsequent to the asterism generation, a conventional K-mirror rotator will correct for field rotation to maintain the asterism alignment with the wavefront sensors on the AO bench. It will be placed as close as practical to the pupil formed on the global tip/tilt mirror to minimize its physical size. Due to the small size of the beam pattern at this location, the K mirror can be machined from one solid block of material to maximize stability and minimize alignment requirements. Figure 87 shows a conceptual model of the K mirror assembly mounted on a Newport rotation stage.

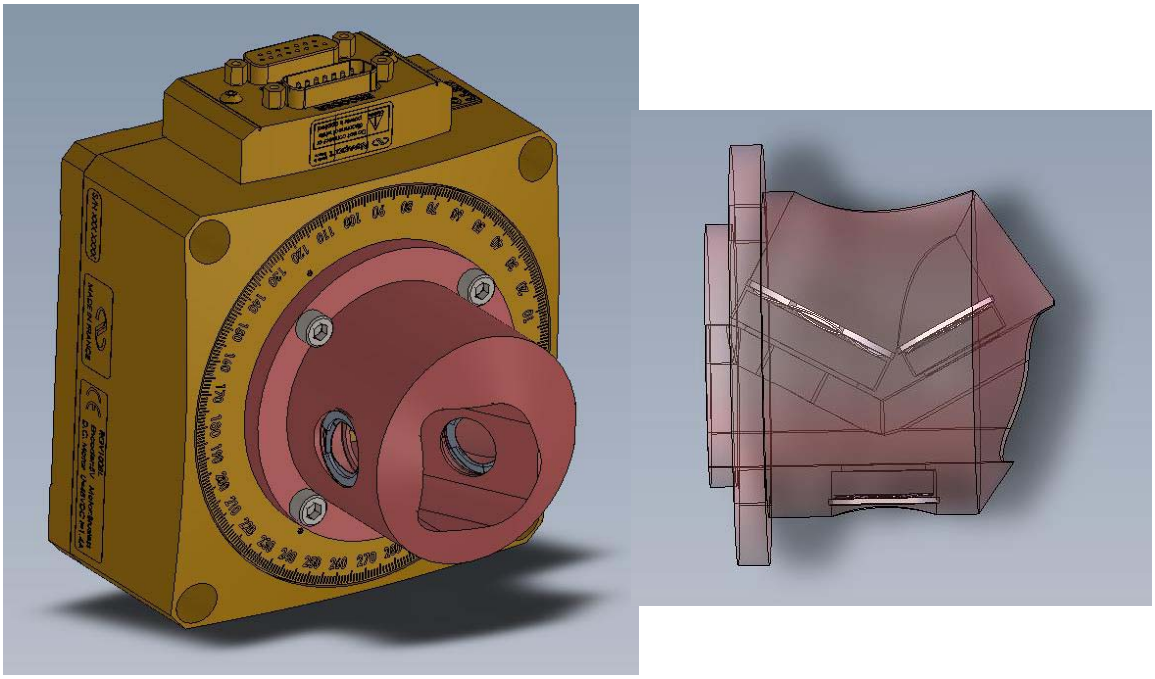

Figure 87: Image rotator

After the rotator, a beam expander is used to expand the laser beams to the required 28.8mm $1/e^2$ diameter beam at the input to the LT. To simplify the steering mirror requirements, a Keplerian telescope layout was used to form a real pupil. The real pupil image allows steering the entire laser constellation with a single tip/tilt mirror without causing pupil misalignment. Without the real pupil image, two coordinated tip/tilt mirrors would be required to maintain proper pupil alignment while steering the asterism. This steering capability is used to correct for flexure and other pointing errors. To produce a compact system, a refractive beam expander design was used with only two elements to maximize throughput.

The Keplerian topology creates a real focus inside the beam expander which is a concern with high power laser systems. The lasers used for the NGAO system, however, are CW which significantly reduces the peak power. The expected peak power density is 2.1×10^8 W/cm^2, which is approximately two orders of magnitude lower than where air breakdown effects are expected to start[1] at 1×10^{10} W/cm^2. If possible, a risk reduction using a comparable CW laser during the detailed design phase to confirm the absence of air breakdown would be beneficial. If breakdown is a problem, the beam expander will be redesigned to use a Galilean telescope layout, and a second steering mirror added to provide the necessary degrees of freedom to properly steer the beam while maintaining pupil alignment.

The finished preliminary design for the beam expander results in an rms wavefront error that varies from 19.0 nm on-axis to 33.5 nm at the edge of the 60 arcsecond field.

The BGS will include a camera to ensure the beams in the generated asterism are at their proper locations. This camera provides position feedback immediately prior to the beam entrance to the LT,

[1] P.X. Tran and C.M. White. Optical Characterization of the Laser-Induced Spark in Air. U.S. Department of Energy Memorandum, retrieved 10/18/2009 from http://www.igrant.demon.co.uk/PAPERS/Tran2.pdf

which allows a closed loop correction for flexure in most of the launch facility. This will significantly improve the pointing performance of the system as a whole. Other diagnostics in the BGS include power measurement from both the asterism camera and from the PSDs at the BGS entrance. These diagnostics can be used to interlock the laser output shutters, as well as to indicate when the overall system throughput is degraded and optical cleaning is needed. The BGS will also provide a shutter and beam dump.

The final element in the LLF is the launch telescope. During the PD phase, a proposal was submitted to the Major Research Instrumentation Program 09-502 for a new Keck II Center Projected Launch System. The current side launch projection system will be replaced by a center launched system to improve the overall performance of the Keck II LGSAO system. The proposal was awarded in June of 2009. Since then, proposals were solicited from five companies, including the Keck I LT vendor, who have produced similar optical systems. Based on the four proposals received, a down selection was made to two vendors. After site visits, the final vendor was chosen based on performance and budget criteria. A partnership between RC Optical Systems in Flagstaff, AZ. and Pacific Defense Solutions, Hawaii was chosen to provide the Launch Telescope. The proposed telescope design is shown in Figure 88. The team has produced similar optical systems for the military and the Air Force Maui Optical Station (AMOS, Figure 89). The Preliminary Design Review date has been set for July 13, 2010 with the delivery of the system in April of 2011. Due to the proximity of the Maui team, the partnership will also support the on-site integration and testing. The NGAO team is working closely with the partnership to ensure the problems experienced by the Keck I LT are remedied in the new design.

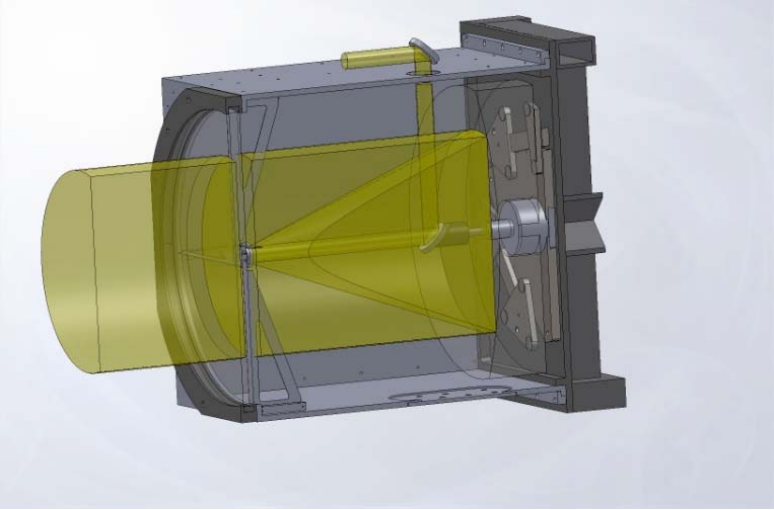

Figure 88: RC Optical's proposed design

Figure 89: RC Optical's 35 kW Laser Beam Director and AMOS Acquisition Telescope

The overall LLF system performance calculations are provided in KAON 686. The goal for the design of the launch system optics was to produce a system with minimal transmission loss and spot size limited only by the atmosphere even in good conditions. This was based on using a launch telescope similar to that used for the recent Keck 1 LGS upgrade. This implies a similar size output beam, from which the output beam Gaussian parameters to minimize the spot size at the sodium layer were determined. Using the mechanical constraints from a conceptual design for the asterism generator, it was then possible to work backwards through the system and determine the required beam sizes. The optical design was then produced to match these desired beam parameters and end in the laser enclosure with a match to the laser beam parameters.

The system throughput has a strong sensitivity on the coating quality and the surface cleanliness due to the number of surfaces. Two cases were examined, one for clean and one for dirty optics (0.5% or 1% degradation/surface depending on location) in the LLF. The number of surfaces is different for the patrolling and fixed asterisms beams so both cases are presented in Table 12. Although the requirement is met for the dirty optics case, periodic cleaning is recommended to maintain the highest possible throughput performance. This results in the need to require durable coatings such as those obtained through Ion Beam Sputtering and mechanical interfaces that will allow easy servicing of the optics. The LLF beam train will also be positively pressurized with dried, filtered air to minimize contamination.

	Throughput		
Asterism	**Requirement**	**Clean Optics**	**Dirty Optics**
Patrolling Beams	60%	85.6%	61.6%
Fixed Beams	60%	85.7%	62.3%

Table 12: Laser launch facility throughput

The spot size at the sodium layer was determined based on the nominal output beam size at the LT. Given this starting beam size, the properties of Gaussian beams define the minimum projected waist size as a function of its distance from the telescope. This also places a limit on the maximum distance at which a beam waist can be placed at. Taking into consideration the resulting spot size for two different sodium layer distances, 85km and 170km (representing zenith and 60 degrees zenith angle), a waist distance of 78km was chosen as a good compromise for spot sizes at all elevations.

Any aberration in the projected beam will tend to enlarge the projected spot from the ideal Gaussian size. To determine the effect of aberrations in the LGSF, a phase screen simulating a random wavefront error was used in Zemax to determine the effect on the spot size (Figure 90).

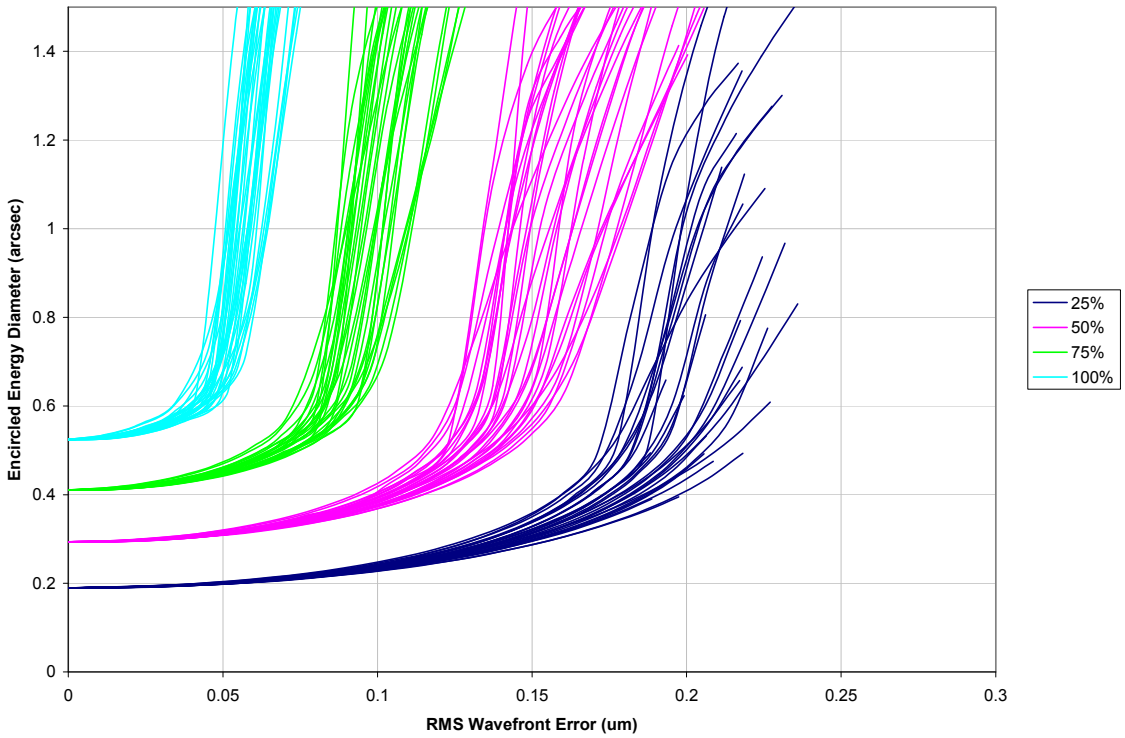

Figure 90: Projected spot encircled energy versus projection optics wavefront error
Each of the multiple lines for a particular encircled energy corresponds to the result for a different phase screen.

The shape of the curves in Figure 90 is due to the fact that the image can be modeled as a combination of the un-aberrated Gaussian spot and a scattered halo from the phase aberrations. As the amplitude of the wavefront phase aberrations increase, more light is diffracted from the core into the halo. For small aberrations, there is much more light in the core than in the halo so the encircled energy diameter is still determined largely by the size of the diffraction-limited core. This holds true until the total energy remaining in the core falls close to the encircled energy threshold in question. After which point, as the aberration is increased further, the encircled energy diameter rapidly grows to include much of the halo.

The current LLF wavefront error, including that from the optics and from the laser itself, is a maximum of 110 nm. This meets the original requirement for a 0.9" spot size without atmospheric effects. As a check, Chris Neyman ran simulations of the up-beam path that included the atmosphere. These were done using the Mauna Kea ridge turbulence model for median seeing conditions. Based on these models, an estimate was determined for the total system wavefront error allowance for the LLT optics (Figure 91). A total value of 110nm rms was selected and is used in the design of the entire launch system. Taking into account the laser wavefront error requirement of 70nm rms, an allocation of 85nm rms was chosen and designed to for the patrolling laser asterism (worst case).

The current laser prototype produces a significantly better wavefront error which will provide additional margin for the LLT optics. If necessary, additional reduction in wavefront error can be implemented by using additional aspheric optical surfaces in the BGS which will increase cost. A further examination will be completed during the DD phase to determine if these remedial steps are necessary.

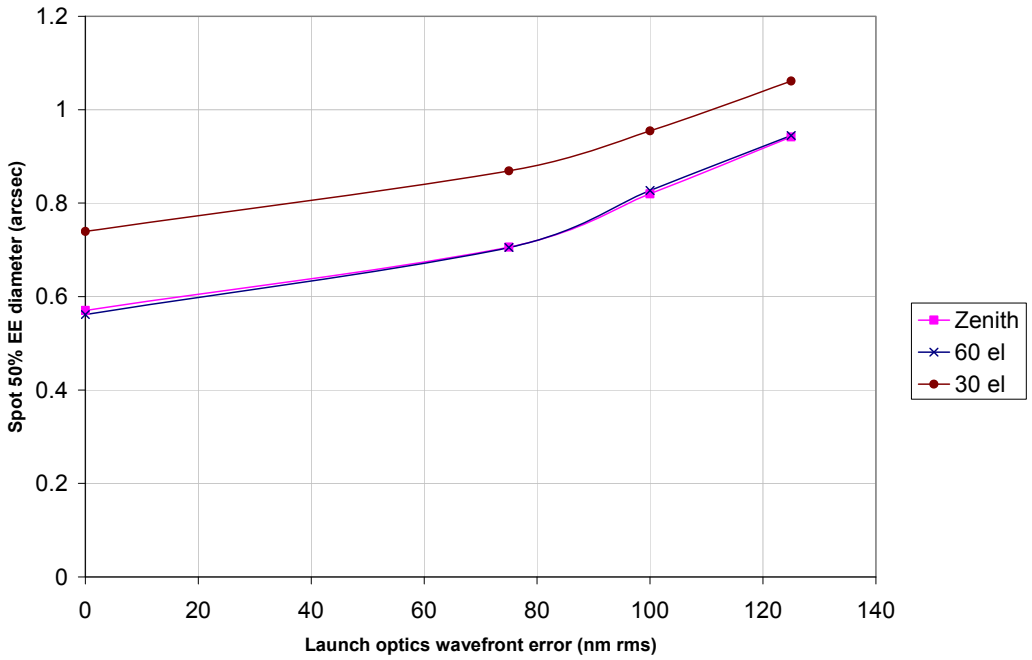

Figure 91: 75th percentile of the 50% encircled energy spot diameter versus wavefront error
Includes atmospheric effects.

Next, the focus of the LLF was examined to determine its impact on spot size. The two largest contributors to focus variations are the distance between the primary and secondary of the LT and the BGS expander optics. The LT impact is mainly induced by the wide temperature swing of +/- 10 °C. In an effort to reduce this impact, the LT primary mirror focal ratio was changed from the f/1 used for Keck 1 to f/1.4. The LT design will include low expansion materials and possibly athermalization based on including small lengths of higher CTE materials at strategic locations to compensate for the expansion of the larger mount components. To reduce this risk further, temperature sensors will be included to allow an open loop focus compensation using the BGS beam expander. To reduce the thermal effects of the BGS expander optics themselves, their mount will be made from Invar 36.

The LLF pointing accuracy (blind pointing) can be divided in two classes, repeatable and non-repeatable errors. The errors can be a combination of flexure, temperature, and alignment positions. Errors prior to the LT entrance can be measured using the BGS asterism camera and corrected in a closed loop. The errors after the BGS such as flexure will be corrected using a look up table based on elevation and possibly temperature or rotator angle.

The first correction loop is a fast tip tilt mirror in the switchyard using the position sensors in the BGS. The use of a single steering mirror per laser will result in a maximum error of 0.27 arcseconds on sky. This error is corrected by the second closed loop pointing correction in the BGS. The

asterism camera and a combination of the BGS global tip/tilt mirror and the patrolling x-y stages will correct any error prior to entry into the LT. The asterism camera itself will have a plate scale of 150 mas/pixel resulting in a 75 mas error if the centroids can be calculated to 0.5 pixel accuracy. As the mechanical design of the BGS develops further during the DD phase, further FEA will be used to determine the overall pointing error.

Since they are after the BGS asterism camera, the LT and the Keck II telescope itself introduce errors that can not be corrected in closed loop. An open loop pointing model will be generated to compensate for these errors as it is currently done for both Keck telescope LGS systems. The current Keck II flexure model incorporates a maximum deviation of about 20" and its performance indicates that the telescope flexure is highly repeatable. The LT pointing requirement is +/- 5" and it is expected to also be highly repeatable, so the combination of the two should be well corrected with a good flexure model. After the laser light is on the AO bench wavefront sensor cameras, a pointing control loop can be closed using their feedback. At this point, the residual error should be determined by the resolution of the stages in the BGS, which are 15 mas for the patrolling beams and 5 mas for the central asterism.

3.4.3 Safety System

The Safety System (SS) will assure the entire LGSF and its components will operate to maintain a safe environment for personnel and equipment. The NGAO lasers are considered Class IV lasers based on their output power. The guidance for laser safety is outlined in the ANSI Standards Z136.1 and Z136.6 Laser Safety for Indoor and Laser Safety for Outdoors. These standards outline the use of control measures to ensure personnel and equipment are protected against hazards.

The physical layout of the SS is shown in Figure 92. The heart of the SS is a Programmable Logic Controller (PLC) located in the AO electronics vault. This controller will maintain status and communications with LGSF subsystems and terminate the beam as necessary to prevent unintended laser radiation. To protect equipment and personnel outside the observatory, the SS PLC communicates with the aircraft/spotters detection system, and the Laser System Interface, from which satellite avoidance, laser traffic control system, and the telescope/dome drive control system are interfaced with. These subsystems provide the necessary permissives allowing the laser to propagate outside of the dome environment.

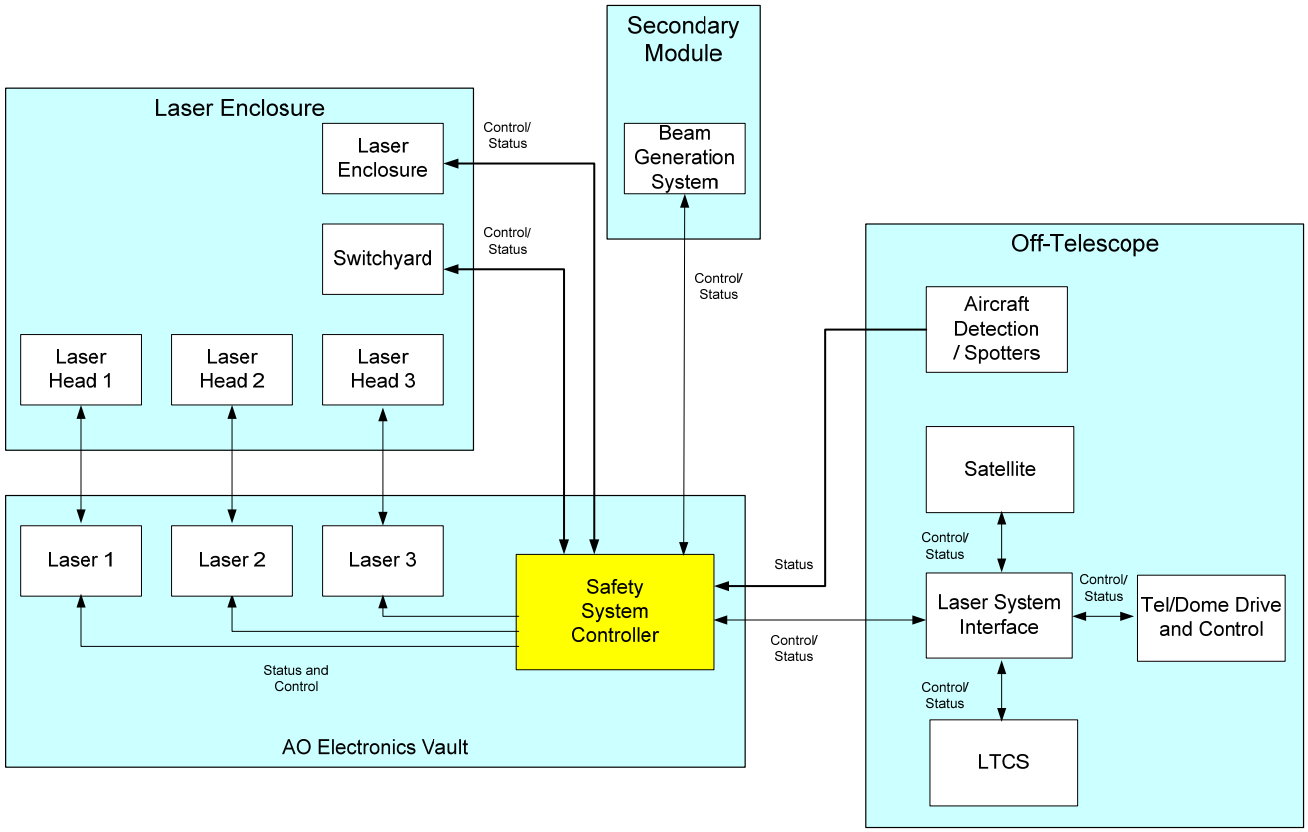

Figure 92: Safety system

The NGAO lasers themselves will be delivered with its own safety measures. The SS PLC will have a direct hardware interface with each laser to shutdown the lasers or close its output shutter. Under normal circumstances, the laser will be controlled by the Multi-Control Sequencer via its TCPIP connection; the SS will only command the laser to shutdown or close its shutter due to an unsafe condition. The SS will monitor the laser enclosure and LLF environment for irregularities such as the triggering of a smoke alarm. If one is sensed, the SS will shutdown the lasers.

In addition to interlocking the LGSF facility to prevent unintended radiation, the SS will also provide status at each locale where personnel will interface with the laser such as the LE and the BGS. Momentary status indicators are provided to operators prior to opening of enclosures. The enclosures themselves will be interlocked to prevent unintended openings. For subsystem operation and servicing, a bank of switches at the PLC assembly will be implemented. These switches are used to bypass interlocks during low power alignments and in-dome lasing. The switches are also used to prevent laser propagations when the LGSF is not in its proper configuration. An example of this is when the secondary module containing the BGS is removed for servicing.

These interlocking conditions are programmed by ladder logic in the PLC. The NGAO PLC will use the Allen Bradley (AB) SLC500 unit which has a proven record as the Keck I LGS SS and as a cryogenic auto-fill systems for the interferometer at the summit. Leveraging of Keck I LGS SS will greatly reduce the design cost and sparing issues. The layout of the PLC assembly is shown in Figure 93. The PLC assembly will be mounted into a standard 19” rack in the AO electronics vault next to

the laser controllers. It is worth noting WMKO has significant experience programming and testing in the AB RsLogix environment.

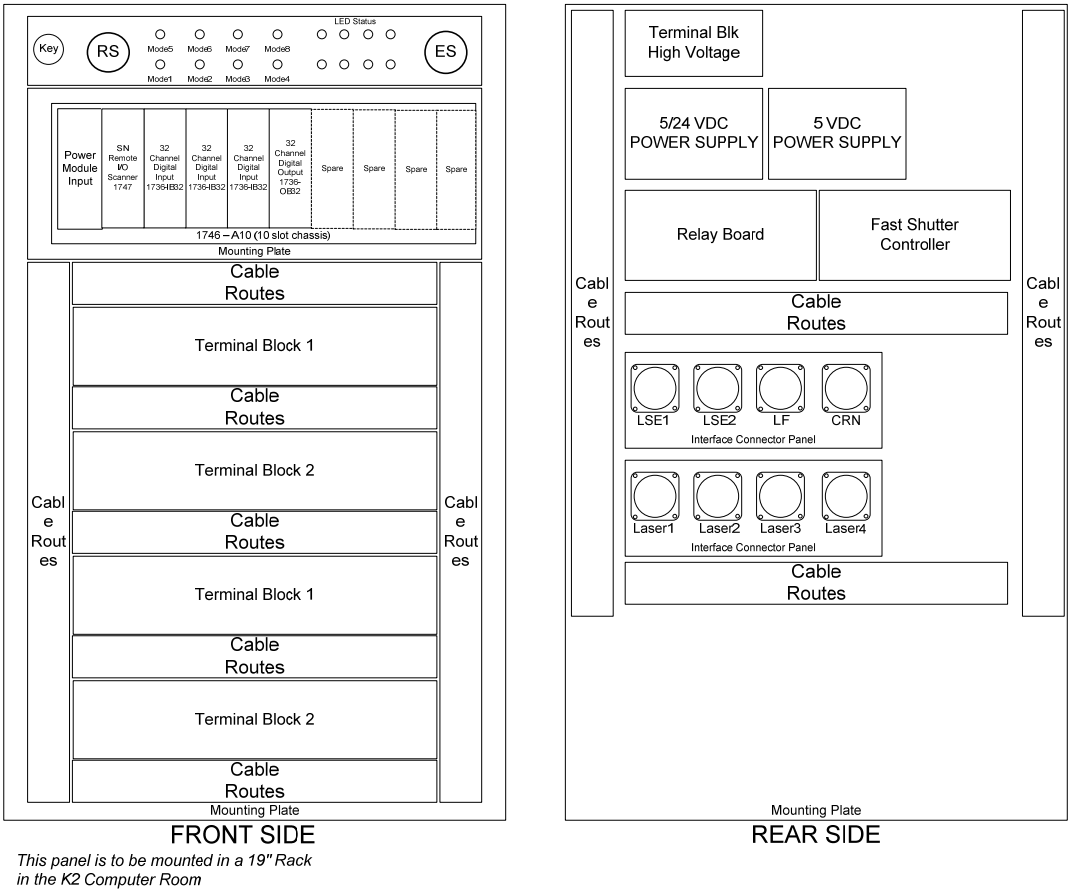

Figure 93: PLC assembly

To support projection of the NGAO asterism outside of the observatory, the SS will receive inputs from the aircraft spotters, satellite avoidance system, Laser Traffic and Control System (LTCS) and the telescope dome drive/control system (DCS). Each one of these systems will provide a permissive to allow the laser to propagate outside the dome. Since Keck has already implemented these systems and protocols for the existing Keck I and Keck II lasers, the subsystems will only need modifications to support the NGAO lasers. The main differences between the NGAO lasers and existing lasers are the use of seven beams in an asterism instead of a single beam. Two methods were considered to account for this difference. The first is to consider all seven beams individually when calculating for laser closure. The second is to treat the seven beams as a cone for the calculations. The second method was chosen due to its simplicity and because the existing keep out zones are sufficiently larger than the asterism cone. This results in minimal change to existing operational parameters.

For satellite permissive, discussions were held with the Laser Clearinghouse (LCH) to determine how best to approach the seven laser asterism. LCH recommended the use of a cone of beams. Although the format of the NGAO lasers are CW and have lower power densities, LCH determined the laser outputs cannot be waived under its guidelines; however NGAO can continue to use the current protocols to support LCH operations.

It is worth noting a risk was brought up during the SDR that LCH closures have increased significantly after a LCH software change in 2007. Since then, WMKO operations team has worked closely with LCH to fine tune the pointing accuracy and Unique Protect List; and have significantly reduced the number of closures (Figure 94).

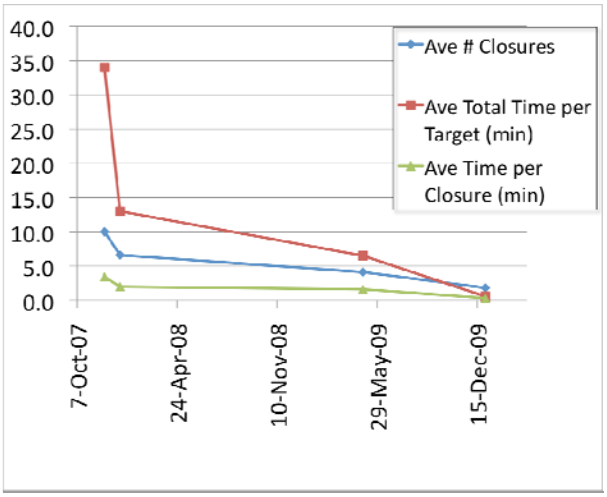

Figure 94: LCH closure rates for Keck II

Aircraft safety for Keck LGS AO observations is currently provided by aircraft spotters as required by the FAA. The NGAO safety system will be designed to use existing engineering controls at the observatory to support aircraft safety. WMKO has been working with the G10-T, a laser safety hazards subcommittee of the Society of Automotive Engineers that sets the relevant aircraft safety standards used by the FAA. This committee is addressing the issue of facilitating a consistent approach to approving control measures. Any benefits resulting from these discussions will also benefit NGAO. Gemini Observatory is developing an all sky camera for aircraft detection that will be implemented as a shared resource on Mauna Kea. WMKO is also testing a transponder system that it hopes will eliminate the use of spotters. Until these measures come to fruition, NGAO will continue to assume the use of spotters. During the DD phase, an application will be made to the FAA to operate the NGAO lasers in the current mode of operations.

3.5 AO Controls

This part of the design manual covers all NGAO controls except for the real-time control (RTC) system. We begin with an overview of the controls infrastructure (section Controls Infrastructure3.5.1), followed by a description of the AO control loops (3.5.2). We then describe the motion/device controls architecture (3.5.3) closing with descriptions for the software controls of the AO (3.5.4) and LGSF (3.5.5) subsystem "controllers" and data server (3.5.6).

3.5.1 Controls Infrastructure

The entire NGAO system can be viewed as a distributed controls system, in which many different components communicate with each other in various client/server or master/slave relationships using possibly several communication networks and protocols. We have represented a high-level abstraction of the NGAO system in the block diagram shown in Figure 95.

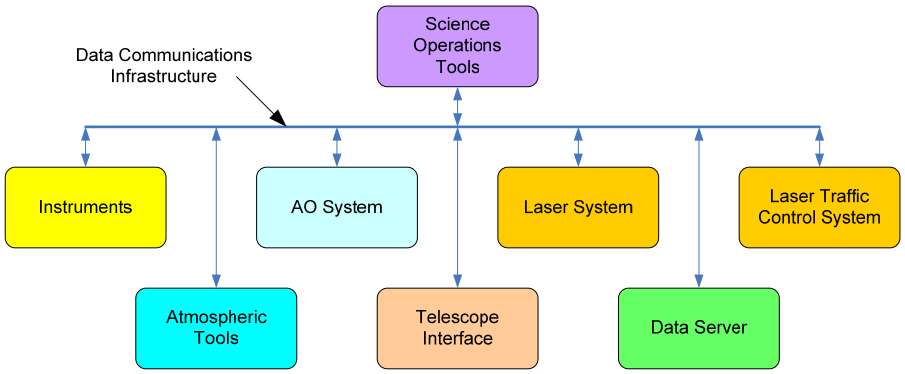

Figure 95: Block diagram of the NGAO system viewed abstractly as a distributed controls system

Each block in the diagram represents a set of control functions unique to a particular system or subsystem that can logically be grouped together. The grouping is an abstraction, as the various functions represented by each block are actually to be implemented using multiple software and hardware components that may also be distributed.

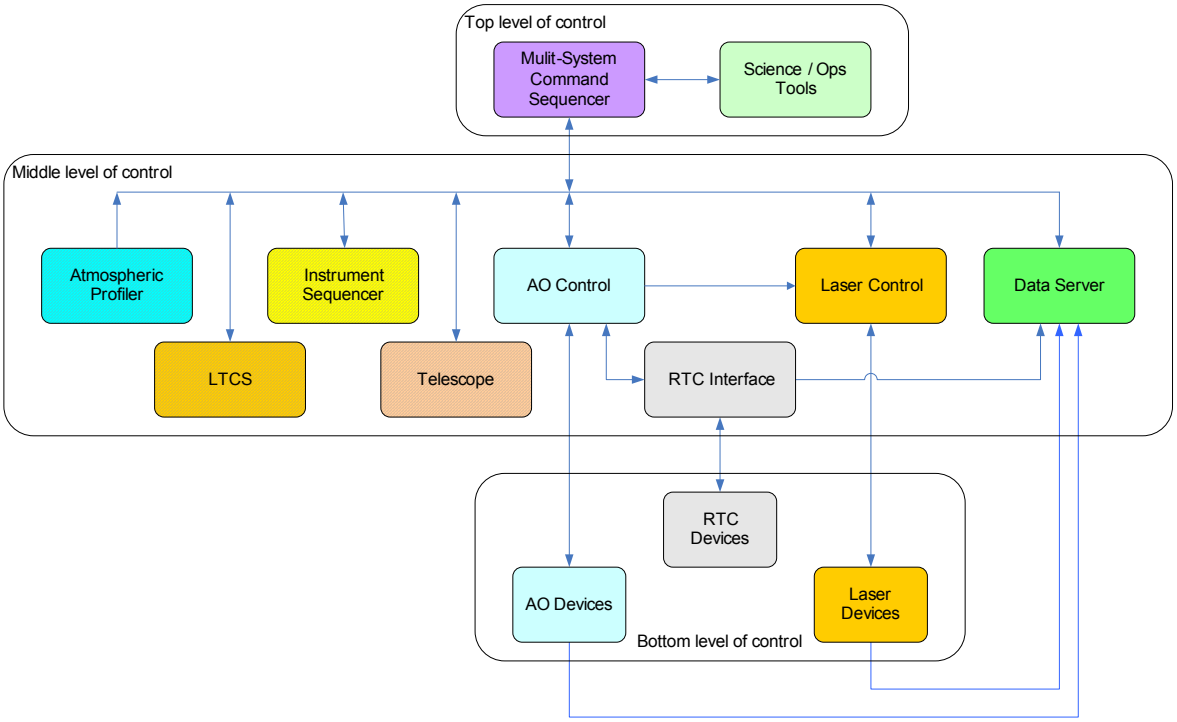

Figure 96: A block diagram of the NGAO controls infrastructure

Figure 96 depicts the controls system as a software hierarchy. At the top level are the main interfaces to the various subsystems (some of these interfaces are referred to as sequences in the diagram). All user commands to the subsystems pass through these top level interfaces. The middle level of the hierarchy represents an abstraction of more complex lower level control tasks, namely the basic

control functions for that subsystem. Users do not access the system at this level except for engineering or troubleshooting purposes. Finally, at the bottom level of the hierarchy are the devices controlled by the control system themselves. The telescope, LTCS, instrument, and atmospheric profile are outside of the direct control of the NGAO system.

The current Keck telescope and AO software and controls infrastructure relies on the EPICS control system middleware, Sun workstations and VxWorks real-time CPUs in VME crates. Since NGAO and an upgrade of the Telescope Control System (TCS) were both in the early design phase we took this opportunity to look at whether options to EPICS might provide a better match to our requirements including ease of development and maintenance. We therefore began the NGAO architecture design process (see KAON 679) by looking at a number of communication middleware packages and software frameworks and also reviewed similar comparisons performed by groups working on the Australian Square Kilometre Array Pathfinder and the ESO E-ELT TCS.

The software architecture we have chosen to build the NGAO controls system uses a framework based on the Advance Technology Solar Telescope's (ATST) Common Services Framework (CSF). We have dubbed this architecture the "Keck Common Services Framework", or KCSF. The KCSF provides the base infrastructure needed to develop a distributed control system. In collaboration with the TCS Upgrade project we will perform one more comparison of CSF versus EPICS to ensure that we have chosen the optimal path for NGAO and TCS by early in the NGAO detailed design.

In a distributed system, components will need to communicate with each other, perform certain actions, and work together in a pre-defined way to form a larger system. The KCSF framework enables this by providing common communications, common data types, common commands and common tools throughout. The solution uses a Component Based Development (CBD) model that supports methods, attributes and properties. The framework provides a kernel API which hides all the details of network access and provides object browsing, discovery and common services. Refer to KAON 671 and KAON 679 for more details.

3.5.2 AO Control Loops

KAON 705 provides a high level summary of the AO control loops used during night-time operation.

3.5.2.1 Devices

Figure 97 provides an overview of the devices used in closed loop operation.

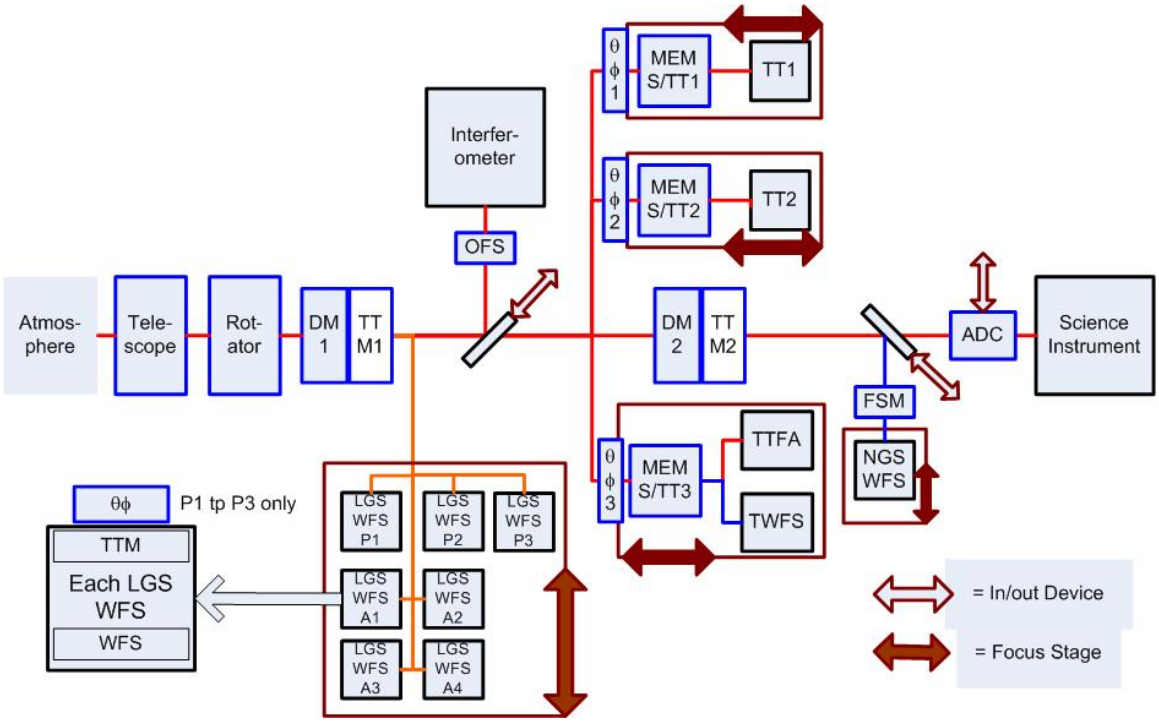

Figure 97: AO device overview.

Here is a brief explanation of each of the devices, proceeding roughly from left to right in Figure 97:

- Telescope. The telescope tracks the science object.
- Rotator. The rotator tracks to keep the field or pupil fixed.
- Deformable Mirror 1 (DM1). The Low Order DM in the wide field relay.
- Tip-Tilt Mount 1 (TTM1). The high bandwidth TTM on which DM1 is mounted.
- Laser Guide Star (LGS) WaveFront Sensor (WFS). There are seven laser guide star (LGS) WFS. The LGS WFS corresponding to the central fixed asterism are labeled A1 through A4. The LGS WFS corresponding to the three patrolling lasers are labeled P1 to P3. Each patrolling LGS WFS is positioned on the corresponding patrolling LGS with a θϕ probe arm (non-tracking). All LGS WFS's include a TTM and a WFS (as pictured in the lower left of Figure 97). The LGS WFS's are mounted on a single tracking focus camera stage (FCS) to maintain conjugation to the sodium layer.
- Interferometer. A dichroic beamsplitter can be inserted into the beam to feed light to the interferometer. The interferometer uses a pair of object field selector (OFS) mirrors (non-tracking) to transmit the on-axis object and acquire an off-axis object (these are controlled by the interferometer).
- Low order wavefront sensor (LOWFS). There are three near-infrared LOWFS. Each is positioned on a NGS using a θϕ probe arm (non-tracking). All three LOWFS contain a MEMS deformable mirror and a fast tip-tilt mirror (MEMS/TT in the figure). The first two, labeled 1 and 2 in Figure 97, have a tip-tilt (TT) sensor. The third LOWFS, labeled 3 in Figure 97, contains a tip-tilt-focus-astigmatism (TTFA) sensor. Co-mounted with the TTFA is a truth wavefront sensor (TWFS) that uses the visible light. All three LOWFS have focus

translation stages (non-tracking) to position them, as a function of field position, conjugate to the science instrument or interferometer focus.

- Deformable Mirror 2 (DM2). The High Order DM in the narrow field relay. This is higher order than DM1.
- Tip-Tilt Mount 2 (TTM2). The low bandwidth TTM on which DM2 is mounted. This is suitable for tracking but not for atmospheric correction. See KAON 669 for more discussion.
- Natural Guide Star (NGS) WFS. A dichroic beamsplitter can be inserted into the beam to feed light to the NGS WFS. A pair of field selector mirrors (FSM) (non-tracking) is used to acquire the NGS. The NGS WFS is mounted on a translation stage to position its focus, as a function of field position, conjugate to the science instrument or interferometer focus. The NGS WFS can be used in a mode where it acts as a TTFA/TWFS type LOWFS.
- Atmospheric Dispersion Corrector (ADC). The science instrument ADC that compensates for atmospheric dispersion as a function of zenith angle and direction. It can be moved into or out of the science path with a translation stage.
- Science instrument. Only one science instrument, DAVINCI is planned initially, although the NGAO system will be capable of feeding a second future instrument. No tracking devices are currently planned in the instrument, but multiple devices (e.g., filter wheels, gratings) will be changeable between science exposures.
- Not shown are the sources that can be inserted on the telescope side of the rotator (via a fold mirror) for alignment, calibration and testing purposes. These are not expected to be required during routine night-time operation.

3.5.2.2 NGS AO Control Loops

Figure 98 and Figure 99 show the control loops used in NGS AO mode with the science instrument and interferometer, respectively.

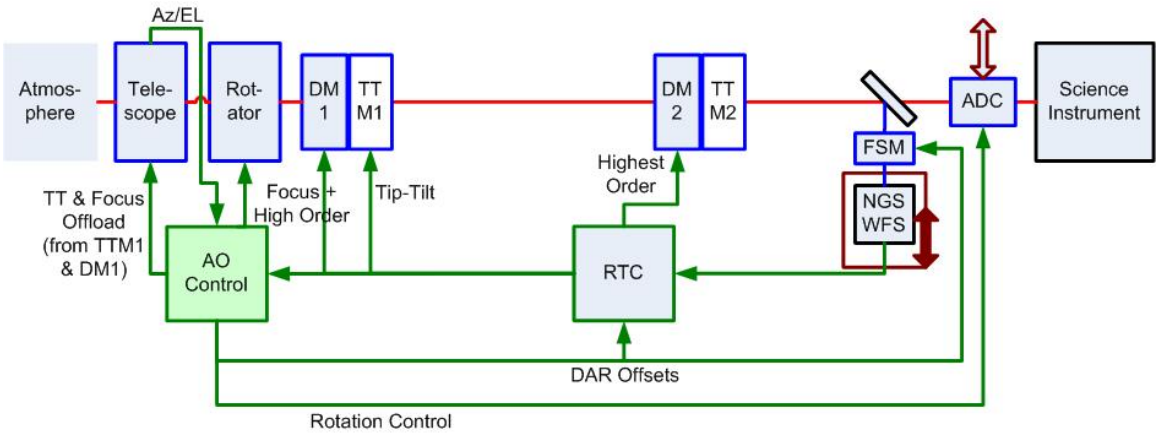

Figure 98: NGS AO control loops for the science instrument

The real-time wavefront sensing is provided by the NGS WFS. The NGS WFS camera data is fed to the real-time control (RTC) system. The RTC computed tip-tilt is sent to TTM1 and the higher order commands are sent to DM1. In the case of the science instrument the highest order corrections can

be applied to DM2 (DM2 is fixed, nominally flat, for the interferometer); these are higher order terms than DM1 is capable of correcting.

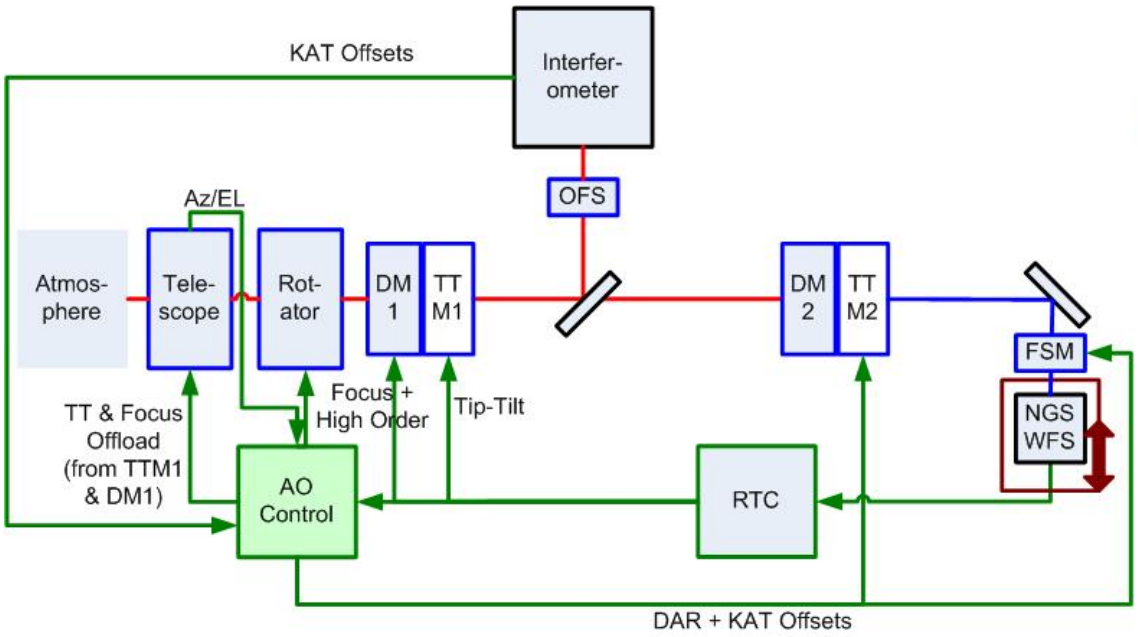

Figure 99: NGS AO control loops for the interferometer

The AO control system keeps track of the tip-tilt applied to TTM1 and the focus applied to DM1. Tip-tilt and focus are then periodically offloaded to the telescope pointing and focus (secondary piston). Telescope Az/El position information is used to make the transformation to telescope coordinates.

The AO control system provides tip-tilt offsets. These are applied to the FSM when the tip-tilt loop is open. For the science instrument case the offsets are used as centroid offsets by the RTC when the tip-tilt loop is closed. For the interferometer case these offsets are applied to TTM2 when the tip-tilt loop is closed. The AO control system computes differential atmospheric refraction (DAR) between the NGS WFS wavelength and the science instrument or interferometer wavelength. Keck angle tracker (KAT) offsets are provided by the interferometer and are combined with DAR offsets in the case of the interferometer. Any pre-measured tip-tilt errors from the ADC rotation can also be included as part of the AO control system provided offsets. Differential tracking can also be handled with offsets.

The AO control system provides position and rotation control for the science instrument ADC when it is in the science path. This control is based on the Az/El of the telescope, the rotator orientation and the science instrument wavelength band. Any tip-tilt errors introduced by the ADC rotation should be corrected via AO control system offsets to TTM2 (based on a previously calibrated lookup table or algorithm).

3.5.2.3 LGS AO Control Loops

Figure 100 shows the control loops used in LGS AO mode with the science instrument. Two "AO Control" boxes are used in the figures for drawing simplicity; these are the same system. Two "RTC Tomo." boxes were used for the same reason. The real-time wavefront sensing is provided by a central set of four fixed LGS WFS, three patrolling LGS WFS and the three LOWFS.

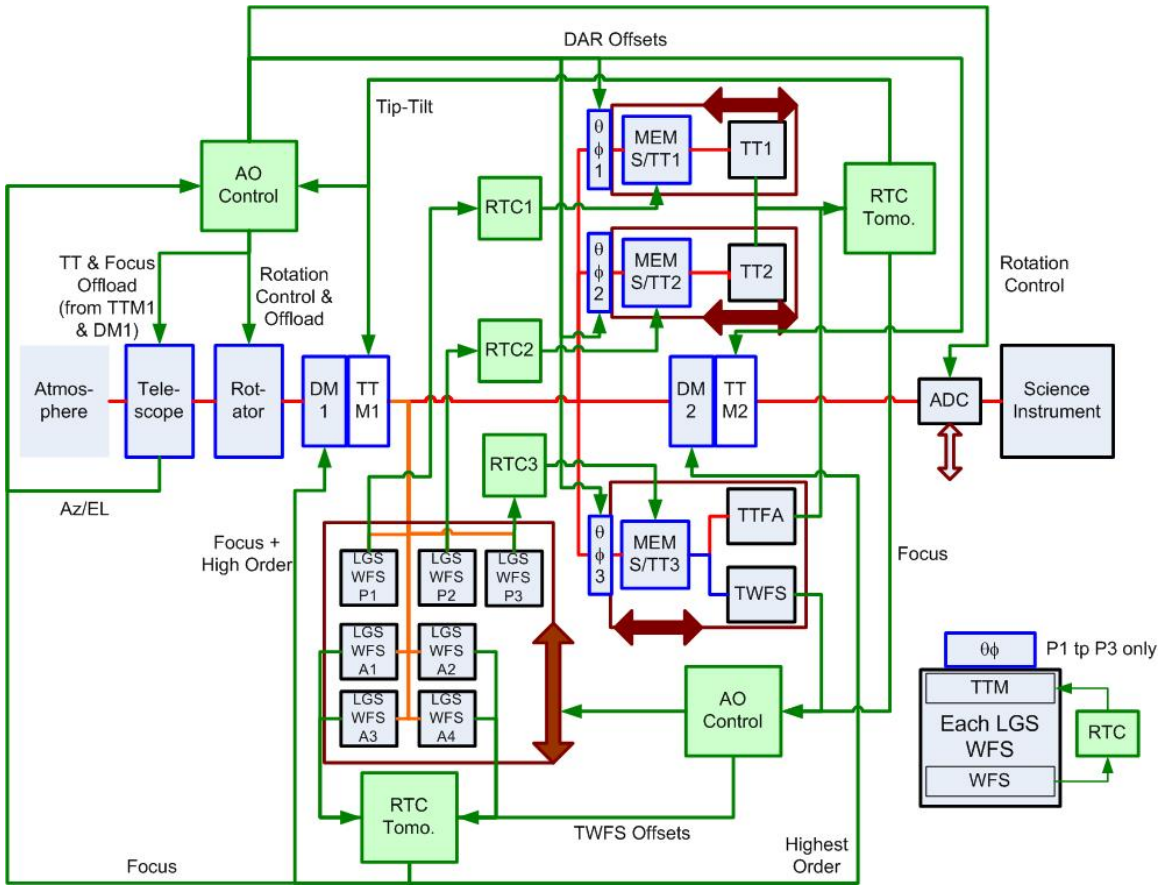

Figure 100: LGS AO control loops for the science instrument

Data from the central fixed asterism LGS WFS and LOWFS are used by the real-time control (RTC) tomography engine to compute the best correction to be applied to the science path. Two options will exist as to how to distribute the science path correction between DM1 and DM2. One option is to apply the ground layer turbulence to DM1 and the high altitude turbulence to DM2. The second option is to apply the lower order corrections to DM1 and the higher order (higher than DM1 can handle) corrections to DM2. In either case DM2 must deal with the highest order terms that cannot be handled by DM1. In the interferometer case DM2 is nominally flat so all of the possible correction must be applied to DM1.

The real-time wavefront sensing data from each patrolling LGS WFS is used to control the MEMS in the corresponding LOWFS via a separate RTC control loop (labeled RTC1, RTC2 and RTC3 in the figures).

The tip-tilt information from the three LOWFS is used via the RTC tomography engine to control TTM1. This information is also used by the AO control system to determine if there is any field rotation; which could be corrected with an offload to the rotator.

Offloading of tip-tilt and focus from TTM1 and DM1 to the telescope is done in the same way as for NGS AO mode. Science instrument ADC control is also the same as for NGS AO mode.

The seven LGS WFS are mounted on a tracking focus camera stage (LGS FCS) to maintain conjugation to the sodium layer. Fast focus information from the TTFA (via the RTC) is used by the AO controller, with appropriate time averaging, to provide a focus correction to the FCS. On a slower time scale more accurate focus information from the TWFS is used by the AO controller to provide a focus correction to the FCS.

The AO control system provides tip-tilt offsets (for DAR, KAT offloads and differential tracking). These are applied to the three LOWFS $\theta\phi$ probe arms when the tip-tilt loop is open. The offsets are applied to TTM2 when the tip-tilt loop is closed (this is different than for the NGS case).

Figure 101 show the control loops used in LGS AO mode with the interferometer. The real-time wavefront sensing is provided by the four fixed LGS WFS and by the LOWFS/TWFS mode of the NGS WFS (the fold dichroic that feeds the interferometer does not transmit NIR light to the LOWFS). Data from the central fixed asterism LGS WFS and single LOWFS are used by the real-time control (RTC) tomography engine to compute the best correction to be applied to the interferometer science path using DM1. The tip-tilt information from the LOWFS is used via the RTC tomography engine to control TTM1.

Offloading of tip-tilt and focus from TTM1 and DM1 to the telescope is done in the same way as for NGS AO mode.

The LGS WFS are mounted on a tracking focus camera stage (LGS FCS) to maintain conjugation to the sodium layer. Fast focus information from the single TTFA (via the RTC) is used by the AO controller, with appropriate time averaging, to provide a focus correction to the FCS. On a slower time scale more accurate focus information from the TWFS is used by the AO controller to provide a focus correction to the FCS.

The AO control system provides tip-tilt offsets (for DAR and KAT offloads). These are applied to the NGS WFS field steering mirrors when the tip-tilt loop is open. The offsets are applied to TTM2 when the tip-tilt loop is closed (this is the same as for the NGS case).

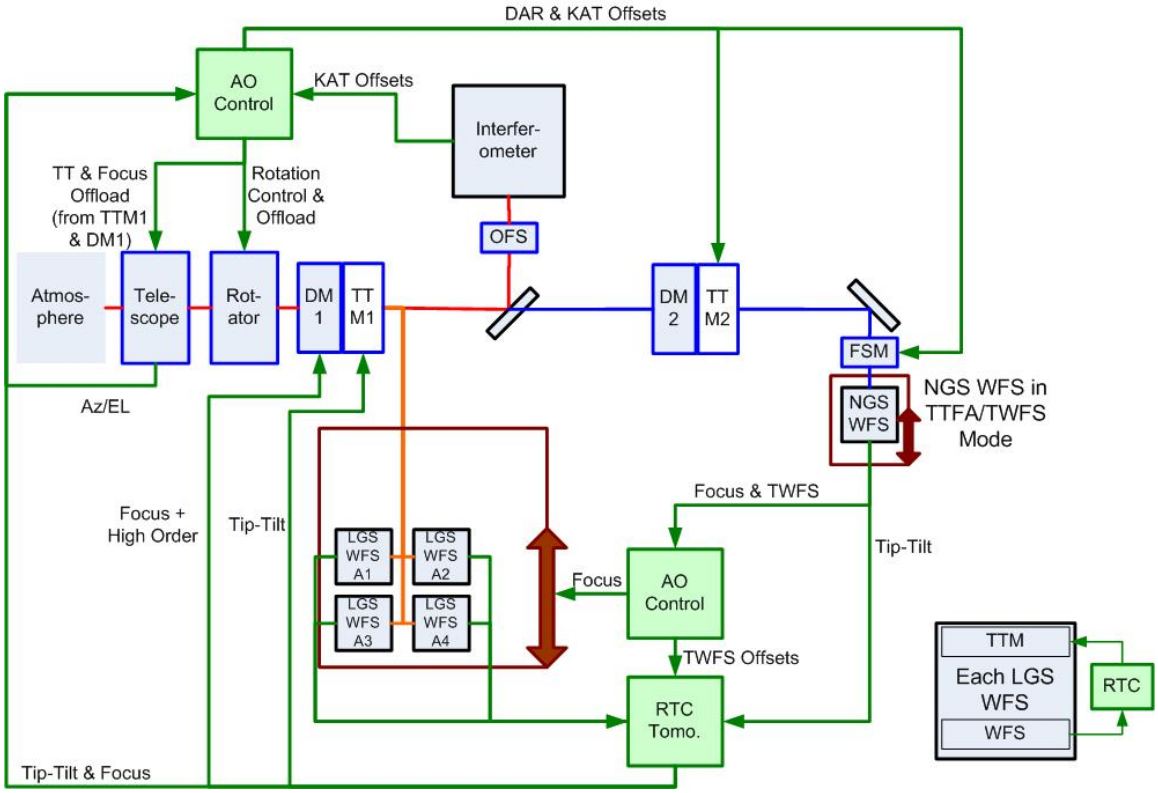

Figure 101: LGS AO control loops for the interferometer.

3.5.3 Motion / Device Control

3.5.3.1 Motion Control Electronics

Approximately 90 moving axes are needed to support the AO and Laser Guide Star systems. There are four primary areas NGAO devices will be located. The devices on the cooled AO bench and those outside of the AO bench (AO Room) will be located on the Left Nasmyth Platform. The devices for the Laser Switchyard will be on the elevation ring. The Beam Generation System (BGS) devices that control the fixed LGS asterism and steering of the patrolling LGS will be in the secondary socket on the telescope.

Components of the motion control system will be required to operate reliably and within specification in the designated environment: -15°C for cold enclosure components, -10°C in other locations, and operating specifications may require derating based on the 4200m elevation of the observatory. In order to preserve the environment, the motion control system must not create EMI, no light pollution is allowable, thermal dissipation must be managed, and the design should minimize vibration. Measures must be taken to protect personnel and equipment from injury or damage, including (but not limited to) e-stops, limit switches, software protections, thermal monitoring and diagnostics.

The motion control architecture will be distributed in nature. The number of devices has decreased significantly as the subsystems have matured, making centralized control more practical, but there are still benefits to a distributed approach.

The concept of a control category, first introduced in KAON 643 (Motion Control Architecture Study), has been used by the controls team to help partition the design. The four categories are described below.

1) Low precision in/out
   - simple in/out devices
   - actuators other than motors (e.g., solenoid, pneumatic, etc.) may be considered
   - switches or hard stops may be used to define positions
   - knowledge of position and velocity while moving, although desirable, may not be required
   - a dichroic or fold, for example, that is either in beam or out of beam
   - moved during configuration, not during an observation
2) Non tracking
   - moved during configuration, not during an observation
   - generally used to position an element for focus or alignment
   - some devices with tight position tolerances
3) Tracking
   - position calculated from and synchronized to external information (telescope az/el, etc)
   - servo loops closed during an observation, update rates from 25ms to 100s of seconds
   - various levels of precision required
   - ADC, rotators
4) Special Consideration
   - coordinated motion with other DOF(s)
   - may be constantly moving during an observation, update rates ≥ 1Hz
   - mechanical design may require the device to servo in position
   - may require a high precision actuator, not a servo motor
   - examples include steering mirrors, tip/tilt stages, and object selection arms
   - pickoff arms require spatial position constraints to avoid collision

3.5.3.1.1 Controllers and Actuators

Servo motors will be controlled via multi-axis motion controllers. Controllers should be capable of performing the conversion between engineering units and encoder units. The ability to define coordinate systems is highly desirable to reduce overhead on the control system. Although a vendor has not been selected, the Delta-Tau PowerPMAC looks to be a good candidate given its programmability and scalability. Equipment will be mounted in standard 19inch equipment racks. Rack mountable equipment is preferred, although equipment with non-standard chassis can be placed on shelves within the rack.

For the lower precision, type 1 devices with intermittent motion, smart motors are recommended. A smart motor is a servo motor with an integrated controller. These devices can be chained together on a single communication port and power supply, providing a significant reduction in cabling. These motors have a NEMA17 or NEMA23 frame, so stages will need to be selected with that in mind. For cases where a smart motor is not useable, a conventional DC servo with shaft encoder will be used. The motor could be either brushed or brushless and depending on the location, a PWM amplifier could be used.

Some type 2 devices may be grouped with the type 1 devices and controlled via smart motor. The remainder will likely be actuated with a conventional servo motor and shaft encoder. The motor could be either brushed or brushless. Assuming electrical noise from PWM amplifiers is managed, linear amplifiers may not be required. Servo loops will be tuned to achieve commanded position within reasonable settling time; performance while stage in motion (following error, damping) is less critical.

Type 3 devices will be actuated with brushed or brushless servo motors with shaft encoders. Assuming electrical noise from PWM amplifiers is managed, linear amplifiers may not be required. However, the torque jitter present in PWM driven loops may not be acceptable and depending on the required performance, dictate the use of linear amplifiers. These devices have more stringent requirements on servo loop performance, including minimal following error.

Type 4 devices require special consideration due to one or more requirements on their performance. These DOF will be actuated with a combination of motors, piezo and voice-coil actuators. Some of these DOF are required to track in some observing modes. Motorized devices may require linear drive amplifiers. Piezo devices may not be suitable for use with a 3rd party controller. OEM controllers are available to match the specific actuator. These are provided with either a digital (serial/Ethernet) or analog interface. In general, these devices will not require a high control bandwidth; tracking is used for flexure compensation and the rates are slow. If higher bandwidth is required, the interface and update rates will need to be carefully considered once the devices have been chosen to ensure that the tracking performance requirements are met. Some of these devices require custom homing sequences to move two more axes in coordination.

3.5.3.1.2 PWM Drives & EMI

Manufactures of servo drives are increasingly making use of Pulse Width Modulation (PWM) to efficiently transmit power to motors. PWM has several advantages and a few disadvantages. Of primary concern to NGAO is the generation of electromagnetic interference (EMI). PWM signals have relatively fast rise times and may be required to switch high currents through long lengths of cable; a scenario that leads to noise. Detectors on the AO bench are extremely sensitive and will likely not tolerate the presence of electrical noise. EMI could also affect analog feedback signals from strain gauge type sensors commonly used on piezo motion stages. The MEMS deformable mirrors may also be susceptible to EMI.

Even with the good cabling design and careful routing with sufficient physical isolation, PWM drives must not be used, or any cabling routed near, any of the various detectors, deformable mirrors or devices with analog feedback.

The architecture does not prohibit the use of PWM drives. In the case of smart motors, the drive signals are extremely short (several cm) which significantly reduces the magnitude of EMI. Many motors are not located near a sensitive device and careful cable design and routing may allow use of a PWM drive. In addition, many DOF only move during bench setup when sensitive devices are idle or could tolerate a slight elevation in EMI without an impact on performance.

When selecting PWM drives, they must be matched to the motor characteristics and, whenever possible, a path for changing to a linear drive should be identified.

3.5.3.1.3 Room for Expansion

The baseline NGAO motion control architecture will budget space for a 10%, or nearest sensible incremental increase in the total number of servo motor axes, beyond what is outlined in the Master Device List. It is acknowledged that some of the devices listed may not be implemented during initial commissioning, however these are included in the design and not considered expansion. The intent is to provide rack space, or if available, crate space for the additional controllers and amplifiers. Depending on the power supply configuration, power will be available or space will be available for an additional power supply. Communication ports will be reserved as well. Given the difficulty of modifying the cold enclosure, the design will make provisions for at least five additional motion cables passing through the enclosure wall. This will likely be a blank panel that is not populated with connectors.

3.5.3.1.4 Support Equipment

The motion control system is required to halt all devices in response to the observatory emergency stop. Circuitry will be required to remove power from the motion control amplifiers. Recovery from the e-stop event will be faster if the encoders and limits remain powered; re-initializing the devices would not be necessary.

Some digital inputs and outputs will be required to control and monitor the status of the motion controllers. Inputs will be required to monitor the health of the controllers. Outputs will be required to reset a controller.

Controllers will be connected to the Ethernet, either directly or via a protocol converter if their native protocol is RS-232 or USB.

Some controllers will need an analog setpoint and provide analog position feedback. Depending on the required bandwidth, either an Ethernet ready analog I/O module, an analog output from a motion controller or PLC, or an analog card in a control computer will be required.

Remote control of the power feeding servo amplifiers and motion controllers will be included.

3.5.3.1.5 Cabling

For servo motors, a generic two DOF cable will be designed. This will provide the primary connection between the motion controller distribution panel and the motion axis. It is envisioned that the cable will have Mil-spec connectors on each end with conductors sized according to the demands of the motion axes. The length of this cable will be a function of the source and destination. The intent is to include cabling in the NGAO 3D model in order to avoid excess. Breakout cables will be required at each end of this cable to connect the distribution panel to the motion controllers and to convert the circular connector to the axis specific connector at the stage. This scheme will need to be adjusted for brushless motors to accommodate the additional phase and sensor conductors.

Non-servo stages will have different requirements that may not allow more than one DOF per cable. This will be evaluated on a case by case basis. The goal is to reduce the number of individual cables and connectors as much as possible, while maintaining reliability and serviceability.

3.5.3.1.6 Location of Equipment

The proposed architecture places controllers in the AO Electronics vault and the Laser Service Enclosure. The use of smart motors puts some control on the AO bench.

The planned layout of the AO Bench, AO room and Electronics vault is shown in Figure 102. Although a single block is shown for the servo controllers, this may not reflect the final hardware implementation with all DOF on a single controller.

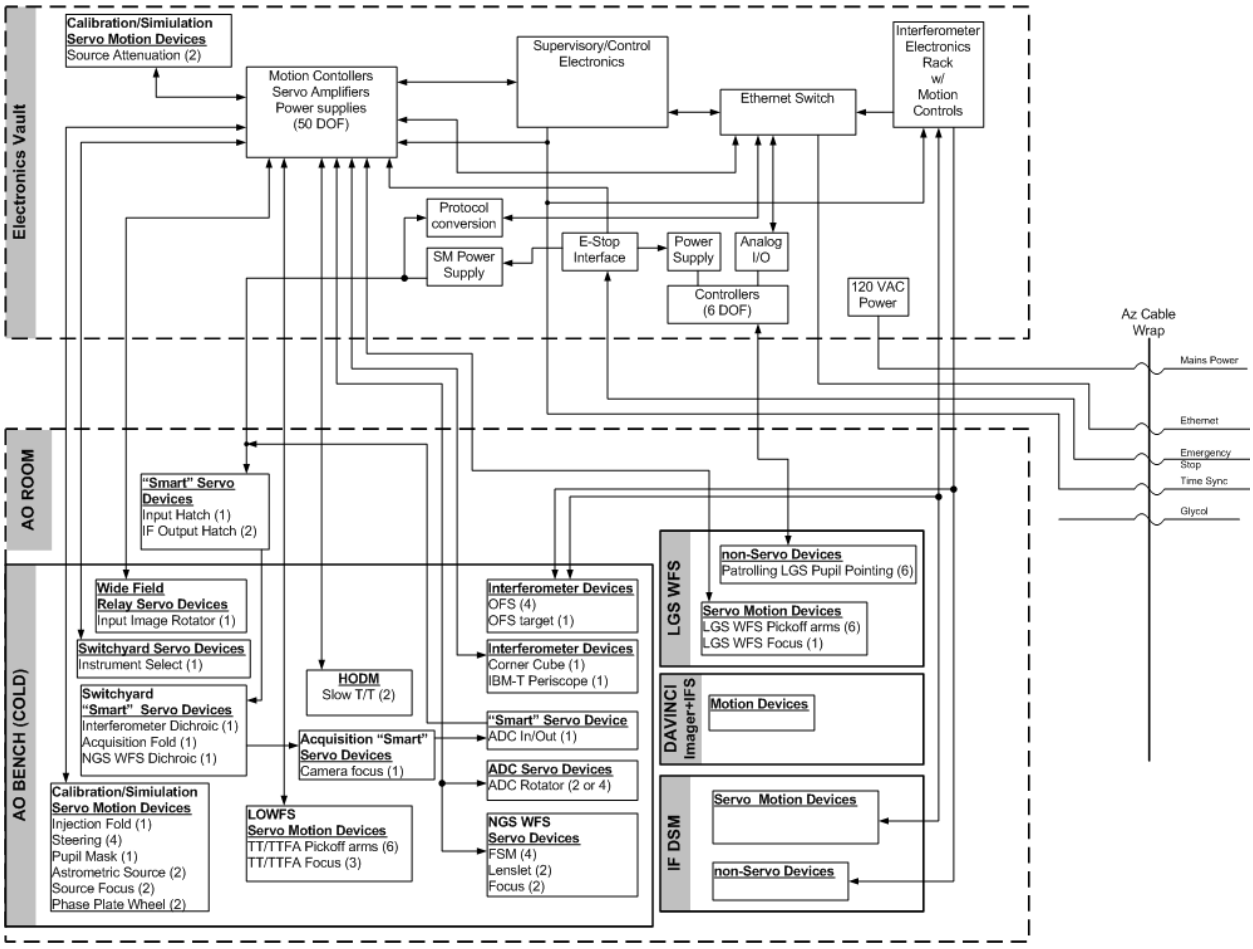

Figure 102: AO Motion Control Layout

Controllers for devices in the laser switchyard and beam generation system will be located in the Laser Service Enclosure (LSE), as shown in Figure 103. This helps by shortening the cable run and does not require significant use of the elevation cable wrap. This approach will also simplify integration of the laser switchyard devices. Cabling between the LSE and secondary should be designed to include two or more devices per cable, where possible. This architecture is quite feasible.

The present LSE design will accommodate the volume of the equipment and glycol cooling that is already required.

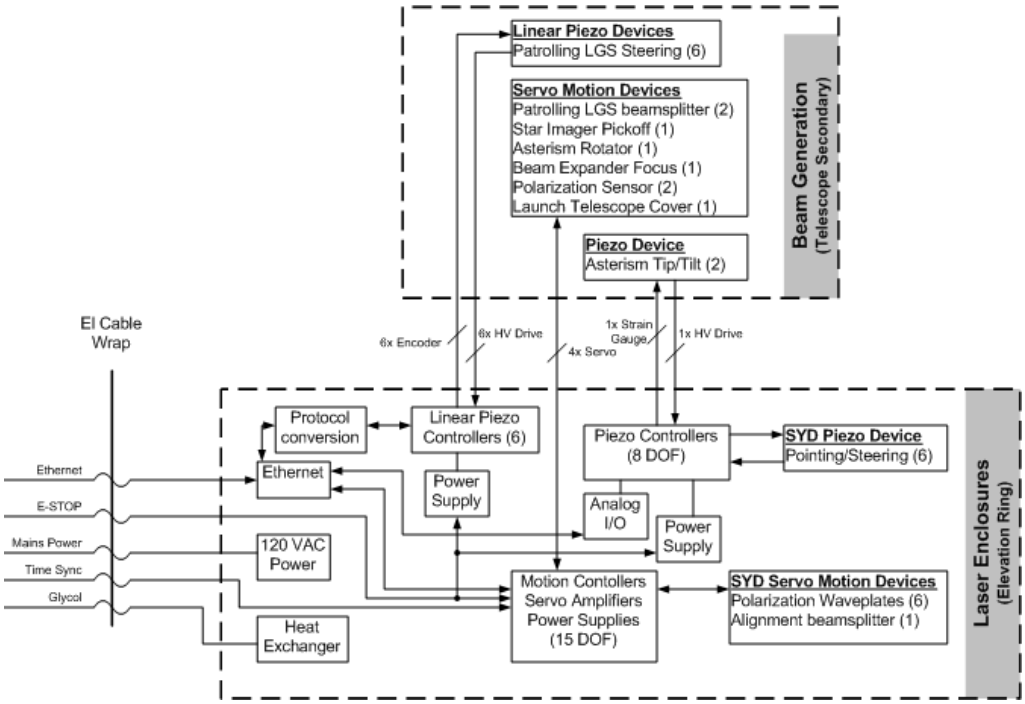

Figure 103: Laser Motion Control Layout

For more details on the motion control hardware, refer to KAON 715 and KAON 643.

3.5.3.2 Motion Control Software

The low level motion control functions consist of one or more device drivers that implement an API for interacting with the motion control system to provide the most basic level of control. This device driver will most likely be supplied by the manufacturer of the motion control electronics. An abstraction layer will be added above the low level driver as part of AO Controls. This layer would hide all the hardware specifications and implementation of the actual motion control hardware. At the top of this control block is a generic state machine that implements the basic coordinated functions required for controlling a motion control device with an arbitrary number of degrees of freedom. This concept is used in the existing Keck AO and Interferometer systems.

KAON 715 identifies all of the current device types / categories required by NGAO. In order from least complicated to most demanding, they are:

- Shutters
- Low precision non-tracking devices
- Medium precision non-tracking devices
- High precision non-tracking devices
- Tracking devices
- Extremely high precision tracking and non-tracking devices
- Coordinated high precision tracking and non-tracking devices

From a software perspective, these are grouped into the following generic categories:

- discrete commanded devices
  - shutters
- non-tracking devices
  - low precision non-tracking devices
  - medium precision non-tracking devices
  - high precision non-tracking devices
  - extremely high precision non-tracking devices
  - coordinated high precision non-tracking devices
- tracking devices
  - tracking devices
  - extremely high precision tracking devices
  - coordinated high precision tracking devices

The intent is to develop each type once and instantiate it for all the necessary devices. This will simplify implementation and allow for quick and easy changes or addition of new devices. Each of these types is discussed in the following sections.

3.5.3.3 Device Control Electronics

Device control is, in general, low speed without tight timing constraints; the commands are frequently single events (e.g., GUI button press) and are expected to be executed on the timeframe of a second. Ethernet will be the primary means of communicating with devices for control. If a device does not have an Ethernet interface, there may be simple Ethernet solutions which exist (e.g., terminal servers to communicate with RS-232 based devices, or digital I/O modules with an Ethernet interface to generate digital I/O signals). This approach has a number of benefits:

- Control can easily be distributed as needed
- Cabling issues associated with centralized control can be minimized
- Solutions based on an industrial computer and real-time operating system, e.g., VxWorks and VME crates, can be minimized to those areas requiring tight real-time control which do not fall under the device control architecture discussed in this document.
- Ethernet-based solutions are easily interfaced to the NGAO control system.
  - To reduce software integration efforts, Ethernet devices should support an industrial protocol (Modbus TCP/IP, Fieldbus, etc) rather than a web (HTTP) based interface whenever possible.

The following is a summary list of all of the common control methods/interface/signal types that will be needed to support the NGAO controls system. For more details on each type refer to KAON 668.

- Remote Power Control
- Camera / Detector Control
- Discrete (Digital) Input/Output
- Analog Input
- Analog Output
- COTS Controllers

- Remote Reset control
- Video
- RS-232 and USB
- Ethernet
- Time Distribution / Synchronization

3.5.3.4 Device Control Software

Under the KCSF infrastructure, the concept of a digital I/O acquisition (DAQ) controller would be built and any component needing to interface to a device would create a DAQ specific controller to match the IDaqDevice interface. In our case we would use the NIDAQ Device Controller. This device controller uses the NI-DAQmx API from Nation Instruments and supports the ICE IDaqDevice interface. The NI-DAQMmx driver supports a number of device types:

- Multifunction DAQ
- Analog output
- Digital input/output
- Counter/timer
- High speed digitizer
- Dynamic signal acquisition

A DAQ Client will run as part of the application and will be responsible for setting up the IO, alarming and reading/writing to the devices via the ICE interface.

Serial and Ethernet interface device types, which are not supported by NI-DAQmx, as well as special camera or detector controls, will be handled independently under the existing KCSF iDevice infrastructure. For more details refer to KAON 679.

Non-motion device control not covered by the above IDaqDevice interface will be described case by case in the following sections. However, they should all be able to fall under the KCSF device infrastructure and be designed with the generic IDevice interface. The IDevice interface allows a device to access the *get, set, execute* and *xxxMonitor* methods which should be able to support the full command set for each device.

3.5.4 AO Control Software

KAON 714 should be referred to for more details for the following section.

3.5.4.1 AO Control Sequencer

The AO control sequence is implemented by the *AOFacilityComposite*, which is the main interface between the various AO controls functions and the rest of the NGAO system. The AO Sequencer is responsible for the management and coordinated execution of the entire AO controls system. The Facility Composite implements the high-level device sequences that will perform the system configuration, target acquisition, and closed-loop observing. The Composite executes these sequences by directing commands to each of the dependent subsystems depicted in Figure 104, and discussed in the following sections.

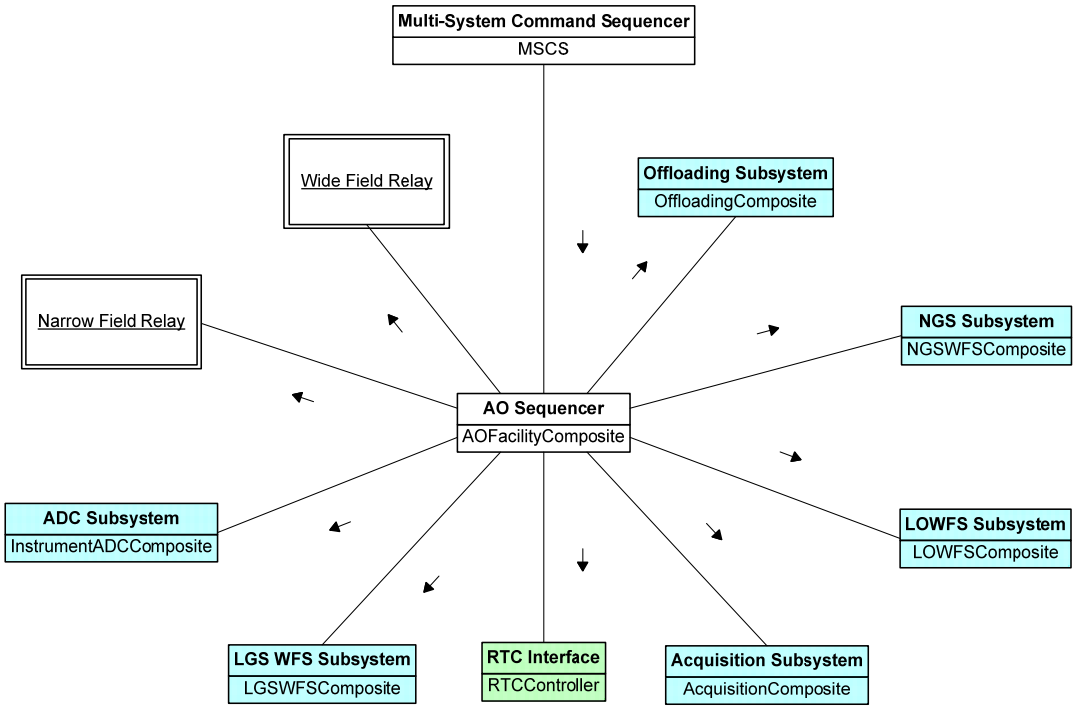

Figure 104: AO Control Sequencer Collaboration Diagram

The AO control sequence covers everything from bringing up the software system to acquisition, and finally shutting down for the night. The sequence itself can be divided into phases each covering a specific state of the system during a typical night's observing. These phases are (listed in order of execution):

- Startup
- Initialize
- Configure
- Acquire
- Observe
- Halt
- Power-down

For the most part these phases can be executed straight through to perform NGAO corrections for a science target. However there is flexibility allowing the sequence to return to a previous phase or jump forward to a latter phase. A detailed review of the AO sequences is described in KAON 735. The following sections briefly discuss the AO subsystem composites controlled by the AO Sequencer.

3.5.4.1.1 Wide Field Relay

The Wide Field Relay covers the low-order atmospheric correction hardware and miscellaneous first-relay and low-order devices, which includes the entrance hatch cover, the rotator, the low order

deformable mirror (LODM) , the tip-tilt stage on which the LODM is mounted and the IF fold dichroic.

The Wide Field Relay subsystem is a logical grouping of these hardware devices, but is not actually implemented as a standard KCSF component due to the very different management and control requirements of the individual devices. Although other devices may also be considered part of the wide field relay, they are grouped and managed under other subsystems (see the LGS and LOWFS subsystems).

The following sections detail the NGAO controls loops implemented by the Wide Field Relay devices.

Rotator Control Loop

Due to the design of the Keck telescopes, as a target is tracked across the sky it will appear to rotate on the science instrument. Similarly, as the telescope elevation changes, additional rotation is added to the field and pupil due to the rotation of the telescope's tertiary mirror (optical axis) of the telescope with respect to the Nasmyth platform. The image rotator is designed to correct for these rotations and keep either the field or pupil stable relative to the instrument.

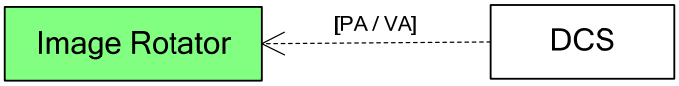

Figure 105: Image Rotator Control Loop

In fixed-field observing we want the sky field to remain at a fixed orientation relative to the detector. In this mode the rotator should track the position angle of the target (the apparent angle of rotation on sky) which will be constantly changing as the telescope tracks the target. While in fixed-field the pupil is allowed to rotate freely.

In fixed-pupil we want the telescope pupil to remain at a fixed orientation relative to the detector. To maintain a stable pupil the rotator will track the telescope vertical angle. The vertical angle changes as the telescope slews in elevation. While in fixed-pupil mode the field is allowed to rotate freely.

LOWFS Rotation Correction Control Loop

During LGS observing the LOWFS sensors will be tracking the tip and tilt of the natural guide stars. From this information the system can determine the appropriate tip-tilt correction to apply to TTM1, and determine if there is any residual field rotation not corrected by the *Image Rotation* control loop.

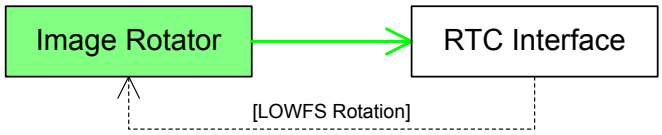

Figure 106: Field Rotation Offset Control Loop

The NGAO RTC Interface Controller will calculate the residual rotation seen by the three LOWFS and make this information available as telemetry. The Image Rotator Controller will subscribe to this telemetry and correct for any residual field rotation.

3.5.4.1.2 Acquisition System

During the NGAO acquisition phase of the observing sequence, the operators, science tools, and controls system will need to be able to view the sky to determine the current pointing and alignment of the telescope. This is possible by imaging the field with the acquisition camera. With this device clients can determine the precise pointing of the telescope and the orientation and position of the laser asterism. The functionality for this capability is provided by the Acquisition Subsystem. The Subsystem is responsible for the management and control of the following devices: acquisition camera, acquisition fold mirror, filter wheel and focus stage. The Acquisition Subsystem does not implement any control loops.

3.5.4.1.3 LGS Wavefront Sensors

The LGS Wavefront Sensor Subsystem is responsible for the management and control of the LGS wavefront sensors and related hardware. The subsystem provides the initialization and acquisition functionality to position the patrolling pickoffs; align the patrolling and tomography LGS beacons; configure the WFS RTC cameras; and manage the focus for the entire LGS assembly. The LGS WFS Subsystem also provides capabilities to perform background calibrations and respond to alignment errors by offloading to the laser facility global tip-tilt and asterism rotator.

The following sections detail the offload control loops of the LGS WFS subsystem. Each control loop is implemented in part or in full by one or more of the NGAO controllers.

LGS WFS Focus Control Loop

As a tracking device, the WFS Focus Stage Controller will be monitoring the state of the system and responding to events. Focus information is derived from the LOWFS calculated focus and the telescope zenith angle.

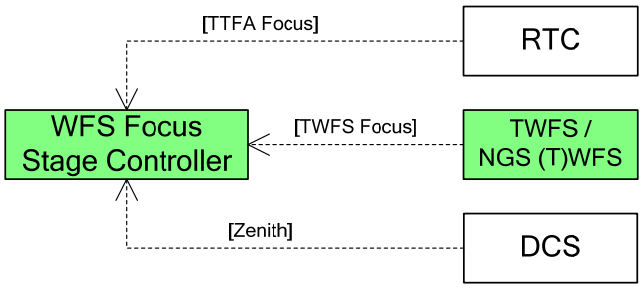

Figure 107: WFS Focus Control Loop

WFS focus tracking is an event driven control loop triggered by telemetry events from the RTC, the TWFS camera, and DCS telescope zenith angle keywords. The RTC provides time-averaged data from the Tip-Tilt Focus and Astigmatism (TTFA) WFS to determine the error in the LGS WFS focus position. More accurate focus information is provided at a slower rate (~1Hz) directly by the Truth Wavefront Sensor (TWFS). The TWFS images will be processed by the NGAO controls system to

determine focus and centroid offsets and published as telemetry. When the controller receives input from these items it will recalculate the sodium layer altitude and apply the appropriate compensation to the stage.

As the focus position is driven by measurements calculated from LGS beacon information, disturbances in seeing, hardware obstructions, or device failures can cause the control loop to receive erroneous data from the WFS. To ensure the focus is tracking a real target and not noise or reflections, the controls system will monitor the sensor data quality. This may involve periodic checks of flux intensity or the rate of focus degradation. Extreme changes in the monitored properties can be used to automatically stop focus correction until the seeing improves.

LGS WFS Offloading Control Loop

During observing the LGS WFS will periodically have to offload tip-tilt errors to the Beam Generation System to maintain alignment of the LGS beacons. Two types of offload control loops are implemented: one for the tomography sensors, and another for the patrolling WFS. The offload control loop has been divided in this way based on the specific offloading hardware. As with the LGS WFS focus control loop, data quality monitoring will be performed to ensure the offloads are genuine and not a product of tracking noise or reflections.

Tomography WFS Offload

The Tomography WFS Controller uses a single offload task to manage the tip-tilt offload for all four WFS. Offloads are performed when the average of all the tomography tip-tilt stages exceeds a specified threshold. This task is responsible for maintaining a balanced tip-tilt average across the asterism.

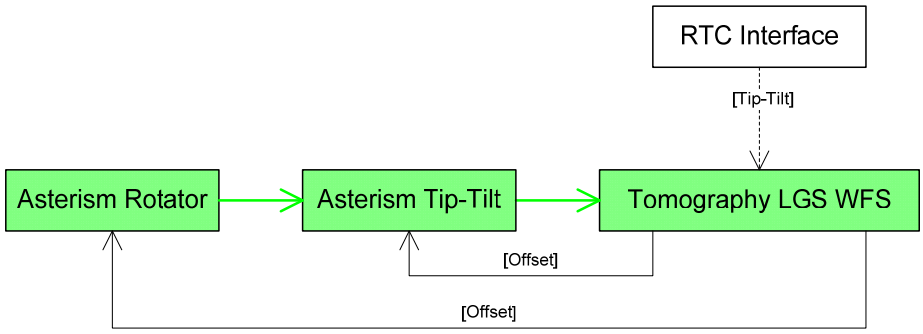

Figure 108: Tomography LGS WFS Offloading

Tip-tilt information from each of the WFS TT mirrors is provided through the RTC telemetry, and is used to calculate average tip-tilt across the tomography sensors. The offload task will determine the offset to apply to the BGS up-link Tip-Tilt and Rotator for asterism shift and rotation, respectively. The BGS offsets will be seen by the WFS as rapid motion away from the increasing tip-tilt. This will result in the RTC compensating by moving the WFS TT mirrors towards their zero point.

Patrolling WFS Offload

Each of the patrolling WFS Controllers implements their own tip-tilt offload control loop. This loop is responsible for periodically offloading the accumulated tip-tilt of the WFS TT mirror (the mirror itself is controlled by RTC) to the BGS patrolling steering arm.

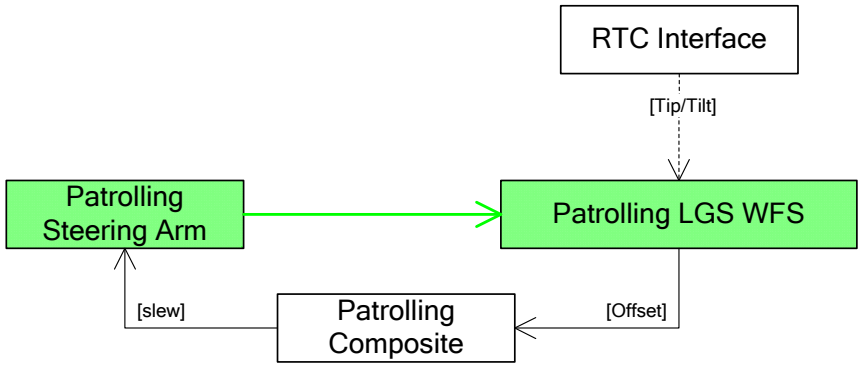

Figure 109: Patrolling LGS WFS Offloading

When the RTC WFS loop is closed the real-time system will be using the WFS tip-tilt mirror to keep the LGS spot stable on the sensor. Over time the tip-tilt will build up and if not offloaded can cause the TT mirror to reach its limit, and eventually lose the LGS beacon all together. When the tip-tilt exceeds a defined threshold, the LGS WFS Controller will calculate the offset required by the steering arm to bring the beacon closer to true center (zero tip-tilt). The WFS will see this as the beacon moving rapidly out of center in the opposite direction of drift, and will compensate by moving the TT mirror to bring the spot back to center. This should consequently return the TT mirror to near its center of range of motion.

3.5.4.1.4 Low Order Wavefront Sensors

The Low Order Wavefront Sensor subsystem is responsible for the management and configuration of the low order wavefront sensors (LOWFS) and related hardware. The LOWFS are responsible for providing tip-tilt and focus information to the RTC and AO Controls system. RTC will apply corrections to the low-order relay TTM1 to correct for full-field tip and tilt. Focus and rotation offloading will be managed by the AO Controls and will be applied to the LGS focus stage and AO rotator.

There are a total of three LOWFS assemblies, each with a dedicated deformable mirror, pickoff arm, focus stage, tip-tilt mirror and sensor. In addition to tip and tilt, one of the LOWFS sensors also provides focus and astigmatism information (TTFA) to the RTC. Co-mounted with the TTFA is a truth wavefront sensor (TWFS). This sensor provides more accurate focus information, but at a slower rate than the TTFA. The TWFS sensor is under the direct management and operation of the AO Control system.

All three LOWFS and the TWFS are managed by the *LOWFSComposite*. This NGAO component provides a simple interface to initialize, acquire, and manage the devices during observing. The following detail the control loops managed by the LOWFS subsystem.

TWFS FOCUS AND CENTROIDING CONTROL LOOP

The TWFS Controller will be responsible for processing images to determine high accuracy focus and centroiding errors. A Shack-Hartmann technique is used to estimate the wavefront and calculate the overall focus of the light and its average centroid. The focus information will be published to the LGS WFS focus stage, and centroid information will be sent to RTC to improve AO corrections.

If the controller detects that the NGS target has been lost or the flux is too low to track against, the focus and centroid calculations will be suspended until seeing improves.

3.5.4.1.5 Narrow Field Relay

There are two devices that comprise the Narrow Field Relay: the high-order DM (HODM) and high-order tip-tilt stage (TTM2) on which it is mounted. The DM is under the direct control and management of the RTC, and is used to correct for the remaining atmospheric distortion that could not be removed by the Wide-Field Relay DM. TTM2 is under the direct control of the NGAO controls system.

As a low-bandwidth device, TTM2 is used primarily for tracking of differential atmospheric refraction (DAR); correcting ADC tip-tilt errors; and offloading for the Keck Angle Tracker (KAT). In addition, TTM2 will be able to execute science dithering routines, either as scripts or built in sequences, to move the field in a coordinated fashion. The following sections identify the control loops defined for the Narrow Field Subsystem.

ADC Tip-Tilt Errors Control Loop

It is expected that the Atmospheric Dispersion Compensator (ADC) will cause position translation errors in the science image. Fortunately these errors can be compensated for by the High-Order Tip-Tilt device.

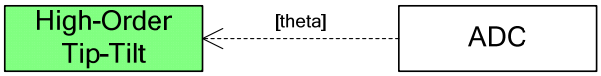

Figure 110: ADC Tip-Tilt Error Correction Control Loop

The High-Order Tip-Tilt Controller will listen to position events from the ADC (as orientation of the corrector stages), and using a table of premeasured tip-tilt error values find the appropriate compensation to apply to the stage.

KAT Offloads Control Loop

During IF observing the Keck Angle Tracker (KAT) will need to periodically offload target centroids while tracking. The TTM2 mirror will correct for KAT offloads.

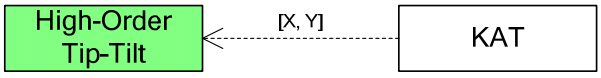

Figure 111: KAT Tip-Tilt Error Correction Control Loop

The High-Order Tip-Tilt Controller will listen to offload events from KAT as an X / Y field offset. The controller will convert these offsets into the appropriate tip-tilt offsets which will be corrected up-stream by the NGS WFS.

3.5.4.1.6 NGS Wavefront Sensor

The NGS WFS Subsystem is implemented by the *NGSWFSComposite*, and is responsible for the management and operation of the NGS devices. This includes the NGS WFS, focus stage, lenslet array, and field steering mirrors. The Composite presents a simple high level interface to the client to initialize, configure, and acquire the guide star from the field. The NGS WFS Composite is managed directly by the AO Sequencer subsystem.

The NGS WFS camera is under the direct control of the real-time system. The NGAO controls system is responsible for the initialization and configuration of the sensor, and commanding RTC to open and close the WFS control loops. The other NGS devices are all under the direct control of the Controls System. Outside of the RTC NGS control loops, the NGS Subsystem does not implement any tracking or offload tasks. The majority of device control is performed during configuration and acquisition.

The NGS WFS subsystem does not currently implement any servo control loops.

3.5.4.1.7 Atmospheric Dispersion Corrector

The ADC is responsible for compensating for the effects of refraction caused by light travelling through the atmosphere. This system uses a set of adjustable prisms to converge the dispersed wavelengths to their original shape and position. The *ADCComposite* is responsible for the management and operation of the ADC subsystem. The subsystem comprises the ADC devices and in-out stage. The following detail all of the tracking control loops implemented by the ADC subsystem.

ADC TRACKING CONTROL LOOP

As a tracking device the ADC Controller will be listening to system event and responding automatically to changes. The ADC dispersion corrector control loop takes as input the telescope zenith angle and rotator orientation. (The science instrument wavelength is also needed, but this is set before the start of a sequence.)

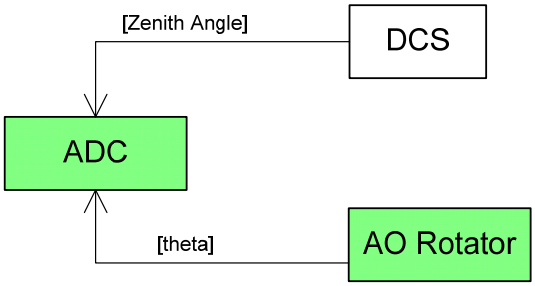

Figure 112: ADC Tracking Control Loop

The input values are used to index a table of premeasured dispersion values and combined to determine the appropriate correction to apply with the ADC. The ADC correction loop is event driven and can potentially run at the rate of the fastest telemetry item. Decimation can be used to reduce the correction rate if appropriate.

3.5.4.1.8 RTC Interface

The Real-Time Controller (RTC) is responsible for calculating the atmospheric distortion and applying corrections to the NGAO system by controlling the operation of the deformable mirrors and various tip-tilt stages. Tomographic and atmospheric reconstruction calculations are performed at multiple kilohertz rates to provide fast real-time atmospheric correction of the science field.

The RTC Interface is implemented by the *RTCController*, and provides all of the AO controls functionality exposed by RTC. The RTC Interface Controller does not implement any control loops.

3.5.4.1.9 Offloading

The Offloading Composite manages two stand-alone offload tasks: *TelescopeOffloadController* and *DAROffsetController*. These controllers are responsible for calculating and applying offsets to the associated devices.

The Telescope Offload task offloads the focus and tip-tilt build-up (as measured by DM1 and TTM1) to the telescope secondary and pointing, respectively. In open loop mode (during target acquisition) focus and tip-tilt information will be provided by the LOWFS and NGS WFS. The DAR Offset task is responsible for calculating the effects of DAR between the science instrument and WFS (either LOWFS or NGS), while taking into account the other optics and filters in the beamtrain. These offsets are applied to the High-Order Tip-Tilt stage, or as centroid offsets to RTC. Both tasks are event driven; where the telescope offload is based on focus and tip-tilt thresholds; and the DAR task is based on changes in telescope elevation.

The following control loops are managed by the Offloading Subsystem.

TELESCOPE OFFLOAD CONTROL LOOP

The *TelescopeOffloadController* is responsible for offloading tip-tilt, focus, and coma from the low-order relay to the telescope. During observing, focus and field tip-tilt will be corrected by the low-order DM and TTM1 stage, respectively. Periodically these quantities will need to be offloaded to the telescope to ensure the AO devices have sufficient range to correct for the atmosphere. Tip-tilt is offloaded to the telescope AZ / EL position of the telescope, and focus / coma is offloaded to the secondary piston and tip-tilt.

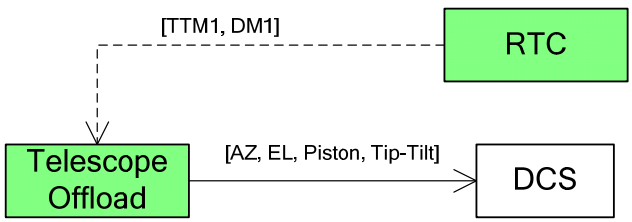

Figure 113: Telescope Offload Control Loop

The *Track* action is responsible for starting the telescope offload task, and represents the bulk of the controller's functionality. While tracking, the controller will be listening to events from the low-order relay DM and Tip-Tilt Mirror (TTM). If the controller determines that the focus applied to the DM or the position of the TTM exceed configurable thresholds, the controller will take action to offload the buildup to the telescope.

DAR OFFSETS CONTROL LOOP

The DAR Offset controller is responsible for calculating and compensating for the affects of DAR on the NGAO system. DAR is a measure of the refraction of light between two wavelengths caused by atmosphere at different elevations. From the perspective of the WFS it will appear as if the target is slightly offset from its expected position due to the wavelength of light the sensor can see. If the diffraction effects are not corrected the WFS alignment will suffer and the science target will not be on-axis for the science instrument. (See KAON 221 for more information on Differential Atmospheric Refraction.)

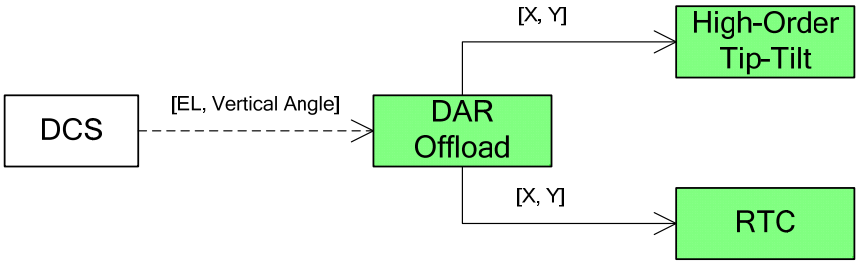

Figure 114: DAR Offset Control Loop

DAR is a relative calculation based on the wavelength of the science instrument, tip-tilt WFS (either LOWFS or NGS WFS), and the current telescope elevation and vertical angle. In NGS mode or LGS with the Interferometer the DAR calculation is performed relative to the NGS WFS, and is applied to the RTC as centroid offsets. During LGS with an instrument the DAR is calculated relative to the LOWFS wavelength and is applied directly to TTM2. The DAR calculation is triggered whenever the telescope elevation / vertical angle changes.

The DAR Offset Controller is not responsible for initializing, configuring or acquiring the device dependencies. The Offset Controller assumes the devices are in the proper operating state and capable of accepting offsets when tracking.

3.5.4.1.10 Other Composites

CALIBRATION SIMULATION

The Calibration Subsystem is comprised of a number of devices responsible for the generation and propagation of simulated sources including: stimulus devices, tip-tilt fold mirrors, and focus stages. The Calibration System is implemented by the NGAO *CalibrationComposite* class.

The calibration subsystem is a loose collection of device controllers. The subsystem is primarily responsible for initializing the devices and catching run-time errors. Control and execution of calibration sequences will be performed by the MSCS or other high-level operator tools, which will interface directly with the devices (see KAON 739 for a summary of the calibration sequences).

AO ENCLOSURE

The AO enclosure, which includes the cold-bench, AO room, and electronics vault, contain a number of diagnostic and environment sensors. These sensors will be distributed throughout the AO enclosure to obtain global and localized measurements of environmental conditions. The readings from these sensors will be used primarily to monitor these conditions and ensure the safe operating environment for the AO hardware.

Currently this subsystem does not manage any motion control devices, and as such has a very simple software design and limited functional requirements. Although the sensor information will be freely available to the NGAO Controls System, it is not actively used during regular observing.

Unlike other NGAO control subsystems, the AO Enclosure Subsystem will typically be left running at all times, even during shutdown at the end of an observing night. Information published by the enclosures should always be available so operators and technicians can monitor the well being of the system, even during down time.

3.5.5 Laser System Software

KAON 714 should be referred to for more details for the following section.

3.5.5.1 Laser Control Sequencer

The Laser Control Sequencer is implemented by the *LaserFacilityComposite*, and is responsible for managing and configuring the entire laser facility, and executing the various sequences. The Composite sits above all of the other laser system components, and coordinates their state and task execution during observing. The Laser Sequencer is under the direct control of the MSCS, and is the primary interface to the laser system.

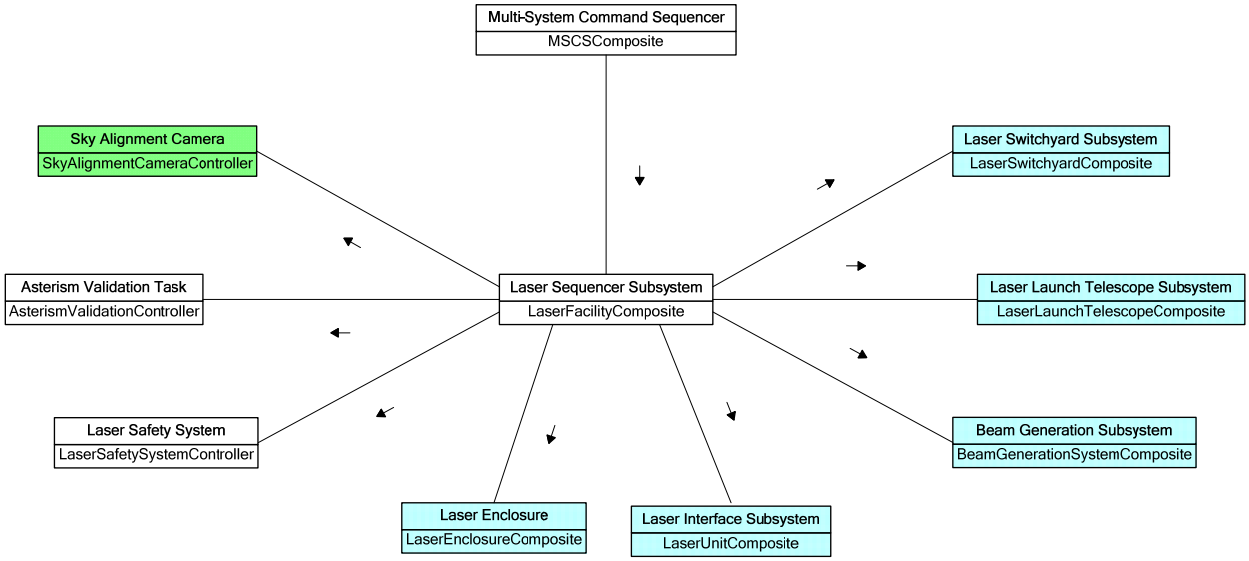

Figure 115: Laser Control Sequencer Diagram

The Laser Sequencer exposes a simple set of high level actions to the MSCS. These actions provide the Command Sequencer with the ability to initialize and configure the laser facility; acquire LGS targets; and shutdown the system. The composite in-turn takes the action data and distributes it among the relevant subcomponents; invoking their corresponding initialization, configuration, acquisition, and shutdown actions.

As with other composites, the Laser Sequencer will reflect the overall state of its subcomponents: effectively the health and state of the entire laser system. The MSCS will monitor the state of the composite to ensure its continued safe operation, and to respond to any errors that may occur.

A detailed review of the Laser sequences is described in KAON 736. The following sections briefly discuss the AO subsystem composites controlled by the AO Sequencer.

The following sections detail the control loops of the Laser Control Sequencer. Each control loop is implemented in part or in full by one or more of the NGAO components.

3.5.5.1.1 Asterism Validation Control Loop

NGAO makes use of high-intensity lasers to produce the LGS beacons. If the lasers are not properly aligned they can cause significant damage to the laser facility hardware and injury to personnel. As such, the laser propagation must be periodically validated to ensure the proper alignment and performance of the system. An asynchronous task will be created to monitor the health of the laser system. If the task identifies any major changes to the asterism structure, such as the loss of an LGS beacon, an automated response will be taken to ensure the safety of the laser facility.

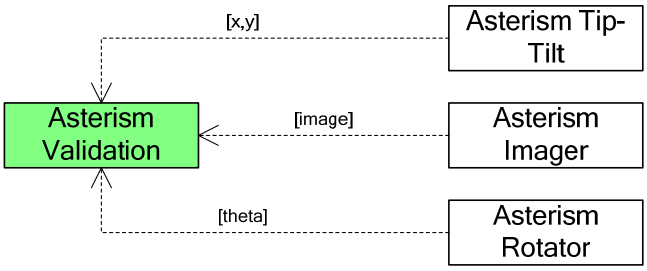

Figure 116: Asterism Validation Control Loop

The *AsterismValidationController* is designed to perform asterism validation and error handling during the acquisition and observing sequence. The control loop implements an image processing routine that takes images from the Asterism Imager Camera and compares the laser beacons against their expected positions in the field. These positions are based on the coordinates of the tip-tilt targets, position of the asterism tip-tilt mirror, and the orientation of the rotator. If there are any major changes to the asterism structure, such as the loss of an LGS beacon, the validation controller can take an automated response to ensure the safety of facility.

Three failure modes have been identified for the laser asterism and will be monitored by the validation controller. The failure modes are:

- Loss of a laser or beacon – If the asterism validation identifies that there are fewer than the expected LGS beacons in the image the sequence will be halted and the laser system will be put into a shuttered safe state.
- Additional beacons – Potentially the laser system could be configured incorrectly to produce additional beacons when a reduced subset is desired (e.g. fixed-pupil or a single TT target). If the validation task identifies more than the expected number of LGS beacons the sequence will be halted and the laser system will be put into a shuttered safe state.
- Incorrect beacon position – Potentially caused by a number of factors (offloading, flexure compensation, etc.) the laser beacons may drift over time. As all of the beacons are accounted for, only displaced, there is no imminent safety concern for the system. The validation task will assume the system is performing correctly, but will warn the operator that the asterism has changed and that performance could suffer.

The validation task is event driven and will be executed for each new frame produced by the asterism imager camera. The initial positions of the beacons will be calculated when the validation task is started based on the sky position of the tip-tilt targets. The positions of the beacons will be recalculated whenever the BGS rotator or tip-tilt mirror is moved, and should only require a translation and rotation matrix transformation. The validation task is started at the beginning of the science sequence and halted at the end of integrations.

As a high-level subsystem, the Composite relies on the low-level subsystems for the majority of hardware control. Although the Laser Control Sequencer is capable of directly interacting with any hardware in the laser facility, there are only a few hardware devices it manages directly. The following sections briefly discuss the laser subsystem composites controlled by the Laser Sequencer.

3.5.5.1.2 Laser Switchyard

The Laser Switchyard control system is implemented by the *LaserSwitchyardComposite*. This component is responsible for controlling the individual devices and distributed software controllers that implement the switchyard functionality. This includes the low-power fold mirror, steering mirrors, beam polarizers, and beam positioning sensors.

The Switchyard Composite is managed directly by the Laser Facility Composite, and presents a simple high-level interface to initialize, acquire, and halt the switchyard devices. The Composite's primary responsibility is to prepare the switchyard devices for closed loop observing. The majority of the Switchyard Composite functionality exists as part of the configuration and acquisition sequence. During observing tracking components are independently controlled or run closed-loop with the rest of the system.

The following sections detail the tracking and offload control loops of the Switchyard subsystem. Each control loop is implemented in part or in full by one or more of the switchyard subsystem controllers.

LASER TRANSPORT CONTROL LOOP

The laser transport control loop is responsible for maintaining the proper alignment of the lasers from the laser enclosure to the BGS. This control loop is needed to compensate for flexure as the telescope tracks a target; and uses a combination of the telescope elevation and feedback from the beam positioning sensors to calculate the appropriate position of the laser steering mirrors.

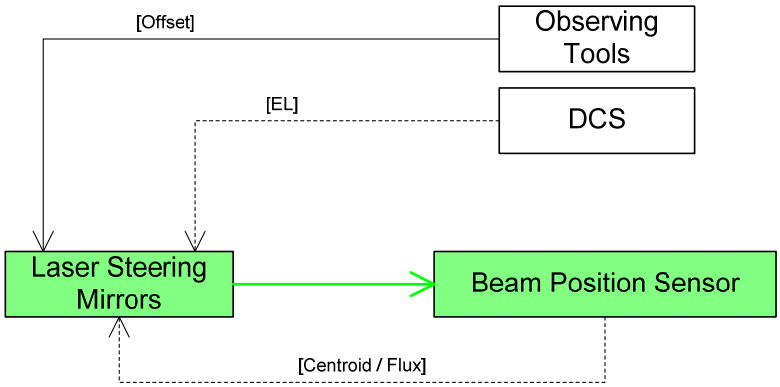

Figure 117: Laser Steering Control Loop

Although the laser transport tracking loop (implemented by the Laser Steering Mirror controller) uses inputs from DCS and the positioning sensors, it does not use both of them at the same time. The laser facility can propagate the lasers in high-power and low-power modes, depending on the position of the low-power fold mirror. When the fold mirror is in the beam path, all but a small percentage of the laser light is diverted to a beam dump. The leakage is allowed to propagate through the system and can be used for alignment and tests with little risk to hardware or personnel. When the fold mirror is retracted the full beam is allowed to propagate.

The laser transport control loop will use the flux value from the beam positioning sensors to determine if the system is configured for low or high-power propagation. If the flux is below a certain threshold the control loop will use the current telescope elevation from DCS. The elevation will be used to index a simple table to determine the appropriate flexure compensation to apply to the steering mirrors. These values will have been derived from empirical tests and will be interpolated to find the appropriate tip-tilt to apply to the stage.

If the positioning sensor threshold reports sufficient laser light, centroid information will be obtained from the detector and will be used to calculate the compensation required to keep the laser aligned with the BGS.

LASER POLARIZATION CONTROL LOOP

During observing the laser asterism needs to have the proper polarization as seen by the AO wavefront sensors. Fortunately this polarization is directly related to the elevation of the telescope and incidence angle of the laser with the sodium layer. The control loop to maintain the desired polarization is implemented by each of the polarizer controllers.

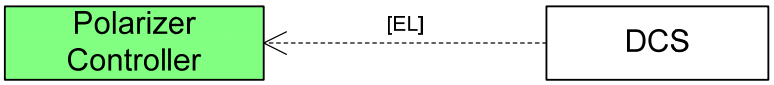

Figure 118: Laser Polarization Control Loop

The polarizer controller tracking loop is event driven and responds to telescope elevation events from DCS. When an event is received the controller will lookup the required orientation of the polarizer in a table based on the current elevation. The table will be defined through empirical tests at regular telescope elevations. The actual polarizer orientation will be interpolated based on these values.

The Half and Quarter Polarizer tracking loop can be remain closed throughout a night's observing.

3.5.5.1.3 Laser Beam Generation System

The *BeamGenerationSystemComposite* is a high-level multi-device manager that is responsible for acquiring and configuring the hardware on the BGS. These devices include the patrolling steering arms, beam splitters, asterism rotator, tip-tilt mirror, and beam expander focus.

The BGS Composite is managed directly by the Laser Facility Composite, and presents a simple high-level interface to initialize, acquire, and halt the BGS devices. The majority of the BGS Composite functionality exists as part of the configuration and acquisition sequence. During observing the majority of the subcomponents are independently controlled or run closed-loop with the rest of the system.

The BGS subsystem is responsible for configuring and positioning the hardware to obtain the desired laser constellation. The constellation is based on the number and position of the wide-field targets, the position of the telescope, and the desired image orientation as seen from the science detector. The BGS subsystem will take this information and calculate the required positions for each of the associated devices.

The BGS subsystem also manages the focus and propagation of the lasers and implements various safety processes to ensure the safety of the laser generation system.

The following sections detail the tracking and offload control loops of the BGS subsystem. Each control loop is implemented in part or in full by one or more of the NGAO controllers.

Focus Tracking Control Loop

During observing the BGS subsystem will have to track the changing focus of the LGS asterism. Focus is primarily based on the current telescope elevation and launch telescope temperature. As the telescope elevation changes, the beam length of the laser from the telescope to the sodium laser will fluctuate. As the distance to the sodium layer changes the beam expander will have to compensate to maintain LGS focus. The temperature of the launch telescope also affects the focus of the laser. This information is derived from the environmental sensors within the LLT.

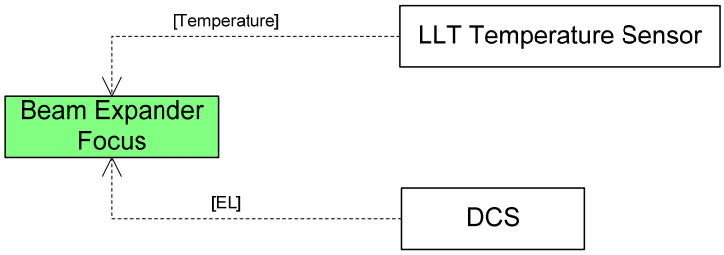

Figure 119: Laser Focus Tracking Control Loop

Beam expander tracking is an event driven control loop triggered by telemetry events from the LLT environment sensors and DCS telescope elevation keywords. When the controller receives input from these items it will calculate the LGS asterism focus compensation and apply it to the stage. A lookup table should be sufficient to define focus compensation based on telescope elevation and temperature.

Rotator Tracking Control Loop

During observing the laser asterism will need to track the LGS targets as the telescope rotates. This is to ensure that the asterism maintains alignment with the LGS WFS detectors. In fixed field mode this is based on the position angle (PA). In fixed pupil mode the rotator will track the vertical angle (VA).

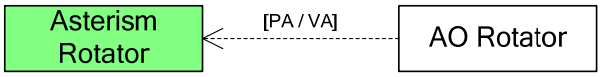

Figure 120: Asterism Rotator Tracking Control Loop

Rotator tracking and offloading is event drive. The Asterism Rotator Controller will receive the position and vertical angle from the AO rotator through a telemetry stream. The asterism rotator will process this information and track with telescope and field rotation.

Flexure Compensation Control Loop

Changes in telescope elevation will induce flexure on the BGS and launch optics. As the telescope tracks a target the asterism tip-tilt will need to compensate for flexure to keep the asterism stable on the sky..

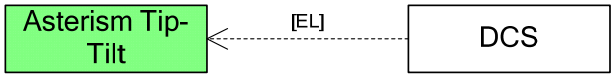

Figure 121: Flexure Compensation Control Loop

The Asterism Tip-Tilt Controller implements an event driven tracking loop. Primary input to the control loop is the telescope elevation and is made available from DCS through the Channel Access service. A simple look-up table can be used to interpolate the required flexure compensation for the current elevation.

3.5.5.1.4 Laser Safety System Interface

The LSS Interface is implemented by the *LaserSafetySystemController*, and provides the operational interface to the laser control system. The LSS Controller provides clients with actions and attributes to set permissives, execute device commands, and read-back state information about the lasers.

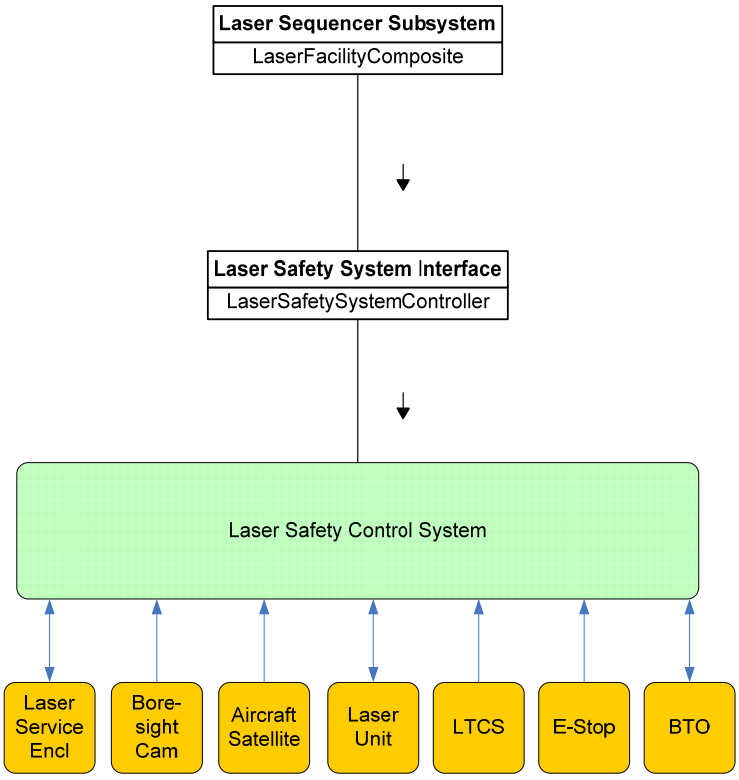

Figure 122: Laser Safety System Collaboration Diagram

As shown in Figure 122, a number of facility components interact with the Safety System including the Laser Traffic Control, Aircraft and Satellite detection, laser service enclosure, E-Stop and the laser units. The LSS utilizes these connections for commanding and feedback. The NGAO Controls

system does not need to be directly aware of the state of these components, and instead can rely on the LSS to provide telemetry information indicating the overall safety / health of the laser system. Other safety permissives such as spotter and OA acknowledgments must be provided by the NGAO LSS Controller.

The Safety System Interface subsystem does not directly manage any tracking control loops.

3.5.5.1.5 Laser Service Enclosure

The *LaserEnclosureComposite* manages the environmental sensors found in the laser unit enclosure. These sensors are responsible for providing the current temperature, humidity, and particulate level.

As sensors are simple on / off devices without motion control requirements, the composite itself is very simple, and provides the basic capabilities to initialize the system for observing. The composite will collect data from each of its sensors and will provide a summarized health status as telemetry and alarming. The Laser Enclosure subsystem does not manage any control loops.

3.5.5.1.6 Laser Interface

The Laser Interface Subsystem is implemented by the *LaserSystemComposite*, and manages the three individual laser units and provides propagation control through the Laser Safety System.

This Laser System Interface provides a single unified command and status interface to all three lasers units. Clients can treat the laser sources as a single instance, allowing them to issue a single command in place of three. Additionally, health and status information for all three laser units will be consolidated and made available to the control system for easy reference.

The Laser System Composite is managed directly by the Laser Facility Composite. The Laser System Interface does not implement any control loops.

3.5.6 Data Server

The Data Handling System for the AO Controls has been called the “Data Server”. The NGAO Data Server is defined as a computer in the network, with associated software, that is dedicated to the data storage and retrieval needs required by the AO Controls System. It holds the database management system, the databases and is part file server capable of housing non-database files such as FITS. In addition to providing data persistence, retrieval and data management there will be a telemetry data recorder, an ad-hoc data recorder, an alarm recorder, general logger, and configuration. High speed RTC data will be stored in its own data recording system.

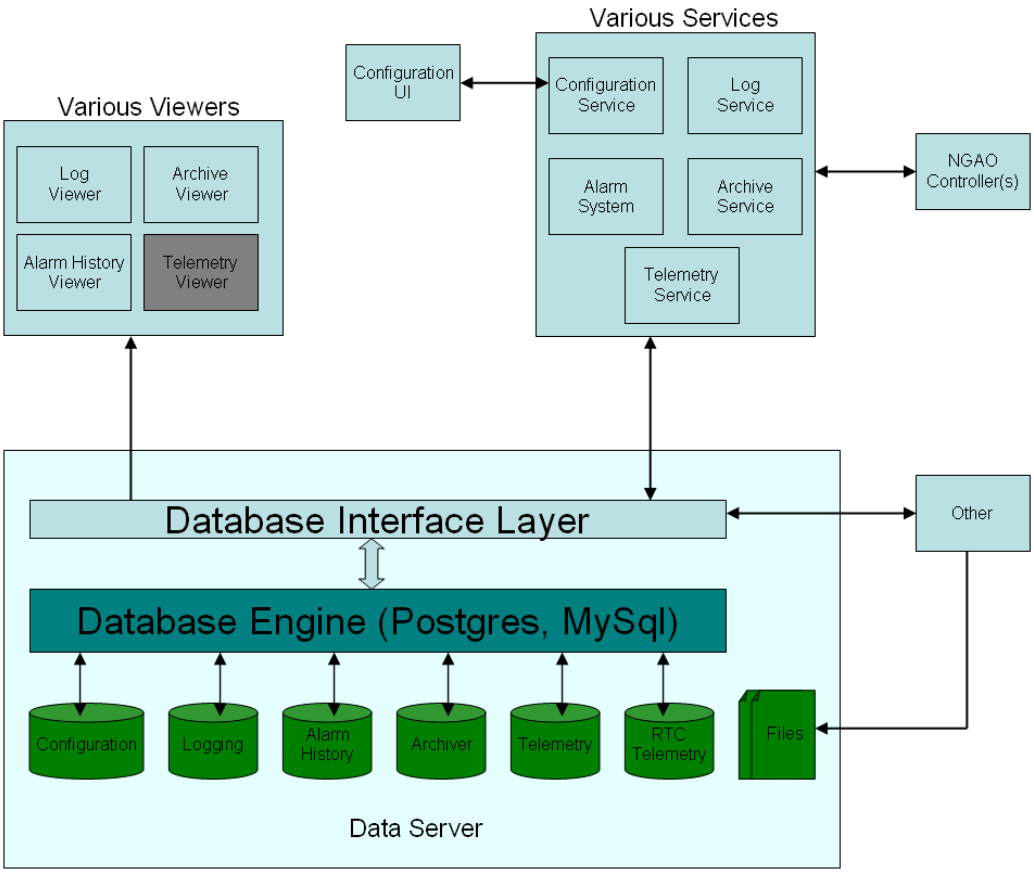

Figure 123: Data Server Overview

Figure 123 shows a high level overview of the data server. The data server hardware consists of expandable and reliable (RAID) hardware capable of supporting multiple databases. More details of the Data Server design can be found in KAON 732.

3.5.7 Real Time Control

3.5.7.1 Introduction

The Real Time Controller (RTC) is a specialized computer system designed to perform all of the wavefront sensing, tomography calculations, and deformable mirror control processing at rates that keep up with atmospheric turbulence induced optical aberrations. The RTC data flow and computer architectures have been designed to achieve the tomography precision, noise suppression, and bandwidth requirements implied by the science-case driven wavefront error budgets.

An equally important consideration in the RTC design is the need to keep the cost and complexity manageable. Simply scaling earlier implementations of single conjugate AO RTC reconstructors using traditional central processing units (CPUs) is infeasible because of the multiplying effect of multi-guidestars and multiple deformable mirrors on computer speed requirements. To address this issue, we have taken advantage of the parallelizability of wavefront reconstruction and tomography algorithms and mapped them on to a massively-parallel processing (MPP) compute architecture. This

architecture scales in size and complexity much more favorably than doing the same calculations on CPUs, and can be readily implemented with commercial off the shelf technology building blocks called field programmable gate arrays (FPGAs). Additional details of this design approach are given in a section on implementation later in this report, and given in greater detail in KAON 696.

We first describe the main line real-time tasks that the RTC must perform. Then we describe the essential ancillary support tasks relevant to the RTC such as communicating with the supervisory controller configuration and calibration information, providing offload signals, and providing diagnostic data. In the final section we explain the MPP implementation, describing processor hardware, interface hardware, and software development methodology.

3.5.7.2 RTC Tasks

The RTC, at the core, performs the following tasks in LGS mode:

- Accept digitized pixel data from the LGS WFS and LOWFS, and perform basic image processing (dark and bias subtraction, flat-fielding).
- Calculate wavefront tilts from the LGS WFS and LOWFS using a choice of noise-optimal centroiding algorithms, and compensate for non-linearities in the centroiding methods.
- Reconstruct wavefront phase at each sensor and transmit this information to the tomography processor.
- Use cone-beam projection tomography techniques to reconstruct the three-dimensional volume of atmospheric index-of-refraction variations above the telescope and over the field of view of interest, given the wavefronts from various directions as measured by each wavefront sensor. This algorithm also takes inputs from the tip/tilt and tip/tilt/focus/astigmatism sensors to break volume solution ambiguities inherent in laser wavefront measurements.
- Integrate through the volume of index estimates along the path to the science instrument – either on-axis for the narrow field science modes, or across a modest FoV (sacrificing peak on-axis performance for more uniform AO correction.)
- Compensate for deformable mirror influence functions and nonlinearities, deriving voltage commands for the DM's given desired wavefront distortion corrections to be placed on them. Split the control between commands to the tip/tilt mirror, moderate-order (woofer) DM, and high-order (tweeter) DMs.
- Incorporate control compensation dynamics to keep the system stable and achieving a given temporal bandwidth.

In LGS mode the RTC also computes high-order wavefront control commands for DMs in the tip/tilt sensors, sharpening the IR tip/tilt stars.

In NGS mode, the RTC acts as a traditional single conjugate AO system. It takes inputs from one NGS sensor, reconstructs the wavefront, and computes commands to be split up amongst the tip/tilt mirror, woofer DM, and tweeter DM in the narrow field science path.

All these RTC tasks take place at the frame rate of the fastest wavefront sensor camera, up to 2,000 frames per second.

As shown in the Figure 124 schematic, large chunks of compute tasks are associated with either wavefront sensors or DM's and thus can be parallelized across them. Furthermore, algorithms running within the sensor and actuator subunits, as well as within the tomography engine, are highly parallelizable when implemented in the Fourier domain, and thus will each map onto an MPP architecture as described earlier.

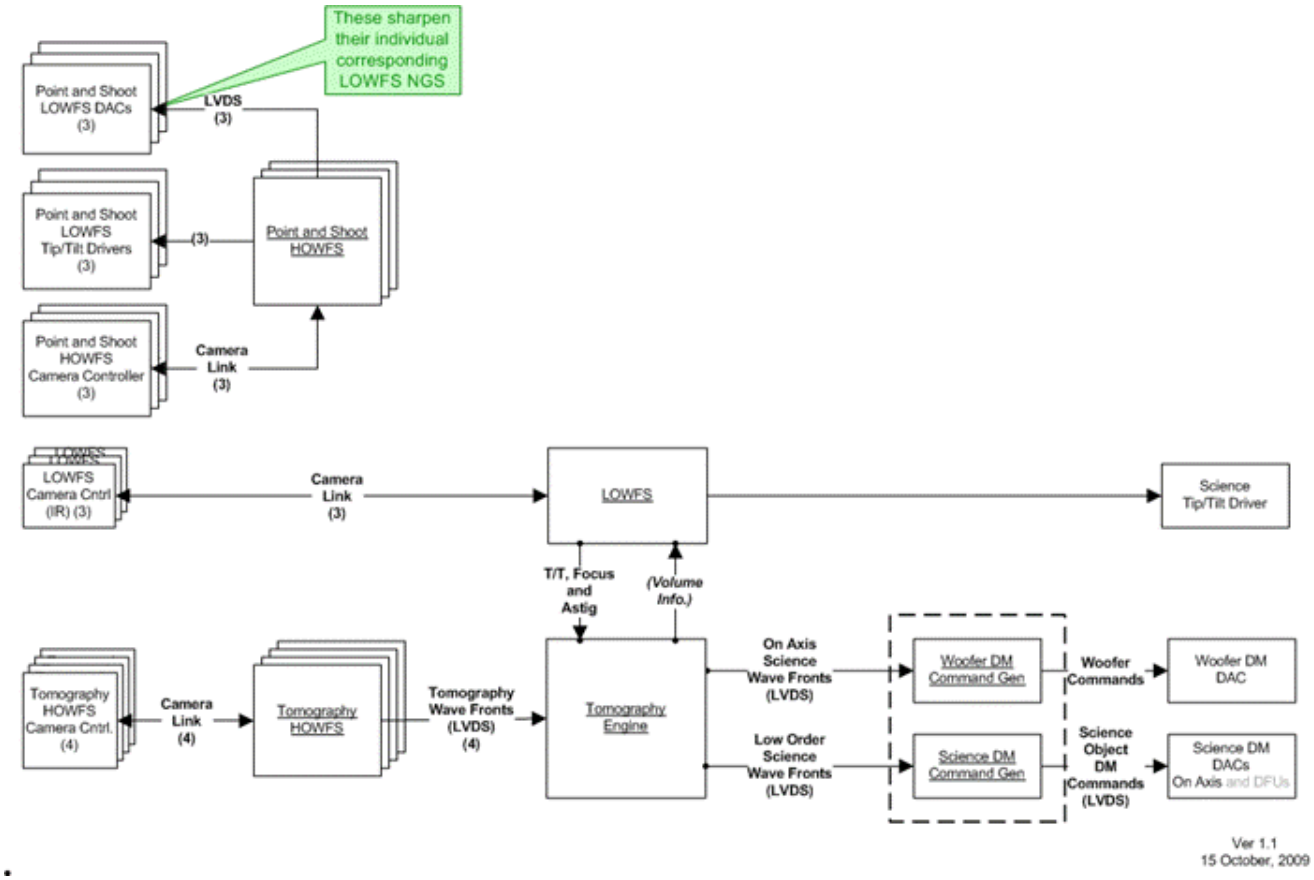

Figure 124: Multi-guide star tomography data flow and parallel processing

3.5.7.3 Parametric Input, Optimization, and Reconfigurability

3.5.7.3.1 Minimum Variance Reconstruction Optimization

The RTC iteratively solves a large set of linear equations associated with wavefront reconstruction and tomography. These equations have a generic form. By loading the RTC with the proper set of parameters it can implement a wide variety of reconstructor/controller solutions, including weighted-least-squares, statistical minimum variance, Fourier mode optimized gain, pseudo-open-loop, steady-state Kalman, and wind-predictive estimation and control solutions. Furthermore, slowly varying parametric data that affect the solution can be continuously adjusted during real-time operation. For example, the minimum variance solutions depend on certain a-priori data, which the RTC accepts as parametric input. These include:

- Volumetric turbulence strength (Cn2 profile, discretized at layers)

- Number of layers of turbulence
- Brightness of guide stars
- Wind speeds at layers

C_n^2 can be provided either as a-priori input, or as derived from external measurements, for example, from a MASS/DIMM sensor. The preparation and processing of this data is left to the external supervisory control system; the RTC simply takes in a set of normalized C_n^2 strength numbers, one per layer, at a rate that is slow (e.g. once per second) with respect to the real-time tasks. As an option, the RTC's tomography engine will provide statistical average rms aberrations resolved by layer, which can be used to adjust C_n^2 profile numbers dynamically.

Similarly, wind speeds can be incorporated from external data or deduced internally from past histories of estimates.

3.5.7.3.2 Calibration Parameters

The truth wavefront sensor will provide long-term average wavefront data designed to normalize out systematic biases due to either non-common path optical aberration or Hartmann sensor biases due to variations in the sodium layer thickness and altitude. The RTC will process these wavefront sensor data like any other wavefront sensor and use the results to adjust zero-set points in the overall reconstructor.

In a like manner, prior measurements will have determined calibration set points for each wavefront sensor, giving the definition of a "flat" wavefront for each sensor. The set points for LGS wavefront sensors will depend on field position and zenith angle. Thus the multi-system command sequencer, with knowledge of the telescope and AO system configuration, will periodically update the RTC wavefront sensor sub-processors as to which parameter set to apply to the wavefront reconstruction.

The optical system will unavoidably have pupil-mapping distortions between DMs and WFS pupil planes. The RTC will use a set of distortion definition coefficients to interpolate wavefront samples, mapping them to a common physical grid. This will also effectively control the errors introduced by perspective elongation due to non-normal beam incidence angle off of DMs. Correction to a physical grid makes the tomography self-consistent to a well-defined atmospheric volume. Calibration parameters are determined ahead of time, either through analysis of laboratory measured pupil image data or via optical ray-trace models.

3.5.7.3.3 Reconfiguration

The processing units and algorithm will be made reconfigurable to allow for each of the observing modes envisioned for NGAO. Configuration parameters include:

- Number and field-positions of laser guide stars.
- Number and field-positions of tip-tilt guide stars.
- Field position of TTFA (tip/tilt/focus/astigmatism) sensor.

Furthermore, the scalloped pupil of the Keck primary mirror will rotate with respect to the wavefront sensors and DMs in some science observing scenarios. The wavefront and tomography reconstructors

utilize a model pupil as a "valid data" mask (a loadable parameter), so this model will be set and updated at the appropriate rate within the RTC.

3.5.7.4 Interfaces

3.5.7.4.1 Offloading

The RTC will provide offload signals to the telescope so that the high speed wavefront controllers don't saturate. The offload signals flow to the non-RTC supervisory controller at a relatively low data rate, on the order once per second. Offloading signals include:

- Tip-tilt to the telescope guider.
- Focus to the secondary piston.
- Other low order modes TBD to the telescope primary segment control system.

3.5.7.4.2 Diagnostics and Telemetry

Diagnostic data is defined as data intended for monitoring the health of the RTC and AO system, and for display to the operator. Centroid data from wavefront sensors, signals going to DMs, and other indicators are transmitted at relatively low, human readable, data rates to the external systems.

The diagnostic data, as well as the offloading data mentioned above, will be low-pass filtered by the RTC to avoid aliasing, which reduces the noise and jumping due to sparsely sampling high frequency data. The anti-aliasing bandwidths for all data streams are adjustable parameters.

Telemetry data is defined as up to full-frame rate streaming of portions or all of the intermediate data to high-speed data capture units. This data is useful for a number of post processing tasks such as

- Debugging or tuning of parameters.
- Analysis of seeing conditions and performance of the AO system.
- Point spread function determination.

Data that would be streamed for data capture include:

- All wavefront sensor centroids, intensities, and wavefront sensor reconstructed phases.
- All tip-tilt and TTFA sensor centroids and intensities.
- All commands to the DMs and tip/tilt mirrors.
- All tomography volume estimate data.
- Ancillary information associated with the operations so as to be able to reconstruct the state of the RTC at the time, including internal data tables, C_n^2 numbers, wind numbers, calibration sets, etc.

Additional data storage capability will be needed to record full frame rate raw pixel data from the wavefront and tip/tilt sensors.

3.5.7.4.3 Command State

The RTC at any time will be operating in one of a number of possible states. Examples of such states include:

- Narrow field science LGS AO control (hybrid closed loop on the woofer and open loop on the narrow field tweeter and tip-tilt and TTFA tweeters).
- Narrow field science NGS AO control (closed loop on the woofer and tweeter).
- Control on tip-tilt only.
- Calibration modes (for alignment/registration, push matrix generation, linearity calibrations).
- Uncontrolled or idle, with static values as loaded for the DMs and tip/tilt mirrors.

The supervisory control system will transmit the state transitions to the RTC control processor which will configure parameter sets for the RTC real-time hardware accordingly (and also report back its state on demand). The maintenance of state transition rules will be the responsibility of the multi-system command sequencer.

Additional flags will be maintained for turning on and off various diagnostic and telemetry streams.

Figure 125 shows the architecture of communication amongst the supervisory (AO) control system, RTC, and hardware elements. It shows the flow of commands and status information between supervisory control and the RTC via the coordinating function of the RTC control processor. It also shows how the high speed telemetry data is streamed to disk storage and enabled for later retrieval for post-processing.

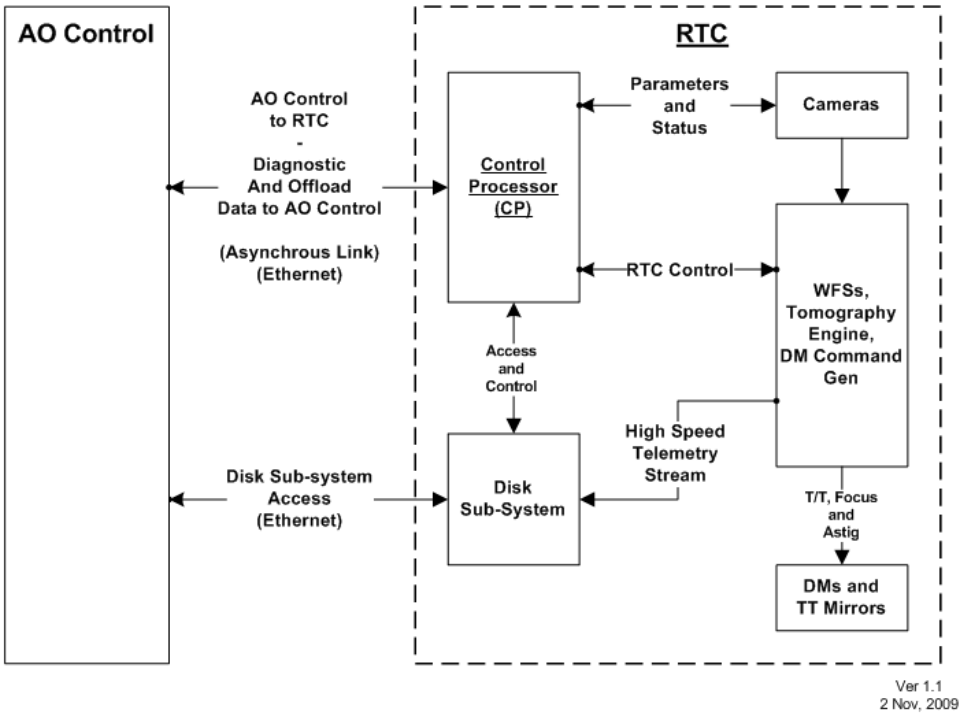

Figure 125: RTC to supervisory controller interface and communications architecture

3.5.7.5 Implementation

3.5.7.5.1 Algorithms

Algorithms for wavefront phase reconstruction from Hartmann slope data have been analyzed since the beginning days of AO. We anticipate using a modern fast-iterative technique such as the ones described by Vogel and Yang (Appl. Opt. IP 45, 705, 2006) and Gilles et al. (Appl. Opt. 42, 5233, 2003). Such techniques can take advantage of parallelism if they are implemented in the Fourier domain. Regularizations taking into account the signal-to-noise of the measurement and filters for suppressing the waffle mode can also be implemented in the Fourier domain. The pupil boundary conditions (outside of which the measurements must not be assumed as zero but allowed to be free variables) force the algorithm to be iterative as described in the above references, but 3-5 iterations of a Fourier-domain pre-conditioned solver have been shown to be adequate for meeting our error budget.

Inverse tomography algorithms using wavefront measurements from multiple directions have been developed recently (see Gilles et al. (Appl. Opt. 42, 5233, 2003) and Gavel (SPIE 5490, 1356, 2004)). These algorithms are mapped to massively parallel operations through the use of the Fourier domain but solutions must be iterated because of the finite spatial extent of the measured wavefront data. Figure 126 depicts the operations in the tomography engine's iterative solver loop. Repeated forward and backward propagations of rays through the sample volume are used to refine estimates of the volumetric distribution of atmospheric aberrations until a forward propagation matches the wavefront sensor data. The pre-conditioning step helps convergence by applying an approximation of the inverse to the key set of linear equations in the Fourier domain. The Fourier domain inversion is exact on an infinite aperture, so applying the pupil mask in the spatial domain is crucial to ensure that the solution is driven only by the valid WFS data, which is available only inside the telescope pupil.

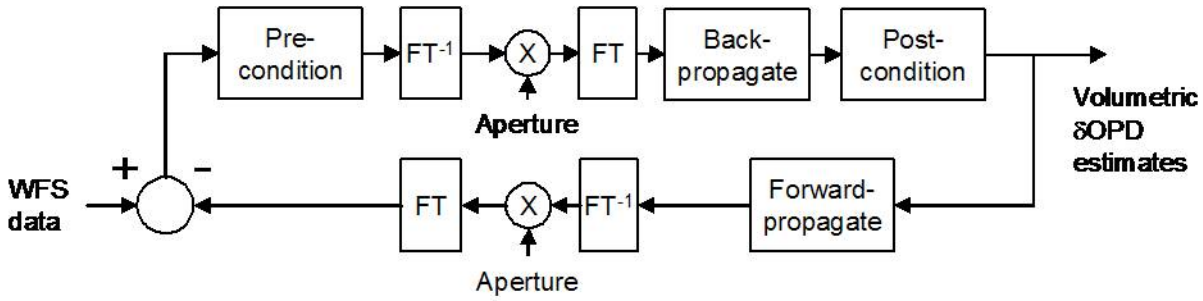

Figure 126: Rough outline of the iterative back-projection tomography algorithm

Finally, fitting the deformable mirror to the desired wavefront correction can be accomplished with parallel processor implementations that carry an inverse model of each DM.

- MEMS open loop control is decoupled into a linear cross-coupling, which is solvable in the Fourier domain, and independent nonlinear functions for each actuator, solvable with nonlinear lookup tables in parallel. The MEMS are repeatable go-to devices and this open-loop model has been proven to be quite accurate (see Morzinski et al. (SPIE 6888, 2008)).

- The woofer DM, likely a piezo-actuator device with cross-coupling and hysteretic effects, will be controlled via a linear Fourier domain deconvolution only. We will rely on the fact that this mirror is in "closed loop" (upstream of the wavefront sensors) and so any residual mis-fitting will be measured and sent to the more accurately responding tweeters. Bandwidth shouldn't suffer because the woofer is correcting the lower order, and hence slower evolving, atmospheric modes.

More details on algorithm implementation are given in KAON 695.

3.5.7.5.2 Hardware

The multi-processor units are implemented as banks of field-programmable gate arrays (FPGAs) arranged on custom circuit boards. The technology of FPGA programming has advanced to the point that the design and configuration of these boards, intimately coupled to the algorithm distribution on the processor chips themselves and data flow needs, is accomplished entirely using standardized computer aided design and simulation tools. The details of distributing the NGAO RTC architecture onto these processor units are given in KAON 696, sections 5 to 8.

The processor units end up being many repetitions of identical processing elements, making them interchangeable and therefore easy to spare. Except for specialized I/O interfaces, the boards can be configured to process wavefront sensor data, do a piece of the inverse tomography, or process DM commands.

3.5.7.5.3 Hardware Interfaces

High throughput I/O must be used to get data from wavefront sensors to processor units and DM command data to the D/A converter hardware associated with each DM or tip/tilt mirror. Similarly, high throughput I/O must be used to get telemetry data to data storage units. For the most part, industry standard hardware is now commonly available that will handle our anticipated data rates, and an industry standard protocol (LVDS) is called out in the conceptual design. These data interconnects will be implemented on reliable high speed interconnects, such as fiber optic links.

3.5.7.5.4 Programming and Design Process

There are a number of FPGA manufacturers and each has commercial design packages to aid in the design of the programming and interconnections. MPP programming is in common practice today in industry and the required skills are taught in university computer and electrical engineering courses.

3.5.7.5.5 RTC Physical Implementation

The very demanding computation and data storage requirements of the NGAO RTC lead to the important questions of power and space usage. The RTC system is large enough that in the nominal design substantial portions of the controller are located off the Nasmyth platform. With limited space and power available on Nasmyth, only the crucial elements are placed there, such as the camera controllers and DM high-voltage drive electronics. These end-units have strict restrictions on the distance of the analog lines between drivers to their respective parts on the AO bench.

3.5.7.5.5.1 Data Transmission Links

Connection between the Nasmyth electronics and the rest of the computer system is via digital optical fiber channel (FC) links. A lot of these are required as the data rates are high. The downlink rates from wavefront sensor cameras amount to 2.2 GB/sec. Serialized transfer via optical fibers at about 1 Gb/sec/fiber capacity will require a bundle of 22 fibers. The uplink rates to the DM and Tip/Tilt drives amount to a smaller value, 25 MB/s which can be handled by one additional fiber. Such fibers and the optical codecs required at each end are standard commercially available items. For example, EDT Corporation, which also makes the frame-grabbers compatible with our choice of WFS CCD controllers, makes compatible fiber optic transmission systems.

The transmission distance for data fiber is rated well in excess of the anticipated distance from Nasmyth to computer room. The round trip transmission time delay affects the control bandwidth, since these links are in the control loop. With fiber transmission speeds about ½ the speed of light, a 100 m distance from Nasmyth to computer room amounts to about one microsecond of delay in an overall latency budget of 500 microseconds.

3.5.7.5.5.2 Power Utilization

Power usage of the RTC as a whole may seem daunting given that the RTC has operation counts rivaling that of a moderate sized supercomputer. The tomography processor requires a number of FPGA devices mounted on custom designed circuit boards. The FPGA manufacturers provide guidelines on power utilization as a function of chip line, on-chip logic utilization, clock speed, and I/O utilization. In the RTC tomography engine the dominant calculation is the Fourier transform where data communication rate between FPGA chips can reach capacity before processor utilization, although the ongoing board design process will attempt to choose chip family and board layout to optimally balance communication and computation utilization. Assuming 100% communication utilization, and logic and processor utilization of about 50%, the resulting power usage for the Xilinx Vertex-6 chips tops out at 15W/chip. With an estimated maximum of 150 chips needed for the system, this yields a 2.25 KW requirement for the tomography engine.

The GPUs assigned to DM command generation use about 200W each, resulting in an additional 1KW needed for 5 DM-dedicated units.

The SATA drives used for diagnostic data capture consume a considerable amount of power owing to the multiplicity of systems needed to support the aggregate 3 GB/s sustained data rate. An 80 TB RAID system running at full capacity will consume about 8 KW.

Rounding out the real time control system is a dedicated RT/Linux system to process tip/tilt controls and another system to act as the RTC control processor (CP). These are standard rack-mount CPU-board based systems using about 500 W each. The total off-Nasmyth power utilization for the RTC, adding in all the other miscellaneous electronics, communications support, power supply, and cooling systems, is under 10 KW. Adding the data-streaming diagnostics capture system roughly doubles this need to on the order of 20 KW.

On-Nasmyth, the driver electronics for 10 WFS camera controllers (7 WFS CCDs and 3 LOWFS infrared cameras) amounts to 500W. The Cilas woofer DM driver takes about 100W while the

MEMS tweeter DM and 3 LOWFS MEMS DMs consume a total of about 100W. The grand total on-Nasmyth, including cooling fans, is on the order of 1 KW.

3.5.7.5.5.3 Space Utilization

Initial analysis indicates that all of the critical on-Nasmyth drive electronics can be fit into 2 ½ standard height 19" racks. These include the multiple camera controllers, with their LVDS interfaces on the data output side, and the DM drivers, which use LVDS control and data signaling input converted to analog and boosted to 200V range.

The tomography engine is situated on up to 5 large custom boards, all mounted in a non-standard enclosure complete with cooling system. The cabinet is approximately 2 standard racks wide but must have additional room to fold open for access to the FPGA boards. Probably a footprint of 1 x 1.5 meters of the computer room will be occupied by this system. The RAID disk systems, GPUs, CPUs (running tip/tilt and CP functions), and fiber communication electronics will occupy another approximately 3 full racks of space.

3.5.7.6 Progress during the Preliminary Design

Significant progress during the PD phase has led to a mature design for the RTC and has established good confidence in the system meeting its goals. This is in view of the fact that the RTC is utilizing novel architectural concepts for AO real-time control – taking advantage of massive parallelization and heavy use of the Fourier domain, and calls for a state-of-the-art compute hardware platform with significant portions being custom designed.

3.5.7.6.1 Hardware to Algorithm Mapping

We have completed a full analysis of the suite of algorithm components needed in real-time and have established strong mappings to the compute hardware. This included documenting all algorithmic details (see KAON 695) and validating that each will operate on the respective platform correctly. The FPGA-based operations (WFS processing, slopes to phase reconstruction and tomography) were tested using an FPGA definition and simulation tool suite (Verilog HDL). The GPU-based operations (DM command generation) were tested on a state-of-the-art NVidia multicore GPU (C-1060) available at the LAO.

In addition to the basic operations of wavefront reconstruction and tomography, the RTC must implement a variety of support operations in its sequence of real-time processing. These include: pupil distortion correction using datapoint interpolation, correction of wavefront sensor centroids using non-linearity lookup tables, implementation of the HODM/LODM control split, and implementation of the MEMS open-loop control inverse model. Each of these have been defined in considerable mathematical detail (refer to KAON 695), and have been strongly mapped to their respective hardware implementations (KAON 696).

The convergence and accuracy of the wavefront reconstruction and tomography algorithms have been validated using IDL simulations.

3.5.7.6.2 Design of Tomography Engine Compute Hardware

Phase 1 of the design of the FPGA boards for the tomography engine computer has been completed under a contract with Axelsys LLC. The design work completed so far has provided us with a board layout, board to board and chip-to-chip interconnection definitions and analysis, partitioning of the computations amongst FPGA chips, definition of power supply needs, and an analysis of the heat load and thermal dissipation requirements. Axelsys has experience taking FPGA board designs from layout through fabrication and installation. They also have experience fielding systems in harsh environments and in our design are taking into account the special needs of the NGAO high-altitude implementation.

3.5.7.6.3 High Speed Interfaces to WFS and DM Drives

The hardware for the high speed interfaces to WFS cameras and to DM drive electronics has been established. LVDS digital communication is identified as a standard for the electrical interfaces and fiber-link for the long-haul between Nasmyth and computer room. DIO, DAC, and communication components, all off-the-shelf components, have been identified and quoted.

3.5.7.6.4 Power and Space

The power supply, thermal dissipation, cabling, rack space, and communication fiber needs are now determined (see section **Error! Reference source not found.**). Details of rack layouts, networks, etc. are given in KAON 696.

3.5.7.6.5 Telemetry Data Capture System

The telemetry system has been specified with the capacity of 3 GB/s sustained data rate and a storage capacity of 80 TB. This will enable storing full frame data for a few nights of science operations. Since this system is optimized for high-speed data recording and not intended for long-term data storage or database service, an off-line ancillary system (see section **Error! Reference source not found.**) will back up the data capture system during off-peak hours. We have begun discussion with potential vendors for the telemetry data capture system.

3.5.7.6.6 Subsystem Testing

A plan for the acceptance testing of both commercial off-the-shelf and custom hardware has been outlined, as well as a procedure for validating the software algorithms as they are implemented on the compute hardware. Project management has asked that the RTC be delivered as a working subsystem prior to NGAO system I&T. As such, the RTC program plan through Full-Scale-Development (FSD) phase has been scoped to include a subsystem integration and test plan for the RTC. RTC subsystem testing will include a point-by-point validation of the system operations at full frame rate given a set of dummy input data with the output signals validated against benchmarks. A testbed and related testing equipment will include input signal generators and data capture systems necessary to validate full frame rate operation.

3.6 Science Operations

This section discusses the hardware and software needed to control the overall NGAO facility for science operations at both the operator and astronomer levels and the pre- and post-observing support tools.

3.6.1 Science Operation Model

The overall goal of NGAO science operations is to maximize the science return from the allocated observing time, given i) the science cases, ii) a performance budget for the instrument suite, iii) an operation-cost for the Observatory and iv) a scientific skill set for the astronomers. There exists a wide range of science operations models to accomplish this overall goal, as a function of the instrument functionalities, the Observatory budget and the *modus operandi* and size of the scientific community.

3.6.1.1 Observing Model: Classical with Built-in Flexibility Tools

A trade study of possible observing models was performed in KAON 476: it recommended that NGAO science operations follow the Keck classical observing model. NGAO nights, particularly LGS nights are scheduled and allocated 6-9 months in advance. Astronomers, assisted by Keck Observatory support personnel, are performing the observations remotely either from Keck HQ or from a partner institution: the astronomers-observers are therefore fully engaged in their observations and can make on-the-fly decisions for the observing strategy.

The suite of NGAO pre-observing tools including simulation and observations planning tools should allow the astronomer to easily and quickly assess the feasibility of a scientific program during the observing proposal submission phase or any phase prior to the observations, and make the best use of the allocated time. Astronomers will want to adapt the scientific program with the observing conditions for the scheduled observing night(s). Using the planning tools, they can make on-the-fly decisions on the observing strategy and take advantage of the various observing configurations with NGAO: NGS/LGS switch, AO science instrument switch, non-AO instrument switch during any night.

One of the risks encountered with the classical observing model is that the data collected be incomplete (e.g., due to bad weather or low observing efficiency) preventing the astronomers from fully exploiting the data and publishing, resulting in a lower science return and visibility for the AO instruments. Our model trade study proposes a scenario that can be phased in with NGAO science operations with low impact on the Observatory support: Each TAC may decide to encourage its astronomers' pool to collaborate for a subset of TAC-allocated nights: the scientific programs could be ranked as a function of required observing conditions, and be given observing priorities till the data is complete. This level of schedule flexibility would likely benefit the overall science return while maintaining Observatory operation costs. The flexibility and scheduling burden would be distributed among the astronomers within the partner institutions. The experiment could be stopped at any time should it be not satisfying.

3.6.1.2 Science Operation Requirements: Observing Efficiency

The requirements from the NGAO science cases (KAON 455) and the observing scenarios for these science cases (KAON 571) led to a set of requirements for the science operations from the astronomer point-of-view that are detailed in the System Requirement Document - SRD (Sect. 6.1.4 in KAON 456). In addition, we have reported on the lessons learned from the LGS science operations at Keck (KAON 463) including weather impact on LGS and observing efficiency budget. From this report and other sources, we have developed a second set of Observatory Operational requirements for the science operations in the SRD (Sect. 6.2.5 in KAON 456).

One of the most important requirements is the percent of time collecting science quality data. Our goal is to achieve at least 80% open shutter science time for "faint field" observing program (programs requiring 1 to 4 hours of total integration time with individual integration time of > 20 min) and 70% for "bright field" observing programs (programs requiring less than an hour of total integration time and including many fields through the observing night). For comparison note that OSIRIS and NIRC2 currently get 65% and 50% open shutter time, respectively.

In accounting for the open shutter science time, we make the following assumptions:

- Weather impact is not included in the calculation of the open shutter science time. Time loss due to weather in LGS mode accounts for ~25% of the total allocated time (KAON 463). We will track the statistics from time losses due to weather in both LGS and NGS mode. Yet given the Observatory option for the classical observing model, this loss cannot be accounted against the NGAO science operation efficiency. The weather statistics will be included in more general discussion on observing model.
- Open shutter time spent on science acquisition, centering the object, checking the SNR, etc is considered overhead.
- Open shutter time spent for on-sky telluric, photometry, astrometry, PSF calibration is considered science time but we will keep track of its contribution to the total time.

While developing the observing scenarios, we have created a simple efficiency budget tool (http://www.oir.caltech.edu/twiki_oir/bin/view/Keck/NGAO/NGAOObservingScenarios) that can be used for each science case and provide a preliminary assessment on the observing efficiency. A snapshot of the tool is presented in Figure 127. The estimates for the overhead for the acquisition sequence are detailed in KAON 567. We have considered minimum, median and maximum estimate for each of these contributions and calculate a weighted average equivalent to *(min + 4*med + max) / 6*. We estimate for the current study that the maximum values represent instances of technical difficulties. Therefore we have not allocated any additional time for technical problems. These estimates have also been checked against current performance.

We can reach ~83% observing efficiency on the high-z galaxies science case, including calibrators. There are still a few contributors to the total overhead whose impact is difficult to mitigate. Any dedicated time for calibration standards has a strong impact on observing efficiency since these objects are "bright field" observed for a few minutes (< 5 to 10 min), with ~100% time overheads (slew, acquisition, SNR check, etc). In the Figure 127 example we have estimated ~27 min for any overhead due to the Laser Traffic Control System (LTCS). LTCS interrupts are due to either 1) a

plane flying in the vicinity of the beam, 2) beam collision with other telescopes, 3) planned request for no-propagation (closure event) from the Laser Clearinghouse (LCH), and 4) on-the-fly phone call request for no-propagation at all from the LCH. A recent change in the LCH operations could lead to additional time losses.

The number of interrupts due to planes is estimated to ~2 per year, making it a non-issue. The number of interrupts due to beam collision with other telescopes will be reduced once the new "first on target" LTCS rule is agreed upon and applied for all Mauna Kea telescopes (currently the new rule is used between the Keck and Gemini telescopes). Under this rule, the first telescope on target gets priority to keep observing (currently telescopes projecting a laser have lower priority and the laser is shuttered for any collision). One gets the most benefit from this rule if it used in parallel with the collision preview tool that can predict the collisions before the telescope slew to a new target, hence allowing the observer to select a target that is clear of "planned" collisions. The benefit from this new rule has yet to be fully assessed.

	A	B	C	D	E	F	G	H
4			Time (min)					
5			min	med	max	(min+4*med+max)/6	Total	
6								
7	Galaxy Field 1	Telescope slew	1	3	6	3.17		
8		Adjust pointing	0.5	1	2	1.08		
9		NGS acquisition	0.5	1	4	1.42		
10		NGAO acq	2	4	6	4.00		
11		Fine centering	1	2	4	2.17	**11.83**	
12		Ind. Science integration	15	20	30	20.83		
13		Total Science Integration	90	150	240	155.00	**155.00**	
14		repeat	6	7.5	8	7.44		
15		Re-Fine centering	1	2	4	2.17		
16		# of re-centering	0	2	4			
17			0	4	16	5.33	**5.33**	
18		Dither/setup/readout	0.08	0.25	1	0.35		
19		x # of repeats	0.48	1.875	8	2.58	**2.58**	
20								
21	Telluric calibration 1	Telescope slew	0.25	0.5	1.5	0.63		
22		Adjust pointing	0	0	0	0.00		
23		NGS acquisition	0.5	1	2	1.08		
24		NGAO acq	1	2	3	2.00		
25		Fine centering	0	0	0	0.00	**3.71**	
26		Ind. Science integration	1	2	3	2.00		
27		Total Science Integration	2	4	8	4.33	**4.33**	
28		repeat	2	2	2.67	2.17		
29		Dither/setup/readout	0.08	0.25	1.00	0.35		
30			0.16	0.5	2.67	0.75	**0.75**	
31								
32	**Total field #1**	**Total Observing**					**183.54**	
33		**Total Open Shutter**					**159.33**	**0.87**
34								
35	Flux standard	Open shutter				4.33		
36	(eq. to telluric std)	overhead				0.75	**5.08**	
37		repeat per night					**2**	
38	**Total Std Flux**	**Total observing**					**10**	
39								
40	**LTCS interrupts**	ind integration time	20.83	20.83	20.83			
41		re-fine centering	2.17	2.17	2.17			
42		# of interrupt	0	1	3			
43			0	23	69	26.83	**26.83**	
44								
45								
46								
47								
48	Available hours/night		9.1	10.25	11.3	10.23		
49			546	615	678	613.50	**613.50**	
50								
51	Number of field/night					3.14		
52								
53								
54								
55								
56	**Efficiency**	**Total Observing**					**613.50**	
57		**Total Open Shutter**					**509.14**	
58		**Total overhead**					**104.36**	**613.50**
59		**Observing efficiency**					**0.83**	
60								

Figure 127: Efficiency estimate for the high-z galaxies science case

The planned LCH requests for closure on a specific target direction can be included in the observing planning tool and can result in minimal impact on the observing time losses *as long as they are less than 10 min and rare*. LCH closure requests were rare and insignificant from 2003 to 2007. After LCH released the SPIRAL 3 software, closures increased dramatically (up to several hundred closure events per night). The AO Ops Team has documented the pointing accuracy of the LGS for LCH and LCH has reduced the half-cone angle to 0.1º for Keck II and 0.5º for Keck I. On Keck II, this has reduced LCH closures to 0-2 per target per night with each closure lasting <10 seconds. It is possible that with more lasers and new pointing control, the LCH half-cone angle will increase initially for NGAO. Once the pointing control of the NGAO LGS facility is proven, we anticipate that LCH will reduce the half-cone angle.

Last minute phone call request for no-propagation from LCH have a huge impact on efficiency for the given night since this stops all LGS operations for durations of 1 hour up to the entire night.. As of 2010, the number of these incidents is on the rise. The AO Ops team is exploring how to reduce these "blanket closures". Last but not least, the ability to abort a science exposure quickly and either get ready for a new exposure or move to a new target faster should contribute to reduce the impact from LTCS events.

3.6.2 Science Operations

3.6.2.1 Operation Control Infrastructure

For a given observing model, the observing efficiency is *the* important design requirement for the individual components (e.g., reading out the camera), but not mostly for the integrated system (e.g., offset to sky). The current Keck II LGS system feeding NIRC2 or OSIRIS performs routinely with ~ 30 - 50% overhead depending on the science program (KAON 463). Its limited efficiency as an integrated system is primarily due to the serial architecture for the command interfaces between subsystems (AO/laser/telescope/science instruments) and the lack of multi-system coordination sequences.

To address the efficiency requirement with NGAO as an integrated system, we are proposing a new integrated design. Our conceptual design includes 1) a multi-system sequencer for commanding the sub-systems in parallel (e.g., offset the telescope as the science instrument writes the FITS file to disk) and 2) a sequencer for each subsystem (AO, laser, science instrument) to quickly and reliably handle complex command for a given subsystem (e.g., set AO subsystem for NGS field acquisition).

The overall control infrastructure is documented in section 3.5. The three main components of the NGAO science operations are:

1. The Pre- and Post- Observing Tools
2. The Operation Control GUIs
3. The Multi-system Command Sequencer

The pre- and post-observing tools and operational control GUIs comprise the NGAO Science Operations Tools GUI suite and further details on these tools can be found in KAON 744. These functions will be covered by four or five tools. In the current system, planning is divided between the

web-based AO Guide Star Tool, to find NGS, and the stand-alone OSIRIS Observing Planning GUI (OOPGUI), to define observing sequences. These functions may be combined into an NGAO Planning Tool, or left separate as the Acquisition Planning Tool and the Observing Planning Tool. For further discussion, we will assume separate tools. The other three stand-alone tools will be the Execution Client, the Observer's Status Display, and the Operator's Status and Control Display. We highly recommend that the current ethos of separating form and function be continued.

1. The web-based Acquisition Planning Tool will inherit strongly from the AO Guide Star Tool used by the current LGSAO system. The planning tool will require an internet connection to provide catalogs and images and will produce a data product that inherits strongly from the current LGS starlist format and will be compatible with the MAGIQ acquisition and guiding system of the telescope. This data product will be compatible with the Execution Client and will be executed as an acquisition sequence.

2. The Observing Planning tool will inherit many features of the OOPGUI and will be a stand-alone tool. It will allow the observer to define an observing sequence that includes configuring the science instrument, data taking, dithering, and offsetting. It will produce a data product that is compatible with the Execution Client and will be executed as an observing sequence.

3. The Execution Client will inherit many features of the OSIRIS Data Execution Client (ODEC) and will be the main interface to the Multi-System Command Sequencer (MSCS). The Execution Client will read in all sequences (calibration, acquisition, setup, and observing) and output them in a common format to the MSCS.

4. The Observer's Status Display will inherit from the Laser User Interface (LUI) tool developed for the current system; it provides the information needed for filling out log sheets, for making tactical observing decisions, and for automatically answering observer's questions as to why a certain step in the acquisition sequence is taking longer than usual. Although targeted toward the needs of the observer, the Observer's Status Display will be useful to the NGAO operator under nominal operating conditions. Initially, the NGAO operator may be a separate position, but eventually could be the observing assistant (OA) or support astronomer (SA).

5. The Operator Status and Control Tool will incorporate the functionality of an alarm handler along with direct status and control functions needed to optimize performance and troubleshoot fault conditions. We envision this tool to use a simplified light path to aid in troubleshooting.

In addition to the five top-level tools, the NGAO Science Operations Tool suite will provide tools to coordinate targets with the Laser Clearinghouse (LCH), to optimize NGAO given observing conditions and NGS "constellation", and to characterize the point spread function (PSF) as a function of time, field position, and wavelength.

In Figure 128, we present a block diagram for the science operations architecture using a view that complements the architecture information from KAON 569. The configuration for the NGAO and the science instrument depends on the science program and the observing strategy and is determined during the pre-observing phases. Using a set of planning tools, the astronomer will develop the detailed observing plan and save all relevant parameters in configuration files. These configuration files can be loaded by the Operation Control GUIs. From the Operation Control GUIs, the operator and the observer will command & control the observation sequences: AO & science acquisition, system tune-up, observing sequences (snapi, dither, offset, filter, etc). The observation sequences are managed by the Multi-system Command Sequencer (MSCS): complex sequences for one subsystem are handled by the subsystem sequencer (e.g., "setup AO bench for NGS" is performed by the AO sequencer) or executed directly from the MSCS for simple command.

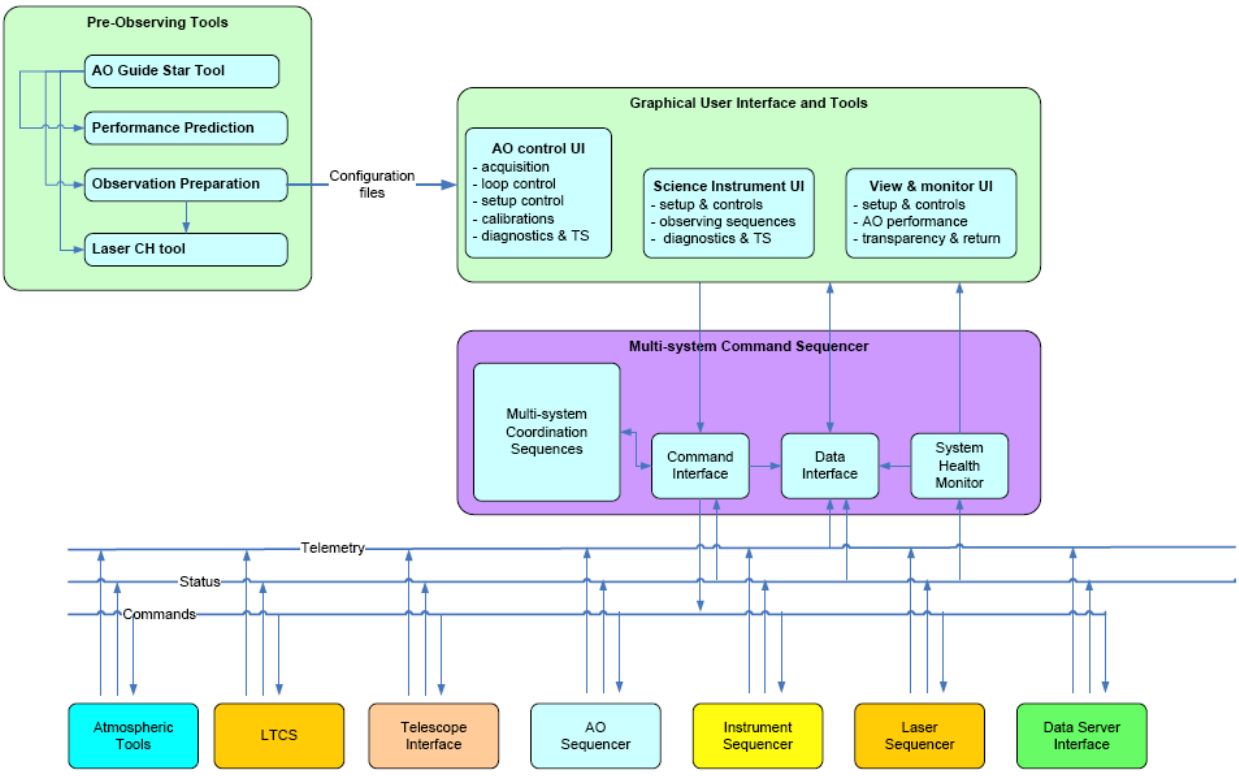

Figure 128: Science operations tools block diagram

The post-observing tools have been omitted in Figure 128. The pre- and post- observing tools are described in more detail in the next section.

3.6.2.2 System Configurations Matrix

The purpose of the system configuration matrix is to help map requirements to components. The NGAO system configuration is shown in Table 36 (section 5.4.1). It represents a total of 5 different configurations in NGS mode and 5 in LGS mode for acquisition, calibrations and science observations with the science instruments (interferometer, imager, IFS). Some of the configurations include more options (e.g., rotator mode in fixed field or fixed pupil). This matrix is also key to the

design of the sequences of commands to the subsystems and individual components during calibrations, setup and observing sequences.

3.6.2.3 System Calibration: Routine and Maintenance Calibrations

The calibrations include 1) routine calibrations, and 2) maintenance calibrations. The routine calibrations are calibrations that are required on run-to-run or night-to-night basis such as fine laser alignment and power calibrations, DM to lenslet registration, non-common path aberrations, etc. The maintenance calibrations are performed following a schedule and may include detector response, noise and offsets calibrations, TT and DM interaction matrices (poke matrices), motion control tune-ups, throughput, etc.

We anticipate that the daily calibrations will be performed by the observing support team using the high-level science operation tools. The maintenance calibrations may be implemented at the sub-sequencer level when applicable. The corresponding calibration sequences will be coded and implemented at the MSCS and/or at the subsystem sequencer level. Note that the use of the keyword architecture as currently implemented at Keck will allow the scientists to easily prototype and validate the calibration algorithm using their programming language of choice during the I&T phases.

3.6.2.4 System Operations: Acquisition

The NGS and LGS acquisition requirements and conceptual design are discussed in KAON 567. This includes a trade study between near-IR and visible detector technologies that found that a commercial CCD is sufficient for the NGS acquisition task. The NGS acquisition will also rely on data retrieval from multi-color astronomical catalogs (USNO-B, GCS-II and SDSS). KAON 567 lists and studies the possible risks during the acquisition process. The specifications for the acquisition conceptual design are presented in Table 13.

Table 13: Acquisition conceptual design level specifications

Title	Specifications
Field of view	≥ 120"
IR field identification	a) Image sources in the near-IR (1.0-2.0 μm) b) Image sources in the visible (0.5-1.0 μm) In both cases, use supplementary information about target locations from catalogs and surveys
Point source sensitivity	V=22 or J=19, exposure ≤ 10 s, SNR ≥ 10
Position accuracy	≤ 0.050" rms, random errors in determining source positions in an acquisition camera image
Minimal time overheads	Total acquisition process time typically < 50 s, worst case < 120 s. Includes time for telescope moves, camera exposure, and analysis.
Photometric imagery	Photometric error of 0.2 magnitudes, in standard astronomical bands such as Johnson, UKIDDS, or SDSS
Registration accuracy	≤ 0.020" rms, random error in determining positions of acquisition camera with respect to telescope optical axis
Diagnostics and troubleshooting tools	Report metrics for automatic acquisition and to aid observer decision-making, including manual override by astronomer or observing assistant
Data products	Store acquisition images as FITS files, and appropriate diagnostics, in the NGAO data server
Interface to observer planning tools	Acquisition software will receive target information from the NGAO observer planning tools
Guiding mode	Used for testing when wavefront sensors not available

The telescope pointing accuracy is currently the largest risk for the observing efficiency. The observing efficiency budget depends on the brightness of the NGS and acknowledges the difficulty of acquiring fainter stars. A single camera design is feasible for LGS and NGS acquisition using a CCD sensor. High level requirements and interfaces to other NGAO subsystems are also discussed in KAON 567.

Table 14 presents a generic description for the acquisition sequence for NGAO with an emphasis on the parallel steps. The NGAO planning tools will assist the astronomer to select the next science target. All relevant configuration information will be loaded by the Operation Control (OC) tools.

Table 14: Generic NGAO acquisition scenario

Step	Observing Step	Parallel Steps	Remarks
0	Select next target: - assess science priority - check target elevation range - check observing conditions - check LTCS conditions	Complete integration on current science target or calibrator. When target selected from Planning Tools, then information is loaded in OC tools.	It is not clear yet whether the astronomer will have to run these checks manually or whether it will be automated.

1	Upon completion of readout of science array, LGS is shuttered, AO loops open and key-system feedback parameters are saved then the operation control tools trigger the telescope slew.	OC tools parses information, and get ready for execution: - NGS parameters for acquisition - AO configuration - Instrument configuration	
2	Telescope slews	The OC tools send commands to the multi-system sequencer. Setup sequences are executed as appropriate by the AO, laser & science instrument sequencers.	
3	Telescope Pointing Adjustment on one of the NGS (brightness allowing). This step is automatically performed by the NGS acquisition subsystem with the visual check of the Observing Assistant (OA). Upon success, pointing corrections are applied and next telescope slew is commanded from the OC tools.	There is no need to use the acquisition camera for the LGS acquisition: LGS pointing model is accurate enough to get all laser spots centered within the capture range for the HO WFS.	This step may be required only when the NGS V>18 mag. (TBC) or when the telescope slews by more than x° in elevation/azimuth range.
4	Telescope coarse registration on the science field. NGS acquisition subsystem runs an automated routine to record and process image, ID the NGS in the field with respect to catalog data then compute required offset. Visual check of process by OA. Upon success, position offsets are applied to telescope.	LGS propagation and acquisition steps initiated. Laser pointing correction and uplink TT correction loops closed with very low gain. Pickoff mirror positioning and LOWFS setup complete including background.	Need to implement the acquisition for the vibration/wind shake reference. Need additional study for telescope guiding. Not clear if the HOWFS will require a background.
5	Telescope fine registration on the science field: If photons not detected at the expected SNR on the LOWFS (or NGS not on Pointing Origin), then NGS acquisition subsystem runs a 2nd iteration. Visual check of process by OA. Iterate if necessary (to be detailed). Upon completion adjust telescope pointing model.	Pick-off mirrors for science and TWFS in position	Need to check the conditions for the dichroic during this step. Need to be able to adjust pointing model for telescope even though PO != REF.

6	AO subsystem control: 1) low gain on woofer & MEMs, 2) increase gain on UT, 3) start telescope guiding, 4) adjust woofer & MEMs gain, 5) initiate TWFS + tomography optimization	Science instrument is setup: optics and read modes are set and confirmed. May record first exposure to check centering with point-source and expected SNR/coadd. Monitor image quality and assess optimization progress.	UTT acquisition requires more design. Assuming redundant information from USNO-B, GSC-II & SDSS uncertainty in field centering should be < 0.2".
7	Science integration starts		

The main contributions to the centering error budget during NGAO acquisition in LGS mode are:

1. The accuracy for the knowledge of the separation distance and position angle between the stars and the galaxies from the literature. This information is provided by the astronomer, and can be < 0.01" if the field has been observed (recently) with HST cameras. The USNO-B on-line catalog provides an astrometric accuracy of 0.2", and the astrometric solution for the USNO-B, GSC-II and SDSS catalogs are improved as the proper motions are being calibrated using GSC-I (KAON 467).
2. The pickoff arm positioning accuracy for each science target with respect to the TT closed-loop reference position for the LOWFS, which is the total of:
    a. The internal positioning accuracy and position stability for each individual pick-off arm.
    b. Registration accuracy and stability between LOWFS and science arms including TT stage positioning accuracy.
3. The differential atmospheric refraction between the LOWFS and the science instrument.
4. The total contribution from the optical distortions due to thermal gradient, alignment error, woofer and MEMs positioning between the science array and the LOWFS.

3.6.2.5 System Operations: Dithering and Offsetting

Several approaches to dithering and offsetting were proposed and discussed in KAON 558. The rationale for reviewing the dithering and offsetting scenarios comes from the important overhead (~30 seconds per move) it currently takes to perform these important observing steps.

The selected approach (KAON 669) avoids any telescope move and AO pause/resume sequence, unless necessary. Most field repositioning on the science array is performed to account for pixel/spaxel response, background emission or super-sampling and are of relatively small amplitude (< 2"). They could be performed by a tilt on the second-relay MEMS. This implementation leaves the LOWFS, TWFS and LGS WFS closed during the entire observing sequence, and allows for maximum flexibility and efficiency for centering the science target, tracking, correcting for DAR, etc. We believe that the internal optics have the required pointing accuracy and could result in minimal overhead (< 5 second).

Offsets of larger amplitude are performed by requesting a telescope offset, repositioning the probe arms at a different field location and re-acquiring the guide stars on the AO sensors. This may take about ~ 15 to 30 seconds depending on the detailed implementation.

We are confident that the combination of these scenarios along with parallel commands to different subsystems will address the efficiency requirement for dithers and offset for the key science cases.

3.6.3 System Control

The high-level control of the system is performed through the Operation Control GUIs and executed by the Multi-system Command Sequencer (MSCS). A schematic view for these controls was presented in Figure 128.

3.6.3.1 Multi-System Command Sequencer

The MSCS is the main interface between the Operation Control GUIs (configured and controlled the by AO operator, the expert user and the observer) and the control of each subsystem. The important design concept we have opted for, is to have all complex observing sequences under a central supervisory control system that will send and coordinate commands with the AO, Laser, science instrument(s) and other subsystems (see section 3.5.1).

The MSCS has four main components: a library of multi-system coordination sequences, a command interface, a data interface and a system health monitor. The functions of these four main components are as follows:

- Multi-system coordination sequences. The multi-system coordination sequences are a collection of functions which implement complex sequences of commands for the underlying control subsystems (AO, Laser, etc). A multi-system coordination sequence allows the user to send a simple command to the MSCS, while it commands and coordinates all of the many tasks required by this command and returns the status to the user. The coordination sequence receives a command from the user and then sends multiple commands appropriate for the task to be accomplished to the underlying multi-systems using the main command interface discussed below. Examples are: the LGS setup sequence that is used during slew to startup, initialize and setup AO, Laser and science instrument for the next LGS acquisition sequence. A key task during the PD phase will be to identify all of the coordination sequences required for the MSCS and to specify their requirements. Note that we will likely require some flexibility in the management of this sequence library as we plan to add sequences to the library, mostly diagnostic and troubleshooting sequences, during the I&T and early operation phases of the system. The reliability and efficiency of the NGAO operations strongly rely on the successful implementation of the multi-system coordination sequences.
- Command interface.
- Data interface (see Section 3.5.6).
- System health monitor. The system health monitor is a task that monitors the status of the MSCS functions and tasks.

3.6.3.2 Operation Control (Graphical) User Interfaces

The operation control GUIs are the main interface between the Users (AO operator, expert user and observer) and the control of components and execution of sequences with the NGAO and science instrument.

For NGAO, the operation control GUIs will be the Execution Client and the Operator's Status and Control Display. The NGAO Execution Client will be able to read in all products of the Acquisition Planning and Observing Planning Tools and send these to the MSCS in the form of a common structure. These include NGAO calibration sequences, configuration sequences, acquisition sequences, and observing sequences.

The detailed design for the operation control GUIs for the science instruments will be defined in the science instrument manual. We anticipate that the Observing Planning Tool and the Execution Client will comprise the operation control GUIs for the science instrument and that the science instrument team will develop instrument status and image display software. We will work with the science instrument team to ensure a cohesive design.

We have opted for the following preliminary set of design choices:

- The GUIs will be modular (as shown in Figure 128) and include three main parent components: 1) NGAO controls, 2) science instrument controls and views, and 3) system-view and performance monitoring displays.
- The implementation of these tools should be fully compatible with the pre- and post-observing tools.
- Several GUIs may be required during the operations per parent component. We will attempt to limit the total numbers of GUIs. Due to the limited integrated software development, our current LGSAO control includes as many as 30 displays and leads to some confusion during LGS operations.
- The control GUIs will include two types of command controls: controls for direct commands with no parameters e.g., open AO loops, (re-)close AO loops and controls for more complex commands requiring some parameters e.g., an acquisition sequence using a configuration file.
- The operation control GUIs will be designed to be user-friendly and include/display the minimal complexity. All complex commands will be implemented at the lower levels in the MSCS and subsystem sequencers. Additional complex commands could be controlled using specific calls to a different set of GUIs (e.g., a somewhat complex calibration widget could be called from the NGAO GUI).
- The user can select the parameters for complex command either by loading a previously saved configuration file (these configuration files are also the outputs of the planning tools) or by manually entering values in the configuration fields.

3.6.4 Pre and Post-Observing Tools

3.6.4.1 Pre-observing Tools

The pre-observing tools will allow the observer to simulate, evaluate and plan for an observing program using the NGAO and the science instrument(s) any time prior to the observations,

particularly during the observing time proposal submission process. The astronomer will likely go through a second phase of observation planning in the month prior to, and days leading to the observations. During the observing night, the observer may use the same sets of tools to check and refine the observing strategy, if necessary.

The pre-observing tools are the Acquisition Planning Tool and the Observing Planning Tool. The Acquisition Planning Tool will inherit strongly from the excellent AO Guide Star Tool, while the Observing Planning Tool will inherit many features of the OSIRIS Observing Planning GUI (OOPGUI).

Like the AO Guide Star Tool, the Acquisition Planning Tool will be a web-based utility that displays survey images and catalog positions of possible guide stars. Observers can determine whether a guide star is within reach of the system and add it to their starlist. Once complete, the observer may submit their starlist via this tool in the proper format. Additionally, the Acquisition Planning Tool will have the ability to:

- Load images from surveys other than DSS (SDSS, Pan-STARRS, LSST)
- Load user-supplied images
- Search online image archives and create links to images (HST, Subaru, etc.)
    - often, these archives do not serve images like DSS, but rather allow registered users to download raw or reduced FITS files
- Cross-check available catalogs to flag:
    - high proper motion stars
    - galaxies
    - magnitude or coordinate disagreements among catalogs
- Provide access to an online ephemeris calculator such as JPL Horizons for nonsidereal targets
- Perform rudimentary color transformations to estimate magnitudes in the proper band if no measurements are available
    - given Rmag, b-v, and b-r, one can, for example, estimate Jmag and Hmag assuming the star is “normal”
- Overlay brightness and accuracy of astrometry onto images
- Allow users to upload their own catalog information in either absolute or relative coordinates
- Estimate the AO performance (Strehl ratio, encircled energy, field dependent PSF) given median conditions with the selected NGS “constellation”
- Estimate the time required to acquire and optimize NGAO with the selected NGS “constellation”

The Observing Planning Tool will permit the astronomer to define the observing sequence that the Execution Client can use to collect data. An observing sequence can include instrument configuration(s) such as pixel scale, filter, integration time(s) and dither and offset patterns. The output from such planning will be a text file that will be readable by the Execution Client which will communicate with the MSCS. Additionally, the Observing Planning Tool will have the ability to:

- Read the starlist (acquisition sequence) and import target and NGS positions
- Load a sky survey image (DSS, SDSS, Pan-STARRS, LSST)
- Load a user-supplied image
- Overlay the dither pattern on the sky image (this is the most requested feature of the OOPGUI)

- Estimate the SNR and precision of astrometry and photometry of an observation given median conditions, the predicted NGAO performance, the source flux, and the total integration time
- Estimate the total integration time needed to obtain the required SNR given median conditions, the predicted NGAO performance, and the source flux
- Estimate the companion sensitivity of an observation given median conditions, the predicted NGAO performance, the source flux, the companion separation, and the total integration time
- Alert user if dither sequence does not dwell long enough for TWFS optimization (NGS mode only)

The requirements for these tools are a combination of derived-requirements from the science cases and operational requirements. A block diagram for the pre-observing tools architecture design was shown in Figure 128.

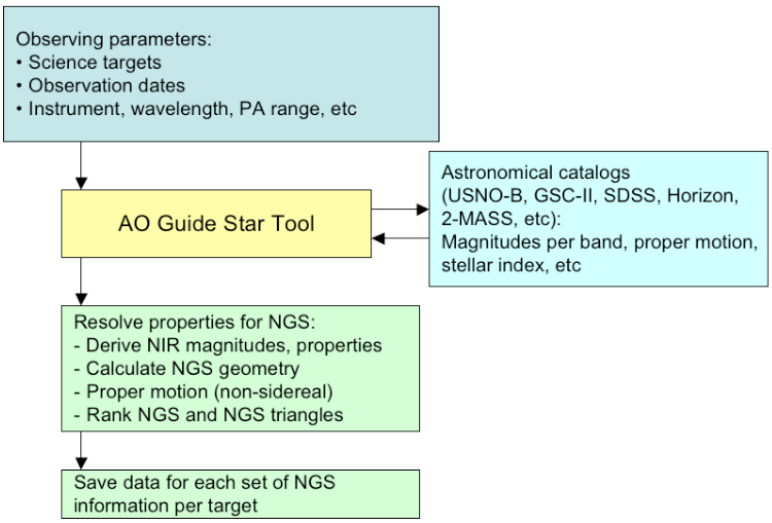

Figure 129: AO guide star tool workflow

During the proposal phase, Acquisition Planning and Observing Planning Tools need to assist the astronomer in identifying suitable Guide Stars and providing a first order estimate for the image quality, the exposure time and expected SNR and the observing strategy, given a basic science instrument setup. The information saved by the user might be inserted in the technical justification of the proposal. The tools need to be user friendly and easily portable on most computer's OS.

During the detailed observation planning, the same tools will be used to evaluate, optimize and prepare the observations sequences. The output parameters for the guide stars and instrument configurations will be saved in a format shared by the NGAO observing tools. The information will be loaded by the observing tools during night time operations.

Finally, during the observations, these tools may be used to preview and assist the on-going observations and for any on-the-fly change to the observing strategy.

Figure 129, Figure 130 and Figure 131 succinctly present the workflow for the AO guide star tool, the performance simulation and exposure time calculator, and the observation preparation tools, respectively.

The Acquisition Planning Tool is used for both LGS and NGS cases. It is a versatile tool that will make requests to astronomical catalogs, resolve target names, find and select AO guide stars for the NGAO science cases based on their derived NIR brightness and save the results. It is required to find a single star for NGS and sets of triplets for LGS. The sets of triplets will be ranked according to the estimated total residual error on the estimation of the TT mode and quadratic null modes. The results will be saved in the valid format for the telescope and the tools.

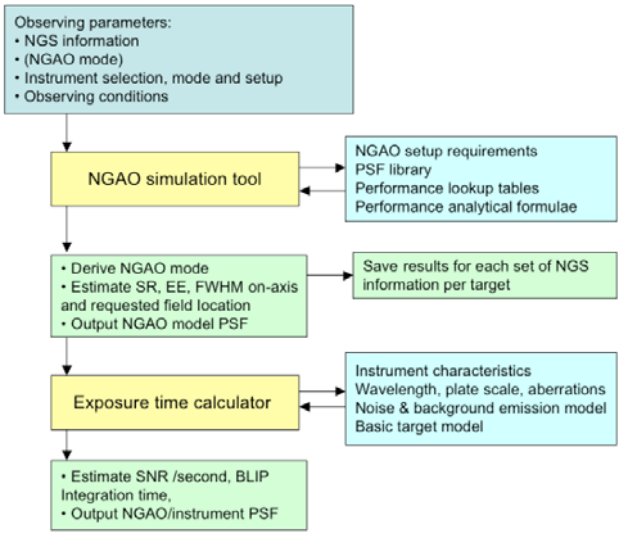

Figure 130: NGAO performance estimation tool and exposure time calculator workflow

The Observing Planning Tool will take as inputs the AO Guide Star(s) information, the AO mode, the selected instrument and the (anticipated) observing conditions. As it will run on the host computer, or through a web-server, it will not be able to (re-)run a full NGAO simulation for each new observing program. Instead, it will make use of a combination of PSF libraries, performance lookup tables and analytical formulae to estimate AO quantities such as SR, EE, FWHM and possibly a 2-D NGAO model PSF for the science field(s). The tool will allow the user to compare performance results from different AO Guide Star(s) and different LGS asterisms configuration. The output results and the parameters used for the simulation will be saved in a file. The parameters and the algorithm for the simulation tools are yet to be defined.

Once the AO performance has been estimated it is then possible to calculate the exposure time to achieve a desired SNR given the instrument selection and setup, the detector read mode, a model for the noise and background emission, as well as a (simple) flux distribution model for the target. The tool will also estimate the background limited performance time and check that the detector is used in its linear range.

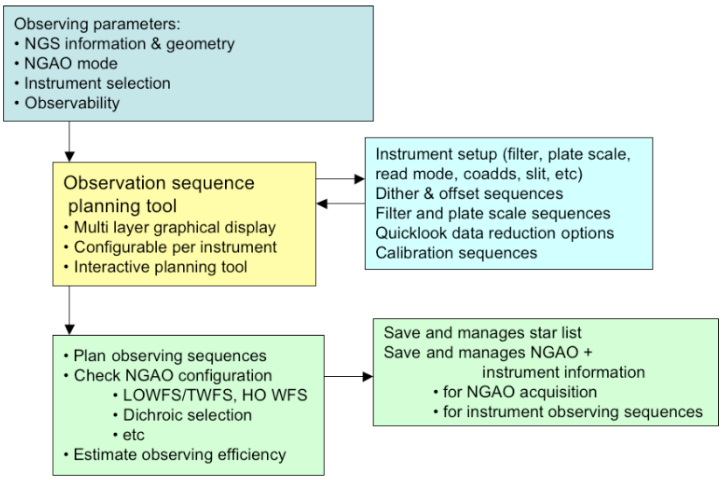

Figure 131: Observation preparation tool workflow

The Observing Planning Tool will take as inputs the information from the selected AO guide star(s), the NGAO mode, the instrument selection and when required, the observability of the target. The astronomer will define the parameters for the observing sequences that are possible for this observing mode. The tool will check the NGAO configuration e.g., dichroic configuration and expected NGS flux on the LOWFS compatible with the selected observing wavelength. The parameters to be set for the observing sequences are yet to be defined. The tools are anticipated to allow for flexible and versatile use of the instrument. The configuration for the observing sequences will be saved in files that will be loaded at the time of the observations. We have yet to define how these files will be managed. A manual management for these various configuration files (guide star and science targets information, NGAO configuration, instrument configuration, observing sequence information, etc) could lead to confusion. We will consider implementing an automated file management from the observing proposal phase to the final execution at the telescope.

3.6.4.2 Post-observing Tools

The post-observing tools and interfaces are:

- Data quality metrics: the purpose of this tool is to reduce and analyze data collected during the observations and output quantities such as total residual wavefront error, seeing, photometric stability, Na return, observing efficiency, etc. These quantities have yet to be defined during the PD and DD phases. The results will be saved and stored with the final data product.
- Data product management tool: the observer and the support staff will use this tool to define which data needs to be saved and stored with the science data. This data product management may also help manage the data that does not need to be stored and can be deleted.
- PSF reconstruction tool: based on the WFC data stored on the data server, the C_n^2 information, and other system parameters the PSF reconstruction tool will provide an estimate for the PSF in specific locations in the science field. The algorithms for the PSF reconstruction are yet to be defined. We have started the development of a prototype algorithm for the current NGS and LGS system for the on-axis and off-axis cases.

3.7 Science Instruments

3.7.1 Science Passbands

The NGAO system passbands, as defined by filters in DAVINCI, are summarized in Table 15. Additional details on the NGAO passband definitions can be found in KAON 530.

Table 15: NGAO system passband and observing band characteristics

Passband name	Cut-on λ (μm)	Cut-off λ (μm)	Notes
NGAO Visible	0.68 (0.62 goal)	1.07	Goal is useful Strehl at Hα
NGAO I	0.700	0.853	
NGAO Z	0.818	0.922	
NGAO Z spec	0.855	1.050	Custom NGAO z band for spectroscopy
NGAO Near-IR	0.97	2.40	
NGAO Y	0.970	1.07	UKIDSS photometric
NGAO Y spec	0.970	1.120	
NGAO J	1.170	1.330	UKIDSS/Mauna Kea photometric
NGAO J spec	1.100	1.400	
NGAO H	1.490	1.780	UKIDSS/Mauna Kea photometric
NGAO H spec	1.475	1.825	
NGAO K	2.030	2.370	UKIDSS/Mauna Kea photometric
NGAO K spec	2.000	2.400	

3.7.2 DAVINCI

DAVINCI, the Diffraction limited Adaptive optics Visible and Infrared iNtegral field spectrograph and Coronagraphic Imager is the first light science instrument for the Keck Next Generation Adaptive Optics system (NGAO) at the W. M. Keck Observatory (WMKO).

DAVINCI is a fully cryogenic instrument providing imaging at the diffraction limit over a wavelength range of 0.7 μm to 2.4 μm with a fixed plate scale of 7 milliarcseconds (mas). The field of view (FOV) for imaging is 28.7" x 28.7" using a Teledyne Hawaii-4RG detector with 4096 x 4096 pixels and a 2.5 μm cut-off wavelength. The imager provides a selectable coronagraph mask and a large selection of photometric, continuum, and narrow band filters. A tracking cold pupil mask is provided for H and K band observations, and an additional selection of pupil masks is provided for the shorter wavelength bands and for the coronagraph mode.

DAVINCI also provides integral field spectroscopy (IFS) with 112 x 60 spatial samples over a wavelength range of 0.7 μm to 2.4 μm. Samplings scales of 10, 35, and 50 mas are provided, resulting in FOVs of 1.12" x 0.6", 3.92" x 2.1", and 5.6" x 3".

The central portion (~6") of the DAVINCI FOV can be sent to the IFS, allowing simultaneous spectroscopy and imaging. Fixed gratings are provided for each wavelength range, operating in the first order near the blaze angle with R ~4,000. The IFS is optimized for narrow band observations (~5% bandpass) and uses a lenslet image slicer combined with novel reformatting optics to provide 6 virtual slits (680 pixels per spectra) on a Hawaii-4RG detector with a 2.5 μm cut-off wavelength.

In the following sections we summarize the design and performance of the DAVINCI instrument. A more detailed discussion is provided in the DAVINCI Preliminary Design Report (KAON 761); the references mentioned here can also be found in that KAON.

3.7.2.1 DAVINCI Science Drivers

DAVINCI is expected to offer high performance imaging and spectroscopy for science observations with NGAO. The top level science driven requirements (Table 16 and Table 20) for DAVINCI are:

1. Diffraction limited imaging from 0.7 to 2.4 μm with at least 3 pixel sampling to 1 μm, and 2 pixel sampling to 0.7 μm
2. High throughput
3. Imaging over an FOV that is as large as possible for NGAO, ~20" to 30" diameter
4. Integral field spectroscopy from 0.7 to 2.4 μm with spatial scales suited to the diffraction limit and the maximum ensquared energy provided by NGAO
5. Coronagraphic imaging with contrast of at least 10^{-4} from 1 to 2.4 μm over an inner working angle of 200 mas

NGAO offers a significantly extended parameter space for these observations, both in terms of spatial resolution and wavelength range. Detailed studies of the performance for various science cases and sky coverage fractions support the view that imaging capability suited to the diffraction limit will provide excellent results over the wavelength range of 0.7 to 2.4 μm. The combination of the AO system and imaging capability are expected to support high accuracy relative photometry and high accuracy astrometry. The imaging capability is also expected to have high throughput and appropriate background suppression in order to take advantage of the low backgrounds provided by NGAO, and the imaging capability must provide a coronagraph to support the detection and characterization of planets around nearby low mass stars.

An integral field spectrograph (IFS) is recognized as an ideal way to take advantage of the image quality offered by NGAO because of its ability to provide spatially resolved spectroscopy of diffraction limited images without suffering from losses due to a mismatch between a long slit and the shape of a complex object. IFS data can provide information essential for deconvolution of the point spread function (PSF) and offers a comprehensive tool for determining kinematics, mass distributions and velocity dispersions.

3.7.2.2 Imaging Science with DAVINCI

DAVINCI's imaging capability represents a general purpose tool that will be expected to serve a wide range of scientific needs as well as provide a tool for characterizing the performance of the NGAO system. The imager's performance requirements are in turn defined from two viewpoints, the NGAO science cases, and a technical viewpoint that defines the requirements for performance measurement. Here we will consider the science driven performance requirements with an understanding that satisfying the most demanding of these will also provide the performance needed for AO system characterization.

The general purpose nature of the imaging capability is reflected in the number of NGAO science cases that require imaging. Based on a review of those science cases, the important performance parameters for the imaging capability are summarized by science case in Table 16.

Several of these science cases identify the desirability of accessing wavelengths below 1 μm, either for specific diagnostic lines such as the Ca II triplet (~850 nm), or for the improved spatial resolution available at the shorter wavelengths. A number of the science cases also require high levels of performance from astrometric and photometric measurements obtained from NGAO observations. Initial evaluation of the I band for color-color diagrams indicates that extending coverage to this band will prove highly beneficial to the study of stellar populations.

Table 16: Summary of the primary science driven parameters for DAVINCI imaging

Science Case	Wavelength Coverage†	Field of View	Spatial Sampling	Sensitivity and SNR	Other requirements
Measurements of General Relativity Effects in the Galactic Center*	H, K (1.49 to 2.37 μm)	10" x 10"	At least λ/2D sampling	Better than current AO system with NIRC2	Astrometric performance > 0.1 mas
Imaging and Characterization of Extrasolar Planets around Nearby Stars*	Y, J, H, K (0.97 to 2.37 μm) Also below Y to 0.9 μm	< 5"	Diffraction limited sampling. At least 1.5 x better than λ/2D sampling at J (goal Y)	10^{-4} contrast at 200 mas separations, goal of coronagraph with inner working angle of 70 to 100 mas. ΔH = 13 at 1" separation, H = 25 for σ = 5 in 20 minutes.	R ~100 spectroscopy? Relative photometry to accuracy ≤ 0.1 magnitudes, astrometric precision of 2 mas. 6 λ/D general purpose coronagraph.
Multiplicity of minor planets*	Z, Y, J, H, K (0.818 to 2.37μm)	≤ 4"	Diffraction limited, λ/3D for J, H, and K-bands, or λ/2D for R and I-bands		
Gravitational Lensing	I, Z, Y, J, H, K (0.7 to 2.37 μm)	≥ 15" dia., goal of 30" dia.	Diffraction limited, λ/2D		Relative photometry to accuracy ≤ 0.1 magnitudes
Size, shape, and composition of minor planets	Z, Y, J, H, K (0.818 to 2.37 μm) I band to 0.7 μm desirable for asteroid shapes	≤ 4"	Diffraction limited, λ/3D for J, H, and K-bands, or λ/2D for R and I-bands	R = 29 for 5σ in 1 hour (from NGAO proposal, table 14)	R ~100 spectroscopy?
Characterization of Gas Giant Planets	J, H, K (1.17 to 2.37 μm)	≥ 30" dia. in K, ≥ 20" dia. in J,H	Diffraction limited, λ/2D or finer sampling	Moons are very bright, need a large dynamic range, short exposures	
Resolved Stellar Populations in Crowded Fields	I, Z (0.7 to 0.922 μm), J, H, K (1.1 to 2.37 μm)	≥ 15" dia.	Diffraction limited, λ/2D or finer sampling	K = 27 for σ = 5 in one hour	

* = NGAO key science driver

† = Photometric filter passbands

3.7.2.2.1 Imager Sensitivity

The imager photometric passbands, zero points, and background predictions for DAVINCI imaging are shown in Table 18. The sensitivity predictions for DAVINCI imaging are shown in Table 19. The background predictions are based on a cooled AO system operating at a temperature of -15 °C and emissivity for the LGS observing mode assuming degraded optical transmission due to dust and aging of coatings. The background predictions include the effects of moonlight (50% dark time) for the I and Z bands. Average transmission in each passband is used for the atmosphere, telescope, and AO system. The DAVINCI imager transmission values for each passband are shown in Table 23. Thermal background within DAVINCI is suppressed by operating the instrument at 120 K in a vacuum dewar.

The zero point magnitudes and the sensitivity predictions (Table 19) are based on the detector characteristics summarized in Table 17. Sensitivities are calculated assuming the delivered NGAO Strehl based on 170 nm wavefront error. The required aperture for a diffraction limited image is assumed to be that needed for a well compensated image (Hardy, 1998, p. 42), i.e. a diameter equal to $2\lambda/D$ where D is the diameter of the telescope aperture, and λ is the long wavelength cut-off in the passband of interest.

Table 17: Hawaii-4RG performance parameters

Parameter	Min. Value	Notes
Dark Current	0.01 e^-/s	Median dark current of all imaging pixels
Charge Storage Capacity	100,000 e^-/pixel	Array average number of electrons where the photon transfer curve first deviates from a straight line
Read Noise	15 e^-/pixel	Per CDS read
Quantum Efficiency	0.80 0.75 0.70	970 to 2400 nm 850 to 970 nm 700 to 850 nm

.

Table 18: Zero points and background magnitudes for DAVINCI imaging

Photometric Passband	Cut-on, nm	Cut-off, nm	CWL, nm	Zero point	Background, mag./sq. arcsecond
I band photometric	700	853	776.5	27.34	22.13
Z band photometric	818	922	870	27.16	21.28
Y band photometric	970	1070	1020	26.92	17.28
J band photometric	1170	1330	1250	26.96	16.04
H band photometric	1490	1780	1635	26.95	13.76
K' band photometric	1956	2291	2124	26.39	13.86
K band photometric	2030	2370	2200	26.37	13.44

Table 19: DAVINCI imaging sensitivity

Photometric Passband	Ave. Strehl (170 nm wavefront error)	Time per exposure	5σ mag.	Time for single exposure to background limit, mag. = 27
I band photometric	15%	120 s	27.5	9.2 h
Z band photometric	22%	120 s	27.62	8.3 h
Y band photometric	33%	900 s	27.92	2800 s
J band photometric	39%	900 s	27.32	900 s
H band photometric	59%	900 s	26.37	120 s
K' band photometric	77%	900 s	26.14	220 s

K band photometric	79%	900 s	25.9	150 s

Point source limiting magnitude for 4 co-added exposures to reach 5σ in 1 hour for Y through K bands, and 8 minutes for I and Z bands

3.7.2.3 Spatially Resolved Spectroscopy with DAVINCI

DAVINCI's IFS capability is intended to meet the needs of a range of Galactic and extra galactic science observations. We have evaluated the key IFS performance parameters and determined that the parameters most critical to IFS science are wavelength coverage including the placement of the short wavelength cut-off, spectral resolution, FOV, spatial sampling, and sensitivity. Table 20 gives the values of these parameters for each of the science cases that represent the primary drivers of IFS performance for DAVINCI.

Table 20: Summary of the primary science driven parameters for an IFS

Science Case	Wavelength Coverage	Spectral Resolution	Field of View	Spatial Sampling	Sensitivity and SNR
Galaxy Assembly and Star Formation History*	Z, Y, J, H, K (0.818 to 2.4 μm), narrow band coverage acceptable since redshifts will be obtained before IFS observations	R >3000 (for OH line removal and discrimination of key diagnostic lines (Hα vs. NII)	1" x 3" or greater	Optimized for 50% ensquared energy, range of 50 to 100 mas acceptable	K band performance improvements needed (lower background). Seeking 5 times better sensitivity than OSIRIS on current Keck AO system
Nearby Active Galactic Nuclei*	Z, Y, J, H, K (0.818 to 2.4 μm, or at least to below 850 nm for the Ca II triplet)	R ~3000 to 4000	≥ 5" dia.	20 mas in the near-IR, 8.5 mas in Z	High spatial resolution and precision radial velocities
Measurements of General Relativity Effects in the Galactic Center*	H, K (1.475 to 2.4 μm), primarily narrow band observations of specific absorption lines	R ~4000	≥ 5" dia., goal of 10" dia.	20 mas (H band) and 35 mas (K band)	RV precision at least 10 km/s
Gravitational Lensing	I, Z (0.7 to 1.05 μm), J, H, K (1.10 to 2.4 μm)	R ~4000	> 4" dia., goal of 8" to 10" dia.	50 mas or smaller	RV precision at least 20 km/s (1 σ)

* = NGAO key science driver

In the IFS design one of the key performance trades is the relationship between spectral coverage, spectral sampling, and FOV. For a given number of detector pixels one can trade between these three parameters, finding that certain combinations are more efficient in using the available detector area than others. Our analysis indicates that the NGAO science cases requiring IFS observations are generally more concerned with obtaining a larger FOV than they are with full coverage of an entire IR or visible passband in one exposure.

3.7.2.3.1 IFS Sensitivity

The predicted zero points and background magnitudes for the DAVINCI IFS are shown in Table 21. This table is based on the predicted transmission of the IFS, and the assumptions for Strehl, atmospheric transmission, background, and detector as described in §3.7.2.2.1.

Table 21: Zero points and background magnitudes for DAVINCI IFS

Passband	Cut-on, nm	Cut-off, nm	CWL, nm	Zero point	Background, mag./sq. arcsecond
I band spectroscopic	700	853	776.5	26.31	22.13
Z band spectroscopic	855	1050	952.5	26.74	20.68
Y band spectroscopic	970	1120	1045	26.35	17.05
J band spectroscopic	1100	1400	1250	26.72	16.33
H band spectroscopic	1475	1825	1650	26.19	13.79
K' band spectroscopic	1956	2291	2124	25.45	14.08
K band spectroscopic	2000	2400	2200	25.61	13.62

3.7.2.4 Design and Build-to-Cost

DAVINCI originates within the design and build to cost requirement for NGAO, and is based on a design and build to cost approach supported by six principles:

1. Ensure that the instrument capabilities are well matched to key science requirements
2. Ensure that the instrument capabilities are matched to the AO system in order to maximize the science gains
3. Understand which requirements drive cost
4. Resist the temptation to add features
5. Maximize heritage from previous instruments
6. Evaluate ways to break the normal visible/near-IR paradigm of using different detectors in separate instruments

The concept developed for DAVINCI is aimed at satisfying principles 1 and 2 as fully as possible. The main aspects of the concept as described here are then intended to address the remaining principles with a clearly cost driven approach supported by sound engineering and technical decisions. The design adopts significant portion of subsystem designs from previous instruments, in particular the MOSFIRE (McLean et al., 2008) and OSIRIS (Larkin et al., 2006) instruments. To meet the cost requirements DAVINCI incorporates two instrument capabilities (imaging and spectroscopy) in a single cryogenic dewar with common fore-optics. The single dewar offers significant cost savings by eliminating the need to duplicate the dewar itself as well as cryogenic cooling and a number of control and supervisory systems such as temperature control and pressure monitoring.

A second important aspect of the design concept addresses principal 6, and that is the use of substrate removed HgCdTe infrared focal plane arrays (FPAs). The substrate removed FPAs have good (~70%) QE down to 500 nm, and although the single CDS read noise is higher than typical science grade CCDs (~15 e^-/read for a Hawaii-2RG vs. 5 e^-/read for a deep depletion CCD, see Adkins, 2009)

the low power dissipation of the FPA read out integrated circuit and non-destructive pixel read out allows many Fowler or up the ramp samples and results in essentially the same readout noise levels for exposures where the exposure duration allows time for the required number of reads. While the QE of a CCD will be at least 20% higher at 1 μm and below, this seems to be the only penalty for not using a CCD below 1 μm. This represents another important component of the cost reduction needed in order to ensure that DAVINCI supports the NGAO design and build to cost requirement.

3.7.2.5 The DAVINCI Concept

A block diagram of DAVINCI is shown in Figure 132. DAVINCI is a fully cryogenic infrared and optical (to 0.7 μm) imager and IFS enclosed in a vacuum dewar. The dewar contains two optical systems, one for the imager shown at the bottom center of the block diagram and one for IFS, shown on the right half of the block diagram. The imager and IFS share the fore optics shown in the left half of the diagram. The fore optics includes a selection of coronagraph masks, a selection of filters, and a selection of pupil masks. The FOVs of the imager and IFS are both at the center of the NGAO science FOV as illustrated in Figure 133.

Starting at the left side of the block diagram, light enters the dewar from the AO system through a vacuum window ~120 mm in diameter. The window is coupled to the NGAO system's cooled enclosure via a light and air tight bellows. The bellows isolates the two structures mechanically, and since the AO enclosure is cooled to -15 °C and filled with dry air, the emissivity of the window is reduced and the issue of condensation or ice on the window is eliminated during normal operation. A mechanism such as a dry air purge will be provided for the window during servicing or testing to prevent condensation when the window is exposed to ambient conditions.

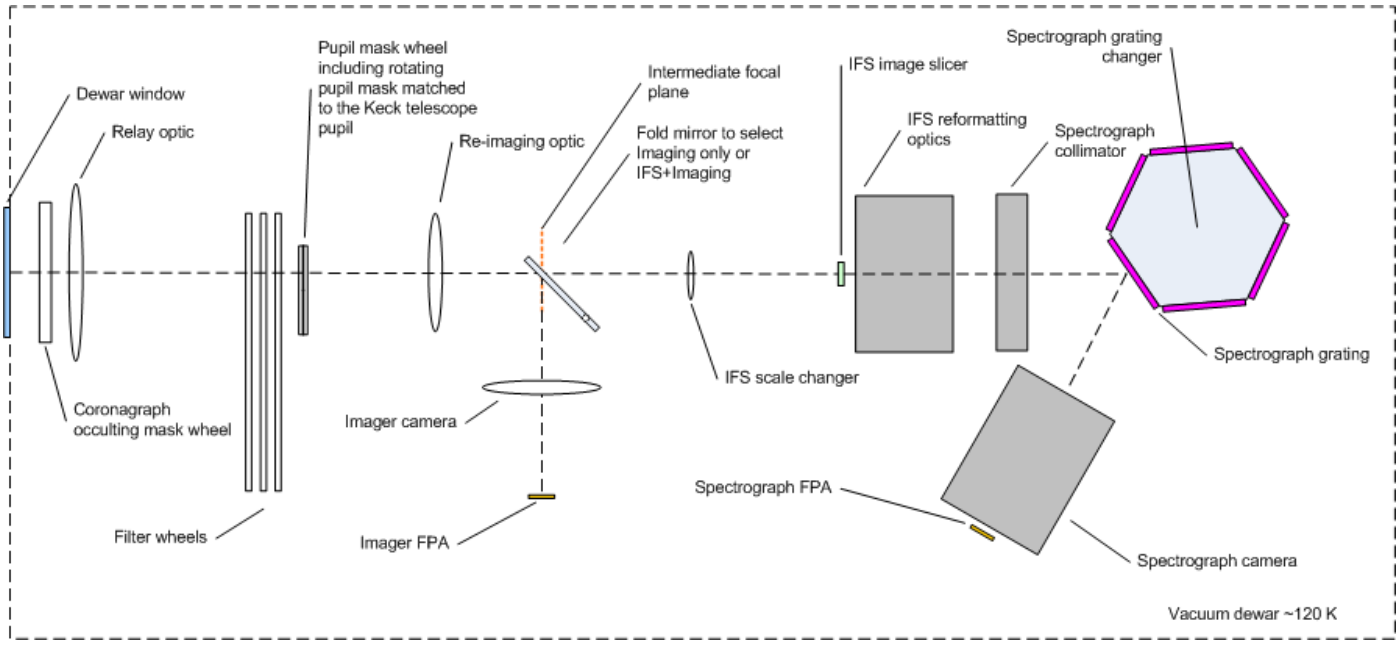

Figure 132: DAVINCI opto-mechanical block diagram (not to scale)

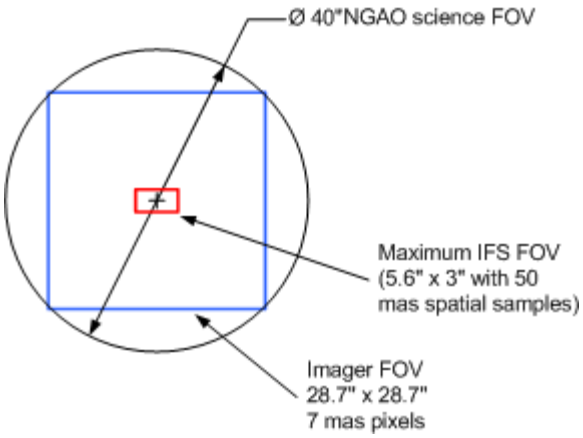

Figure 133: DAVINCI FOVs

The AO system's science focal plane is located inside the dewar where a wheel is located providing a selection of coronagraph occulting masks. A relay optic forms a pupil image at a wheel carrying a selection of cold pupil masks for imaging and coronagraphy including a tracking pupil mask matched to the primary mirror aperture and central obscuration of the Keck telescope.

A set of filter wheels is located just in front of the pupil plane, with ~45 filters shared between the imager (24) and the IFS (17). Each wheel will contain ~15 filters plus an open position. After the pupil mask a re-imaging optic forms an intermediate focal plane. Continuing to the right along the IFS optical path the beam enters the IFS scale changer, which has three selectable scale changing optics to provide the three spatial sampling scales for the IFS. The scale changer focuses the light onto a 112 x 60 element lenslet array which performs the image sampling. After the lenslet array a reformatting mirror system formats the rectangular array of pupil images formed by the lenslet array into six virtual slits of 1120 spatial samples each. The spectrograph collimator is a single off-axis aspherical mirror which illuminates a grating working in the first order, and the dispersed light is then imaged onto the spectrograph detector by a second TMA. Multiple gratings will be used with a rotary grating changer to select the appropriate grating for each waveband.

Returning to the center of the block diagram, a fold mirror near the intermediate focal plane sends the light to imager camera and detector. The fold mirror is a plane mirror mounted at 15 degrees that can be rotated in that plane to position a hole (~ 6.5" diameter) in the mirror to allow light to reach the IFS. This allows simultaneous imaging of the field around the IFS field for imaging to support PSF monitoring or for astrometry. Locating this mirror near the intermediate focal plane minimizes the vignetting of the imager field.

A pupil imaging mode is provided by a lens (not shown on the diagram) that can be deployed into the imager optical path to allow imaging the telescope pupil to ensure that the instrument's pupil masks are properly aligned.

3.7.2.6 DAVINCI Optical Design

3.7.2.6.1 Imager and IFS Scale Changer

DAVINCI provides three operating modes: imager, coronagraph, and IFS. All three modes of operation are contained in a single dewar, and are fed by a single output of the second AO relay of the NGAO system. An optical layout of the DAVINCI instrument, including the imager light path and the IFS scale changer, are shown in Figure 134. An annotated Zemax shaded model is shown in Figure 135 .

Referring to Figure 135, the entrance window for the DAVINCI dewar lies in the converging beam of the AO relay's science feed, ~200 mm before focus. The masks for the coronagraphic mode of the instrument are located at the AO focal plane inside the dewar. The AO relay provides a telecentric output to DAVINCI with a focal ratio of f/46.38. Using a focal ratio of f/13.66 for the Keck telescope the resulting image scale at the focal plane of the AO relay is 2.46 mm/", resulting in a 40" focal plane approximately 98 mm in diameter.

Approximately 1 m after the focal plane is an OAP (OAP1) with a radius of curvature of 1998.7 mm, an off-axis angle of 41.5°, and a diameter of 150 mm. This OAP has been optimized in off-axis angle and focal length to produce a high quality, 25mm pupil image at the cold stop. This was accomplished in Zemax by producing a configuration in which the primary mirror of the telescope was the object. Geometric rays from the primary mirror "object" were used to evaluate pupil image quality after passing through both the AO relay and DAVINCI's OAP1. OAP2 is used to produce an intermediate focal plane near the IFS selection mirror (FM3). The distance between OAP1 and OAP2 is long, almost 1.5 m, because of the slow input f/#, the desired 25 mm pupil size at the cold stop, and the need for telecentricity on the input to the IFS. Therefore a fold mirror (FM1) is located 586 mm before the cold stop for packaging. The 40 mm diameter bandpass filters are placed before the cold stop in collimated light.

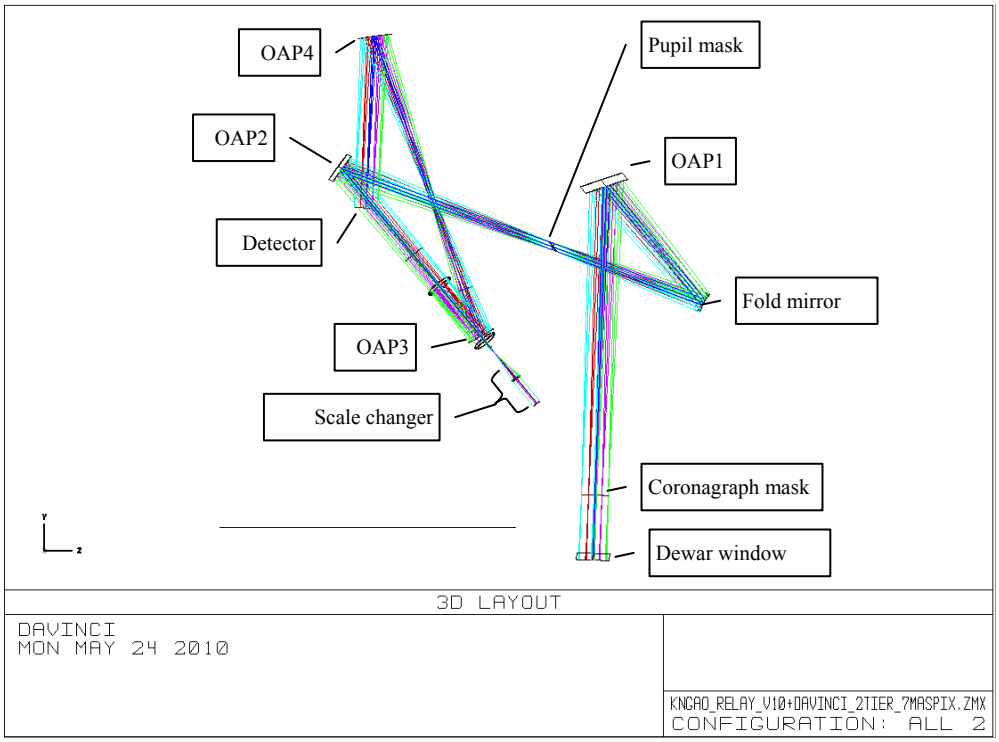

Figure 134: The DAVINCI optical layout, as seen from directly overhead

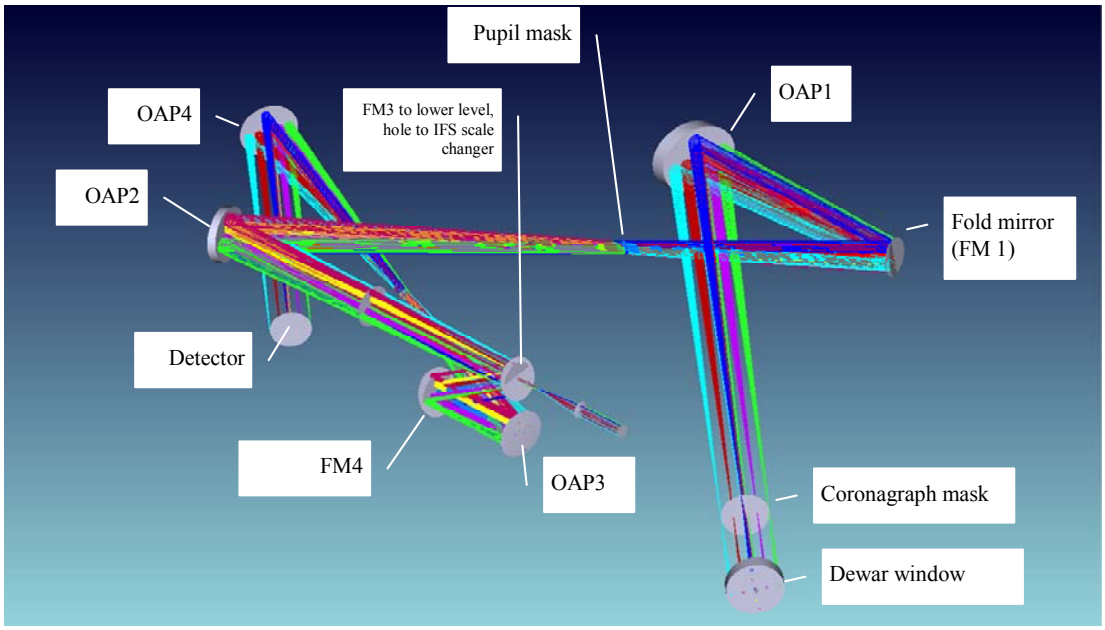

Figure 135: The DAVINCI optical layout, shown in perspective to emphasize the 2-tier design

As noted in §3.7.2.5, all modes of operation share a common pupil image as a cold pupil mask or Lyot stop location, thus the first OAP relay of the instrument is shared between all modes.

The image scale required at the detector is 2.143 mm/", and this corresponds to an f/40 beam. Because the optics of the DAVINCI imager must provide a scale change, OAP2's focal length is shorter than OAP1's (they are not a matched pair), giving an image scale of 1.9 mm/" at the intermediate focal plane. Because this focus also acts as the feed to the integral field spectrograph, which unfortunately requires a larger focal ratio, so we chose to accomplish the focal ratio reduction for the imager with both OAP relays. OAP2 has a radius of curvature of 1531.9 mm, an off-axis angle of 30.2° and a diameter of 120 mm. It is placed one focal length away from the cold stop to provide a telecentric beam to the IFS scale changer and the second relay of the imager.

To allow access to mechanisms (coronagraph mask wheel, filter wheels, pupil mask wheel, and IFS scale changer wheels) we have divided the DAVINCI imager's optical path into two tiers, with the input optical path up to the intermediate focal plane located on an upper tier, and the optical path to the imager and detector on a lower tier. Near the image plane of the first OAP relay in DAVINCI is the first of two mirrors which fold the beam down at an incidence angle of 15° to a lower level of the dewar. This is the rotating mirror with the hole that allows light to reach the IFS. A matching (15°) fold mirror completes the periscope to the second level. The vertical distance between levels is 150 mm.

To complete the scale change required by the imager's detector size, a second, also unmatched, OAP relay is used. OAP3 has a radius of curvature of 1044 mm, an off-axis angle of 20°, and a diameter of 120 mm. It produces a collimated beam in which a pupil image is formed one focal length away from OAP3. This pupil image is not utilized, so its quality is not relevant. The final OAP in the imaging system has a radius of curvature of 1226 mm, a diameter of 100 mm, and off axis angle of 22.1°. It produces an image plane ~61 mm in diameter for a 28.7" diameter field of view.

3.7.2.6.2 IFS Scale Changer

Figure 134 illustrates the optical design of the IFS scale changing optics. Following the first OAP pair of DAVINCI is an intermediate focal plane where a rotating fold mirror with a hole is located that allows light to enter the IFS scale changer.

The integral field spectrograph is required to work at three different sampling scales. The sampling is achieved by a 250 μm pitch lenslet array at the focal plane of the IFS scale changer. The scale changer is required to remain a constant length, regardless of sampling scale, to keep the lenslet array and all following optics stationary. The scale changer is also required to work at wavelengths from 0.7 μm to 2.4 μm (I through K bands). To help in meeting throughput requirements it was desirable that the scale changer contain as few elements as possible.

Table 22 provides the different sampling scales, the maximum field size on the 112 x 60 lenslet array, their physical size at the IFS pickoff, and the magnification required.

Table 22: DAVINCI IFS scale changer requirements

Sampling scale (mas)	Max. field size (arcseconds)	Size at IFS pickoff focal plane (mm)	Magnification required
10	1.12	2.13	13.3
35	3.92	7.45	3.8
50	5.6	10.64	2.63

A pair of BaF_2 singlets in a 4f configuration is used for each of the three sampling scales. Two wheel mechanisms are used to select each pair of lenses with the two wheel mechanisms spaced ~117 mm apart. This arrangement is very similar to that used in the OSIRIS instrument (Larkin et al., 2006).

3.7.2.6.3 Image Quality

An overview of the performance of the current optical design for the DAVINCI imager is shown in Figure 136. The images are diffraction limited at wavelengths ≥ 1 μm with a maximum grid distortion of 1%. The form of the distortion is barrel shaped and well behaved.

When optimizing a design based on OAPs there is a trade off to be managed between distortion and image quality. In addition, the OAP design does not completely remove the field curvature. A design incorporating an refractive field flattener placed ~ 4 mm away from the detector with a radius of 75 mm on the convex surface removes the field curvature and produces diffraction limited images across the field at 0.7 μm but with ~5% grid distortion.

3.7.2.6.4 Transmission

The transmissions shown in Table 23 for the DAVINCI imager were estimated using reflectance and transmittance values from the NGAO throughput and emissivity flowdown budget (KAON 723). It is assumed that all reflective optics are gold-coated, and all transmissive optics have a broadband AR coating. A pupil mask matched to the shape of the Keck telescope primary mirror and center obscuration is provided for the H and K bands, and a circular mask is provided for the Y and J bands.

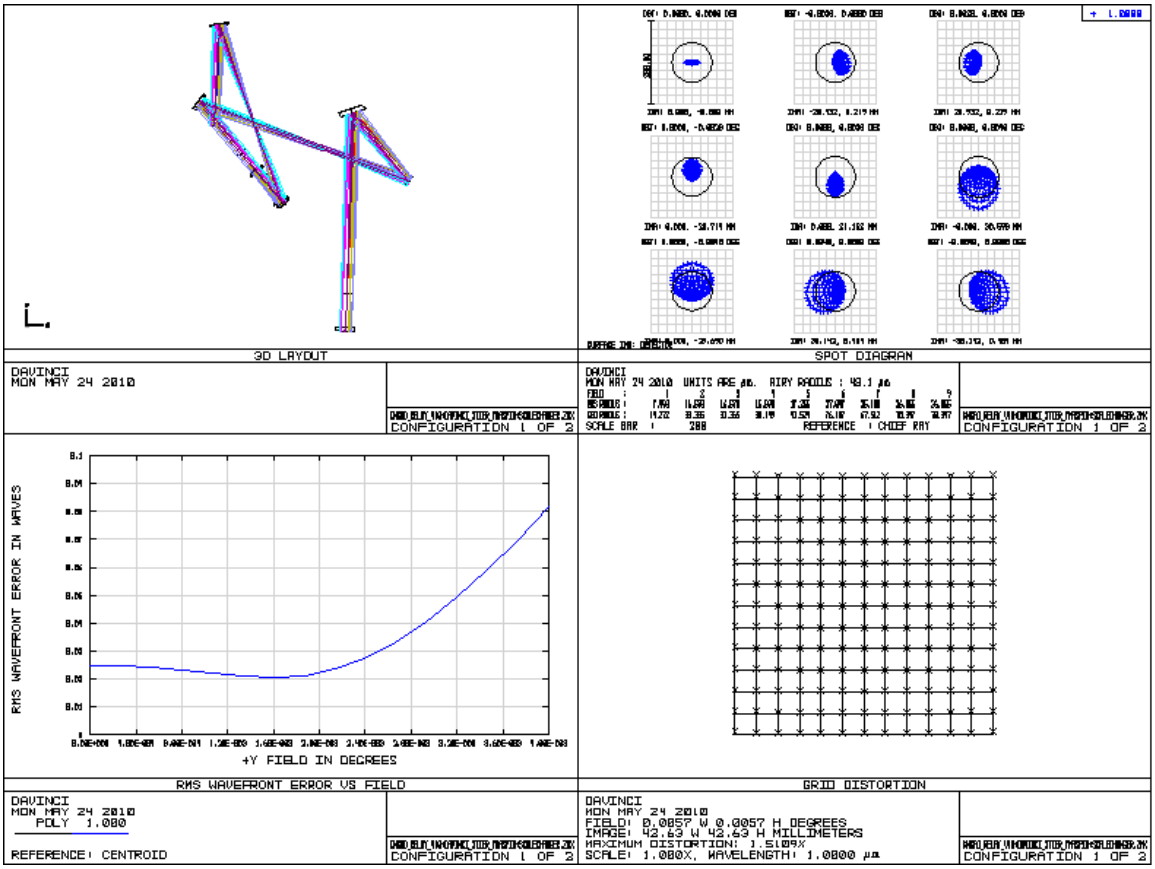

Figure 136: Image quality metrics at the DAVINCI imager's detector plane

Table 23: Transmission estimates for the DAVINCI imager

	%T						%R					
Surface	**I band**	**Z band**	**Y band**	**J band**	**H band**	**K band**	**I band**	**Z band**	**Y band**	**J band**	**H band**	**K band**
Dewar Window												
Infrasil 302, 25 mm thick	99.23%	99.23%	99.23%	99.23%	99.23%	99.23%						
Coating, 2 surfaces	97.83%	97.84%	94.95%	95.83%	95.50%	96.77%						
Coronagraph Mask												
Infrasil 302, 2 mm thick												
Coating, 2 surfaces												
FM1							97.65%	98.53%	98.79%	99.00%	99.03%	99.17%
OAP1							97.65%	98.53%	98.79%	99.00%	99.03%	99.17%
Cold stop	100.00%	100.00%	97.00%	97.00%	97.00%	97.00%						
Filter	90.00%	90.00%	80.00%	85.00%	85.00%	92.00%						
OAP2							97.65%	98.53%	98.79%	99.00%	99.03%	99.17%
FM3 (hole to IFS)							97.65%	98.53%	98.79%	99.00%	99.03%	99.17%
FM4 (periscope)							97.65%	98.53%	98.79%	99.00%	99.03%	99.17%
OAP3							97.65%	98.53%	98.79%	99.00%	99.03%	99.17%
OAP4							97.65%	98.53%	98.79%	99.00%	99.03%	99.17%
Totals												
%T	87.37%	87.37%	73.11%	78.40%	78.13%	85.69%						
%R							84.68%	90.18%	91.80%	93.17%	93.40%	94.33%
Combined	73.99%	78.79%	67.12%	73.05%	72.98%	80.84%						

3.7.2.7 Coronagraph

DAVINCI will include a coronagraph, and our initial design is a simple Lyot coronagraph. We wanted to evaluate the performance of this approach first, but more sophisticated approaches will also be considered such as an apodized Lyot coronagraph (Soummer, 2005) or a vortex or four quadrant phase mask coronagraph. An apodizer would ideally be located exactly at a pupil plane ahead of the coronagraph mask. There is a location near a pupil plane at the second deformable mirror in the AO system, otherwise additional optics will be required to form a pupil plane for the apodizer.

3.7.2.7.1 Coronagraph Assumptions

The high contrast imaging expected performance for DAVINCI ("Keck," 2008) may be summarized as:

1. $\Delta J = 8.5$ (or contrast ratio of 4×10^{-4}) at 100 mas with a goal of $\Delta J = 11$ (4×10^{-5}) at 100 mas
2. $\Delta H = 10$ (or contrast ratio of 1×10^{-4}) at 200 mas with a goal of $\Delta H = 13$ (6.3×10^{-6}) at 1'
3. $\Delta K = 10$ (or contrast ratio of 1×10^{-4}) at 100 mas

The FOV considered for coronagraphy is only 1" therefore the field aberrations – and the pupil distortions – are negligible. We did consider a hexagonal pupil, although the shape of the aperture is not the limiting factor in the final performance.

Simulations have been done using an f/46 input beam and a Lyot stop of 25mm. We studied the performance in three observing bands, J (1.2 μm), H (1.6 μm) and K (2 μm).

Median seeing for Keck is assumed to be 0.8" and the effect of the turbulence is corrected using a square region of 62 x 62 actuators in a MEMS deformable mirror (DM). Assuming an rms wavefront error of 170 nm, the Strehl performance of the AO system for this application depends on the wavelength and is: K: 75%-82%, H: 60%, J: 40%-56%, I: 10%-22% (Dekany et al., 2009).

In theory and without aberrations, the optimum focal plane mask (FPM) depends on the wavelength, the shorter the wavelength, the smaller the FPM. However, the Strehl ratio decreases with wavelength, meaning that the halo fraction will increase leading to the need for a bigger FPM than for the perfect case. This is expected to reduce the number of different sized FPMs needed in practice.

3.7.2.7.2 Coronograph Simulation Results

The performance of a simple Lyot coronagraph was simulated using an IDL program. The code is based on the fact that focal planes and pupil planes are related by a Fourier Transform.

The simulation is based on an f/46 beam converging onto the focal plane mask at each wavelength. The sampling resolution of the diffraction limited spot in the simulation is arbitrarily set to 12 simulation pixels per FWHM (defined as f# x λ). The pixel size in the focal plane is thus (f# x λ)/12.

The FPM is either an opaque dot or a 10% transmission dot to be able to eliminate most of the light coming from the parent star but still see the star for astrometry and photometry (some precise calibration will be needed). Such technique is being used on NICI (Chun et al., 2008).

The energy distribution in the following pupil plane or Lyot plane is the Fourier transform to get to the Lyot plane where we put an aperture to block the diffracted light from the FPM.

By the definition of the Fourier Transform, the pixel size on the pupil plane is equal to (λ x f1)/(n x θpixel), where f1 is the focal length of the first lens and θpixel the pixel size in the focal plane. We chose f1 from the f# and the diameter of the pupil in the Lyot plane (f1 = f# x d).

As stated earlier, the aberrations of the wavefront in the pupil plane are negligible because the FOV of that particular mode is very small (only 1"). Our initial simulations consider the effects of AO correction with a first approximation that considers only fitting error, using a high pass filter with a cut-off frequency set by the number of actuators. Another more accurate technique is to consider a parabolic filter instead of a Heaviside function (Sivaramakrishnan et al., 2001). The most precise estimation of the performance would be obtained by simulating true point spread functions after correction with the Keck NGAO. More thorough simulations including Strehl will be done to determine if the results found here will hold with less optimum corrections. Indeed, the Strehl in these initial simulations was kept relatively high (around 80%) which is a good approximation for K band but not for J band. We also will consider the effects of a 90% opaque FPM to account for astrometry and photometry

Performance was estimated by determining the contrast obtained as a function of separation. The separation is given both in arcseconds and in cycles per aperture where one cycle per aperture is defined by the pitch of one actuator on the second DM in the AO relay.

Naturally, the results depend on the wavelength both because of the size of the spot at the focal plane and the AO correction obtained. They also depend on the size of the FPM and the size of the Lyot stop. We therefore studied contrast curves as a function of Lyot mask and FPM sizes. The goal is to define the best combination (Lyot, FPM) as a function of wavelength.

The FPM size d was varied from 2 to 12 λ/d. For the Lyot stop, only sizes bigger than 60% of the full aperture were considered because for smaller apertures, the transmitted flux goes down significantly.

The following graphs show the resulting contrast curves for the best combinations (Lyot mask, FPM), for the three different bands. A common solution was sought for the three bands in order to minimize the number of masks needed. In the following, the FPM sizes are given in λ/d. For the 3 wavelength chosen, there is a factor of 1.6 and 1.3 respectively between J and K, and between J and H. To reach the 100 mas inner working angle, an FPM equal or smaller than 5 λ/d is required for K band, 6 λ/d in H and 8λ/d in J. The Lyot mask remains the same size in all three bands. A reduction of the Lyot mask size from 90% to 75%, causes a decrease in sensitivity of 2.5 x Log(0.833^2) or 0.4 magnitudes.

3.7.2.7.2.1 J Band

For J band the Strehl is overestimated using the simple method of a Heaviside high pass filter. The requirements ask for an inner working angle smaller than 100 mas. The diffraction-limited spot is 25 mas and the maximum FPM size is thus 8λ/d diameter at 1.2 µm. For this band we varied the FPM radius from 3 to 8 λ/d by increments of 1 λ/d and the Lyot size from 75 to 90% by increments of 2.5%.

The best combination using the biggest size Lyot stop is (82.5%, 8), which is at the limit of the required separation (Figure 137). To increase the inner working angle and optimize the same FPM for a different wavelength, we need to reduce the size of the Lyot mask to 75% and use an FPM of diameter equal to 5λ/d (Figure 138). This reduces the transmission, but in this exercise the goal is to optimize the inner working angle instead of the flux. One could consider increasing the FPM to increase the Lyot stop mask and therefore increase the flux.

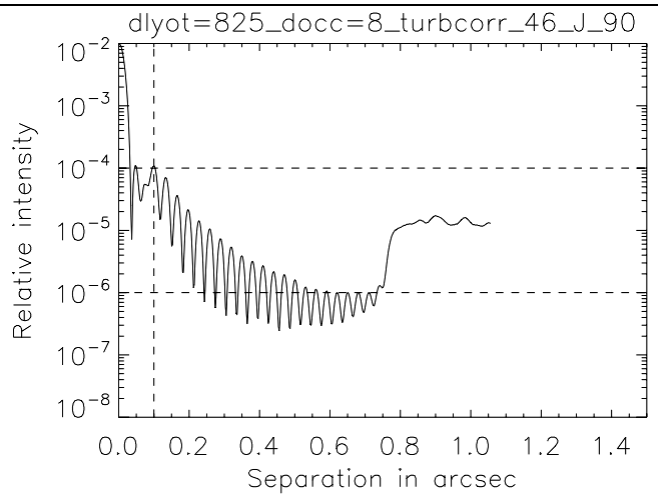

Figure 137: J band contrast (82.5%, 8) case

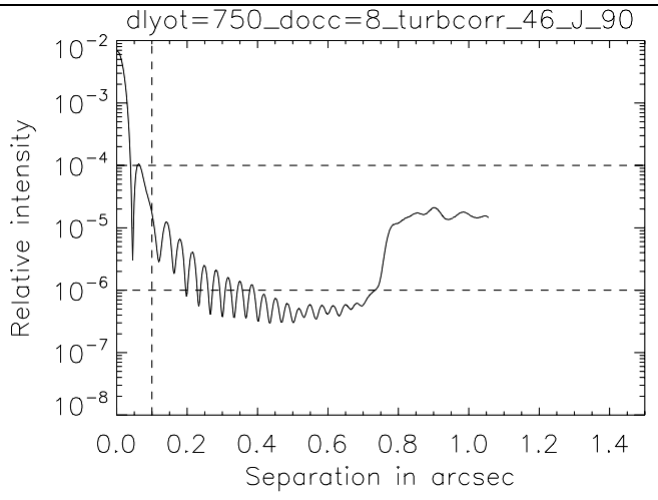

Figure 138: J band contrast (75%, 5) case

The plateau at about 0.8" is due to the limit at which the DM can control and correct the wavefront.

3.7.2.7.2.2 H Band

The requirements ask for an inner working angle of 200 mas. The diffraction-limited spot is equal to 33 mas and the maximum FPM size is thus 12λ/d radius at 1.6 µm. For this band we varied the FPM radius from 3 to 12 λ/d by increments of 1 λ/d and the Lyot size from 75 to 90% by increments of 2.5%.

The best combination is (90%, 4) to meet the requirements both at 200 mas and 1'. To minimize the changes in FPM sizes and Lyot stops between different wavelengths so far (J and H); one would have to choose the combination (75%, 6). The resulting contrast is even better at this wavelength.

3.7.2.7.2.3 K Band

The requirements ask for an inner working angle of 100 mas. The diffraction-limited spot is equal to 41 mas and the maximum FPM size is thus 5λ/d diameter at 2 µm. For this band we varied the FPM radius from 2 to 5 λ/d in increments of 1 λ/d and the Lyot size from 75 to 90% by increments of 2.5%. Because of previous results, we increased the range of the FPM size to 6λ/d.

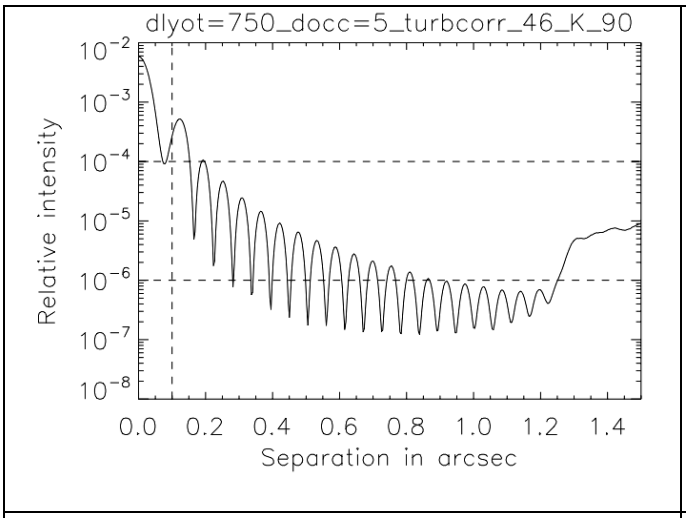

Figure 139: K band (75%, 5) case

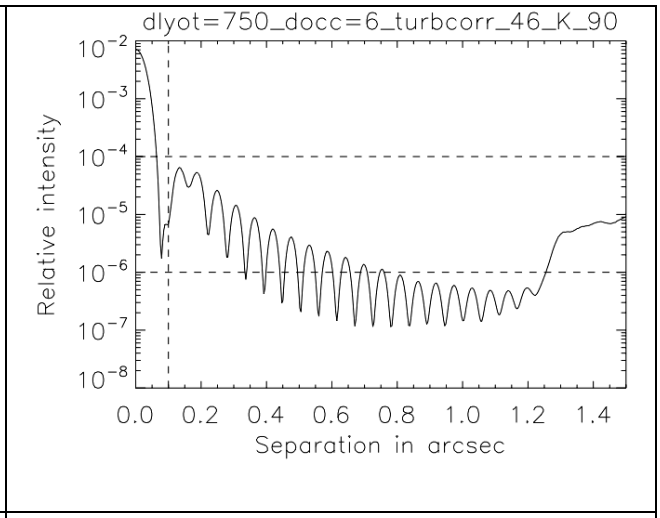

Figure 140: K band (75%, 6) case

To keep an inner working angle of 100 mas without loosing too much light, the best combination is (75%, 5) as seen in Figure 139. However, the contrast at 100 mas is higher than 10^{-4}. The combination (75%, 6) leads to better performance for a slightly bigger inner working angle (Figure 140).

3.7.2.7.3 Sensitivity

The SNR vs. exposure time for companions of K band magnitudes of 18 and 24 are shown in Figure 141 for the (75%, 6) and (100%, 6) cases.

3.7.2.7.4 Coronagraph Conclusions

A simple Lyot coronagraph meets our requirements if the transmission losses and some compromises of inner working angles are acceptable. The best common combination is to use a Lyot mask of 75% the nominal pupil size and a focal plane mask of 100 mas. In order to further improve performance, we will need to use an apodizer, or consider other techniques such as a vortex coronagraph or quadrant phase masks.

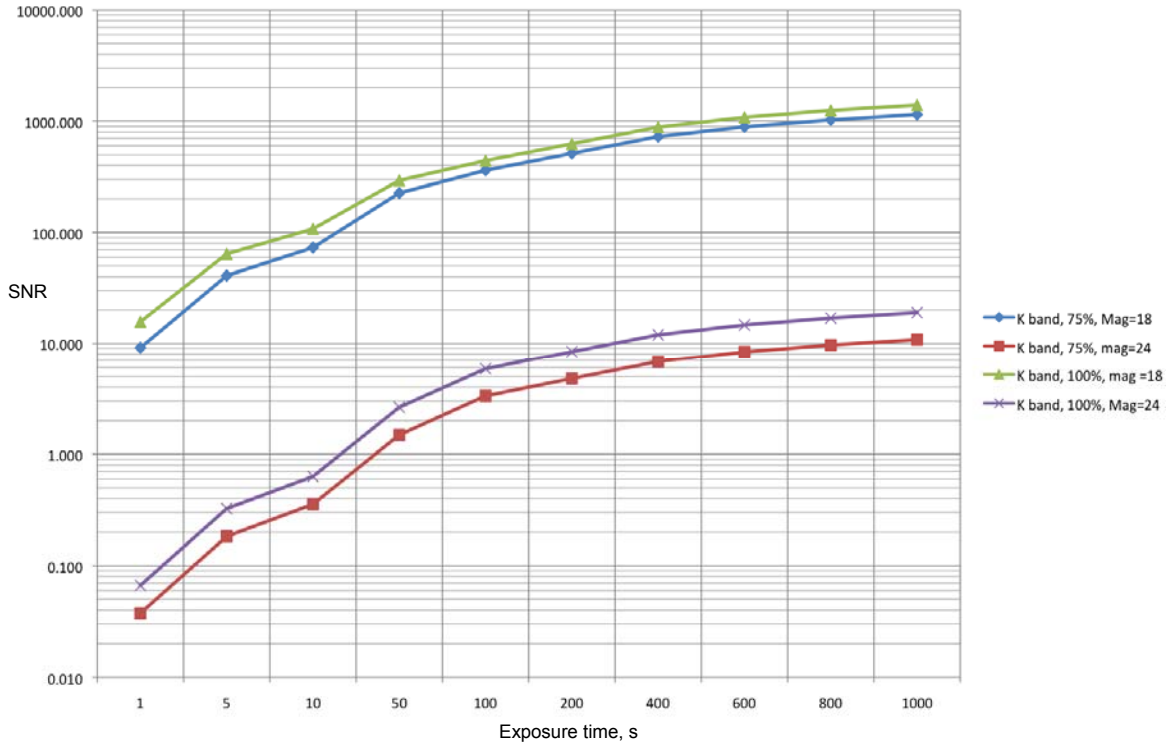

Figure 141: DAVINCI coronagraph companion sensitivity in K band

3.7.2.8 DAVINCI IFS

As discussed in §3.7.2.3 the DAVINCI IFS requirements are driven by science where FOV and sensitivity are more important than simultaneous coverage of a single observing band. The IFS is also expected to provide spatial sampling scales suited to the diffraction limit and spatial sampling scales that optimize the ensquared energy in each spatial sample. There should be a minimum of two pixels per sample on the detector in the spatial direction, and two pixels per resolution element in the spectral or dispersion direction on the detector.

The design and build to cost requirement of NGAO leads to a concept for the DAVINCI IFS where the fore-optics (coronagraph, filters, and pupil masks) are shared with the DAVINVI imager. In order to ensure the image quality delivered to the IFS is the very highest, the IFS field is located at the center of the NGAO science relay FOV, and therefore at the center of the imager FOV. Using a pick-off mirror arrangement to send light to the IFS it is possible to image objects around the IFS field (such as PSF stars) during the IFS observation. Separate detector readout systems will provide for exposure control and readout cadences appropriate to each of the observing modes.

We have developed two concepts for the IFS, one based on a lenslet slicer similar to the OSIRIS instrument (Larkin et al., 2006), and a second concept that uses a lenslet array to perform the initial image sampling, and then reformats the array of pupil images formed by the lenslet array into a series of virtual slits.

3.7.2.8.1 IFS Design Considerations

An integral field spectrograph (IFS) instrument takes a certain, usually contiguous field of view (FOV), spatially samples the image, normally on some uniform grid, and then produces a spectrum over some wavelength range for each of the spatial samples. In the simplest form the IFS must accomplish three functions: image slicing, spectral dispersion, and detection of the dispersed spectra. Image slicing is a term used to describe the process of taking the spatial samples, effectively slicing the image into pixels, analogous to a CCD imager, but instead of becoming an intensity value each spatial pixel or "spaxel" is used to produce a spectrum. To avoid confusion with the common usage of the word pixels to mean detector pixels, the term spatial pixel or "spaxel" is often used to describe the image samples taken by an image slicer. The size of the spatial pixel determines the spatial resolution of the image formed by the image slicer output. Just as with a CCD, where each pixel exhibits a characteristic point spread function (PSF), the image slicer also has a PSF determined by the performance of the image slicer's optical elements.

In general the design of the spectrograph portion of an IFS instrument is similar to a conventional slit spectrograph for the same wavelength range. There are three approaches to image slicing that have been used to build visible or infrared IFS instruments: fiber optics, mirrors and lenslets. The image slicer is placed at an image focal plane, often after scale changing optics which adjusts the plate scale of the telescope to match the desired physical size of the image samples. To illustrate the basic operation of each concept, we will use a small scale example with 16 spatial samples, arranged in a 4 x 4 grid.

3.7.2.8.1.1 Lenslet Slicers

A schematic of the operation of a lenslet slicer is shown in Figure 142. Lenslet slicing (Bacon et al., 1995; Larkin et al., 2006) employs a two dimensional array of small lenses located at a focal plane to take each part of the image and focus it to a small pupil spot. The two dimensional pattern of spots effectively forms the entrance slit of a spectrograph, and the array of pupil spots is collimated and dispersed into spectra. By rotating the lenslet array slightly with respect to the dispersion axis of the grating the spectra from some number of consecutive lenslets in the column wise direction of the lenslet array will be interleaved between consecutive lenslets in the row wise direction. Increasing the rotation also allows adjacent spectra to be separated from each other, but this will decrease the number of spectra that will fit on the detector. The lenslet rotation also causes the spectra to be staggered on the detector as shown in Figure 142.

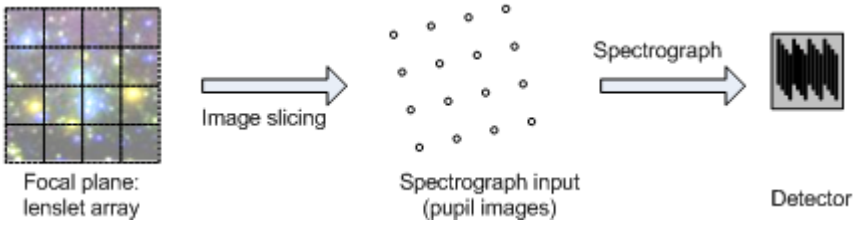

Figure 142: Lenslet slicer based IFS

Lenslet slicers have the advantage that each spatial sample is completely independent in both the spectral and spatial directions. High quality arrays of lenslets with very well matched focal lengths and nearly perfect fill factors are routinely made using specialized manufacturing techniques. The

difficulty with lenslet slicing is that due to the lenslet rotation adjacent spectra are displaced with respect to each other on the detector in a pattern that repeats at the row pitch of the lenslets, this can result in bright features in one spectrum being next to fainter features in an adjacent spectrum. The displacement also leaves some of the detector area unused.

Without introducing additional optical elements, the f-number of the spectrograph collimator input is set by the need to match the f-number of the lenslet array. The combined focal lengths of the collimator and camera must match the input spatial sampling to the desired sampling on the detector (typically 2 pixels). Increasing the FOV in a lenslet slicer drives the collimator to a larger aperture and a longer focal length for a fixed f-number leading in turn to a larger aperture in the camera. The physical size of the collimator and camera apertures eventually limit the FOV of a lenslet based IFS from purely practical considerations.

3.7.2.8.1.2 Mirror Slicers

The operation of a mirror slicer is illustrated in Figure 143. Mirror slicing (Content, 1998; Eikenberry et al., 2006) employs an array of mirrors located at a focal plane to deflect portions of the image light in different directions. Each mirror is equal to the physical width of a single spatial sample in one direction, and equal to the length of n spatial samples in the other direction, where n = 4 for the example of 4 x 4 spatial sampling shown in Figure 143. The light from each slicing mirror is collected by a second set of mirrors that format the slices into one or more rows in a virtual slit for the spectrograph. Flat or powered mirrors may be employed, and additional mirrors or lenses may be needed to place the pupil image at the correct conjugate in the spectrograph optical path.

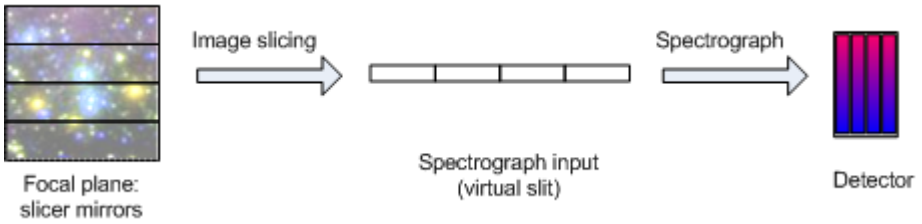

Figure 143: Mirror slicer based IFS

Mirror slicers have the advantage that the virtual slit approach can be more efficient in the use of the detector pixels. The disadvantages are greater light losses and additional sources of aberrations that can impact the quality of the spatial sampling. Light is lost at the input focal plane due the fact that the tilted mirrors move through focus, causing some light to be lost at each end of the long axis of each spatial sample. The mirrors are relatively small, typically between 0.3 and 0.5 mm in the narrow dimension. The mirrors only separate the samples in one dimension, so aberrations of the slicer mirror surfaces, as well as the aberrations through the spectrograph all contribute to loss of wavefront quality in the spatial direction. In a mirror slicer design the aperture of the collimator is set by the virtual slit length, and ultimately the total slit length will be limited by the practical size of the slicer and collimator, and the related down stream focal ratio and grating size considerations.

3.7.2.8.1.3 Hybrid Slicer Design

Comparing the lenslet based slicer, and the mirror slicer, one notes two important considerations. First, for slicers operating at the diffraction limit, the higher quality of the sampling in both spatial

dimensions is a benefit. Second, the mirror slicer avoids the problem of the staggered spectra and the problems of bright feature/dark feature cross talk between adjacent spectra, and provides more consistent pixel to wavelength calibration for spatial samples along a given virtual slit, and makes more efficient use of detector pixels.

The technology for making lenslet arrays is capable of producing very precise arrays with high fill factors (≥ 97%), very low transmission losses, excellent focal length matching and very low wavefront error. With a proper choice of focal length the lenslet array can produce very clean samples of the focal plane image, and spatial sampling is not degraded by the optical performance of the spectrograph. After considering an initial evaluation of the feasibility of a given FOV using either a mirror slicer or a lenslet array we have realized that a combined system might offer the best combination of low wavefront error and efficient detector utilization. A "straw man" design for this approach is shown in Figure 144.

In this hybrid design the lenslet array forms a series of pupils that are then reformatted by a slicer stack and a series of pupil mirrors into rows of virtual slits at the entrance of the spectrograph. This design has the advantage of maintaining the well isolated spatial samples of the lenslet array design all the way to the detector and avoids the problem of overlap between staggered spectra on the detector.

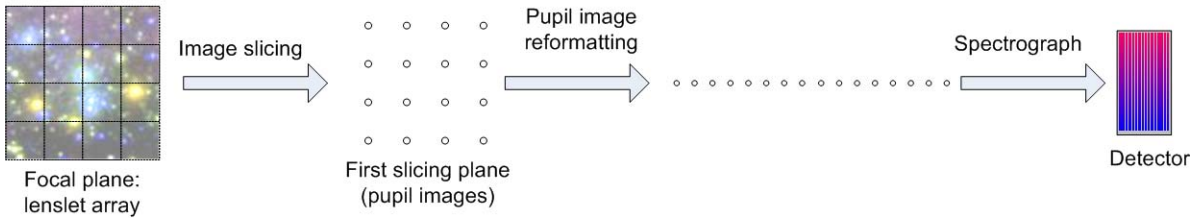

Figure 144: Hybrid slicer based IFS

A hybrid slicer will require a greater distance between the pupil image plane and the lenslet array to allow for mirrors to redirect columns of pupil images to the formatting optics. However, the lenslet focal length is not constrained by the need to achieve a small pupil image size in order to fit the desired number of lenslet images between the row pitch that results from rotation of the lenslet array.

3.7.2.9 IFS Optical Design

The overall arrangement proposed for the IFS is shown on the right half of Figure 132. At the center of the block diagram, a fold mirror near the intermediate focal plane sends the light to imager camera and detector. The fold mirror is a plane mirror mounted at 15 degrees that can be rotated in that plane to position a hole (~ 6.5" diameter) in the mirror to allow light to reach the IFS. This allows simultaneous imaging of the field around the IFS field for imaging to support PSF monitoring or for astrometry. Locating this mirror near the intermediate focal plane minimizes the vignetting of the imager field. The rotary motion should result in very reliable centering of the field between the imager only and IFS+imager modes, allowing an initial imager observation of the full field to be used to refine the telescope pointing prior to beginning the observation. It is also possible to have a third

position of this mirror with a partially reflective area instead of a hole, allowing the center of the DAVINCI FOV to be used for PSF imaging at the same time as an IFS observation.

As noted earlier, there are two concepts for the IFS image slicer, a lenslet slicer, and the hybrid slicer. The lenslet slicer employs an 80 x 80 lenslet array with a 200 µm pitch. The hybrid slicer employs a 112 x 60 lenslet array with a 250 µm pitch. The IFS scale changing optics are described in §3.7.2.6.2.

3.7.2.9.1 DAVINCI IFS Passbands

The DAVINCI IFS passbands each cover ~5% of each of the major spectral bands, I, Z, Y, J, H, and K in order to limit the length of the spectrum from each spatial sample and allow more spatial samples to fit on the detector, allowing a larger FOV. Table 24 shows the initial DAVINCI IFS passbands. Each of the adjacent narrow bands in each major spectral band overlap at their respective cut-off and cut-on wavelengths by ~10% of the bandpass in each narrowband.

Table 24: IFS passbands

Passband	Narrowband 1				Narrowband 2				Narrowband 3				Narrowband 4			
	Cut-on	Cut-off	CWL	Bandpass	Cut-on	Cut-off	CWL	Bandpass	Cut-on	Cut-off	CWL	Bandpass	Cut-on	Cut-off	CWL	Bandpass
Ia, Ib	700.00	784.15	742.08	84.15	776.50	853.00	814.75	76.50								
Za, Zb	855.00	962.25	908.63	107.25	952.50	1050.00	1001.25	97.50								
Ya, Yb	970.00	1052.50	1011.25	82.50	1045.00	1120.00	1082.50	75.00								
Ja, Jb, Jc	1100.00	1210.00	1155.00	110.00	1200.00	1310.00	1255.00	110.00	1300.00	1400.00	1400.00	100.00				
Ha, Hb, Hc, Hd	1475.00	1571.25	1523.13	96.25	1562.50	1658.75	1610.63	96.25	1650.00	1746.25	1698.13	96.25	1737.50	1825.00	1781.25	87.50
Ka, Kb, Kc, Kd	2000.00	2110.00	2055.00	110.00	2100.00	2210.00	2155.00	110.00	2200.00	2310.00	2255.00	110.00	2300.00	2400.00	2350.00	100.00

3.7.2.9.2 Lenslet Slicer

The baseline configuration for the IFS employs a lenslet based image slicer similar to the OSIRIS instrument. The initial analysis presented in the following paragraphs was developed with reference to OSIRIS optical design notes (OODN0300 and OODN0400 by James Larkin). The lenslet array is located at the focus of the scale changer and forms a pupil image from each spatial sample that in turn becomes the effective entrance slit of the spectrograph. The lenslet array is rotated with respect to the spectrograph causing successive lenslets column wise to produce adjacent, staggered spectra on the detector. By choosing a rotation such that 24 such spectra are produced for each row wise step across the lenslet array, the 4096 pixel wide Hawaii-4RG detector will accommodate 80 to 85 row wise steps. In the other dimension a total of 4 rows of staggered spectra can be accommodated with ~1024 pixels per spectrum for a total of 85 x 96 spectra on the detector. The 1024 pixels per spectrum imply that narrow band filters are used to limit the length of each spectrum.

An 80 x 80 lenslet array with a pitch of 200 µm results in a total area of 16 mm x 16 mm for the lenslet array. This is the same size as the OSIRIS lenslet array but with a smaller lenslet pitch. The lenslet array is rotated with respect to the spectrograph to produce 24 staggered spectra corresponding to 24 columns of lenslets (compared to 16 in OSIRIS). With a 50 mas spatial scale an 80 x 80 lenslet array will result in an FOV of 4".

The pupil size at the spectrograph based on 200 µm pitch lenslets and 24 spatial samples (lenslet columns) in the space of one lenslet pitch (1/24 stagger) is 8.3 µm for the 50 mas plate scale. The f-number of the lenslets is 3.4, and the collimator should match this f-number. With a larger detector

(Hawaii-4RG) the spectrograph camera will require a somewhat larger field size (~1.6 times on each axis), but the required f-number is only 11 based on a 16 mm x 16 mm lenslet array and 15 µm detector pixels.

The focal length of the collimator will be determined by requirements to illuminate the proper area on the grating, and the combined focal length of the collimator and camera will be selected to ensure that the spectra are properly imaged on the detector. The baseline concept is to use a different grating for each of the instrument's passbands. For efficiency the gratings will be chosen to operate close to the blaze condition ($\alpha - \theta B = \beta - \theta B$).

3.7.2.9.3 Hybrid Slicer

The hybrid slicer design uses a 112 x 60 spatial sample configuration with a 250 µm pitch lenslet array. Figure 145 shows the overall optical layout of the hybrid slicer. After the lenslet array the array of pupil images formed by the lenslet array is magnified by two doublets (~6x magnification) to allow room for the reformatting mirror arrays. The magnified field is split in the 60 sample direction (the y axis of the IFS FOV) by a tent shaped arrangement of two mirrors at a 45° angle to the optical axis, and each 112 x 30 half of the field is directed to two sets of slicing mirrors by a second 45° fold mirror. Each of the two half fields is then reformatted by the two sets of slicing mirrors, the M1 and M2 shown in Figure 146. The result of the vertical split and the reformatting of each half field by an M1 and M2 mirror pair is that the IFS FOV is treated as 4 quadrants of 56 x 30 spatial samples by the reformatting mirror system.

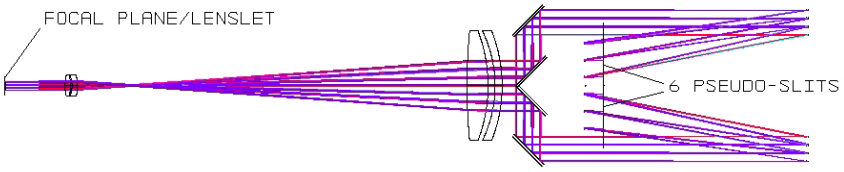

Figure 145: Optical layout of the hybrid slicer

Figure 147 shows how the M1 and M2 mirrors reformat one quadrant of the lenslet array. The M1 mirror consists of a stack of 30 rectangular mirrors (1.22 mm x 67 mm) with spherical front surfaces (R = 600 mm). Every 10 mirrors of the M1 stack reformat a 56 x 10 sample rectangular field into a staggered row of 10 sets of 56 spatial samples. The M2 mirrors, also spherical (R = 48 mm) rearrange the staggered row into a single row to form a virtual slit with 560 spatial samples.

Figure 148 shows how the four quadrants are formatted into the six virtual slits with 1120 spatial samples each.

The M1 and M2 slicing mirrors not only reformat the lenslet array in each quadrant but also provide the following optical functions:

1. De-magnification of the field by 12.5x to achieve a reasonable size for the pseudo-slits. M1 and M2 are separated by F1+F2 distance preserving the telecentricity at the slit plane.

2. Collimate the beams in the M1 to M2 space. This is achieved by placing M1 at one focal distance from the intermediate focal plane. This helps to keep the beam footprint small at M2.

Each group of M1 mirrors arranges the beams into a single staggered row. Each group of M2 mirrors creates one virtual slit. Figure 149 shows one-half of 3 of the virtual slits (corresponding to one quadrant of the lenslet) at the slit plane.

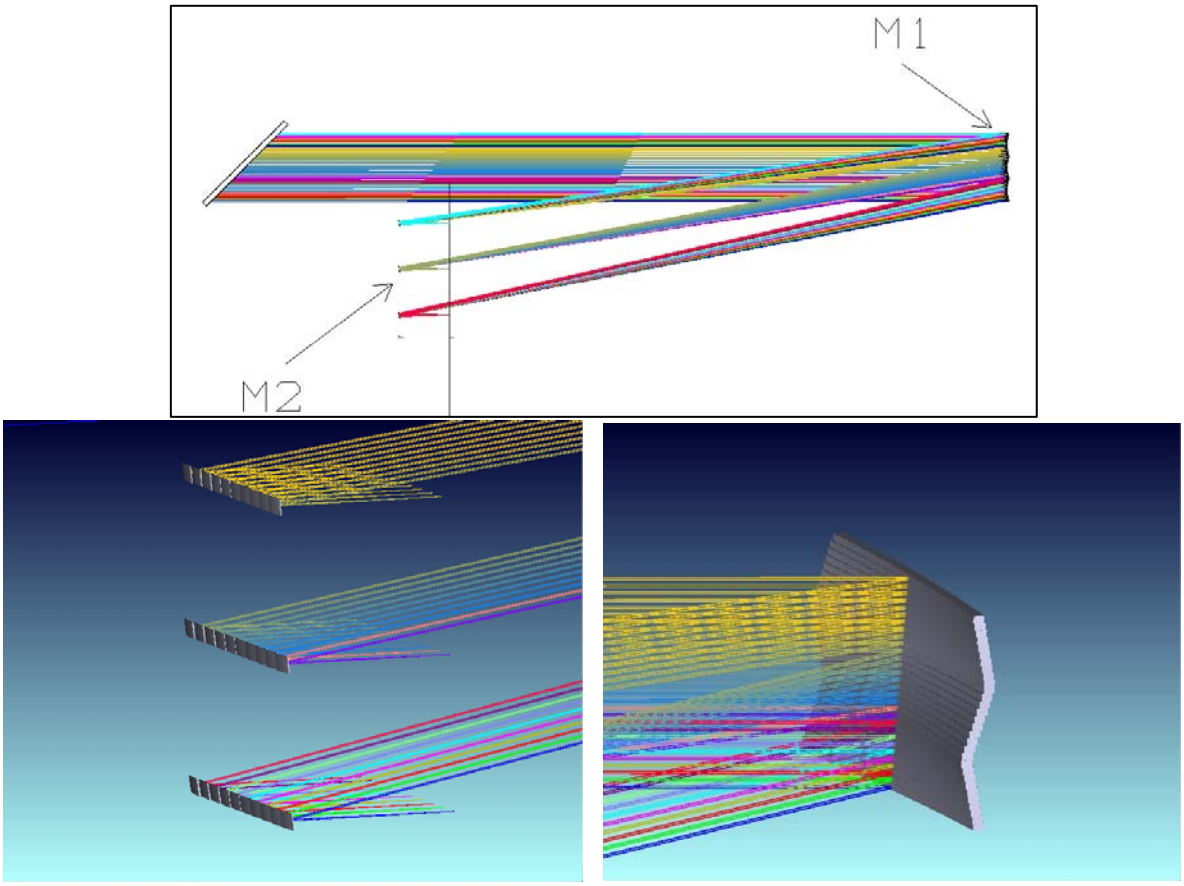

Figure 146: Slicing mirrors

The first set of slicing mirrors (M1) reformats the rectangular field into a staggered line. The second set of mirrors (M2) rearranges the staggered line into a single line. For clarity only one set of M1/M2 mirrors is shown that cover one quadrant of the FOV.

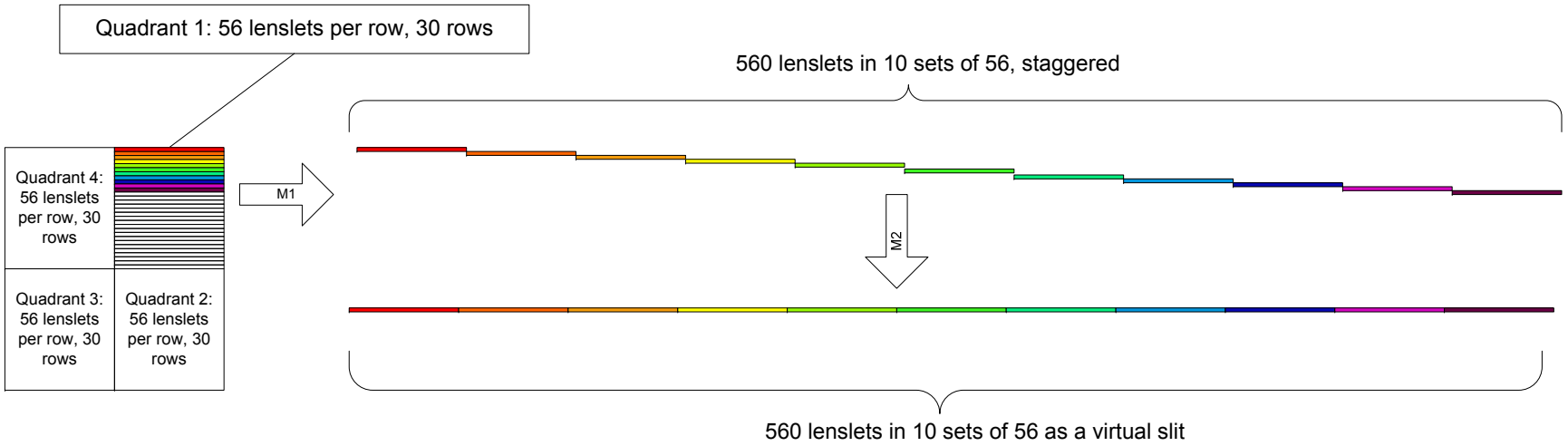

Figure 147: Reformatting 10 lenslet rows from one quadrant of the 112 x 60 sample pupil plane into a virtual slit

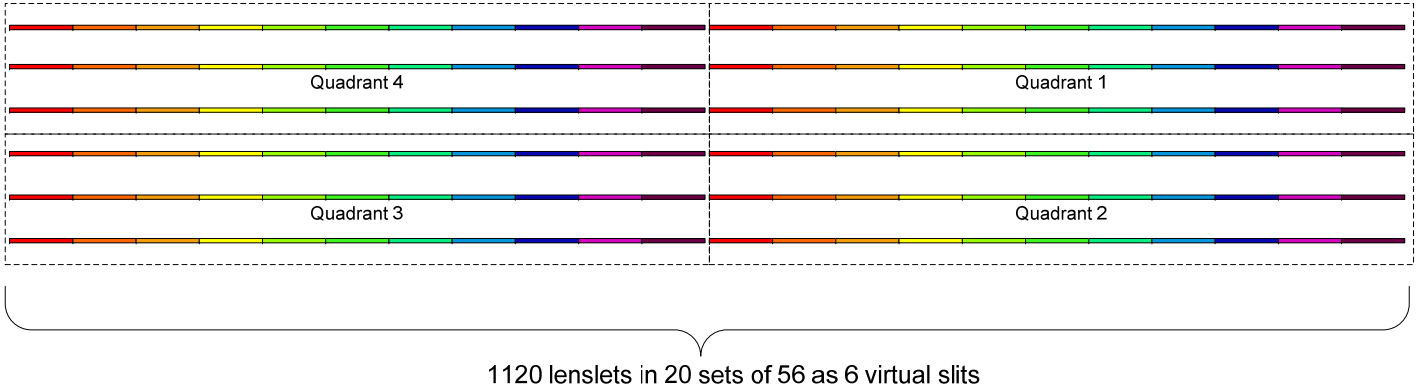

Figure 148: Virtual slit format for all four quadrants of the 112 x 60 lenslet array

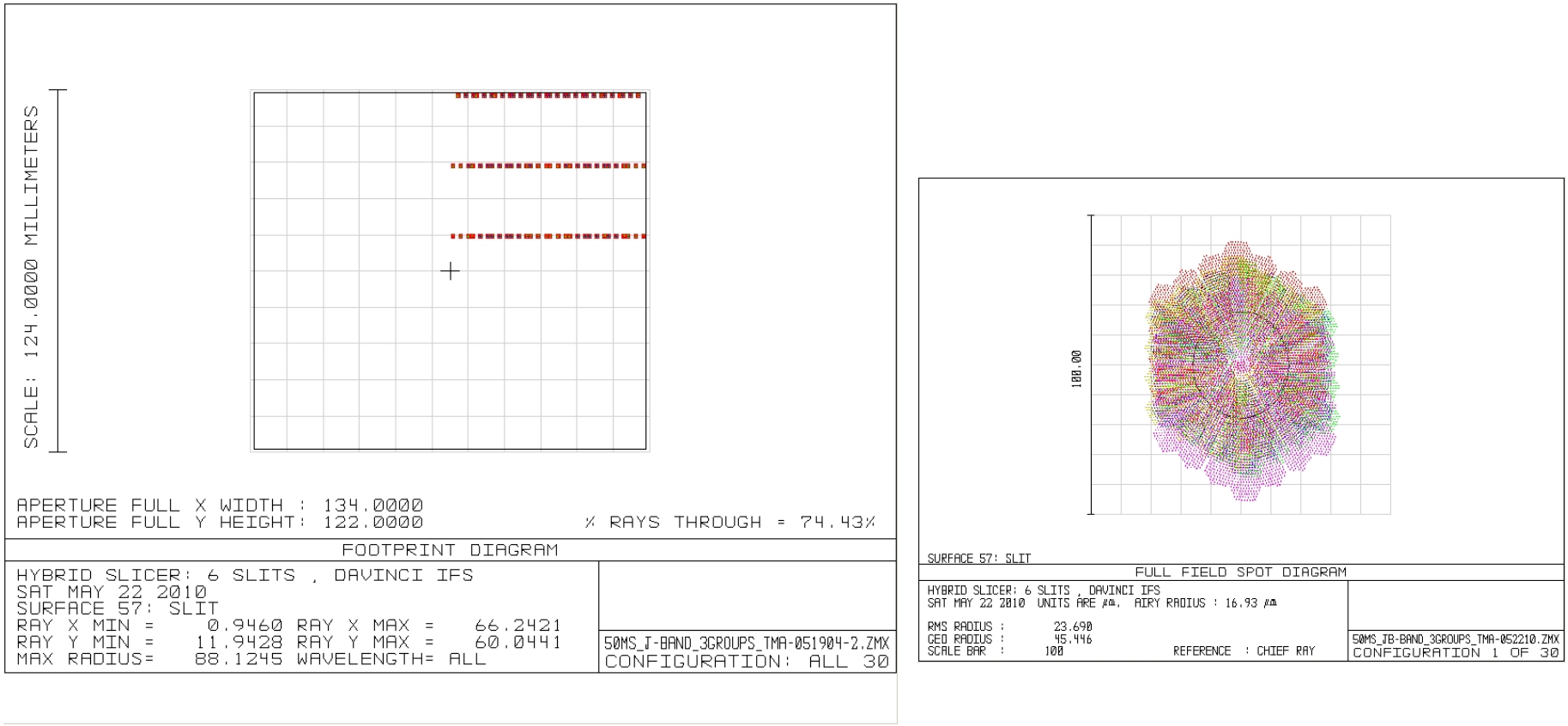

Figure 149: The layout for one half of 3 of the virtual slits (left) and the pupil image for a single sample (right)

3.7.2.9.4 Hybrid Slicer and IFS Transmission

For the image slicer design with all reflective components coated with bare gold the total transmission is 95% in the J, H, and K bands. The end to end predicted transmission of the DAVINCI IFS is shown in Table 25 when the hybrid slicer combined with the DAVINCI fore-optics and a three mirror anastigmat (TMA) is used for the collimator and the camera.

Table 25: DAVINCI IFS transmission estimate

Surface	I band	Z band	Y band	J band	H band	K band	I band	Z band	Y band	J band	H band	K band
Dewar Window												
Infrasil 302, 25 mm thick	99.23%	99.23%	99.23%	99.23%	99.23%	99.23%						
Coating, 2 surfaces	97.83%	97.84%	94.95%	95.83%	95.50%	96.77%						
Coronagraph Mask												
Infrasil 302, 2 mm thick												
Coating, 2 surfaces												
FM1							97.65%	98.53%	98.79%	99.00%	99.03%	99.17%
OAP1							97.65%	98.53%	98.79%	99.00%	99.03%	99.17%
Cold stop	100.00%	100.00%	92.00%	92.00%	98.00%	98.00%						
Filter	90.00%	90.00%	80.00%	88.00%	85.00%	95.00%						
OAP2							97.65%	98.53%	98.79%	99.00%	99.03%	99.17%
Scale changer	84.93%	84.93%	84.93%	84.93%	84.93%	84.93%						
Lenslet	95.00%	95.00%	95.00%	95.00%	95.00%	95.00%						
Reformatter							91.26%	93.75%	94.47%	95.07%	95.18%	95.58%
Collimator TMA												
1							97.65%	98.53%	98.79%	99.00%	99.03%	99.17%
2							97.65%	98.53%	98.79%	99.00%	99.03%	99.17%
3							97.65%	98.53%	98.79%	99.00%	99.03%	99.17%
Grating							60.00%	60.00%	60.00%	60.00%	60.00%	60.00%
Camera TMA												
1							97.65%	98.53%	98.79%	99.00%	99.03%	99.17%
2							97.65%	98.53%	98.79%	99.00%	99.03%	99.17%
3							97.65%	98.53%	98.79%	99.00%	99.03%	99.17%
%T	70.49%	70.50%	55.95%	62.12%	63.69%	72.13%						
%R							44.22%	49.25%	50.78%	52.09%	52.31%	53.20%
Combined	31.17%	34.72%	28.41%	32.35%	33.32%	38.38%						

3.7.2.9.5 IFS Spectral Formats

The science requirements for the DAVINCI IFS indicate that a spectral resolution of $3000 \leq R \leq 4000$ is required to resolve OH lines and support kinematic measurements. Two virtual slit configurations for the hybrid slicer were considered, one with 8 virtual slits with 20 sub-slits each (mapping 80 x 80 spatial samples into 20 x 40 x 8) and 6 virtual slits with 28 sub-slits each (mapping 82 x 82 samples in to 28 x 40 x 6). The configuration with six virtual slits has been selected after consideration of required spectral resolution and the aperture requirements for the collimator and camera optics.

Each sub-band listed in Table 24 will be selected by combination of a bandpass filter and the rotation angle of the diffraction grating. We want to evenly distribute 6 spectra along 4096 pixels utilizing as many pixels as possible for each spectrum. For a given spacing between the virtual slits, there are three parameters that affect this distribution. They are diffraction grating dispersion, angle of constant deviation (between a beam incident at the diffraction grating and a diffracted beam) and the effective focal length of camera optics. As a baseline for selecting diffraction gratings we can use Table 26 which lists the maximal grove frequency to fit a sub-band spectrum in 680 pixels (six virtual slits).

We will use G numbers from the Newport Richardson stock list of plane ruled grating to select a proper grating for each spectral band. This should reduce the cost of the gratings although we have to

note that stock gratings with suitable G may not be usable because their blaze angles are not appropriate for our application.

Table 26: Baseline for groove frequency G (1/mm)

# of slits	Ia	Ib	Za	Zb	Ya	Yb	Ja	Jb	Jc	Ha	Hb	Hc	Hd	Ka	Kb	Kc	Kd
6	848	848	665	665	865	865	649	649	649	741	741	741	741	649	649	649	649

To show how spectra from 6 virtual slits are distributed along the detector we use a constant deviation angle of 90° and an EFL of 280 mm for the camera optics. The latter is based on a 900 mm collimator EFL. Table 27 shows parameters for selected diffraction gratings (α = CWL incident angle, β = diffraction angle, D_β = angular dispersion, R = resolution). Again, for simplicity, a band CWL was used for any sub-band when deriving the listed values. To center a set of six spectra for each band on the detector, the diffraction gratings should be adjusted in the angle of rotation as shown in Figure 150. Using the diffraction grating with these parameters will yield the spectra distribution shown in Figure 151. Again, the shown distribution is mostly for illustration to see relationship between the spectrum positions. If needed, it can also be adjusted by fine tuning the rotation angle.

Table 27: Diffraction grating parameters for a six virtual slit configuration

Passband	cut-on um	CWL um	Cut-off um	G 1/mm	α deg	β deg	Dβ 1/mm	R
Ia	0.700	0.738	0.777	272.3	-36.8	53.2	454.3	3410
Ib	0.777	0.815	0.853	272.3	-36.0	54.0	463.5	3840
Za	0.855	0.904	0.953	210	-37.3	52.7	346.6	3185
Zb	0.953	1.001	1.050	210	-36.4	53.6	353.5	3598
Ya	0.970	1.008	1.045	245	-34.9	55.1	427.7	4381
Yb	1.045	1.083	1.120	245	-34.2	55.8	436.0	4798
Ja	1.100	1.150	1.200	180	-36.6	53.4	302.0	3531
Jb	1.200	1.250	1.300	180	-35.8	54.2	307.4	3906
Jc	1.300	1.350	1.400	180	-35.1	54.9	313.0	4296
Ha	1.475	1.519	1.563	150	-35.7	54.3	256.9	3966
Hb	1.563	1.606	1.650	150	-35.2	54.8	260.3	4250
Hc	1.650	1.694	1.738	150	-34.7	55.3	263.8	4543
Hd	1.738	1.781	1.825	150	-34.1	55.9	267.5	4844
Ka	2.000	2.050	2.100	135	-33.7	56.3	243.2	5069
Kb	2.100	2.150	2.200	135	-33.2	56.8	246.8	5395
Kc	2.200	2.250	2.300	135	-32.6	57.4	250.6	5732
Kd	2.300	2.350	2.400	135	-32.0	58.0	254.5	6080

The spectrum length is maximized at the I-band and Z-band to meet the resolution requirement. This constrains the parameters for the IFS optics, specifically the camera EFL. With these parameters there are large gaps between the spectra for the H-band and the K-band. However the resolution is still sufficient (Table 27).

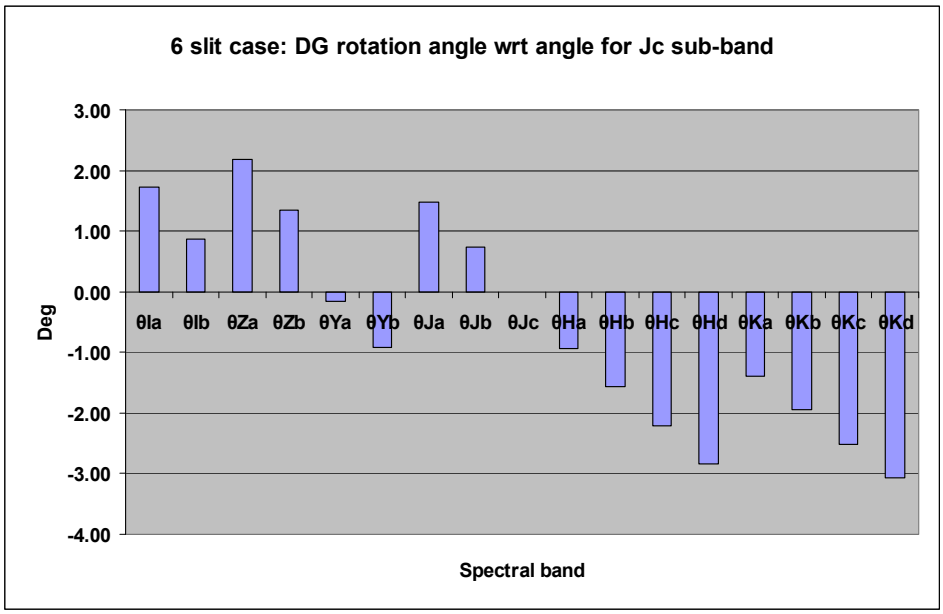

Figure 150: Rotation angles for gratings (six virtual slits)

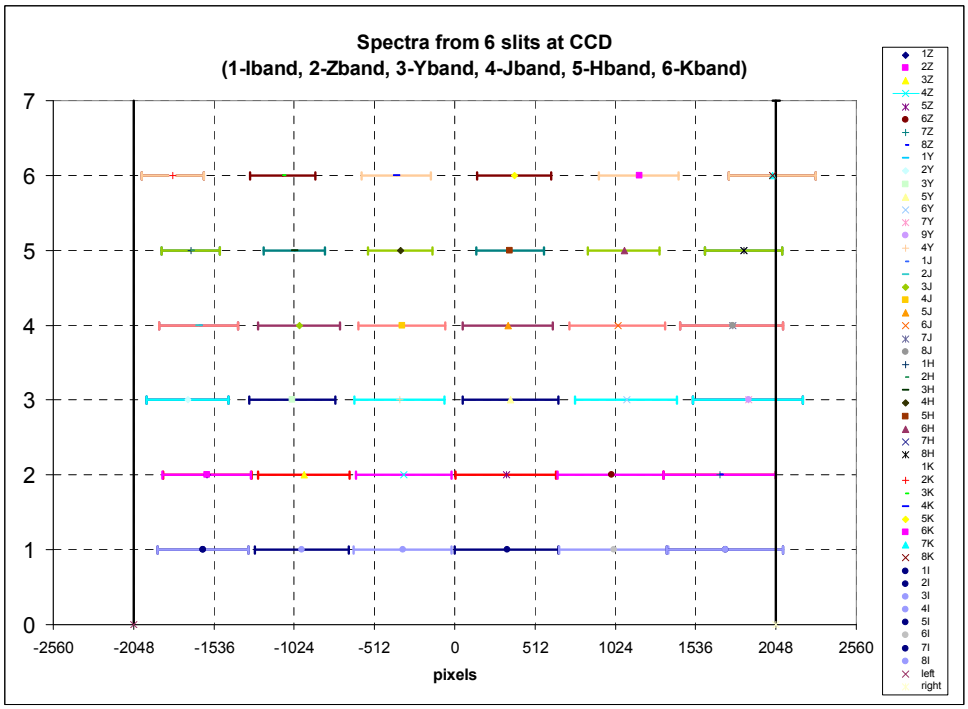

Figure 151: Distribution of spectra on the detector using six virtual slits

3.7.2.9.6 IFS Collimator and Camera

The basic parameters for the IFS collimator and camera with the hybrid slicer are shown in Table 28.

Table 28: IFS camera and collimator parameters

	Slit plane size		Collimator		Camera	
# of slits	X(spatial)	Y(spectral)	EFL	F#	EFL	F#
6	141.1	120.0	900	3.30	274.5	1.01

Figure 152 shows collimating and camera optics developed for the spectrograph using these parameters. The collimator is a single aspherical mirror (R=-1800 mm) working at a 7° off-axis angle. After the collimator the beams are folded by a plane mirror and converge at the diffraction grating. Dispersed light is reimaged by a three mirror anastigmat (TMA) at the detector. The size of footprint requires a grating with ruled area of 120 mm x 110 mm (110 mm groove length). The detector is tilted by 5° with respect to the central axis to provide the best image quality for all slits.

This design for the spectrograph optics provides a good solution to evaluate spectral formatting. But further improvement in image quality is needed and a one solution under consideration is to replace the single collimating mirror with a TMA.

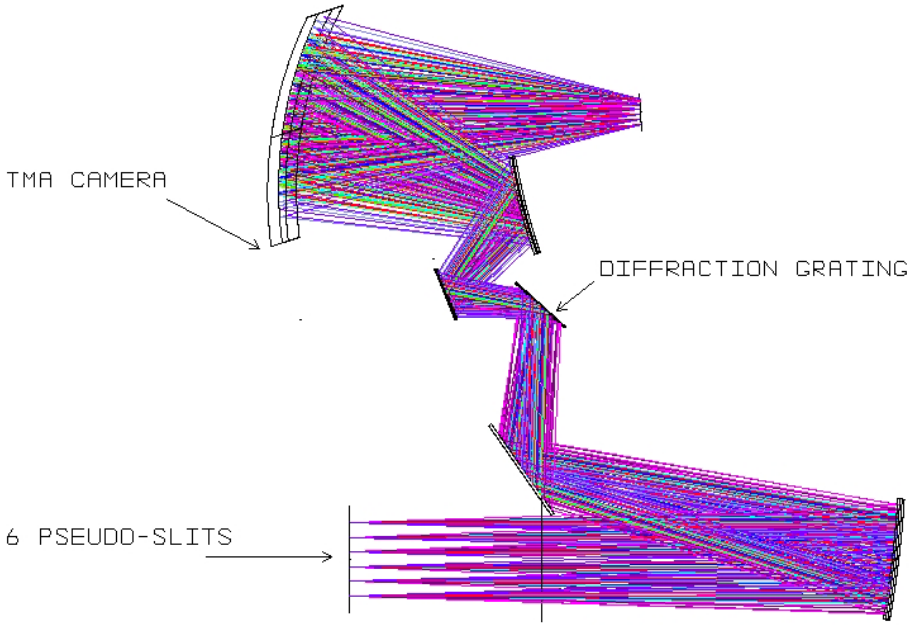

Figure 152: Spectrograph optics

As an example Figure 153 shows distribution of spectra for the Jb-band at one quadrant of the detector. A 190 groove/mm grating is used for this example. Spectral direction is vertical with three sets of spectra from three slits. For clarity only 7 wavelengths are shown. In spatial direction, there are three samples for 1/10 of a half-slit (created by a M1/M2 pair) shown. In total this adds up to 30 samples evenly distributed in the spatial direction.

Note that X-width of the third set of spectra is shorter that the width of two others on the top. This is done deliberately to reduce size of optics. There are still sufficient gaps between sub-sets of samples (in total there are 18 pixel gaps between spatial sub-groups for this set).

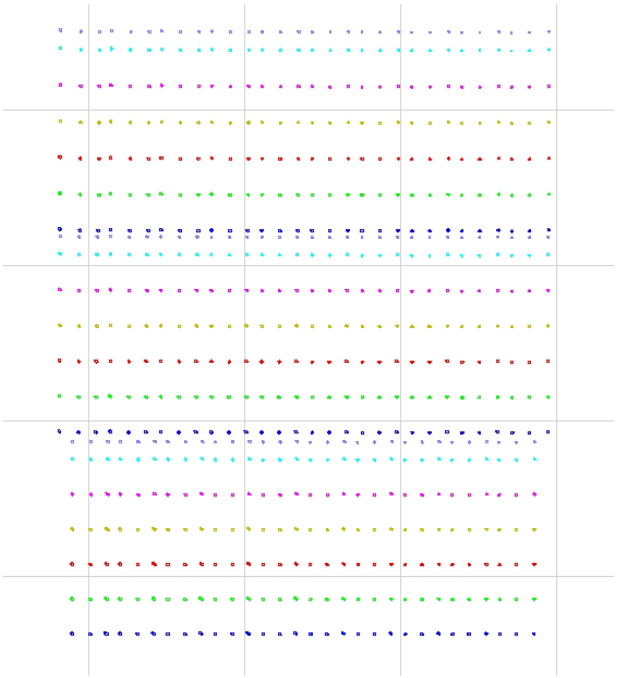

Figure 153: Jb-band spectra at one quadrant of detector. Spectral direction is vertical

3.7.2.10 DAVINCI Mechanical Design

3.7.2.10.1 Mechanical Design Concept

The DAVINCI dewar is shown in Figure 154. The design of this dewar is derived from the design for the MOSFIRE instrument ("MOSFIRE", 2007). This dewar design has proven thermal performance with an internal temperature stability of ~ 1 K through the use of variable speed cold heads in conjunction with a closed loop temperature stabilization system using active heating of the optical bench. MOSFIRE was designed for mounting at the Keck I Cassegrain position, so the dewar incorporated a number of features that were required to control internal flexure. These features are not required for DAVINCI allowing a simplification of the design and lowering the risk with respect to the modifications required for DAVINCI.

Connections between the DAVINCI electronics rack and the dewar are made via hermetic feedthru connectors located on bulkhead plates on the bottom of the dewar. The vacuum pump out port and vacuum gauges are also located on the bottom of the dewar. The CCR heads and the JADE2 interface boards for the imager and IFS FPAs are mounted on the sides of the dewar. All access for adjustment and service is obtained by removing the top cap of the dewar and the internal top cold shield. An overhead crane in the AO enclosure will be provided for this purpose.

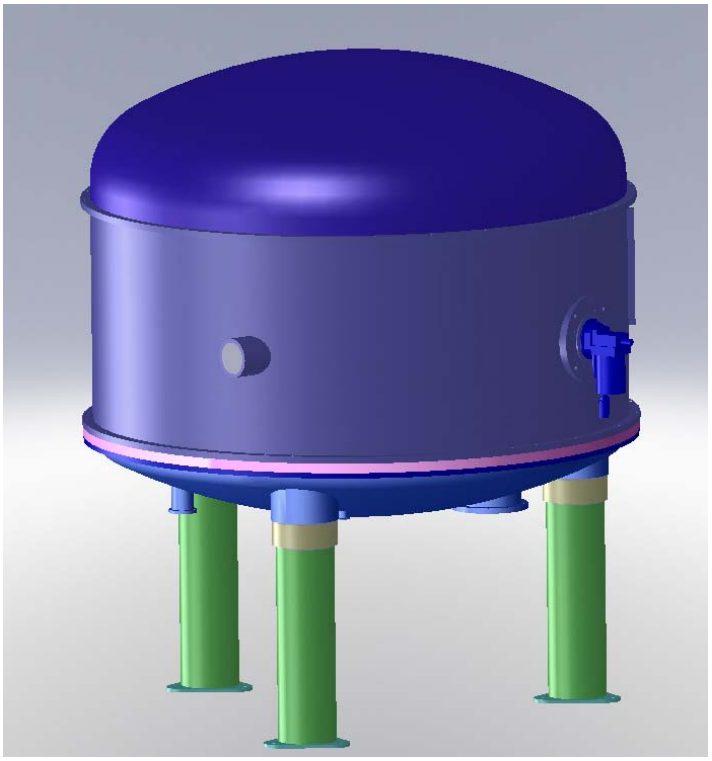

Figure 154: DAVINCI Instrument Dewar

3.7.2.10.2 Mechanisms

The majority of the mechanisms required for the NGAO instrument can be implemented using straightforward rotary or wheel designs derived from the MOSFIRE and OSIRIS instruments. Referring to Figure 132 these include wheel mechanisms for the filters, pupil masks, and coronagraph occulting masks. The instrument's two detectors may be equipped with focus mechanisms derived from MOSFIRE's detector head assembly as well. While the AO system will maintain the focus for the instrument, there are integration and test advantages to being able to shift the detector focus, and it may be important for observing efficiency to maintain parfocality between the imager and IFS channels.

The one mechanism unique to the NGAO instrument is the grating changer. The proposed mechanism for this is a rotary turret carrying the gratings on an outer radius. Each grating can be mounted with precision adjustments to ensure proper alignment in the spectrograph. The requirements on positioning of the gratings will be demanding in order to ensure repeatability of instrument wavelength calibrations. It is likely that this motion axis will require high precision position encoding, perhaps by using either a series of LVDTs, or perhaps optical position sensing.

3.7.2.10.3 Cryogenic Cooling System

The baseline for the instrument's cryogenic cooling system is to reuse the MOSFIRE design which employs two Brooks Automation (formerly CTI) model 1050 single stage closed cycle refrigerator (CCR) heads for cooling the dewar interior. The MOSFIRE detector is cooled by a model 350 two

stage cold head, and two such cold heads will be required for the NGAO instrument. Active temperature stabilization of each detector and the optical bench will be performed by Lakeshore 340 temperature controllers.

3.7.2.10.4 Interfaces

The mechanical interfaces between the NGAO instrument and the telescope/AO system will be simple, provided that analysis of the stability of the mounting of the instrument and the AO system to the Nasmyth platform will support the requirements for relative motion between the instrument and the AO system. This is understood to be primarily driven by the NGAO astrometry error budget.

The instrument will mount to the Keck II telescope left Nasmyth platform on kinematic mounting pads to allow adjustment of the instrument's position for alignment with the AO system's optical axis and science focal plane. The dewar will be supported by a steel tube structure that mounts to the bottom of the dewar shell's main cylinder.

The interface to the AO system's bench enclosure that is used to insulate the cooled bench from the dome ambient will be accomplished by an insulated bellows.

3.7.2.11 DAVINCI Electronics

DAVINCI's instrument electronics are derived directly from the MOSFIRE electronics design. A forced air cooled electronics rack will be located in the AO electronics vault and will contain all of the electronic and electrical systems required by the instrument. A block diagram of DAVINCI's electronics is shown in Figure 155.

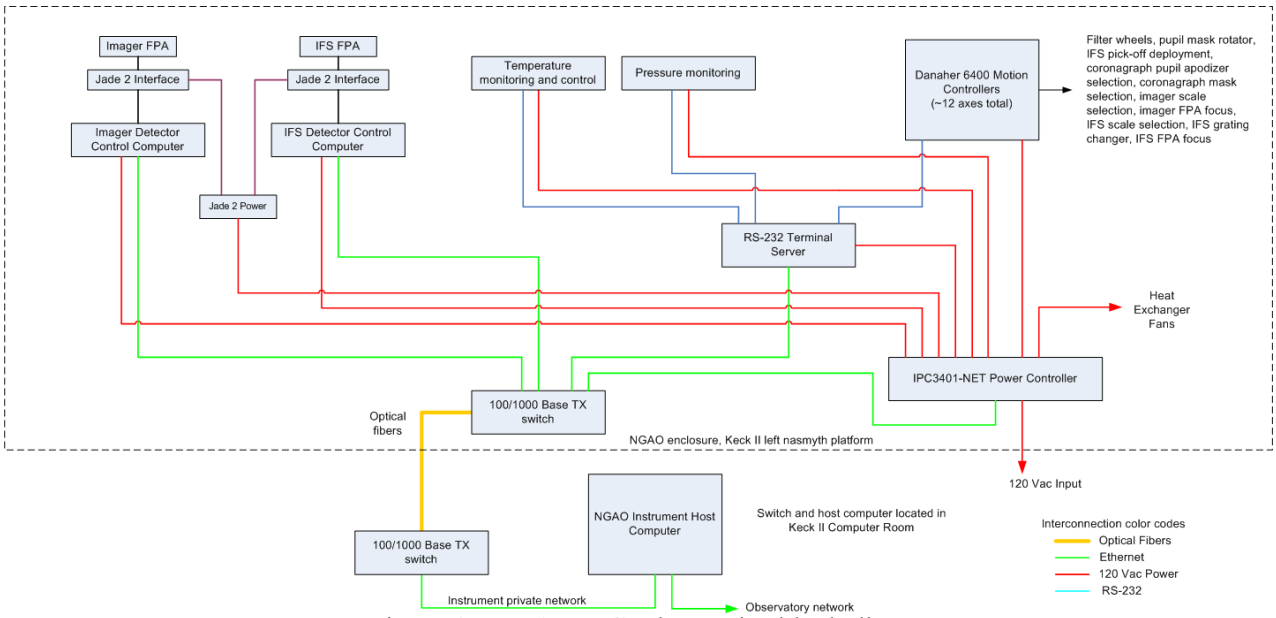

Figure 155: DAVINCI electronics block diagram

3.7.2.12 DAVINCI Software

DAVINCI's instrument software will be based on the software developed for the MOSFIRE instrument. The detector software, temperature and pressure monitoring, power controller and 6400 series motion controller software will be a straightforward port from MOSFIRE. The low level and global server architecture will also be re-used from MOSFIRE. The instrument graphical user interface (GUI) designs are TBD, but they could easily be based on a port of the MOSFIRE desktop and control GUIs.

3.7.3 Interferometer

It is a requirement for the Interferometer to be supported by AO on both telescopes in the NGAO era. A trade study was performed on the issue of Keck Interferometer support during the system design that is documented in KAON 483. The primary requirements are to achieve at least the current level of performance while maintaining a common field orientation and polarization from both telescopes.

The NGAO configuration and control loops in Interferometer mode are provided in KAON 550 and KAON 705 (see also section 3.5.2 of this document), respectively.

An assessment of how well the Interferometer needs are met by NGAO was performed near the end of the preliminary design in KAON 728. The conclusion is that the angles and geometry between Keck I AO and NGAO are quite well matched leaving only the issues of matching material dispersions and dichroic phases. These can be matched by the identified addition of similar windows and dichroic coatings in the Keck I AO system.

3.7.4 'OHANA

Both existing Keck AO systems accommodate an 'OHANA fiber injection module at the output of the AO systems. NGAO should provide an output port where this or a similar fiber injection module could be located, and whose output could be successfully interfered with the light from another telescope. The 'OHANA needs are also addressed in KAON 728 and should be met best by locating the 'OHANA module at the 2nd NGAO instrument location (at least initially).

3.7.5 Thermal NIR Imager

A thermal NIR imager has not been given a high priority and therefore no significant evaluation has occurred for this instrument. An evaluation of the reuse of NIRC2, which extends out to L and M-bands, was performed as part of KAON 493.

3.8 Observatory Infrastructure

The NGAO systems must utilize and interface to the existing Observatory infrastructure. This infrastructure includes the telescope and related control systems as well as mechanical and electrical services. In some cases this existing infrastructure may need to be modified.

The total required facility power and cooling is shown in Table 29. A more detailed explanation can be found in KAONs 759 and 709. Based on historical data, there is a propensity to increase power and cooling requirements as the designs mature. The margin placed on the NGAO design at the preliminary design phase is 50%. With the margin, the amount of power estimated to be needed by NGAO is 77 kW. Measurements were taken to determine the power consumption of the Keck II dye laser system and its supporting systems. The estimated savings from retirement of the Keck II laser is equal to 97 kW. This recovery will be more than sufficient to support NGAO and the proposed margin. There is sufficient capacity on the telescope to support the power requirement; but additional infrastructure wiring will be necessary from the Keck II mechanical room to the computer room to support the RTC.

Current AO and laser operations have also shown how power outages or power bumps can result in significant lost observing time. Subsystems have to be reinitialized and re-calibrated often after power irregularities. To alleviate this problem, the proposed electrical design uses scalable APC Symmetra PX 40 kW UPS. These units are currently used at the summit facilities and have proven to be reliable and effective in providing continuous quality power. Two of these units will be required to provide the required NGAO power and margin.

In additional to providing power, the facility must remove the heat generated from the NGAO system. Two locations are significantly impacted by the NGAO system. The left Nasmyth platform supporting the AO electronics, cold enclosure, science instrument, AO bench, and the laser systems will require significantly more cooling than what is available now. The computer room will require an additional 21 kW of cooling capacity to support the RTC. Based on existing cooling demand in the computer room, the refrigeration unit does have sufficient capacity to support the RTC.

The retirement of the Keck II dye laser will improve the building glycol capacity; but not instrument glycol where it is needed at the AO enclosure. The Keck II instrument glycol system is marginal as it is now and is incapable of supporting the left Nasmyth platform subsystems. To improve the overall Keck II capacity, the design is to tie together the Keck I and Keck II glycol systems. This design will improve the overall Keck II instrument cooling capacity and flow. The design will require piping and pumps to be installed between the Keck I and Keck II mechanical rooms. The Keck I cooling system was recently upgraded to support the Keck I laser. The tying together of the two systems will also provide redundancy for both telescopes. The cost of this design is less than half of that to install a new chiller system in the Keck II mechanical room.

Table 29: NGAO power and cooling requirements

Name	Location	Power (kW)		Cooling
			+ 50%	
Computer Room Electronics	Keck II Computer Room	20.9	31.4	Keck II Computer Room AC
NGAO Instrument CCR Compressor	Keck II Mechanical Room	5.5	8.25	Keck II Building Glycol
NGAO Electronics Racks Power	Keck II Left Nasmyth Platform	11.5	17.25	Keck II Instrument Glycol
Cooling System for NGAO Electronics Vault	Keck II Left Nasmyth Platform	0.67	1.0	Keck II Instrument Glycol
Main AO room for NGAO	Keck II Left Nasmyth Platform	0.67	1.0	Keck II Instrument Glycol
Chiller for NGAO Cold	Within NGAO Clean Room	10.0	15.0	Low temperature glycol from

Bench/Cold Box	Area, on Keck II Left Nasmyth Platform			chiller in Keck II Mechanical Room or local
NGAO Laser Service Enclosure Cooling	Keck II Elevation Ring	0.67	1.0	Keck II Instrument Glycol
Beam Generation System	Keck II Secondary	0.1	0.15	Needs to be cooled by instrument cooling
Keck II NGAO Laser Heat Exchanger	Suspended beneath Keck II Left Nasmyth Platform	0.75	1.125	Heat exchanger cooled with Keck II Instrument Glycol
	Total Power	**51**	**77**	

4 PERFORMANCE BUDGETS

In support of the flow down of requirements from the science case and system requirements to component specification, eight system performance metrics were identified in the science case requirements document. For three of these metrics, background and transmission, wavefront error and ensquared energy, and high-contrast performance, we have produced associated quantitative performance budgets to identify key performance drivers. For photometric precision, astrometric accuracy, and polarimetry we have identified key drivers and documented these in technical reports that have informed the NGAO design. The final two metrics, observing efficiency and observing uptime, have been flowed down to subsystems.

Several of the above performance metrics (in particular astrometry and photometry) will strongly depend on the stability and knowledge of the PSF.

4.1 Transmission and Background

Both AO relays must efficiently transmit the science wavelength light from I-band to K-band (0.7 to 2.4 μm). The first relay must also efficiently transmit sodium wavelength light (589 nm) and the additional L-band light (3.4 to 4.2 μm) for the interferometer. This wavelength range must be efficiently divided between the various sensors (LGS and tip-tilt) and the instruments.

The background and transmission performance budget has been further developed (since KAON 501) into an excel spreadsheet format as part of the performance flowdown budgets (KAON 723). The transmission and emissivity budgets take into account all surface counts in the various NGAO system paths, along with detailed transmission or reflectivity versus wavelength coating models for each surface. Where possible, these models are taken from measurements or vendor designs. Often the NGAO design choice of specific optical coating requires a tradeoff to optimize transmission to different science of AO system sensors and AO system emissivity.

Table 30 is an extract from the "Trans – AO Sys" tab of the performance flowdown budgets spreadsheet. This extract shows the freshly coated transmission in the right hand column for each optical surface (the first 10 surfaces of the AO system are located elsewhere on this same tab). Each numbered row (starting with 11) lists the name of the assumed coating, the temperature of the enclosure in which that optic will reside (only used for the emissivity calculation), the expected percent transmission degradation after one year and the freshly coated transmission for the named coating. The bottom right corner of Table 30 shows a total transmission to the LGS WFS detector of

40.2% after including the one-year degradation numbers plus the sky and telescope. The transmission excluding the sky plus telescope is 64.4%.

Table 30: Fixed Asterism LGS WFS Transmission Budget from KAON 723

				One-year	Wavelength, microns
	Optic	Coating	Temp C	Degradation	0.589
1-10	Total to dichroic				91.2%
1-10	Total to dichroic, Degraded				87.2%
11	NaDichroicWFSpath	CoatingData!dichroic_na	-15.0	0.5%	95.0%
12	Focusing Lens 1	CoatingData!AR	-15.0	0.5%	99.6%
13	Focusing Lens 2	CoatingData!AR	-15.0	0.5%	99.6%
14	LGS Exit Window 1	CoatingData!AR	-15.0	0.5%	99.6%
15	LGS Exit Window 2	CoatingData!AR	2	2.0%	99.6%
16	WFS Probe Arm 1	CoatingData!AR	2	0.5%	99.6%
17	WFS Probe Arm 2	CoatingData!AR	2	0.5%	99.6%
18	WFS Probe Arm 3	CoatingData!AR	2	0.5%	99.6%
19	WFS Probe Arm 4	CoatingData!AR	2	0.5%	99.6%
20	WFS Collimator	CoatingData!AR	2	0.5%	99.6%
21	WFS Collimator	CoatingData!AR	2	0.5%	99.6%
22	Lenslet Array 1	CoatingData!AR	2	0.5%	99.6%
23	Lenslet Array 2	CoatingData!AR	2	0.5%	99.6%
24	Lenslet array, scattering	CoatingData!la_scat	2	0.0%	92.5%
25	Reimaging Optic 1	CoatingData!AR	2	0.5%	99.6%
26	Reimaging Optic 2	CoatingData!AR	2	0.5%	99.6%
27	Reimaging Optic 3	CoatingData!AR	2	0.5%	99.6%
28	Reimaging Optic 4	CoatingData!AR	2	0.5%	99.6%
29	CCD Window	CoatingData!AR	2	0.5%	99.6%
30	CCD Window	CoatingData!AR	2	0.5%	99.6%
	Detector				
SubTotal	To fixed HOWFS input focus				85.5%
SubTotal	**To fixed HOWFS input focus, Degraded**				78.5%
SubTotal	Fixed HOWFS				82.4%
SubTotal	**Fixed HOWFS, Degraded**				73.8%
Total	**Fixed HOWFS + AO, Degraded**				64.4%
Total	**Fixed HOWFS + AO, Degraded + Sky + Telescope**				40.2%

The calculated transmissions for all detectors at relevant wavelengths are listed in Table 31.

Table 31: Percent transmission, including sky and telescope, to each detector

Detector	Wavelength (microns)					
	0.589	0.7	0.85	1.25	1.65	2.2
LGS WFS (fixed)	40%					
LGS WFS (patrolling)	38%					
Acquisition		43%				
Tip-Tilt				29%	31%	
TTFA				27%	28%	
TWFS		18%	20%			
NGS WFS		27%	31%			
Instrument (LGS mode)		14%	17%	34%	37%	35%

The sensitivity delivered by the NGAO system is significantly affected by the total background seen by the science instruments. In the present Keck telescope AO systems, background radiation is recognized as a significantly limiting sensitivity, particularly for the K-band.

Data from the current Keck II telescope AO system was used to help develop a model of the background contributed by sky + telescope + AO system that indicates the AO system optics should be cooled to -12.5°C in order to achieve the requirement that the AO plus instrument contribution must be less than 30% of the sky plus telescope contribution. We have chosen an operating temperature of -15°C for the NGAO bench to provide some design margin.

Table 32 is another extract from the "Trans – AO Sys" tab of the performance flowdown budgets spreadsheet. This extract shows the calculation of the emissivity seen by the Science Instrument as a function of a few wavelength bands. The emissivity from the AO system and Science Instrument in LGS AO mode (5^{th} row from bottom) at 2.2 μm is calculated to be 0.27 photons/sec/m^2/$arcsec^2$/nm. The sky plus telescope emissivity, calculated on the "Trans – Sky + Tel" tab, is listed here as 8.96 photons/sec/m^2/$arcsec^2$/nm. The AO system and science instrument emissivity contribution is therefore only 3% of the sky plus telescope contribution in this case (2^{nd} last row) which is much better than the requirement. As another example, the NGS case with a -2°C ambient temperature, the AO system and science instrument emissivity is 17% of the sky plus telescope contribution at 2.3 μm. We currently therefore have margin and we will re-evaluate how much margin is appropriate as we improve the throughput and emissivity estimates during the detailed design.

Table 32: Science Instrument Emissivity Budget from KAON 723

Emissivity, ph/s/m^2/arcsec^2/nm						
	Optic	Coating	Temp C	**2**	**2.1**	**2.2**
1	AO Window 1	CoatingData!AR	-15.0	7.76E-06	2.44E-05	6.86E-05
2	AO Window 1, surf 2	CoatingData!AR	-15.0	5.19E-06	1.65E-05	4.68E-05
3	AO Window 2	CoatingData!AR	-15.0	5.29E-06	1.68E-05	4.77E-05
4	AO Window 2, surf 2	CoatingData!AR	-15.0	6.84E-06	2.16E-05	6.11E-05
5	Kmirror, surf 1	CoatingData!FSS99_106_45	-15.0	7.94E-06	2.65E-05	7.75E-05
6	Kmirror, surf 2	CoatingData!NaHG	-15.0	7.52E-06	2.33E-05	6.46E-05
7	Kmirror, surf 3	CoatingData!FSS99_106_45	-15.0	8.37E-06	2.79E-05	8.20E-05
8	Fold	CoatingData!NaHG	-15.0	7.93E-06	2.46E-05	6.83E-05
9	OAP1	CoatingData!NaHG	-15.0	8.13E-06	2.52E-05	7.01E-05
10	DM1	CoatingData!NaHG	-15.0	8.34E-06	2.59E-05	7.19E-05
11	NaDichroicSciencePath	CoatingData!dichroic_na	-15.0	1.93E-05	6.00E-05	1.67E-04
12	OAP2	CoatingData!Gold	-15.0	6.35E-06	1.97E-05	5.47E-05
13	Fold	CoatingData!Gold	-15.0	6.46E-06	2.01E-05	5.57E-05
14	OAP3	CoatingData!Gold	-15.0	6.58E-06	2.04E-05	5.67E-05
15	DM2	CoatingData!Gold	-15.0	7.08E-06	2.20E-05	6.10E-05
16a	IR/Vis Dichroic IR Path	CoatingData!None	-15.0	3.77E-02	1.17E-01	3.24E-01
16b	IR/Vis Dichroic IR Path	CoatingData!None	-15.0	0.00E+00	0.00E+00	0.00E+00
17	OAP4	CoatingData!Gold	-15.0	7.21E-06	2.24E-05	6.21E-05
18	Switchyard Mirror	CoatingData!Gold	-15.0	7.21E-06	2.24E-05	6.21E-05
19	IR ADC 1, surf 1	CoatingData!Gold	-15.0	7.68E-03	2.38E-02	6.61E-02
20	IR ADC 2, surf 2	CoatingData!Gold	-15.0	7.82E-03	2.43E-02	6.73E-02
21	IR ADC 3, surf 3	CoatingData!Gold	-15.0	7.96E-03	2.47E-02	6.85E-02
22	IR ADC 4, surf 4	CoatingData!Gold	-15.0	8.10E-03	2.51E-02	6.98E-02
23	Instrument Window 1	CoatingData!ARIR	-196	2.06E-31	1.45E-29	6.88E-28
24	Instrument Window 2	CoatingData!ARIR	-196	1.28E-31	9.00E-30	4.26E-28
25	Collimator	CoatingData!Gold	-196	5.80E-31	4.08E-29	1.93E-27
26	Cold Stop	CoatingData!None	-196	0.00E+00	0.00E+00	0.00E+00
27	Filter	Custom	-196	5.66E-30	3.98E-28	1.89E-26
28	Camera Surf 1	CoatingData!ARIR	-196	1.79E-31	1.26E-29	5.97E-28
29	Camera Surf 2	CoatingData!ARIR	-196	1.80E-31	1.27E-29	6.02E-28
30	Camera Surf 3	CoatingData!ARIR	-196	1.82E-31	1.28E-29	6.07E-28
31	Camera Surf 4	CoatingData!ARIR	-196	1.83E-31	1.29E-29	6.11E-28
32	Camera Surf 5	CoatingData!ARIR	-196	1.85E-31	1.30E-29	6.16E-28
33	Detector Window 1	CoatingData!ARIR	-196	1.86E-31	1.31E-29	6.21E-28
34	Detector Window 2	CoatingData!ARIR	-196	1.88E-31	1.32E-29	6.26E-28
Sub Total	**AO System, wide field relay, Degraded**			0.00	0.00	0.00
Sub Total	**AO System, 1st and 2nd relay, LGS Sci Mode, Degraded**			0.03	0.10	0.27
Sub Total	**AO System, 1st and 2nd relay, NGS Sci Mode, Degraded**			0.07	0.22	0.60
Sub Total	**Instrument only, Degraded**			0.00	0.00	0.00
Total	**Instrument + AO, LGS Mode, Degraded**			0.03	0.10	0.27
Total	**Sky + Telescope**			2.99	2.40	8.96
Total	**Instrument + AO, LGS Mode, Degraded + Sky + Telescope**			3.02	2.50	9.24
Total	**AO System, 1st and 2nd relay, LGS, Degraded as % of Sky + Telescope**			1%	4%	3%
Total	**AO System, 1st and 2nd relay, NGS, Degraded as % of Sky + Telescope**			2%	9%	7%

4.2 Wavefront Error and Ensquared Energy

NGAO performance predictions, in terms of wavefront error and ensquared energy, for each of the key and non-key NGAO science cases are reported in KAON 716, which is recommended adjunct reading to this report. The performance summary from KAON 716 is summarized here in Table 33. KAON 761 also provides a description of:

- The tools, primarily a MS Excel spreadsheet (maintained as KAON 721), and input assumptions used to generate these predictions
- How the spreadsheet tool has been anchored against both detailed wave-optics simulations and as-built measurements of existing AO systems,

- The results of several studies describing the sensitivity of NGAO performance to varying conditions, demonstrating the robustness of NGAO performance.

Table 33: Predicted performance for all NGAO science cases

Cases 1 to 6 are the key science cases. The colors indicate whether the requirement has been met (green), almost met (yellow) or not met (red). Uncolored cells have no explicit performance requirement. The case 3 high order wavefront error requirement is 190 nm rms (see KAON 716).

KAON 721 Case #	Science Case	Science Band	RMS High-order Wavefront Error [nm]	RMS TT Error [mas]	Effective RMS Wavefront Error [nm]	Strehl Ratio	Ensquared Energy in Spaxel			
							10 [mas]	35 [mas]	50 [mas]	70 [mas]
1	Galaxy Assembly	K	158	4.9	180	77%	4%	36%	56%	75%
2	Nearby AGN	Z	158	4.8	176	21%	8%	29%	30%	31%
3	Galactic Center Imaging	K	208	2.2	212	69%	4%	31%	48%	65%
4	Galactic Center Spectra	H	191	2.4	195	57%	5%	38%	52%	59%
5	Exo-planets	H	155	2.9	162	68%	6%	46%	62%	71%
6	Minor Planets	Z	157	4.7	175	21%	8%	29%	30%	31%
7	QSO Host Galaxies	K	158	4.7	178	77%	4%	36%	56%	75%
8	Gravitational Lensing	J	157	4.9	179	45%	8%	45%	53%	55%
9	Astrometry Science	H	169	4.6	188	59%	6%	43%	58%	66%
10	Transients	Z	155	2.9	162	26%	8%	30%	31%	32%
11	Resolved Stellar Populations	I'	168	4.1	181	10%	5%	14%	15%	16%
12	Debris Disks and YSOs	I'	156	4.1	170	13%	7%	19%	19%	20%
13	Size, etc. of Minor Planets	I'	154	3.7	167	14%	7%	19%	20%	21%
14	Gas Giant Planets	K	168	3.4	178	77%	4%	35%	55%	73%
15	Io	Z	116	2.1	119	48%	14%	51%	53%	53%
16	Ice Giant Planets	H	155	2.6	159	69%	6%	46%	62%	71%

4.3 Photometric Precision

Requirements for photometric measurements in the NGAO science cases range from 0.05 to 0.1 magnitudes in relative photometry, and ≤ 0.05 magnitudes for absolute photometry. The fundamental condition for high photometric accuracy is stability of the PSF. Because of the high Strehl delivered by the NGAO system, a more stable PSF is expected. Many of the science cases that require the

highest photometric accuracy are observing a science target of sufficient brightness (H < 16) to permit use of the science target as an on-axis tip-tilt reference, further improving Strehl performance.

Detailed consideration of the physical effects that can degrade NGAO system photometric precision is documented in KAON 474, including AO system performance, stellar crowding, scintillation, atmospheric attenuation, and detector non-uniformities. The key result of KAON 474 is that in order to meet the scientifically required photometric precision, NGAO will need to provide the astronomical user with detailed and reliable information regarding the NGAO point spread function (PSF) on an exposure-by-exposure basis.

We envision 'on-axis' PSF information provide by AO system control and sensing telemetry, in the absence of an appropriate stellar point source reference (which if known will always provide a more accurate, direct measure of the PSF). NGAO will also provide an estimate of the field-dependent PSF based upon integrated recording of $C_n^2(h,t)$ information from the atmospheric profilometer on the Mauna Kea summit ridge (section 3.3.7.7). Work at Palomar (Britton 2006) has shown that real time turbulence monitoring giving C_n^2 data during the observation is also useful in improving the results of PSF post processing. This post processing will also be supported by facility PSF deconvolution software.

4.4 Astrometric Accuracy

Astrometry is important for a number of the Galactic and Solar System science cases. The most demanding requirements are for observations of the Galactic Center where relative astrometric accuracy of 100 μas is required. The current Keck II LGS AO system with the NIRC2 instrument is able to achieve best-case accuracy of 200 μas. Studies of the astrometric accuracy of the current Keck II LGS AO system indicate that source confusion, geometric distortion, differential tilt anisoplanatism between the science target and off axis tip-tilt stars (increasing with increasing distance between the two), and differential atmospheric refraction all contribute to the error in astrometric measurements.

The high Strehl of the NGAO system (~3 times that of the current LGS AO system under similar conditions) will significantly improve accuracy of astrometric measurements by reducing source confusion in crowded fields (such as the Galactic Center). More generally, because NGAO will utilize tip-tilt stars at near-IR wavelengths, sharpened to the diffraction limit, most observations will be able to use fainter tip-tilt stars, located closer to the science target, thus reducing tilt anisoplanatism. Similarly, by using multiple tip-tilt stars, NGAO will further reduce tilt anisoplanatism across the science field; through inclusion of an ADC, NGAO will reduce the differential effects of atmospheric refraction across the field. Finally, by improving Strehl, NGAO observations will detect more stars in a given field, at higher SNR, providing a richer field for astrometric calibration.

Other NGAO design choices have similarly been made to improve astrometric accuracy. The optical design choice of having mutual optical conjugation of the 1st and 2nd relay DM's is an intentional strategy to mitigate NGAO-induced plate scale distortions into the science focal planes. (Because the systematic error floor will be rapidly reached, we are more concerned about long-term stability and

place less emphasis on the potential correction of differential atmospheric tilt jitter afforded by MCAO architectures.) Geometric distortion in the AO system and instruments has been controlled during preliminary design, and we will provide facilities for mapping the small residual distortion during system commissioning. High mechanical stability has been a fundamental part of the design approach of the NGAO system and instruments, driving for example the AO cold enclosure temperature stability requirement of ± 1C. Finally, the same auxiliary NGAO features provided to monitor the PSF and monitor atmospheric turbulence for improving photometric precision will also contribute to improve astrometric accuracy.

Detailed consideration of the physical effects degrading astrometric accuracy for NGAO was documented in KAON 480 during the NGAO system design, including differential atmospheric tilt jitter, geometric distortion, atmospheric refraction, and stellar confusion. During the preliminary design an astrometry error budget tool was begun as part of the performance flowdown budgets spreadsheet tool documented in KAON 723. Containing initial (and occasionally crude) quantitative estimates of the astrometric contribution from various error sources, KAON 723 will be further developed during the detailed design in consultation with Keck and other researchers at the forefront of astrometric science.

4.5 Companion Sensitivity

Another important area for NGAO science is high contrast observations. The near-IR Strehl requirement for NGAO is somewhat lower than for extreme AO systems such as the Gemini Planet Imager but at the same time NGAO will provide higher sensitivity via greater collecting area and sharper diffraction limit. Importantly, NGAO will also provide high-contrast over large sky coverage via LGS operation, greatly exceeding the number of targets accessible via NGS-only extreme AO systems at Gemini and Palomar.

An analysis of the DAVINCI coronagraph performance was already discussed in section 3.7.2.7. During the preliminary design a high contrast error budget excel spreadsheet tool, KAON 723, was also developed that built on work from the system design.

Details of the high-contrast error budget development during the system design are presented in KAON 497. One product of this effort was a preliminary numerical budgeting tool (similar in some ways to the wavefront error spreadsheet tool) that allocated contributions to the residual high-contrast 'dark hole' halo to various physical effects, such as atmosphere fitting error, spatial aliasing, control servo lag, measurement noise, and residual tip/tilt errors. In addition, numerical simulations were performed to evaluate the impact of segment gaps (using the grey pixel approximation), segment vibrations, telescope wind-shake, and coronagraph residual diffraction effects. Partial consideration was made of the residual spatial power spectrum of tomography error, quasi-static LGS calibration errors, telescope static residual errors, and instrument static errors. By taking separate account of the expected residual speckle lifetimes associated with each physical effect, the achievable contrast for a certain observation in a given integration time can be predicted. An example of the high-contrast simulation capability employed in KAON 497 is shown in Figure 156.

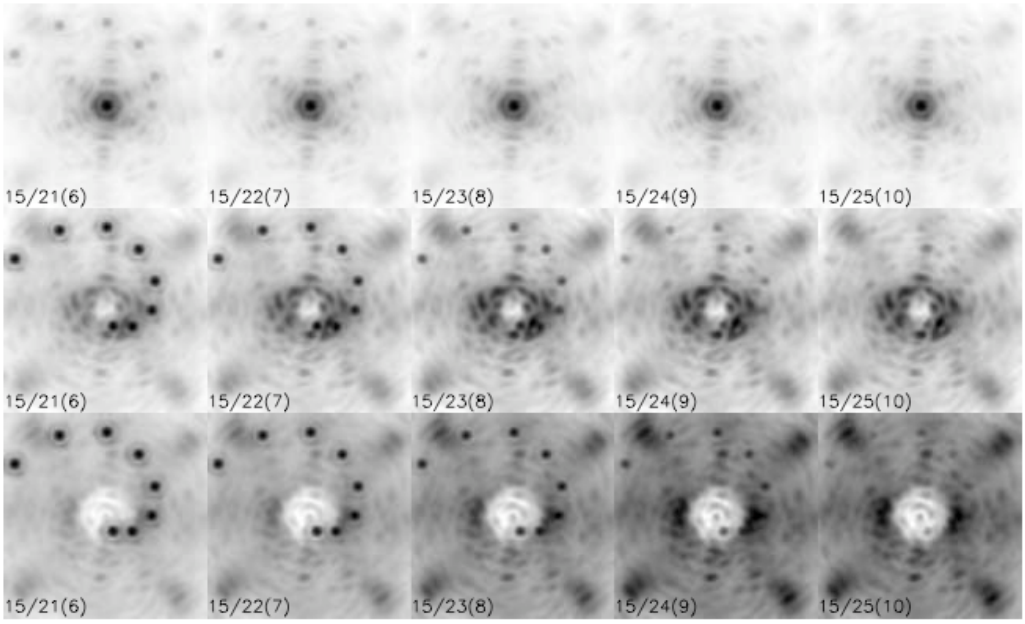

Figure 156: Simulated NGAO J-band science observations with secondary objects inserted
Top row: AO without coronagraph; middle row: AO + coronagraph with 6 λ/D occulation; bottom row: AO + coronagraph with 10 λ/D occulation. The numbers in the lower left corner of each image indicate the primary /secondary / delta magnitudes, i.e. the format is J_1 / J_2 (ΔJ). The images are stretched (asinh) and individually scaled.

The fundamental conclusion of KAON 497 was that NGAO can indeed serve as a powerful high-contrast science engine, particularly in the uniqueness space associated with faint science targets (where NGS-only systems will not be usable). We found that even with the high-order 64x64 actuator NGAO deformable mirror, residual telescope figure errors lead to speckles with troublesome spatial and temporal scales with the greatest contribution to the high-contrast error budget. The analysis indicated that a conventional occulting spot coronagraph with an apodized (hexagonal, rotating) Lyot stop will meet the needs of the majority of the NGAO high contrast science cases.

The level of contrast achieved with NGAO will ultimately depend on the control of systematic errors such as non-static, non-common path aberrations, servo lag error and various sources of speckle. Speckle suppression techniques including spatially resolved spectroscopy will be available for NGAO observations and we intend to incorporate to the extent possible the calibration "best practices" discovered by the GPI project.

4.6 Polarimetric Precision

Polarimetric precision was considered only superficially in the system and preliminary design phases. We identified the K-mirror rotator as a potential detriment to polarimetric precision, but adopted this in our architecture for its other system advantages (simplicity and cost). We do not yet know how stable or calibratable NGAO polarimetry will be.

One potential strategy for polarimetry for further consideration is the use of the K-mirror rotator in a fixed orientation, allowing the science image to rotate on the sky. For high-contrast polarimetry, this may be an acceptable observing mode.

4.7 Observing Efficiency and Uptime

KAON 463 discusses the observing efficiency and uptime of the existing Keck LGS AO system for reference. Observing efficiency has already been discussed in section 3.6.1.2. Flowdowns of observing efficiency and uptime to subsystems are provided in the excel spreadsheet tool maintained as KAON 723.

4.8 PSF Knowledge and Stability

How well do we need to know the PSF and how stable must it be to achieve the NGAO science cases? We have begun to address the PSF science metrics in KAON 762. The overall quality of the PSF subdivides into at least 12 components, everything from the spatial stability of Strehl, to the temporal stability of enclosed energy (see Table 34). Which PSF component provides benefit to a particular science case is highly variable between the key science cases evaluated. Overall a careful characterization of the PSF would benefit both observing efficiency and published uncertainties.

Table 34: PSF characteristics important to each key NGAO science case

For each of four common, yet distinct, figures of merit (Strehl, full-width half-maximum (FWHM), azimuthally averaged (1D) PSF, and the overall 2D PSF), we consider three orthogonal views of its stability: spatial stability across the field of view (Δd), temporal stability (Δt), and wavelength stability (Δλ).

Science Case	Science Sub-Case	Strehl			FWHM			1D PSF			2D PSF		
		Δ*d*	Δ*t*	Δλ	Δ*d*	Δ*t*	Δλ	Δ*d*	Δ*t*	Δλ	Δ*d*	Δ*t*	Δλ
1. Galaxy Assembly and Star Formation History	a. Internal kinematics	☐	☐	☑	☐	☐	☑	☐	☐	☑	☐	☐	☐
	b. Small scale structure (TBD)	☐	☐	☐	☐	☐	☐	☐	☐	☐	☐	☐	☐
	c. Star formation (TBD)	☐	☐	☐	☐	☐	☐	☐	☐	☐	☐	☐	☐
2. Nearby Active Galactic Nuclei	a. BH demographics (TBD)	☐	☐	☐	☐	☐	☐	☐	☐	☐	☐	☐	☐
	b. M-σ relation	☐	☑	☑	☐	☐	☐	☐	☐	☐	☐	☐	☐
	c. Stellar pops, etc (TBD)	☐	☐	☐	☐	☐	☐	☐	☐	☐	☐	☐	☐

3. Precision Astrometry: Measure-ments of General Relativity Effects in the Galactic Center	a. Non-Keplerian	☐	☐	☐	☐	☐	☐	☐	☐	☐	☑	☑	☐
	b. Dark Matter Halo (TBD)	☐	☐	☐	☐	☐	☐	☐	☐	☐	☐	☐	☐
	c. Radial Velocity & Sepctral Type	☐	☐	☐	☐	☐	☐	☐	☑	☑	☐	☐	☐
4. Imaging & Char-acterizing Exoplanets of Nearby Stars	a. Cool & faint (TBD)	☐	☐	☐	☐	☐	☐	☐	☐	☐	☐	☐	☐
	b. SFR young stars (TBD)	☐	☐	☐	☐	☐	☐	☐	☐	☐	☐	☐	☐
5. Multi-plicity of Minor Planets	a. Size and shape	☐	☐	☐	☐	☐	☐	☐	☐	☐	☐	☑	☐
	b. Density	☐	☑	☐	☐	☐	☐	☐	☐	☐	☐	☑	☐
	c. Composition and age	☐	☑	☐	☐	☐	☐	☐	☐	☐	☐	☑	☐

In many or most cases there will not be a PSF in the science field. For NGAO we are currently planning to provide a PSF reconstruction tool that will give the astronomer an estimate of the PSF across their field. This is clearly a research field since no astronomical facility currently provides PSF estimates. Our intention is to use the fixed asterism wavefront sensor data to provide a PSF estimate over a narrow field and to use atmospheric profiler data to extend this estimate over the science field.

During the PD phase we have made some progress in this field, but much more work will need to happen during the DD to determine that this is a viable approach. The PD progress included the following activities in order to better understand PSF reconstruction and to reduce risk in this area.

A CfAO funded activity, documented in KAON 626, resulted in a successful demonstration of PSF reconstruction for the bright on-axis NGS case. This project was put on hold in November 2008 with the departure of Ralf Flicker and due to funding uncertainties we were unable to re-hire for this postdoc position. The next step would have been to further develop the noise model component, the r0 estimation, and the covariance matrix model in order to extend this method to fainter guide stars in NGS mode. Anisoplanatism modeling was largely completed including analytical formulas for angular and focal anisoplanatism structure functions, which take into account the finite outer scale.

In support of acquiring real-time wavefront sensor data to develop and test the PSF reconstruction, tools were developed to query the Telemetry Recorder System (TRS) for the existing Keck AO systems and to manage the data. This effort is documented at the TRS Users' Twiki: http://www.keck.hawaii.edu/TWiki/bin/view/Main/AoTrsUsers. Longer term, either a PSF estimate will need to be provided to the observer in semi-real-time, or more likely, the appropriate

raw telemetry data will need to be included in the take-home data set of the observer, along with the software tools necessary to convert the raw data into a PSF representation that can be easily ingested by a standard deconvolution package (e.g., Mistral, IDAC or AIDA).

We determined that NGAO would need an atmospheric profiler in order to determine the off-axis PSF, as demonstrated at Palomar (Britton 2006). Measurements obtained from a seeing monitor could also be useful for predicting how often a PSF reference might be required (especially in the absence of a PSF reconstruction tool). At our request, and due to our ongoing collaborations, TMT donated one of their MASS/DIMM systems to WMKO (we had considerable experience utilizing the data from one of these units during our atmospheric characterization study; KAONs 415 and 420). We then reached an agreement with the University of Hawaii and CFHT, who had plans for a seeing monitor on Mauna Kea, for them to implement the TMT MASS/DIMM. This unit is now operational (section 3.3.7.7).

A Gemini Observatory, Groningen University and WMKO collaboration began in January 2010 to fund Laurent Jolissaint to demonstrate NGS AO PSF reconstruction with Altair and Keck AO. Jolissaint had developed PSF reconstruction code (called OPERA) for Altair while at HIA in 2002-2003 but this code had only been run once on a set of lab data. The OPERA code is now functional and has been run on 20 nights of bright NGS data from Altair. There is good correspondence between the residual wavefront error mode coefficients and the reconstructed PSF, demonstrating the validity of the approach. The next steps are including an estimate of the telescope PSF and compare with the actual science camera PSF data and to get noisier data with fainter NGS and include the noise covariance matrix in the reconstruction process.

Jolissaint has also read KAON 626 and believes that Flicker's approaches will prove to be more powerful in the long term. In May 2010 Jolissaint was given access to Flicker's directory including the IDL source code, the sparse matrix calculation libraries and the day-time and night-time engineering data acquired for this project. Jolissaint plans to continue the OPERA tool test and implementation at Gemini while further developing Flicker's tools on Keck data and ultimately to merge the results.

5 REQUIREMENTS AND CONFIGURATION MANAGEMENT

5.1 Requirements Development

The requirements development process is discussed in KAON 573 and is illustrated schematically in Figure 157. The process began by understanding the goals that the Keck community had for a next generation AO capability at WMKO. This was followed by the development of science cases to understand the science drivers and requirements on this NGAO capability. The Science Case Requirements Document discusses and documents this process and the resultant science requirements. These requirements were developed in parallel with initial performance budgets and analysis to determine feasibility. The science requirements and additional observatory and user requirements were subsequently documented as System Requirements. Both of these sets of requirements were intended to be architecture independent.

The Observing Operations Concept Document (KAON 636) was created during the Preliminary Design to describe how the features and functions of the design will be used to carry out the observations described in the science cases.

As the team developed an architecture and subsystem designs to satisfy the system requirements the next level of implementation dependent requirements were documented in the Functional Requirements. A few Interface Control Documents were developed during the Preliminary Design but primarily the interfaces were defined through a series of controlled documents that all subsystem designers are expected to address as part of their design efforts.

The document you are currently reading is the Preliminary Design Manual shown in the V-diagram as a product of the subsystem design.

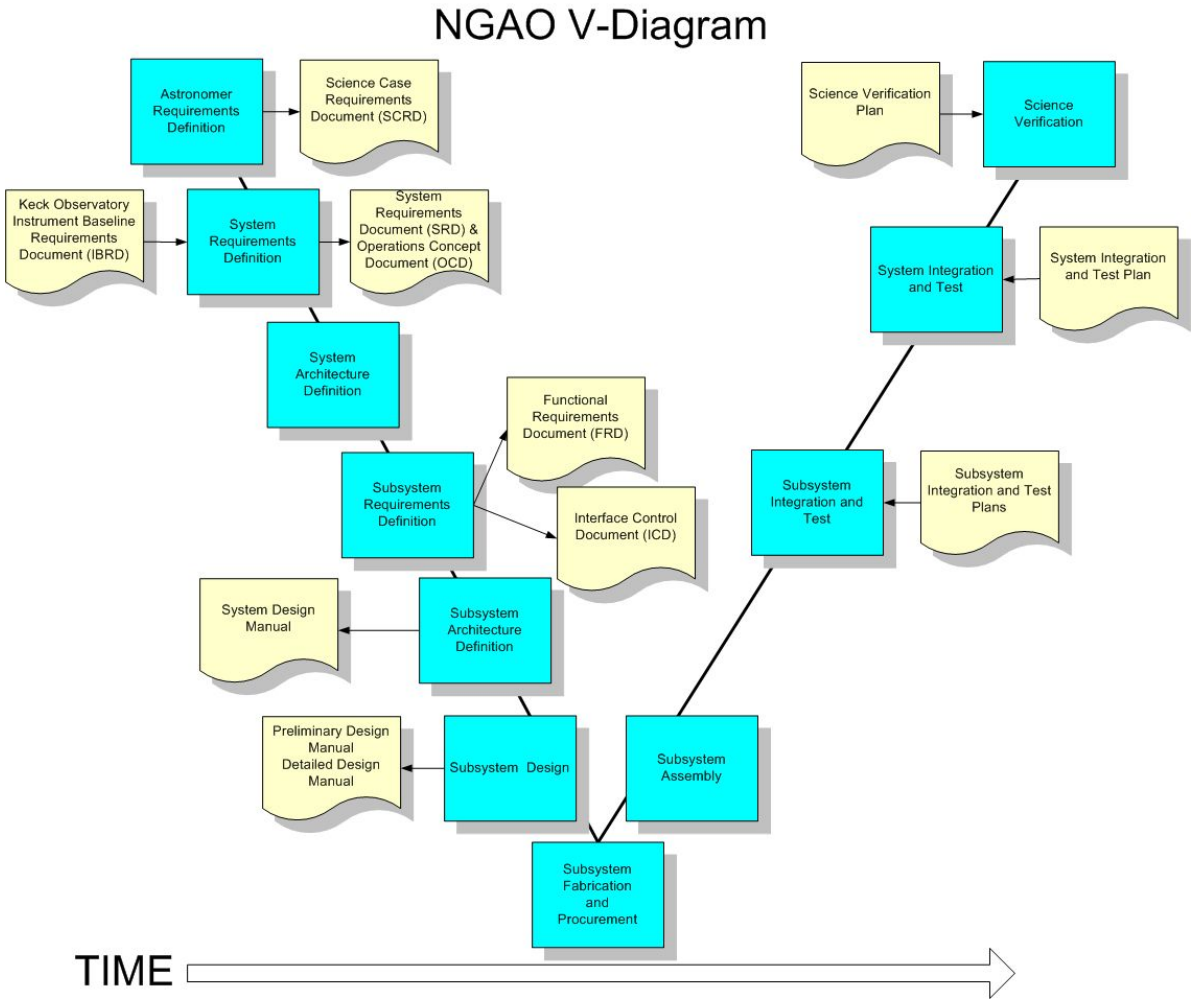

Figure 157: NGAO project V-diagram including the design and development process
Processes are shown in blue and associated documentation in tan.

5.2 Configuration Control

During the preliminary design both the NGAO requirements database and a set of key documents were placed under configuration control. The systems engineering group was given the responsibility for managing the requirements database and documents, using the change control process documented in KAON 638.

The configuration controlled documents are divided into five categories. These categories and the controlled documents within these categories are listed in Table 35. The 2nd last column in this table indicates whether a document is used for interface control. The final column indicates where in this preliminary design manual each document is discussed.

Table 35: Configuration Controlled Documents

Category	KAON	Document	ICD	Section
System Configuration	550	System Configurations		
	636	Observing Operations Concept Document		5.3
	642	Design Changes in Support of Build-to-Cost		
	682	Master Device List (Excel)	Yes	5.4.3
	705	AO-Level Control Loops	Yes	3.5.2
	726	NGAO Mechanical Model (SolidWorks)	Yes	
	727	NGAO Optical Model (Zemax)	Yes	
Performance Budgets	716	Wavefront Error Budgets		
	721	Wavefront Error Budget Tool (Excel)		
	722	High Contrast Error Budget Tool (Excel)		
	723	Performance Flowdown Budgets (Excel)		
Other Budgets	709	Power Consumption & Cabling Budgets (Excel)	Yes	
	724	Mass Budget (Excel) – to be developed during DD	Yes	
Interface Control		Pupil Mapping to DMs (Keck Dwg 1410-CM0010)	Yes	3.3.1
	725	DAVINCI ICD	Yes	

5.3 Interface Control

The approach taken to interface control during the preliminary design is documented in KAON 741. The interfaces between internal subsystems of the NGAO system are primarily defined by the controlled global NGAO documents in Table 35 (identified in the ICD column) rather than subsystem-to-subsystem documents. This approach also extends at a somewhat lesser level to the external interfaces to the telescope and science instruments. There is an ICD for DAVINCI. KAON 741 includes an N-squared diagram of the interfaces between the NGAO subsystems.

5.4 System Configuration Documents

The AO-level control loops are discussed in section 3.5.2.

5.4.1 System Configuration

The configuration of every device in the NGAO system is defined in KAON 550 for the supported science modes. This spreadsheet is reproduced in Table 36 (for display purposes this long horizontal spreadsheet was cut in half with the right half of the spreadsheet pasted below the left half). Five NGS science modes and five LGS science modes are addressed in this spreadsheet.

Table 36: System configurations

To view this long horizontal spreadsheet the left half of the spreadsheet is shown at the top and the right half at the bottom of this figure.

	Observing Mode Definition				LGS Launch Facility				Rotator	Low Order Relay		LGS WFS		IF	Acquis.
#	Configuration	Science λ	Science Field Diameter	Field or Pupil Mode	Asterism Rotation Tracking	LGS Flexure Comp.	Patrol-ling LGS Position	LGS Focus Tracking	Rotator Tracking	LODM	LODM Tip-tilt	Patrol-ling LGS Acquire	LGS Focus Tracking	Interfer-ometer Fold	Acquis-ition Fold
NGS Science Modes															
1a	**Interferometry** of			Fixed field					Fixed field					Science	
1b	bright on-axis NGS	H - L	≤ 2"	Fixed pupil					Fixed pupil	Yes	Yes			reflect	Out
2	Dual star **Interferometry**	H - L	≤ 60"	Fixed field					Fixed field	Yes	Yes			Science reflect	Out
3a	**Imager**		≤ 30"												
3b	**IFS**	Y - K	≤ 5"	Fixed field					Fixed field	Yes	Yes			Out	Out
4a	**Imager**														
4b	**IFS**	Y - K	≤ 2"	Fixed pupil					Fixed pupil	Yes	Yes			Out	Out
5	**Field Acquisition**	Current	Full	Current					Current	Flat	Centered			Out	Mirror
LGS Science Modes															
1a	**Interferometry** of			Fixed field	Yes				Fixed field					Science	
1b	faint on-axis NGS	H - L	≤ 2"	Fixed pupil	No	Yes	No	Yes	Fixed pupil	Yes	Yes	No	Yes	reflect	Out
2	Dual star **Interferometry**	H - L	≤ 60"	Fixed field	Yes	Yes	No	Yes	Fixed field	Yes	Yes	No	Yes	Science reflect	Out
3a	**Imager**		≤ 30"												
3b	**IFS**	I - K	≤ 5"	Fixed field	Yes	Yes	1 to 3	Yes	Fixed field	Yes	Yes	1 to 3	Yes	Out	Out
4a	**Imager**														
4b	**IFS**	Y - K	≤ 2"	Fixed pupil	No	Yes	No	Yes	Fixed pupil	Yes	Yes	No	Yes	Out	Out
5a	**Field Acquisition**														
5b	**LGS Acquisition**	Current	Full	Current	Current	Current	Current	Current	Current	Flat	Centered	Current	Current	Out	Mirror

LOWFS				High Order Relay		NGS WFS						ADC	Science Instruments			
NGS Acquis-ition	Focus Adjust	DM + tip-tilt	Visible TWFS	HODM	HODM Tip-tilt	NGS WFS Fold	NGS WFS Acquis.	Field Steering	HO NGS WFS Mode	LOWFS/ TWFS Mode	Focus Adjust	Science ADC	Imager	IFS	Interfer-ometer	OHANA
NGS Science Modes																
				Flat	Tracking	In	Yes	Offloads	Yes		For IF				Single object	Single Object
				Flat	Tracking	In	Yes	Offloads	Yes		For IF				Dual object	Single Object
				Yes	No	In	Yes	Offloads + Dither	Yes		ADC in/out, Instrument	Track or out	Yes Vignetted	No Yes		
				Yes	No	In	Yes	Offloads	Yes		ADC in/out, Instrument	Track or out	Yes or	Yes or		
				Open	Open Lp	In		Open Lp	Open Lp			Current	Current	Current	Current	Current
LGS Science Modes																
No	No	No	Option No	Flat	Tracking	In	Yes	Offloads		Yes	For IF				Single object	Single Object
No	No	No	Option off-axis	Flat	Tracking	In	Yes	Offloads		Yes	For IF				Dual object	Single Object
1 to 3	ADC, Instrum.	1 to 3	Yes	Yes	Tracking + Dithers	Out	No	No		No	ADC in/out, Instrument	Track or out	Yes Vignetted	No Yes		
No	No	No	No	Yes	No	In	Yes	Offloads		Yes	ADC in/out, Instrument	Track or out	Yes No	No Yes		
		Open Lp	Open Lp	Open Lp	Open Lp			Open Lp		Open Lp		Current	Current	Current	Current	Current

In order to understand this spreadsheet we will walk through the primary LGS science mode case, case 3:

- The observing mode is defined in columns 2 to 5. Case 3a is the imager and case 3b is the integral field spectrograph (IFS). Both cases can do science at any wavelength from I-band to K-band. The only difference between these two cases is the science field diameter in the 4th column. This case requires a fixed science field.
- The LGS launch facility configuration is defined in columns 6 to 9. The LGS asterism must be rotated to stay fixed on the sky, the flexure compensation for laser pointing must be on and the laser launch telescope focus must stay conjugate to the sodium layer as the telescope tracks. Normally the 3 patrolling LGS will each be pointed at a NGS; however it is possible to only use 1 or 2 of these patrolling LGS.
- The AO rotator mode is defined in column 10. In this case the rotator will track to keep the field fixed.
- In the Low Order Relay, columns 11 and 12, both the low order deformable mirror (LODM) and the tip-tilt stage it is mounted on will be providing AO correction.
- The LGS WFS, columns 13 and 14, will have its patrolling LGS WFS pointing at the same NGS as the LGS launch facility in order to acquire these LGS and the entire LGS WFS assembly will have its focus tracking as a function of telescope elevation and sodium altitude.
- The Interferometer fold, column 15, that feeds light to the interferometer module must be out of the beam.
- The acquisition fold, column 16, that feeds light to the acquisition camera must be out of the beam.
- The Low Order WFS (LOWFS) configuration is defined in columns 17 to 20. Again normally 3 but as few as 1 NGS must be acquired. The focus of each LOWFS must be adjusted so that they are conjugate to the science instrument focal plane (this focus is a function of what optics are in the beam to the science instrument, such as an ADC). The DMs and tip-tilt mirrors in the LOWFS being used must be controlled by the RTC. The visible truth WFS (TWFS) will be used to provide corrections to the RTC and LGS WFS focus tracking.
- In the High Order Relay, columns 21 and 22, the high order deformable mirror (HODM) will be used for real-time AO correction and the tip-tilt stage it is mounted on will be used for slower AO-loop level corrections.
- The NGS WFS, columns 23 to 28, is not used in this mode. The fold dichroic that feeds light to the NGS WFS must be out of the science beam. No NGS WFS acquisition needs to occur with the NGS WFS field steering mirrors. The NGS WFS is not operated in its high order or low order modes and no focus adjustment is required.
- The science ADC, column 29, can be in or out of the science path.
- The science instrument, column 30 to 33, selected is either the imager or the IFS. It is possible to simultaneously observe with the imager during IFS science but the center of the imager field will be blocked.

5.4.2 Observing Operations Concept Document

The Observing Operations Concept Document (OOCD; KAON 636) was produced during the preliminary design to describe how the science case requirements will be met via observations with

the NGAO system. The document is broken into two major sections: science case observations and use cases.

For each of the five key science drivers, and the gas giant planet case, the imaging and integral field spectroscopy requirements, the assumptions and pre-requisites and the observing model are described. The pre-observing, observing and post-observing tasks are listed in some detail. Observations with the interferometer and using fixed pupil mode are also reviewed.

The specific use cases section includes details of observation planning, acquisition, observing sequences, common troubleshooting and observing support.

5.4.3 Master Device List

The Master Device List (KAON 682) captures all of the controllable devices in the NGAO system. Tabs in the excel spreadsheet capture information on motion devices, non-motion devices and detectors. The motion device tab itemizes all moveable axes along with key performance requirements, location of the stage, manufacturer information (if available) and information supporting the specifications. Non-motion devices include environmental monitors, AC power control, calibration sources, etc. The final tab captures all of the information on the various detectors/cameras used throughout the system. A sample of the Master Device List contents is shown in Table 37. These 8 rows, of the 54 rows in the "motion devices" tab, show the Laser Launch Facility Beam Generation System devices.

Table 37: Beam Generation System devices from the Master Device List

The long horizontal spreadsheet has been divided into thirds with the Device Name repeated in each third..

Device (assembly) Name	RTC	DOF per assy	No of Assy	TL DOF	Type of Motion	Axes	Range	Accuracy / Repeatability	Required Position Knowledge	Runout	Tracking Device?
Patrolling LGS beam splitter		1	2	2	Linear	x	in/out, 12.5 mm	60 um			No
Star imager pickoff		1	1	1	Linear	x	in/out, 50 mm	30 um			No
Patrolling LGS steering		2	3	6	linear	x,y	80 mm	30 um			No
Laser Asterism rotator		1	1	1	Rotational	θ	360 deg	0.05 deg			Yes
Laser Asterism Tip/Tilt		2	1	2	tip/tilt	θ,Φ	3 mrad	3 urad			Yes
Fast Shutter		1	1	0	solenoid	x					No
Patrolling LGS beam splitter		1	2	2	Linear	x	in/out, 12.5 mm	60 um			No
Laser Beam dump		1	0	0	Linear	x		Low precision			No

Device (assembly) Name	Tracking Rate	Slew Rate	load size	load mass	total mass	Device Location	Stage Information
Patrolling LGS beam splitter		1mm/s				secondary	
Star imager pickoff		5mm/s				secondary	
Patrolling LGS steering	slow UTT offload	10mm/s		100-200g		secondary	linear piezo (PI M-683 + PI controller or driver). smarAct SLC-24120
Laser Asterism rotator	Sidereal	min: 10 deg/s goal: 30 deg/s				secondary	Newport RGV100BL, brushless, 30mm apperture, sin/cos encoder
Laser Asterism Tip/Tilt	slow/ flexure					secondary	PI S-330.4SL -> 5mrad range / 0.25urad resolution / 0.5 urad repeatibiity
Fast Shutter		0.1s				secondary	
Patrolling LGS beam splitter		1mm/s				secondary	
Laser Beam dump						secondary	

Device (assembly) Name	Comments	Traceability	source of position command
Patrolling LGS beam splitter	Select number of patrolling beacons 1, 2 or 3		asterism sky location
Star imager pickoff			
Patrolling LGS steering	Position patroling beacons in field Tracking refers to UTT offload.		telescope az/el
Laser Asterism rotator			telescope az/el
Laser Asterism Tip/Tilt	Possible alternative for BTO vibration control may also include UTT offload		tel el (flexure model)
Fast Shutter	part of LaserSafetySystem		
Patrolling LGS beam splitter	Select number of patrolling beacons 1, 2 or 3		asterism sky location
Laser Beam dump	req'd If not built into fast shutter		

5.4.4 Optical and Mechanical Models

The Zemax optical design model of the AO bench has been made a controlled document since it represents the optical interface between multiple subsystems.

The SolidWorks mechanical model, which also incorporates the Zemax optical model, has been made a controlled document since it represents the mechanical interface between AO subsystems and between the AO system and the telescope.

5.5 Performance Budgets

The wavefront error budget is documented in KAON 716. This document also describes the wavefront error budget excel spreadsheet tool (KAON 721) that was used to generate the performance predictions.

A separate excel spreadsheet tool for the high contrast error budget is maintained as KAON 722.

All other performance flowdown budgets are maintained in KAON 723. This excel spreadsheet tool includes budgets (on separate sheets) for transmission and background (see section 4.1), non-correctable wavefront errors, non-common path tip-tilt errors, observing efficiency and system uptime.

5.6 Other Budgets

Two additional excel spreadsheet tools are being developed. KAON 709 contains the power consumption and cabling budgets, and KAON 724 contains the mass budget.

5.7 Requirements Database and Compliance

All of the NGAO science, system and functional requirements are maintained in a requirements database tool called Contour produced by Jama Software. Separate folders are used for the science, system, functional and Keck standards requirements, as well as folders for interfaces and NGAO controlled documents. Within the system requirements folder the requirements are organized by categories such as overall, optical, mechanical, etc. Within the functional requirements folder the requirements are organized to match the NGAO Product Breakdown Structure. The requirements from Contour were output into KAON 771 for the preliminary design review.

In all levels of the requirements, steps were taken to assure that each documented specification is traceable back to its origin or driver. The most relevant sources are the top level NGAO science requirements and essential observatory standards but in many cases requirements are generated based on architectural design decisions, engineering best judgments, or for other reasons. Maintaining requirements traceability enables reasonable change control, so that the systems engineer is able to understand and manage the impact of descopes, engineering "push backs," error budget redistribution, etc.

Compliance matrices were generated for all NGAO subsystems and the results are compiled in KAON 772. The compliance matrices included the system requirements which all subsystems are expected to meet, the overall AO requirements which appropriate subsystems are expected to meet and the functional requirements specific to each subsystem. As a product of the preliminary design compliance matrices were produced for each subsystem.

The result of the system requirements evaluation for each of the subsystems is shown in Table 38.

Table 38: System requirements compliance summary

	N/A	DD	Yes	No	Partial	Goal
Compliance of 11 subsystems for all 102 System Requirements	568	378	170	1	2	3
% excluding N/A		68%	31%	0.2%	0.4%	0.5%

N/A = Not Applicable. DD = Compliance will be determined during Detailed Design. Yes = compliant. No = Not compliant. Partial = Partially compliant. Goal = Compliant as a goal.

The one requirement not in compliance (denoted "No" in the table) is related to the mass limited requirement for systems that are mounted inside the secondary mirror support structure. The LGS Facility design team commented, "The mass of the components will exceed that in the spec. However, there is an existing 700 pound counterweight that will be removed to offset any weight increase by the components in the secondary." This issue will be addressed during the detailed design. The two requirements listed as partially compliant involve documentation requirements. It is not expected at preliminary design review to be able to satisfy the requirement for all final documentation. The other systems all listed this as being verified only at detailed design or during delivery of the subsystem. Two of the three requirements listed at "Goal" are all related to failure testing of the software. Software methodology cannot guarantee compliance during the design phases, the possibility exists of unknown bugs that may not be found until the system is built and

tested. Software, unlike hardware, cannot test many identical units to determine a statistical mean time between failures. NGAO control software will be verified to the extent possible during full scale development of software. The last requirement that is listed as "Goal" involves the requirement to simulate the telescope functions with the AO control software. The software design team commented that they are not currently tracking this as a design feature of controls system, but it could be added during the detailed design phase.

The results of the evaluation of the overall AO functional requirements are listed in Table 39. The one requirement listed at partial involves not blocking the Keck telescope pupil. The NGS WFS team noted that: "The sensors low order 5x5 mode will sometimes loose light (during extreme nutation)." The one requirement listed as a "Goal Only" by the NGS WFS design team involves the non-operational conditions (temperature, humidity, etc.) in the observatory dome environment; no reason was given for the non-compliance. Both issues will be addressed during the detailed design.

Table 39: Overall AO requirements compliance summary

	N/A	DD	Yes	No	Partial	Goal
Compliance of 8 major AO subsystems for all 30 Overall AO functional Requirements	102	80	56	0	1	1

The results of the evaluation of the subsystem specific functional requirements are listed in Table 40 by subsystem.

Table 40: Subsystem Specific functional requirements compliance summary

Subsystem Specific Functional Requirements	DD	Yes	No	Partial	Goal
AO Enclosure	12	18	0	0	0
AO Bench	21	47	0	2	0
LGS WFS	11	24	1	0	0
NGS WFS	10	12	1	0	0
LOWFS	5	11	0	0	0
Acquisition Camera	5	11	0	7	0
Alignment, Calibration, & Diagnostics	2	39	0	0	0
LGS Facility	26	103	1	1	0
Controls	8	48	1	0	0
Science Operations Tools	8	38	0	3	0

The non-compliant requirements will be addressed during detailed design. A brief description of these non-compliant requirements is as follows:

- LGS WFS. The design for the dynamical range of the patrolling asterism LGS WFS is ±0.86" versus the ±1.4" requirement.
- NGS WFS. This appears to be an error in the non-compliant requirement or its interpretation that is being addressed during the PD.
- Alignment, calibration and diagnostics. Four requirements for an atmospheric simulation capability are only partially supported by the design; at present we have deemed that this is acceptable. The team believes that three requirements to do with calibration source brightness

in terms of SNR at the science instrument can be met but no formal verification has been documented.

- The non-compliant requirement has to do with the strength of material for items mounted on or above the telescope. The partial requirement is that the design was modified to require less power at the laser enclosure than stated in the requirement.
- Controls. The non-compliance has to do with providing all functionality by a distributed control system on a single command processor. This requirement would be met by removing the word "single" which we are likely to decide to do.
- Science operations tools. The partial compliance requirements are related to the need to more completely specify the design.

5.8 Performance Compliance

The NGAO architecture we have selected and developed has been demonstrated in our performance budget analyses (KAON 716) to meet the background, wavefront error, ensquared energy and sky coverage science case requirements.

Although not yet demonstrated by performance budgets or analysis we are developing the functional requirements and designs to ensure that the astrometric and photometric requirements will be met. A major element of meeting these requirements will be providing a good calibration of the PSF.

The key elements of the selected architecture flowed directly from the science case requirements. At the highest level these can be summarized as follows:

1. Dramatically improved performance at near infrared wavelengths.
   a. Improved IR sensitivity.
      - High Strehls (≥ 80% at K-band) are required over narrow fields. The flowed down requirements are derived from the wavefront error performance budget and assumption about how these error terms can be met. These flowed down requirements include number of actuators in the narrow field, required system bandwidth, number of LGS, number of NGS, required laser power, etc.
      - Lower backgrounds. This is particularly driven by the high redshift galaxy science. This requirement has driven the need for a cooled AO system and the required temperature.
   b. Improved astrometric, photometric and companion sensitivity performance.
      - Improved IR sensitivity is required (see above).
      - It will also be critical to improve the PSF stability and knowledge. The requirements on the PSF stability and knowledge to achieve the astrometric, photometric and companion sensitivity requirements will be developed during the Detailed Design. The astrometric error budget and PSF reconstruction tools will be developed during the Detailed Design.

2. Increased sky coverage.

- Wide field required. This requirement drove us to the 120" diameter field needed to find suitable NGS for tip-tilt sensing. The field requirement was determined via the analysis documented in KAON 504.
- Ability to use faint NGS. This requirement drove us to the architecture where we provide AO correction of the tip-tilt stars.

3. AO correction in the red portion of the visible spectrum.
   - This drove the need to transmit these wavelengths to the visible science instruments and to share visible light with the LGS and NGS wavefront sensors via appropriate dichroics.

4. Science instruments that will facilitate the range of science programs.
   - This drove the selection and conceptual design of the science instruments described in section 3.7.
   - This drove the providing of locations for these science instruments in the design.

We have also mapped each science case to a configuration of the NGAO system as shown in Table 41 to ensure that the NGAO architecture and subsystems can operationally support each science case (the configurations are maintained in KAON 550). The numbers in the NGS and LGS configuration columns refer to NGAO system configurations in Table 36.

Table 41: Science case mapping to NGAO configurations

#	Key Science Drivers	NGS Configuration		LGS Configuration		Notes
		Primary	Secondary	Primary	Secondary	
1	Galaxy Assembly			3b at z-K		
2	Black Hole masses in Nearby AGNs			3b at I	3b at z-K	
3	General Relativity at the Galactic Center					
	Astrometry			3a at K	3a at H	
	Radial Velocities with IFS			3b at K,H		
4	Planets around low mass stars					
	Survey			3,4		Imaging & IFS; Y to H-band preferred. Coronagraph required.
	Spectra			4,3		Narrow band imaging filters may be adequate
5	Minor Planets as remnants of early Solar System					Differential tracking option needed
	Survey			3a at z-J	4a	Imaging only; z,J-band preferred for survey
	Orbit Determination			3a at I	4a	Imaging; I-band preferred for orbit
#	**Science Drivers**					
1	QSO host galaxies					
	Imaging			3a at z-K		Possible use of coronagraph
	Spectroscopy			3b at z-K		
2	Gravitational Lensing					
	Imaging			3a at z-K	3a at I	
	Spectroscopy			3b at z-K	3b at I	
3	Astrometry in sparse fields			3a at H-K		
4	Resolved stellar populations in crowded fields			3a at I-K	3b	
5	Debris disks and Young Stellar Objects					
	Imaging	3a,4		3a at I-K, 4a		Need coronagraph. Polarimetry useful.
	Spectroscopy	3b,4		3b at z-K, 4b		
6	Size, shape & composition of Minor Planets			3a at I	3a at z-J, 3b	Differential tracking option needed
7	Gas Giant Planets and their moons	3	3 at I	3		Differential tracking option needed
8	Ice Giant Planets	3	3 at I	3		Differential tracking option needed

6 ALTERNATE SYSTEM ARCHITECTURES AND TRADE STUDIES

During the selection of the system architecture described in the system design manual (SDM; KAON 511), several alternate architectures were also evaluated and ranked. Each of these architectures, along with our adopted cascaded relay, are described and evaluated in KAON 499.

1. Split relay. The LOWFS, NIR deployable IFU and LGS wavefront sensor are fed directly from the telescope (and therefore must rotate). The narrow field science instruments are fed by a refractive AO relay including a K-mirror and ADC. Some technical evaluation details for this architecture are discussed in KAON 506.
2. Adaptive secondary mirror. All of the science instruments and wavefront sensors are fed directly by the telescope. An adaptive secondary trade study was performed in KAON 485. The existence of an adaptive secondary could potentially improve the performance on seeing limited instruments, and would offer the optimal approach to a ground layer AO system (see KAON 472).
3. Large relay. A large rotator and AO relay feed all of the science instruments and wavefront sensors. This is the architecture that was described in the NGAO proposal (KAON 400).
4. Keck I upgrade. Quite similar to the selected cascaded relay approach. The NIR deployable IFU and LGS WFS both follow the existing AO relay. A second, higher order relay feeds the narrow field science instruments. The difference is that this is an upgrade to the existing system, rather than a fresh start. KAONs 500 and 502 describe this upgrade in some detail. During preliminary design, we will look more closely at interim benefits to the Keck I LGS system that could be realized as part of our NGAO risk mitigation.

A number of trade studies were performed early in the SD phase to inform the system architecture down select and design choices. A list of these trade studies is provided in Table 42 and their results were briefly summarized in the SDM (KAON 511). These trade studies were key inputs to the architecture down selection process described in KAON 499.

Table 42: List of trade studies performed during the system design

Trade Study Title	KAON #
MOAO & MCAO	452
NGAO Versus Keck AO Upgrades	462
Adaptive Secondary Mirror Option	485
Keck Interferometer Support	483 (& 428)
GLAO for non-NGAO Instruments	472
Instrument Reuse	493
Telescope Wavefront Errors	482
Observing Model	476
Rayleigh Rejection	490
LGS Wavefront Sensor Type & number of subapertures	465
Low Order Wavefront Sensor number & type	470
Low Order Wavefront Sensor Architecture	487
LGS Asterism Geometry and Size	429
Variable Versus Fixed LGS Asterism Geometry	427
Uplink Compensation	509

A major set of trade studies were performed as part of the build-to-cost exercise. The resultant design choices are described in KAON 642 and the performance evaluations in support of these design choices are described in KAON 644.

A few trade studies were performed during the preliminary design to support design decisions:

- As part of the build-to-cost exercise several alternate optical relay designs were considered in KAON 628. The conclusion was to continue with the baseline cascaded relay design.
- A number of motion control architectures were evaluated against the NGAO needs in KAON 643. The conclusion was to use a combination of centralized control for high precision devices and distributed control, with smart motors, for devices with less demanding requirements.
- KAON 680 looked at options for vibration mitigation and recommended a parametric oscillator approach similar to that being used with the Keck Interferometer.

7 GLOSSARY

Table 43 defines the acronyms and specialized terms used in this document.

Table 43: Glossary of Terms

Term	Definition
"	Arc seconds
'	Arc minutes
ACS	Active Control System
ADC	Atmospheric Dispersion Corrector
AO	Adaptive Optics
API	Application Programmer Interface
BGS	Beam Generation System
BTO	Beam Transport Optics
DAVINCI	Diffraction limited Adaptive optics Visible and Infrared iNtegral field spectrograph and Coronagraphic Imager
DCS	Drive and Control System
DD	Detailed Design
DM	Deformable Mirror
DOF	Degrees Of Freedom
EFL	Effective Focal Length
EPICS	Experimental Physics Industrial Control System
FAA	Federal Aviation Administration
FOV	Field Of View
FPGA	Field Programmable Gate Array
FPM	Focal Plane Mask
FRD	Functional Requirements Document
FWHM	Full Width at Half Maximum
GPI	Gemini Planet Imager
HODM	High Order Deformable Mirror
HOWFS	High Order WaveFront Sensor
IBRD	Instrument Baseline Requirements Document
IFS	Integral Field Spectrograph
IFU	Integral Field Unit
KAON	Keck Adaptive Optics Note
KI	Keck Interferometer
KOTN	Keck Observatory Technical Note
LCH	Laser Clearing House

LGS	Laser Guide Star
LGSF	Laser Guide Star Facility
LLF	Laser Launch Facility
LODM	Low Order Deformable Mirror
LOWFS	Low Order WaveFront Sensor
LSE	Laser Service Enclosure
LT	Launch Telescope
LTCS	Laser Traffic Control System
mas	milli-arcsecond
MEMS	Micro Electro-Mechanical System
MSCS	Multi-System Command Sequencer
MTBF	Mean Time Between Failures
NGAO	Next Generation Adaptive Optics
NGS	Natural Guide Star
NIR	Near InfraRed
NIRC2	NIR Camera 2
NIRSPEC	NIR SPECtrometer
OA	Observing Assistant
OAP	Off-Axis Parabola
‘OHANA	Optical Hawaiian Array for Nanoradian Astronomy
OMU	Opto-Mechanical Unit
OSIRIS	OH-Suppression InfraRed Integral field Spectrograph
OSM	Object Selection Mechanism
PAG	Patrolling Asterism Generator
PD	Preliminary Design
PLC	Programmable Logic Controller
PSF	Point Spread Function
rms	root mean square
RTC	Real-Time Control
SA	Support Astronomer
SCRD	Science Case Requirements Document
SD	System Design
SDM	System Design Manual
SRD	System Requirements Document
SS	Safety System
SYD	SwitchYarD
TBC	To Be Completed
TBD	To Be Determined
TEC	Thermo Electric Cooler
TMA	Three Mirror Anastigmat
TMT	Thirty Meter Telescope
WFE	WaveFront Error
WFS	WaveFront Sensor
WMKO	W. M. Keck Observatory